

# INVESTIGATION AND OPTIMISATION OF HYBRID ELECTRICITY STORAGE SYSTEMS BASED ON COMPRESSED AIR AND SUPERCAPACITORS

THÈSE N° 3628 (2006)

PRÉSENTÉE LE 20 OCTOBRE 2006

À LA FACULTÉ DES SCIENCES ET TECHNIQUES DE L'INGÉNIEUR

Institut des sciences de l'énergie

SECTION DE GÉNIE ÉLECTRIQUE ET ÉLECTRONIQUE

ÉCOLE POLYTECHNIQUE FÉDÉRALE DE LAUSANNE

POUR L'OBTENTION DU GRADE DE DOCTEUR ÈS SCIENCES

PAR

Sylvain LEMOFOUET - GATSI

Diplôme de Professeur d'Enseignement Technique de Deuxième Grade en génie électrique,  
ENSET, Université de Douala, Cameroun  
de nationalité camerounaise

acceptée sur proposition du jury:

Prof. J. R. Mosig, président du jury

Prof. A. Rufer, directeur de thèse

Prof. F. Blaabjerg, rapporteur

Prof. A. Bouscayrol, rapporteur

Prof. D. Favrat, rapporteur



ÉCOLE POLYTECHNIQUE  
FÉDÉRALE DE LAUSANNE

Lausanne, EPFL

2006



# Remerciements

Ce travail de thèse, qui a été réalisé entre les années 2002 et 2006 au Laboratoire d'Electronique Industrielle (LEI) de l'Ecole Polytechnique Fédérale de Lausanne (EPFL), a été pour moi une expérience particulièrement enrichissante aussi bien sur le plan professionnel que sur le plan personnel. Les résultats présentés dans ce rapport n'auraient pas été obtenus si je n'avais bénéficié du concours et du soutien multiformes de plusieurs personnes à qui je voudrais ici exprimer ma reconnaissance et ma gratitude.

Je remercie sincèrement et particulièrement le *Prof. Alfred RUFER*, mon directeur de thèse, pour m'avoir accepté comme assistant-doctorant dans son équipe et pour la confiance qu'il a placée en moi en me donnant cette opportunité de travailler sur un sujet aussi intéressant. Son soutien total, sa disponibilité, son ouverture aux idées nouvelles, ses qualités humaines et sociales exceptionnelles à mon égard personnellement comme à celui de toute l'équipe du LEI, ont créé les conditions favorables et stimulantes pour l'obtention de ces résultats.

Je remercie le *Prof. Juan MOSIG* du Laboratoire d'Electromagnétisme et Acoustique (LEMA) de l'EPFL, pour avoir accepté de présider le jury d'évaluation de cette thèse. Je remercie également le *Prof. Daniel FAVRAT* du Laboratoire d'Energétique Industrielle (LENI) de l'EPFL, le *Prof. Alain BOUSCAYROL* du Laboratoire d'Electrotechnique et d'Electronique de Puissance (L2EP) de l'Université de Lille 1 et, le *Prof. Frede BLAABJERG* de l'Institut des Technologies de l'Energie (IET) de l'Université d'Aalborg, pour l'honneur qu'ils m'ont fait en acceptant de faire partie de ce jury.

Ma profonde gratitude va à toute l'équipe du LEI, pour leur soutien et pour cette atmosphère de travail à la fois relaxante et stimulante. Je remercie particulièrement *Fabienne VIONNET*, *Roberto ZOIA* et *Yves BIRBAUM* pour leur appui administratif, informatique et technique respectivement. Je re-

## Remerciements

mercie *Philippe BARRADE* pour ses remarques pertinentes et ces discussions fructueuses dans le domaine de Supercondensateurs. Je remercie vivement *Felix GRASSER* pour la lecture de ce rapport et pour son important soutien, particulièrement dans le domaine de la mécanique. J'adresse également mes remerciements aux anciens collaborateurs du LEI, particulièrement à *Martin VEENSTRA*, *Joseph SONG-MANGUELLE* et *Jean-Sébastien MARIETHOZ* pour leur aide.

Je remercie messieurs *Roland WETTER* et *Sylvain ROBERT* du Laboratoire des Machines Electriques (LME) pour leur assistance lors des essais de caractérisation de la machine synchrone, qui a eu lieu dans leur unité. Je dit également merci à *Monsieur Ivan CYPHELLY* qui m'a fait profiter de sa grande expérience dans le domaine hydropneumatique, à travers ses idées originales et ses conseils techniques pertinents.

Je remercie infiniment toute ma famille et particulièrement mes parents, pour leurs prières, leurs encouragements et leur soutien inconditionnel tout au long de mes études. Ma profonde gratitude à *Natacha*, sans l'aide de qui je n'aurais pas pu venir en Suisse pour ces études doctorales. Je voudrais dire toute ma reconnaissance à *Josiane* mon épouse, pour son soutien indéfectible et son attention particulière pendant ces années difficiles.

Je remercie tous mes amis et connaissances, un peu partout dans le monde, pour leur soutien et leurs encouragements constants. Que tous ceux qui, de près ou de loin, directement ou indirectement et de quelque manière que ce soit, ont contribué à la réussite de cette thèse, trouvent ici l'expression de ma profonde gratitude.

# Résumé

Le recours croissant aux énergies renouvelables est une des solutions clef aux problèmes environnementaux et de ressources liés à l’approvisionnement énergétique mondial. Du fait de la nature aléatoire et répartie de certaines de ces sources (solaires et éoliennes notamment), le stockage est indispensable à une utilisation efficace et économiquement viable de ces énergies. Le stockage d’énergie par air comprimé (sans adjonction de fuel) s’avère, de part ses nombreux avantages environnementaux, hautement compatible avec les énergies renouvelables; cependant ses performances énergétiques limitées constituent le principal obstacle à son utilisation. Ce travail de thèse vise à optimiser le stockage pneumatique afin de le rendre plus efficace, principalement pour les applications d’énergies renouvelables.

Le stockage pneumatique de l’énergie électrique requiert plusieurs étapes de conversion passant par une forme mécanique intermédiaire. La conversion pneumatique-mécanique est donc d’abord étudiée. La suppression de la régulation de pression est proposée afin éviter les pertes d’énergie liées à cette opération. En conséquence, la machine volumétrique fonctionne à pression variable et plus élevée. L’analyse de la caractéristique de rendement de ces machines montre l’existence d’une vitesse optimale qui correspond au rendement maximum et qui dépend de la pression. Une stratégie d’optimisation en temps réel du rendement, basée sur le fonctionnement à vitesse variable commandée par le rendement, est proposée. Les résultats expérimentaux confirment l’efficacité de cette stratégie aussi bien avec les machines pneumatiques qu’avec les machines hydrauliques. Les machines hydrauliques offrent en effet de meilleurs rendements de conversion comparativement aux machines pneumatiques, leur utilisation requiert cependant un interfaçage air-huile dont la réalisation a conduit aux deux systèmes de stockage hydropneumatique présentés. Le fonctionnement à vitesse variable proposé, a permis d’améliorer le rendement de cycle du système de conversion hydropneumatique expérimental d’environ 4% comparé à celui d’un fonctionnement à vitesse constante.

## Résumé

Afin de garantir la qualité et la flexibilité de puissance du système de stockage, une topologie hybride qui associe le stockeur hydropneumatique principal à un stockeur auxiliaire à supercondensateurs, est proposée. La stratégie de variation de la puissance de sortie est basée sur un fonctionnement intermittent du stockeur principal; le stockeur auxiliaire est alors utilisé pour lisser la puissance résultante à travers la régulation de la tension du bus continu commun. La flexibilité de puissance ainsi obtenue rend le système de stockage compatible avec une large gamme de puissances de charge et de source.

L'analyse du rendement montre que les performances du stockeur auxiliaire ont un grand impact sur celles du système global. Le stockeur auxiliaire doit donc avoir un rendement très élevé pour obtenir un rendement global acceptable. Une méthode formelle de dimensionnement du banc de supercondensateurs, qui permet de respecter à la fois les contraintes d'énergie et de tension tout en minimisant les coûts, est présentée. Une stratégie de contrôle du convertisseur DC-DC multicanaux d'interfaçage du banc, qui permet d'optimiser son rendement à charge partielle, est aussi proposée. Elle est basée sur la variation dynamique du nombre de canaux actifs, commandée par la puissance.

Plusieurs autres topologies du système de stockage hybride sont proposées, qui permettent de mieux répondre aux exigences particulières de chaque application tout en optimisant les performances et le coût. Une évaluation comparative de coût du stockage est également effectuée, dans le contexte d'une application photovoltaïque autonome. Elle montre qu'en plus de ses nombreux avantages environnementaux, le stockage hydropneumatique est économiquement plus viable que le stockage par batterie au plomb.

**Mots clef:** Energies renouvelables, Stockage d'énergie, Hydropneumatique, Supercondensateurs, Rendement maximal, Flexibilité de puissance.

# Abstract

An increasing recourse to renewable energies is one of the key solutions to address the current resource and environmental concerns related to the world energy supply. Because of the distributed and intermittent nature of several of them (Solar, Wind), an efficient and economically viable exploitation of renewable energies relies on the use of energy storage means. Fuel-free compressed air energy storage technologies are highly compatible with renewable energies because of their inherent environmental advantages. However their low energy performances have been the main barrier to their widespread utilization. Pneumatic storage is considered in this thesis with the goal of improving its energetic and power performances so as to make it more efficient and suited for renewable sources support.

Storing/generating electrical energy into/from compressed air requires a multiple-step conversion process through an intermediary mechanical energy. Pneumatic-to-mechanical energy conversion is studied first. The suppression of the pressure regulation is proposed to avoid the important energy losses related to this operation. Consequently the volumetric machine must operate at higher and variable pressure. The analysis of the efficiency characteristics of these machines shows the existence of a pressure dependent optimal speed that corresponds to the maximum efficiency. A Maximum Efficiency Point Tracking (MEPT) strategy, based on efficiency-controlled variable speed operation, is proposed for the real time optimization of the conversion efficiency. Experimental results confirm the effectiveness of the proposed strategy both with air machines and oil-hydraulic machines. Oil-hydraulic machines offer higher conversion efficiencies compared to air machines, but require an air-to-oil interface. Two possible ways of realizing such an interface have led to the two hydro-pneumatic storage systems presented. The proposed efficiency-controlled variable speed operation has allowed improving the cycle efficiency of the experimental hydro-pneumatic conversion system by about 4% compared to that of a constant speed operation.

## *Abstract*

In order to provide good power quality and flexibility to these storage systems, a hybrid topology that associates the main, hydro-pneumatic storage subsystem with an auxiliary, supercapacitive storage subsystem is proposed. The power variation is achieved by an intermittent operation of the main storage subsystem and the use of the auxiliary storage subsystem to smooth the resulting power, through the regulation of the common DC bus voltage. The hybrid storage system is thus compatible with a wide range of load and source powers, thanks to the obtained power flexibility.

An efficiency analysis shows that the performances of the auxiliary storage greatly affect that of the global storage system. The auxiliary storage should therefore exhibit very high conversion efficiencies so that an acceptable overall efficiency can be expected. A formal method for optimally sizing the supercapacitive auxiliary storage system is proposed, that allows meeting both the voltage and energy requirements while minimizing the cost. A control strategy to optimize the standby efficiency of the interfacing multi-phase DC-DC converter is also proposed, which is based on “power-controlled variation of the number of active phases”.

Many other application-dependent topologies for the hybrid storage systems are proposed, that help meeting each application’s particular requirements while optimizing its performances and cost. A comparative cost evaluation, realized in the context of a stand-alone photovoltaic home application, shows that in addition to its inherent environmental advantages, hydro-pneumatic storage is cost-effective compared to lead acid battery storage.

**Key words:** Renewable energies, Energy storage, Hydro-pneumatics, Supercapacitors, Maximum efficiency, Power flexibility.



# Contents

<b>Remerciements</b>	<b>i</b>
<b>Résumé</b>	<b>iii</b>
<b>Abstract</b>	<b>v</b>
<b>Notations</b>	<b>xiii</b>
<b>1. Introduction</b>	<b>1</b>
1.1. Energy storage and the challenging energetic context . . . . .	1
1.2. Problematic of the thesis . . . . .	3
1.3. Outline of the report . . . . .	6
<b>2. Generalities on Compressed Air Energy Storage</b>	<b>9</b>
2.1. Brief history of the use of compressed air as "energy carrier" .	9
2.2. Overview of the present compressed air-based storage technologies and their developments . . . . .	11
2.2.1. Classical CAES systems . . . . .	11
2.2.2. Hybrid compressed air and thermal storage systems . .	13
2.2.2.1. Advanced adiabatic - compressed air energy storage (AA-CAES) . . . . .	14
2.2.2.2. Uncooled compressed air energy storage . . . .	15
2.2.2.3. Hybrid thermal and compressed air energy storage (TACAS) . . . . .	16
2.2.3. Purely pneumatic storage systems . . . . .	17
2.2.3.1. Pneumatic storage systems with pneumatic conversion . . . . .	17
2.2.3.2. Pneumatic storage systems with hydro-pneumatic conversion . . . . .	19
2.3. Principle of pneumatic energy storage . . . . .	20

Contents

- 2.3.1. Description of the pneumatic energy storage cycle . . . 20
- 2.3.2. Thermodynamic analysis of the process of pneumatic storage . . . . . 24
  - 2.3.2.1. Pneumatic Joule cycle . . . . . 24
  - 2.3.2.2. Pneumatic Otto cycle . . . . . 29
  - 2.3.2.3. Open gas cycle . . . . . 31
- 2.3.3. Main energy characteristics of pneumatic energy storage 33
  - 2.3.3.1. Actual storage media in pneumatic energy storage . . . . . 33
  - 2.3.3.2. Energy density of closed gas cycle pneumatic storage systems . . . . . 36
  - 2.3.3.3. Energy density of closed gas cycle hydro-pneumatic storage systems . . . . . 41
  - 2.3.3.4. Energy density of open gas cycle pneumatic storage systems . . . . . 44
- 2.4. Chapter summary . . . . . 46

**3. Investigation and Optimization of Pneumatic-to-Mechanical Energy Conversion 49**

- 3.1. Investigation and Optimization of purely pneumatic conversion units . . . . . 50
  - 3.1.1. Suppression of the pressure control valve . . . . . 51
  - 3.1.2. Analytical model for the volumetric air motor . . . . . 53
    - 3.1.2.1. Constant pressure model . . . . . 54
    - 3.1.2.2. Variable pressure model . . . . . 55
  - 3.1.3. Evaluation of the pneumatic-to-mechanical conversion efficiency . . . . . 58
  - 3.1.4. Strategy for maximum efficiency . . . . . 61
    - 3.1.4.1. Principle of maximum efficiency point tracking (MEPT) . . . . . 61
    - 3.1.4.2. Simulation results of the MEPT strategy . . . 64
  - 3.1.5. Extension of the MEPT principle to power-controlled operating modes . . . . . 67
    - 3.1.5.1. Maximum power point tracking (MPPT) operating mode . . . . . 67
    - 3.1.5.2. Variable power-controlled operating mode . . . 71

3.2. Investigation and optimization of hydro-pneumatic conversion systems . . . . .	74
3.2.1. Investigation and optimization of the hydro-pneumatic conversion for BOP-A . . . . .	76
3.2.1.1. Principle of BOP-A: A close gas cycle hydro-pneumatic storage system . . . . .	76
3.2.1.2. Principle of MEPT strategy applied to hydro-pneumatic conversion . . . . .	78
3.2.1.3. Modeling the closed gas cycle hydro-pneumatic storage process . . . . .	78
3.2.1.4. Simulation results of MEPT strategy applied to hydro-pneumatic conversion . . . . .	87
3.2.1.5. Limitations of BOP-A . . . . .	88
3.2.2. Principle of BOP-B: An open gas cycle hydro-pneumatic storage system . . . . .	89
3.3. Chapter summary . . . . .	91
<b>4. Principle of Hybrid Energy Storage Systems based on Pneumatics and Supercapacitors . . . . .</b>	<b>93</b>
4.1. Concept of hybrid compressed air and supercapacitor energy storage (CASCEs) . . . . .	94
4.1.1. Principle of hybrid CASCEs system . . . . .	94
4.1.2. Strategy for output power variation . . . . .	95
4.1.2.1. Principle of power variation . . . . .	95
4.1.2.2. Fixed-frequency power modulation mode . . . . .	96
4.1.2.3. Free-oscillating power modulation mode . . . . .	99
4.1.3. Principle of hybrid energy storage system based on hydro-pneumatics and supercapacitors . . . . .	99
4.2. Evaluation and analysis of the cycle efficiency for the global hybrid storage system . . . . .	102
4.2.1. Expression of the overall system cycle efficiency . . . . .	102
4.2.2. Analysis of the global system efficiency . . . . .	106
4.3. Possible layouts of the hybrid hydro-pneumatic and supercapacitor storage system . . . . .	109
4.3.1. Layout A . . . . .	109
4.3.2. Layout B . . . . .	110
4.3.3. Layout C . . . . .	112

4.3.4.	Layout D . . . . .	113
4.3.5.	Layout E . . . . .	115
4.3.6.	Layout F . . . . .	116
4.3.7.	Layouts comparison . . . . .	117
4.4.	Chapter summary . . . . .	121
<b>5.</b>	<b>Design and Optimization of the Supercapacitive Auxiliary Storage Subsystem</b>	<b>123</b>
5.1.	Description of the auxiliary storage subsystem . . . . .	123
5.2.	Design and optimization of the supercapacitor bank . . . . .	125
5.2.1.	Modeling the supercapacitors bank . . . . .	125
5.2.1.1.	Supercapacitor Cell . . . . .	125
5.2.1.2.	Supercapacitor bank . . . . .	125
5.2.1.3.	Cell voltage balance . . . . .	127
5.2.2.	Sizing of the supercapacitor bank . . . . .	128
5.2.2.1.	Determination of the number of supercapacitors	128
5.2.2.2.	Implications of the dissymmetric topology for the voltage balancing system . . . . .	131
5.2.2.3.	Determination of the useful energy . . . . .	131
5.2.3.	Evaluation and analysis of the supercapacitor bank's efficiency . . . . .	132
5.2.3.1.	Charge-discharge cycle's efficiency evaluation .	132
5.2.3.2.	Analysis of the charge-discharge cycle's efficiency . . . . .	135
5.3.	Design and optimization of the DC-DC converter . . . . .	137
5.3.1.	Analysis of possible topologies and design parameters .	137
5.3.1.1.	Converter's topology . . . . .	137
5.3.1.2.	Phase inductance value . . . . .	141
5.3.1.3.	Switching Frequency . . . . .	146
5.3.2.	Evaluation and optimization of the Converter's efficiency	147
5.3.2.1.	Efficiency evaluation . . . . .	149
5.3.2.2.	Standby operation's efficiency improvement: Principle of "Power-controlled variation of the number of active phases" . . . . .	160
5.4.	Overall efficiency of the auxiliary storage subsystem . . . . .	168
5.5.	Chapter summary . . . . .	170

<b>6. Implementation and Experimental results</b>	<b>173</b>
6.1. Pneumatic conversion system . . . . .	173
6.1.1. Description of the test bench . . . . .	173
6.1.2. Implementation and results of the MEPT strategy . . .	174
6.2. Hybrid hydro-pneumatic and supercapacitors storage system .	178
6.2.1. Description of the test setup . . . . .	178
6.2.1.1. System design . . . . .	178
6.2.1.2. System control . . . . .	181
6.2.2. Implementation and results of the MEPT strategy . . .	183
6.2.2.1. Implementation of the MEPT strategy . . . .	183
6.2.2.2. Experimental results of the MEPT strategy . .	185
6.2.3. Implementation and results of the power variation strategy	189
6.2.3.1. Implementation . . . . .	189
6.2.3.2. Experimental results . . . . .	190
6.2.4. Partial and overall system efficiencies measurement . . .	190
6.2.4.1. Main storage subsystem's cycle efficiency . . .	190
6.2.4.2. Auxiliary storage subsystem's round trip effi-	
ciency measurement . . . . .	197
6.2.4.3. Overall system's round trip efficiency evaluation	200
6.3. Chapter summary . . . . .	201
<b>7. Considerations on Cost, Duty Cycles and Impacts on the Environ-</b>	<b>205</b>
<b>ment</b>	
7.1. Economical considerations: Comparative cost evaluation . . . .	205
7.1.1. Specifications of the studied case . . . . .	205
7.1.2. Layouts of the storage technologies . . . . .	207
7.1.3. Cost evaluation and comparison . . . . .	208
7.2. Considerations on duty cycles . . . . .	209
7.2.1. Service lifetime of storage units . . . . .	210
7.2.1.1. Hydraulic accumulators and high pressure vessels	210
7.2.1.2. Supercapacitors . . . . .	210
7.2.2. Service lifetime of conversion units . . . . .	210
7.2.2.1. Rotating machines . . . . .	211
7.2.2.2. Power electronic converters . . . . .	211
7.2.3. Overall system service lifetime . . . . .	211
7.3. Environmental issues . . . . .	211

*Contents*

<b>8. Conclusion</b>	<b>215</b>
8.1. Contribution and discussion . . . . .	215
8.2. Future work . . . . .	217
<b>A. Control of the PM Synchronous Machine</b>	<b>219</b>
A.1. Principle of Field Oriented Control (FOC) for PMS machine .	219
A.2. Space vector definition and projection . . . . .	220
A.3. Space vector Pulse Width Modulation (SV-PWM) . . . . .	223
<b>Curriculum Vitae</b>	<b>245</b>

# Notations

## Abbreviations

<i>AA</i>	Advanced adiabatic
<i>BOP</i>	Battery with Oil-Hydraulic and Pneumatics
<i>CR</i>	Compression Ratio
<i>CAES</i>	Compression Air Energy Storage
<i>DC</i>	Direct Current
<i>DOD</i>	Depth of discharge
<i>DSP</i>	Digital Signal Processing
<i>EPF</i>	Ecole Polytechnique Fédérale
<i>EPFL</i>	Ecole Polytechnique Fédérale de Lausanne
<i>FPGA</i>	Field Programmable Gate Area
<i>IEA</i>	International Energy Agency
<i>LEI</i>	Laboratoire d'Electronique Industrielle
<i>LCA</i>	Life Cycle Analysis
<i>MEPT</i>	Maximum Efficiency Point Tracking
<i>MPPT</i>	Maximum Power Point Tracking
<i>PR</i>	Pressure Ratio
<i>PHS</i>	Pumped Hydro Storage
<i>PUF</i>	Pressure Utilization Factor
<i>PV</i>	Pressure-Volume, Photovoltaic
<i>TACAS</i>	Thermal And Compressed Air Storage
<i>TSU</i>	Thermal Storage Unit
<i>UPS</i>	Uninterrupted Power Supply

## Roman Symbols

## Notations

$A$	Effective area	$m^2$
$a, A_o$	Constant of the BWR equation of state	
$b, B_o$	Constant of the BWR equation of state	
$c, C_o$	Constant of the BWR equation of state	
$c...$	Interpolation constants	
$c_p$	Constant pressure specific heat	$J/(K.kg)$
$c_v$	Constant volume specific heat	$J/(K.kg)$
$Cyl$	Displacement	$m^3/rev$
$d$	voltage ratio	
$D$	Duty cycle ratio	—
$E$	Exergy	$J$
$f...$	Correction functions	
$g$	Gravitational acceleration	$m/s^2$
$h$	Overall convective heat transfer coefficient	$W/(m^2.K)$
$h$	Enthalpy per unit mass	$J/kg$
$I$	Current	$A$
$J$	Current density	$A/m^2$
$K$	Squareness	
$k...$	Interpolation constants	
$k_m$	Motor torque constant	$Nm/A$
$L$	Length	$m$
$L$	Inductance	$H$
$m$	Mass	$kg$
$\dot{m}$	Mass flow rate	$kg/s$
$M$	Mechanical torque	$Nm$
$n$	Polytropic exponent	
$N$	Rotational speed	$rpm$
$N_1...N_9$	Constants of the ideal gas specific heat equation	
$p$	Absolute pressure (used in bar)	$Pa$
$P$	Electrical power	$W$
$Q$	Heat	$J$
$\dot{Q}$	Heat flux	$J/s$
$\mathcal{R}$	Universal gas constant	$J/(K.kg)$
$R$	Ohmic resistance	$\Omega$
$s$	Entropy per unit mass	$J/(K.kg)$
$S$	Entropy	$J/K$



$t$	Time	$s$
$T$	Temperature or Time period	$K; s$
$u$	Internal energy per unit mass	$J/kg$
$U$	Internal energy	$J$
$U$	Voltage	$V$
$v$	specific volume	$m^3/kg$
$V$	Total volume	$m^3$
$\dot{V}$	Volumetric flow rate	$m^3/s; l/mn$
$W$	Energy, Work	$J$
$\dot{W}$	Mechanical power	$W$
$w$	Mass or volumetric specific energy	$J/kg, J/m^3$
$y$	$N_9/T$ , Variable of the BWR equation of state	

## Greek Symbols

$\alpha$	Constant of BWR equation of State	
$\alpha$	Normalized current ripple amplitude	
$\beta$	Energy factor or energy quotient	
$\gamma$	Ratio of specific heat: $c_p/c_v$	
$\gamma$	Constant of BWR equation of State	
$\delta$	elementary quantity of a physical variable	
$\Delta$	Variation	
$\eta$	Efficiency	—
$\rho$	Mass density	$kg/m^3$
$\tau$	Time constant	$s$
$\Theta$	Shift angle	$rad$

## Indices

0	Standard conditions, Stall
1	Initial state
2	Final state
$a$	Air, Ambient conditions

## Notations

<i>ac</i>	Accumulator
<i>act</i>	Active
<i>ai</i>	Ambient intermediary
<i>as</i>	Auxiliary storage
<i>atm</i>	Atmospheric conditions
<i>avg</i>	Average
<i>bb</i>	Buck/Boost converter
<i>c</i>	Critical
<i>cd</i>	Conduction
<i>C</i>	Charge
<i>cgc</i>	Closed gas cycle
<i>cv</i>	Converted
<i>D</i>	Discharge, diode
<i>dc</i>	Direct Current
<i>dd</i>	Dead
<i>dr</i>	Drive, Drive's converter
<i>e, el</i>	Electrical
<i>e</i>	Extra
<i>f</i>	Forward, Final
<i>e1w</i>	Effective 1 way
<i>fi</i>	Final intermediary
<i>fi</i>	Current fall
<i>fv</i>	Voltage fall
<i>g</i>	Gas or gas mixture
<i>G</i>	Gate
<i>gm</i>	generator/motor
<i>h, hd</i>	Hydraulic
<i>hc</i>	Hydraulic circuit
<i>i</i>	initial, inlet, intermediary, interpolated
<i>J</i>	Joule
<i>liq</i>	Liquid
<i>L, ld</i>	Load
<i>m</i>	Motor, Mechanical, Minimum
<i>min</i>	Minimum
<i>M</i>	Maximum
<i>max</i>	Maximum

<i>mc</i>	Mechanical
<i>ms</i>	Main storage
<i>mp</i>	Motor/pump
<i>O</i>	Otto
<i>o</i>	Outlet, output
<i>ogc</i>	open gas cycle
<i>op</i>	Open cycle polytropic
<i>opc</i>	Open cycle polytropic compression
<i>ope</i>	Open cycle polytropic expansion
<i>opt</i>	Optimal
<i>ov</i>	Open cycle volumetric
<i>ouv</i>	Open cycle unexploited volumetric
<i>oev</i>	Open cycle exploited volumetric
<i>p</i>	pump, parallel
<i>p, ph</i>	Phase
<i>pk</i>	Peak
<i>pre</i>	Pressure regulation energy
<i>pm</i>	Pneumatic-to-mechanical
<i>q</i>	Heat
<i>ref</i>	Reference value or condition
<i>ra</i>	Reversible adiabatic
<i>rac</i>	Reversible adiabatic compression
<i>rae</i>	Reversible adiabatic expansion
<i>ri</i>	Reversible isothermal
<i>ri</i>	Current rise
<i>ric</i>	Reversible isothermal compression
<i>rie</i>	Reversible isothermal expansion
<i>rms</i>	Root means square
<i>rp</i>	Reversible polytropic
<i>rpc</i>	Reversible polytropic compression
<i>rpe</i>	Reversible polytropic expansion
<i>rt</i>	Restored, Round trip
<i>rv</i>	Voltage rise
<i>s</i>	Series
<i>sc, scap</i>	Supercapacitor
<i>scm</i>	Supercapacitor minimum

## Notations

<i>scM</i>	Supercapacitor maximum
<i>scu</i>	Supercapacitor useful
<i>st</i>	Stored
<i>sT</i>	Series total
<i>sw, SW</i>	Switching
<i>T, tl, tot</i>	Total, overall
<i>TH</i>	High side transistor
<i>TL</i>	Low side transistor
<i>Tu</i>	Total per unit
<i>uwe</i>	Unused volumetric energy
<i>v</i>	Volumetric
<i>vhp</i>	Volumetric hydro-pneumatic
<i>vmx</i>	Maximum volumetric
<i>vol</i>	Volumetric
<i>w</i>	Wall

# 1. Introduction

## 1.1. Energy storage and the challenging energetic context

These last decades, the global energy supply system has been facing many problems that even lead to some important crisis, for many reasons:

1. The world energy demand is rising in line with the fast development of emerging countries like China and India, and the production is unable to follow and match this demand [1], [2].
2. The main world fossil fuel resources are concentrated in a limited set of countries and many of which are subject to instability [3]. In addition, while some expert's scenarios are optimistic about the future, some predict the shortage of hydrocarbons to occur probably by the end of this century; if the present energy technologies and policies remain unchanged, considering the known reserves [4], [5]. This situation creates stress on the energy market and increases the volatility of energy prices, which recently reached the highest level ever recorded.
3. The world ecosystem is becoming more and more unstable as the ineluctable climate changes and the increasing number of natural catastrophes show proof. The environmental experts agree that the rising of greenhouse gas emissions is the main cause of this phenomenon. According to the last IEA statistics, hydrocarbons-based energies which represent about 80% of the world energy, are responsible for more than 99% of these emissions [1], [6].

The electric power economy has been seriously affected by the fossil fuels problems for, it strongly relies on these energies, which represent actually more than 66% of its resources [1]. In addition, the recently engaged, worldwide processes of liberalization and deregulation of the electricity market mainly

intended to break monopolies and introduce competition in the field, has also induced more uncertainties and vulnerability in the system, because of the difficulties to share or allocate responsibilities among the different actors, and the technical limitations to implement classical free market rules to a difficult-to-store product like electrical energy: *the Kirchoff laws versus Free-market laws Conflict* [7] [8].

These energy problems and warnings have increased the concerns about the security, reliability and sustainability of the world energy supply system, such that policymakers as well as energy specialists have been proposing many strategies and solutions to improve the situation, with two main long-term objectives [9], [10], [11], [12], [13]:

1. **More efficient and environmentally harmless energy conversion, distribution and use:** This objective requires new energy policies and management, changes in social behaviors for a rational use of energy. The “2000W per capita society” initiative launched in the frame of Swiss EPFs proposes some guidelines for that purpose [14]. It also requires some technology breakthroughs, in the fossil fuels based industry to improve the conversion efficiency and reduce the greenhouse gas emissions, as well as in the end-users infrastructures and equipments to reduce the energy consumption and the  $CO_2$  emissions. Finally, this objective requires a more efficient and reliable electrical energy generation and transmission system: *Energy storage* is expected to play a key role to fulfil this last requirement. In fact, *Storage* can be used on the utility side to support generation through load leveling, peak shaving and energy management. It can be also used to strengthen the transmission and distribution system through voltage control, power quality, system stability and investments deferral. Finally on that side, *Storage* can support ancillary services through frequency regulation, spinning reserve, standby reserve and long term reserve. On the consumer’s side, *Storage* can help ensuring a high voltage quality and the supply availability and reliability [15], [16], [17].
2. **Increasing recourse to alternative energy sources, mainly renewable:** Renewable energy sources are known to be environmentally harmless, however they may exhibit large output power fluctuations in diurnal, monthly and even annual cycles. This stochastic availability associated to their distributed nature will enhance the implementation of

the *Distributed Generation* concept, which in turn will weaken the grid stability and control because of the loss of the effect of the “statistical mean value” of loads that normally smoothes their profile. Again, *Energy Storage* is the key solution to support this generation concept and to guarantee a reliable integration and an efficient and convenient use of renewable energies, by transforming the “*Take it when you can get it*” power into a scheduled power [18], [19], [20].

This thesis mainly deals with this second objective and aims at optimizing pneumatic energy storage, for the purpose of decentralized generation and renewable energy sources integration.

## 1.2. Problematic of the thesis

Renewable energies possess two main characteristics that make them ideal energy sources to address the resources and environmental issues just presented:

1. They are inexhaustible sources since they are renewable.
2. They are harmless to the environment because they produce no problematic waste material and possess a positive greenhouse gas balance when considering their entire life cycle.

However, many of these energies, particularly Wind and Solar energies which are the main concerns of this thesis, are seasons and weather dependant and therefore not always available when needed. Because of this fluctuating nature and random availability, storage technologies are necessary to adapt these renewable energies to the demand and so increase their economical value [16] [20]. However, particular attention must be paid when designing or choosing a storage solution for a given renewable source, to make sure that the limitations and disadvantages of that storage solution do not cancel the main advantages of the renewable source. In other words, important considerations must be made concerning the mid and long term characteristics of the considered storage technology particularly its life cycle and impacts on environment. It is the believe of our research unit that, the integration of renewable energies will be efficient, cost effective and sustainable only if the associated technologies exhibit comparative quality regarding those long term aspects. Hence, the

driving question to this thesis was to know which storage technology is suitable in a sustainable way to a given renewable energy source.

Actually, beside large scale storage solutions like pumped hydro which are mainly dedicated to utility applications; electrochemical technologies are the main candidates in relation with renewable sources support. Figure 1.1 presents the main characteristics of the main commercially available storage technologies. It can be seen that electrochemical batteries are far from fulfilling those mid and long term requirements mainly because of their limited life cycles and, on the environmental aspect, their difficulties to be recycled [21], [22]. They will probably remain the solution for some kind of portable applications, but the conviction of our institute is that, a sustainable support to renewable energy sources requires electrochemical-free storage solutions.

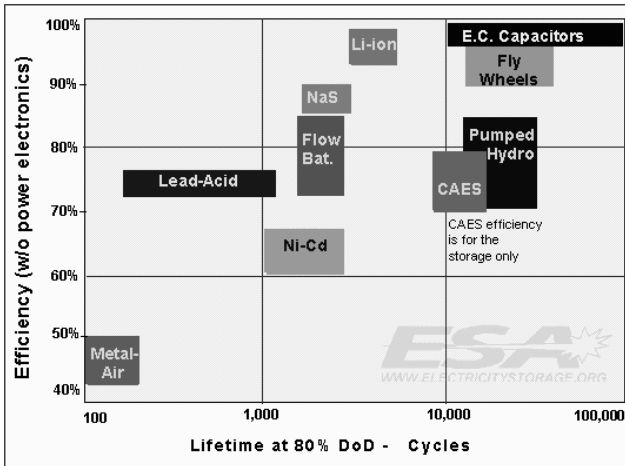


Figure 1.1.: Life Cycle and Efficiency of today's main storage technologies (Source: ESA)

Recently, many alternative storage technologies have appeared, and some are being integrated in real networks. Some are based on high energy fly-wheels and Superconducting Magnetic Energy Storage (SMES) as short term storage mainly for power quality applications [23], [24]; others on thermal en-



ergy storage in solar thermal applications [25], [26]. The idea of hydrogen energy storage has been explored too, with the promised but ever-so-distant reversible fuel-cell or association of fuel-cell and electrolyzer [27], [28]. Flow batteries based on Vanadium-Redox have been investigated also and some test-facilities realized [29], [30]. Some new Compressed Air Energy Storage (CAES) systems have been proposed, from large size facilities with underground storage to Sub-Surface CAES (SSCAES) systems with vessel or pipes storage [31], [32]. A hybrid Thermal And Compressed Air Storage (TACAS) is being evaluated too [33], [34]. Some small size Pneumatic storage systems have been also proposed, that use intermediary mechanical/hydraulic conversion with the so-called “liquid piston” principle [35], [36].

This thesis deals with compressed air technologies and aims at investigating the last concept of pneumatic or fuel-free compressed-air in vessel energy storage, which possesses many practical and long term advantages:

- Air, the “storage media” is available everywhere and does not need to be produced.
- Compressed air can be stored for long time in sealed tank without self-discharge.
- Pneumatic energy conversion is based on simple technologies with high life cycle, and produces no problematic waste and no greenhouse gas emissions, etc.

These advantages provided the pneumatic energy storage with high compatibility with renewable energy sources.

In fact, compressed air has been used as energy storage medium for longer date in the industry, mainly as an energy source for low power tools in hazardous areas [37], [38]. The basic technology for pneumatic energy conversion then exists in a mature industrial market context. However, this storage concept hasn’t known a widespread utilization in storage applications and particularly in the area of renewable energies because of its low conversion efficiency and the low energy density of compressed air.

The purpose of this research work is to improve the technical performances of pneumatic energy storage by addressing these efficiency and energy density

issues. This must be done keeping in mind the environmental and economical concerns, in order to make this technology more efficient and effective for decentralized generation and renewable energy sources support.

### 1.3. Outline of the report

The approach of the thesis is to build a synergy between the simple and mature pneumatic technology and the modern and “intelligent” power electronic and control technology, which appear as complementary to achieve that goal of an efficient, reliable and cost effective storage system. The simplicity and robustness of pneumatics can guarantee the reliability while the intelligence and flexibility of power electronics will allow reaching the objectives of optimal efficiency and flexible operation.

This report is organized in line with the progress of the thesis investigations: Firstly, the investigation and optimization of the operation of pneumatic energy conversion systems thanks to the means of power electronics; secondly the investigation and optimization of the power electronic systems used for that purpose, and finally the overall system performances evaluation.

In chapter 2, after a brief historical review of the use of compressed air energy, several types of compressed air-based energy storage technologies are presented, in order to clearly state the differences between the pneumatic concept studied in this thesis and the other technologies. Afterwards, the basic principles of pneumatic energy storage are studied in order to evaluate some important properties like the energy density and to assess the main technical problems related to this storage concept. The thermal phenomenon linked to gas compression or expansion are analyzed and its impacts on the energy performances of this storage technology are evaluated.

Storing or recovering electrical energy into or from compressed air requires an indirect conversion process with an intermediary mechanical form of energy. For such a multiple-step conversion in energy storage applications, the efficiency requirement for each conversion step is very high in order to achieve an acceptable overall efficiency.

In chapter 3, the Pneumatic-to-Mechanical energy conversion subsystem are investigated in order to optimize its efficiency. These investigations are mainly focus on volumetric machine technology, which is mostly used in pneumatic applications. The analysis of the efficiency characteristic of these machines shows the existence of an optimal pressure dependent operating point that corresponds to the maximum efficiency. An efficiency optimization strategy are proposed to control the machine's operation through the power electronics means, so as to always maintain it at that optimal operating point during the conversion process. The results of this strategy applied to a small air machine are presented and discussed.

Despite the proposed efficiency optimization strategy, the efficiency and pressure ratings of low power pneumatic machines remains unsatisfactory for energy storage applications, due to some mechanical and thermodynamic limitations [39]. Hydraulic machines appear as good conversion alternatives, even though they require an air-to-oil interface which is not always easy to realized. In the second part of this chapter, two hydro-pneumatic storage systems called *Batteries with Oil-hydraulics and Pneumatics (BOP)* [35], [36] are introduced and their conversion performances briefly discussed. The analysis of the efficiency characteristic of volumetric hydraulic machines shows a similar shape to that of volumetric air machines; therefore the efficiency optimization strategy mentioned above is also applied to hydraulic machines and some simulation results presented.

By imposing the speed of the volumetric machine, the efficiency optimization strategy proposed in chapter 3 imposes the level of the converted electrical power. This converted power may not match the load power and/or the source power all the time. A strategy for power flexibility is therefore necessary. This requirement has led to the hybrid storage system based on compressed air and Supercapacitors which is introduced in chapter 4. A control strategy for an efficient management of energy flow between the different subsystems is proposed and the results of which presented. Thereafter, the theoretical round-trip energy efficiency of the hybrid storage system is formally evaluated and commented. This evaluation shows the impact of the multiple-step energy conversion on the overall efficiency and confirms the necessity of optimizing both the efficiency of each unit and the topology of the hybrid storage system. This is illustrated by the other possible configurations of the hybrid system

that are proposed and commented.

The supercapacitive auxiliary storage subsystem is studied in chapter 5. Different configurations of the supercapacitive bank are investigated in order to formalize its optimal design and sizing for pneumatic storage applications. Different topologies and control procedures of the interfacing DC/DC converter are analyzed and compared, for a wide power range and different configurations of the Supercapacitors bank. This aims at easing the determination of the optimal supercapacitive auxiliary storage subsystem for a given application, on the basis of its energy, power and voltage requirements.

In chapter 6, some practical results recorded from the a small test-setup of a pure pneumatic storage system are presented and commented, as well as the results recorded from the prototype of a BOP-A system. These results allow evaluating the practical effectiveness of the proposed efficiency optimization and power flexibility strategies.

In chapter 7, other important characteristics of the hybrid storage system such as life cycle and impacts on the environment are roughly assessed and discussed. Some economical considerations also are made, through a prospective cost comparison of BOP systems and Lead acid batteries, for a day-to-night power shift in a stand alone photovoltaic home application.

## 2. Generalities on Compressed Air Energy Storage

Understanding the origin and evolution of the production and use of compressed air can shed light on the current interests in this storage technique and possibly open doors to future applications. This chapter will begin with a brief history of the industrial applications of compressed air. Then, an overview of the different types of today's storage technologies relying on compressed air will be made so that the pneumatic concepts investigated in the project would be easily identified among all those technologies.

Afterwards, the processes of compression and expansion of air will be reviewed in order to evaluate its energy characteristics. The unavoidable thermal phenomenon linked with these processes and the way it influences these characteristics will be analyzed. This study will show that the isothermal storage cycle targeted in this project is the most efficient and economical way of using compressed air for energy storage.

### 2.1. Brief history of the use of compressed air as "energy carrier"

Compressed air has evolved from its natural primitive origins into a highly technical source of energy. The first air compressor was human lungs used by primitive people to blow on cinders to create a fire. As people began to melt metals such as gold, copper, tin and lead, higher temperatures were needed, and a more powerful compressor was required. Egyptian and Sumerian metallurgists used the wind, then blowpipes for their work. The first mechanical compressor, the hand-operated bellows, emerged soon after, and in 1500 B.C. the more efficient foot bellows came into use. Bellows driven by foot or by water wheel proved a reliable compressor for more than 2,000 years, until in-

ventor John Wilkinson introduced an efficient blasting machine in England in 1776; the machine was an early prototype for all mechanical compressors [40].

The idea of using compressed air to transmit energy became popular around 1800 as metal manufacturing plants grew and emphasized the limited power of steam. The most relevant application was in propulsion and for half a century the air-powered locomotive was a serious contender for the top spot in transportation because of its obvious advantages: *simplicity, safety, economy, and cleanliness*. Air engines were commercially available and used routinely, first as metropolitan street transit, for instance the famous “Mékarski Compressed air Trams” in France in the years 1880s [41], [42] and later for haulage in mines and for pneumatic rock drill in rail tunnel construction [40]. Some trials were given in the field of aviation in 1879 by the French Professor Victor TATIN with a compressed air powered aeroplane [43].

The term “air engine” disappeared from engineering textbooks after the 1930s and the second world war. Internal Combustion Engines (ICE) had been perfected, the oil industry was established, and gasoline was cheap. Serious interest in air cars was rekindled by the energy glitches of the 1970s. Dozens of inventors have patented designs for hybrid, closed cycle, and self-fueling air cars, as well as conversions for existing engines and designs for air cars meant to stop at air stations for refueling. Some actors of the Modern Air Car Movement are: The American inventor Terry Miller with his spring-powered car [44], the French inventor Guy Negre with his compressed air car [45], the British inventor C. J. Marquand with his heat-pipe air car engine designed to recover compression heat [44], and Prof. Tsu-Chin Tsao of mechanical and aerospace engineering at the UCLA Henry Samueli School of Engineering and Applied Science, with his Hybrid Air Engine [46].

The first investigations for the utilization of Compressed air for energy storage in electric power generation can trace its roots to the 1960s, during the early evaluation of gas turbine technology for power production [47]. *Compressed Air Energy Storage (CAES)* gained additional support during the 1970s to provide load-leveling and peak-power support because of its promising fuel efficiency and response capabilities compared to early natural gas turbines. The first commercial unit (which is still in operation) was developed in Germany in 1978, followed by another one in the United States in 1991. A number of follow-

up projects were investigated around the world, but none came to fruition yet. Recently, two other families of compressed air-based storage technology are being developed, which unlike the conventional CAES, are essentially smaller, stand-alone and fuel-free. The first one is mainly characterized by the storage of the compression heat, either in a separated thermal storage unit like in the case of the Advanced Adiabatic Compressed Air Energy Storage (AA-CAES) system, or in the high-pressure vessel together with the compressed air; this is the case of the Uncooled Compressed Air Storage. The second family tries to implement isothermal processes by exporting (and latter importing) the compression heat to the surroundings through various heat exchange techniques. This is the case of the pneumatic storage system investigated in this work.

These different modern compressed-air-based storage systems for power generation will be briefly described in Section 2.2 in order to get a clearer idea and to better define the object of this thesis.

## **2.2. Overview of the present compressed air-based storage technologies and their developments**

### **2.2.1. Classical CAES systems**

Classical CAES systems are with Pumped Hydro Storage (PHS) the only storage technologies in commercial operation, able to provide large-scale deliverability (50 to 300MW) for the use in the whole sale market [47]. The principle of CAES derives from the splitting of the normal gas turbine cycle - where roughly 66% of the produced power is used to compress air - into two separated phases: The compression phase where lower-cost energy from off-peak base-load facilities is used to compress air into underground salt caverns and the generation phase where the pre-compressed air from the storage cavern is preheated through a heat recuperator, then mixed with oil or gas and burned to feed a multistage expander turbine to produce electricity during peak demand. This functional separation of the compression cycle from the combustion cycle allows a CAES plant to generate three times more energy with the same quantity of fuel compared to simple cycle natural gas power plant. The schematic

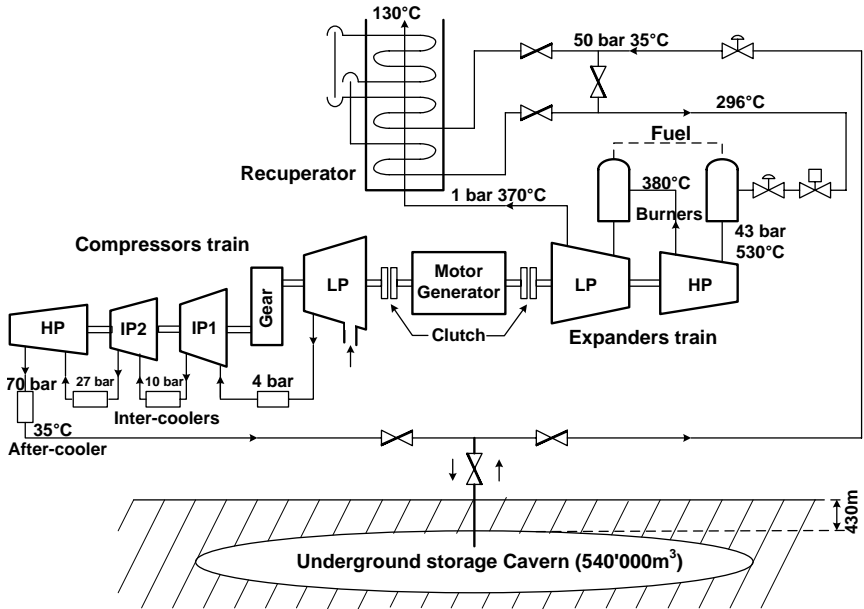


Figure 2.1.: Principle of CAES system: Schematic of the McIntosh plant in Alabama, USA (From Compressed Air Magazine, September 1990)

diagram of a modern CAES facility is presented in Figure 2.1. It consists of five major above-ground components [48], [49], [50]:

1. The motor/generator which employs dual clutches to provide for the alternate engagement of the compressor or turbine trains.
2. The air compressor which may require two or more stages, inter-coolers and after-coolers to achieve efficient compression and reduce the moisture content.
3. The recuperator, turbine train, high and low pressure turbines.
4. The equipment control center for operating the combustion turbine, compressor and auxiliaries, and to regulate and control changeover from generation mode to storage mode.



5. The Balance-of-plant auxiliary equipment consisting of fuel supply, mechanical, electrical, piping and cooling systems.

CAES has the advantages that it doesn't involve huge, costly installations and can be used to store energy for a long time (more than one year). It also has a fast start-up time (9 to 12mn) which makes it suitable for grid operation, and the emissions of greenhouse gases are lower than that of a normal gas power plant, due to the reduced fuel consumption.

The main drawback of CAES is probably the geological structure reliance, which substantially limits the usability of this storage method. In addition, CAES power plants are not emission-free, as the pre-compressed air is heated up with a fossil fuel burner before expansion. Moreover, they are limited with respect to their effectiveness because of the loss of the compression heat through the inter-coolers, which must be compensated during expansion by fuel burning. The fact that conventional CAES still rely on fossil fuel consumption makes it difficult to evaluate its energy round-trip efficiency and to compare it to conventional fuel-free storage technologies. It is likely a more economical way of producing electricity from gas than a pure storage technique as usually understood.

To circumvent the difficulties of large size and limited number of appropriate geological sites of classical CAES, the idea of *Sub-Surface Compressed Air Energy Storage (SSCAES)*, where the natural underground storage is replaced by a sub-surface man-made storage, has been investigated [51]. Unlike CAES, SSCAES will range from 5MW to 20MW and will store compressed air in buried pipes so that the layout can vary. Within that range, SSCAES can use low firing temperature, low cost turbo-expanders and can efficiently use landfill gas as well as coal bed methane gas and natural gas. No commercial project has come to fruition yet.

### 2.2.2. Hybrid compressed air and thermal storage systems

In order to avoid the emissions and fuel dependence of classical CAES, alternative, fuel-free, compressed-air-based storage systems have been investigated, with the main idea of storing the heat generated during compression and later use it to reheat the high pressure air before expansion [52]. In this concept of *unfired* or *adiabatic* CAES, there are many possible ways of storing the

necessary expansion-heat that have led to the different hybrid thermal and compressed air storage systems presented in the next paragraphs.

### 2.2.2.1. Advanced adiabatic - compressed air energy storage (AA-CAES)

The AA-CAES concept has been implemented in the frame of an ongoing European project aims at enhancing the classical CAES so as to develop a pure or non-hybrid storage system based on compressed air. This implies that the heat needed for the expansion process is recovered from the compression and stored in a Thermal Energy Storage (TES) unit for the time interval of the charge-discharge cycle. The simplest arrangement of a AA-CAES power plant is depicted in Figure 2.2.

During charging, the compressed air must be cooled to the cavern inlet

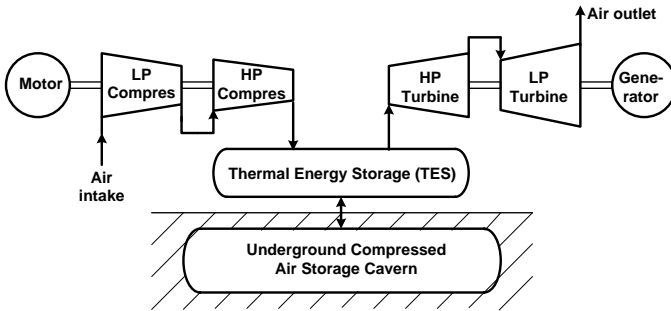


Figure 2.2.: One-stage arrangement of a AA-CAES system (Source: Alstom Power)

temperature which is about  $50^{\circ}C$  for salt caverns. During discharge, the compressed air is heated up to almost the compressor outlet temperature at high heat extraction rates. To reach high pressure with reasonable temperature, the compression and heat storage systems can be divided into two or more stages. In that case, cavern pressure of 160 bars can be reached with compressor output temperature of about  $450^{\circ}C$  [53], [54], [55].

The AA-CAES technology can benefit from higher efficiency and notably zero  $CO_2$  emission compared to classical CAES. However, several technical

difficulties still have to be tackled for an effective and economical realization of this technology: Besides the constraining operating conditions, the broad operating range of the compressor turbo machinery and the sliding-pressure turbine, the Thermal Energy Storage (TES) with its ambitious specifications seems to be the greatest challenge. It would be the main limiting factor regarding the efficiency and storage time of this storage system.

### 2.2.2.2. Uncooled compressed air energy storage

To avoid the difficulty of realizing a cheap and high performance thermal storage unit needed in the other hybrid thermal and compressed air storage systems, a system where the compression heat is stored together with the compressed air in an isolated vessel has been investigated at the Technical University of Clausthal-Germany [56], [57]. The principle of such a system is shown in Figure 2.3.

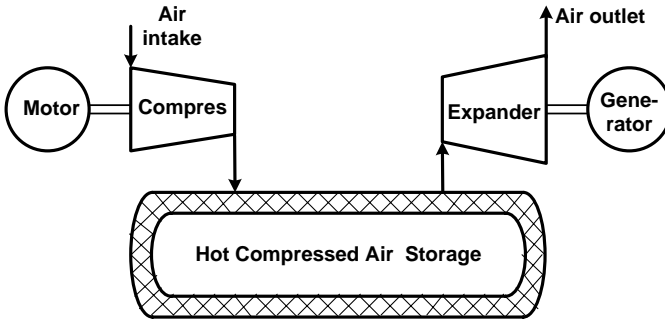


Figure 2.3.: Schematic diagram of the uncooled compressed air storage system

If the system was to really achieve adiabatic processes, the thermodynamic energy efficiency would be 100%. The unavoidable heat-losses due to the non-ideal insulation of the storage vessel limit the storage time; hence, this technology would be mainly dedicated to bridging or short-time storage applications. In addition, to handle the wide temperature variation range related to the adiabatic processes, the system requires costly air motors and compressors with

particular design. The pressure range must also remain very low to limit the maximum temperature.

### 2.2.2.3. Hybrid thermal and compressed air energy storage (TACAS)

The Thermal and Compressed Air Storage (TACAS) is essentially a stand-alone and smaller version of classical CAES, with the main following differences which can be seen on the principle diagram of figure 2.4:

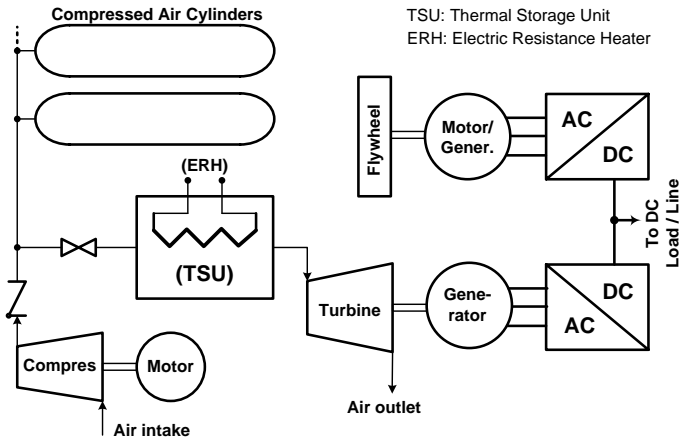


Figure 2.4.: Principle of the hybrid thermal and compressed air storage system (Source: Active Power, Inc.)

- The TACAS system uses conventional high pressure cylinders to store the compressed air, so it can be more easily located on-site at a commercial or industrial facility.
- The needed expansion heat is provided by a steel Thermal Storage Unit (TSU). The TSU is brought to full operating temperature by industrial electric heating resistances, fed with part of the low-cost utility power to be stored. Thus, unlike classical CAES, the TACAS is fuel-free and therefore generates no  $CO_2$  emissions.

- The TACAS system uses a low-cost flywheel to maintain power quality and to provide a few seconds of bridging power during the operation of the system.

Like the previous hybrid thermal and Compressed air storage, the TACAS system is mainly dedicated to short-time storage applications. It was designed to replace battery cabinets in standard Uninterrupted Power Supplies (UPS) systems. Its power ranges are between 40 and 85kW with the extended run times of about 15mn [47], [33].

The hybrid storage systems just presented try to take advantage of the high energy efficiency of adiabatic processes by storing the compression heat and later using it for expansion. But the adiabatic cycle is practically unfeasible because of the limited performances of the thermal storage unit. In addition, these systems require in some cases expensive dedicated machinery designed to handle the high temperatures involved. The storage systems presented in the following sections try to circumvent these difficulties.

### 2.2.3. Purely pneumatic storage systems

Basic thermodynamics proves that energetically speaking, an isothermal cycle is equivalent to an adiabatic one. The isothermal cycle at the atmospheric temperature would have the advantage of needing no thermal storage unit, and therefore having no standby losses and storage time limitation. It will nevertheless need perfect heat-exchangers to achieve constant temperature compression and expansion. This is the basic concept of the Pneumatic storage systems briefly presented in the following paragraphs.

#### 2.2.3.1. Pneumatic storage systems with pneumatic conversion

Pneumatic conversion was the first conversion system used to exploit compressed air for the purpose energy transmission. It consists, for low and medium power ranges or high compression ratio as considered in this project, in using mainly positive displacement (or volumetric) air machines to produce compressed air and later withdraw energy from it. In these machines, the variations of the working fluid's volume in a working chamber produce equivalent displacements of the mechanical member, transmitting thus the energy

and vice versa. The dynamic effect of the fluid is therefore of minor importance, unlike in kinetic (or turbo) machines where the kinetic energy of the working fluid is transformed into mechanical motion and vice versa. There are two main families of volumetric machines: *Rotary machines* for instance lobes, vane, and screw machines, and *reciprocating machines* like diaphragm and piston machines. In the aforementioned range, the piston type is commonly used because of its high efficiency and pressure ratio. The principle of such a conversion system is shown in Figure 2.5.

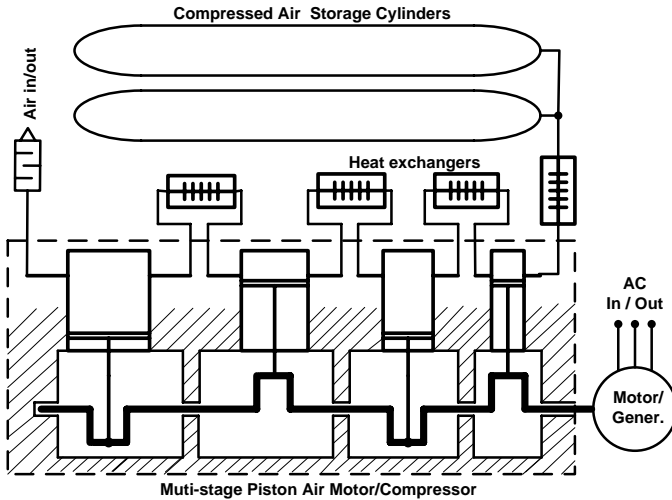


Figure 2.5.: Schematic diagram of a Pneumatic storage with volumetric air conversion system

The Compressed air energy is converted into mechanical energy and vice versa in the compression/expansion chambers. Since it is difficult to achieve an isothermal process in these chambers, the compression/expansion process is subdivided into several stages and heat exchangers are inserted in between as it can be seen on Figure 2.5. Thus the complete cycle is close to an isothermal cycle depending on the performance of the heat exchangers. This principle is as old as the first application of compressed air in propulsion as mentioned in section 2.1, and it is gaining more interest and improvements nowadays with

the new developments in compressed-air-powered cars [45], [58].

### 2.2.3.2. Pneumatic storage systems with hydro-pneumatic conversion

The pressure ratings and conversion efficiency of pure pneumatic conversion system remains low because of the difficulties to implement good heat exchange in the compression/expansion chambers and the important leakage and friction due to the gaseous nature of air. The use of oil-hydraulic machines to circumvent these difficulties has been investigated, as they suffer less from the above problems and therefore exhibit very high conversion efficiencies. The main challenge in using this kind of machine is the oil-to-air interface. Two different ways of interfacing the two fluids in almost isothermal processes are possible and have led to the two hydro-pneumatic storage systems whose principles are depicted in Figure 2.6, and described in [35] and [36] under the acronym “BOP” which stands for *Batteries with Oil-hydraulics and Pneumatics*.

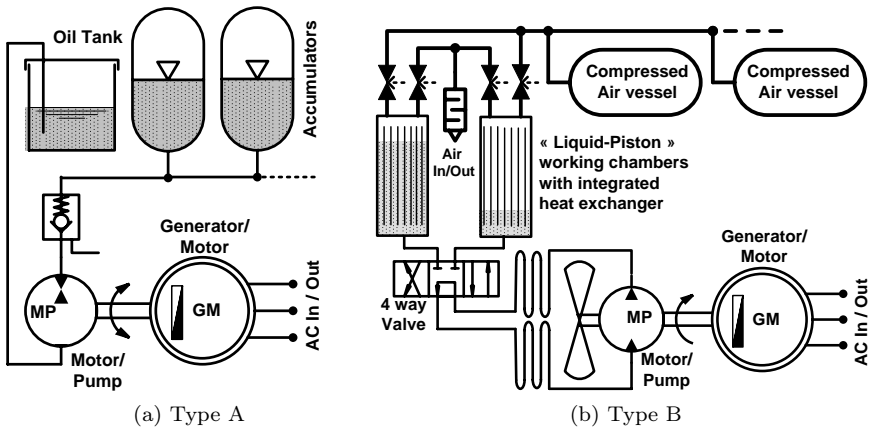


Figure 2.6.: Schematic diagram of a pneumatic storage systems with oil-hydraulic conversion

The first system, *Type A*, is simply an extension of the well-known industrial hydro-pneumatic accumulators to large storage capacity applications. In these devices, there is a physical separation between air and oil, that can be a piston, a bladder or a membrane depending on the type of accumulator. The

isothermal process is achieved by optimizing the “volumetric time constant”<sup>1</sup> of the accumulator. The main drawback of Type A system is its low energy density due to the fixed amount of gas and the outside reservoir needed to store the compressing oil at the discharge state.

The second system, *Type B*, is better in that respect, since it uses a substantially reduced amount of oil working in a closed circuit to compressed fresh air from outside. However, it requires an oil-to-air interface which is based on the “Liquid - Piston” principle and is difficult to realize. These systems will be studied more in details later in this dissertation.

Of all the compressed air-based storage systems presented above, pneumatic-only systems are those who are, regarding the storage time and time-dependent characteristics, more compatible to one of the main target applications of this project: Stand-alone applications powered by solar or wind energy sources. In these applications, storage times of hours, days and even months are necessary; therefore, systems with heat storage would be limited by the important standby losses. This is the reason why pneumatic-only storage technologies are the object of this research project.

## 2.3. Principle of pneumatic energy storage

In this section, we will review the basic physics behind the use of compressed air for energy storage. This review will help highlighting the limitations of this storage technique and the main difficulties that will be addressed by the optimization solutions proposed further. The storage cycle will be described first, then the compression/expansion process and the related thermal phenomena will be studied. Finally the potential energetic characteristics of the pneumatic storage will be evaluated.

### 2.3.1. Description of the pneumatic energy storage cycle

Pneumatic energy storage is often considered as a “gas spring” since it is mainly based on the elasticity of gas. In reality, things are a bit more complicated because, unlike in a mechanical spring, gas elasticity obeys more complex laws as

---

<sup>1</sup>Ratio of the total volume over the oil flow rate



at least 3 different kinds of energy are simultaneously and intensively involved in gas compression and expansion processes: mechanical energy, thermal energy and potential or pressure energy.

To simply illustrate this storage process, a closed piston-cylinder is considered first, that might be for instance a hand pump with orifices (or valves) closed, as sketched in Figure 2.7. The storage cycle is divided into two phases: the *storage phase* which consists in compressing the gas and the *discharge phase* which consists in expanding it to recover the stored energy. The first important remark is that there is no heat-storage unit in this technique as stated in Section 2.2.3; therefore, for each phase, the initial and final temperatures are sooner or later equal to the ambient temperature.

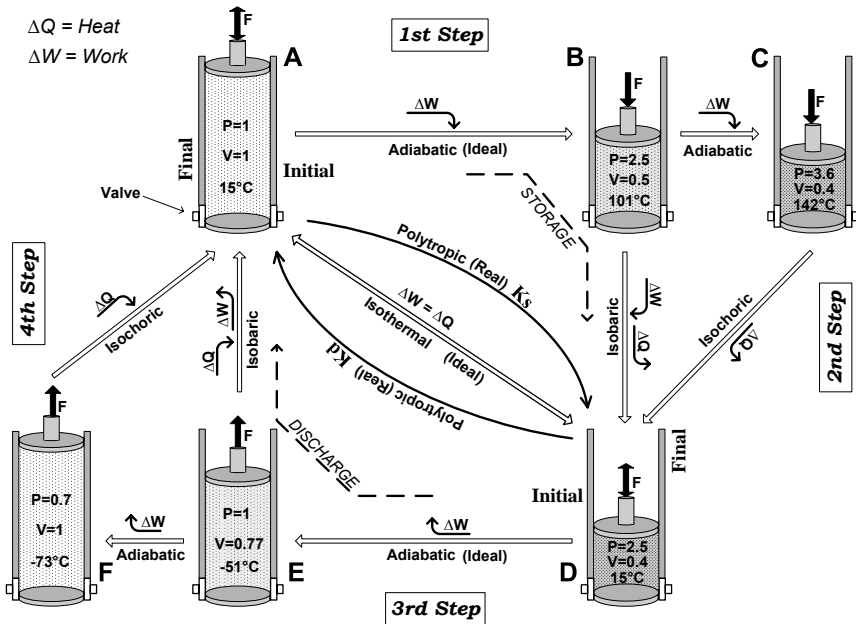


Figure 2.7.: Possible steps for the pneumatic energy storage process

From each initial state, there are 4 possible ways to the final state depending

upon the means used to achieve the work and control the process; they are described below considering the storage phase:

- The first way is to bring the gas to the final volume so rapidly that there is no time for any heat exchange with the surroundings (adiabatic: path  $A-B-C$ ); both the pressure and temperature will therefore rise above the final values (state  $C$ ). Then in the second step, the heat is exported to the surrounding through an isochoric transformation so as to bring the gas pressure and temperature to the desired final values.
- The second way is to bring the gas to the final pressure also through an adiabatic process (path  $A-B$ ); the temperature will rise and volume will remain above the desired values (state  $B$ ), and they will be brought to the final values through a constant pressure or isobaric transformation that evolves cooling of the gas and reduction of its volume.
- The third way is to bring the gas directly to the final volume and pressure in such a way that its temperature remains constant all along the path (isothermal: path  $A-D$ ). This supposes either an infinitely slow compression or a perfect heat exchange with the surroundings.
- The fourth way is an intermediary way called polytropic transformation, which can be considered as a combination of adiabatic and isothermal transformations. In fact isothermal and adiabatic processes are unrealistic because the gas heats up any way, the system is not thermally isolated and the process takes a certain time that allow some heat exchange with the external milieu. The real and practical path will be the polytropic path  $A-B'$  combined with the isobar  $B'-D$  or  $A-B'-C'$  combined with the isochor  $C'-D$ .

The discharge process works the similar way around as can be seen on Figure 2.7. The 4 possible ways to recover work from the compressed gas will be: Path  $D-E-F-A$  for the adiabatic and isochoric process, Path  $D-E-A$  for the adiabatic and isobaric process, Path  $D-A$  for the isothermal process and Paths  $D-E'-A$  for the polytropic process and isobaric process or  $D-E'-F'-A$  for the polytropic process and isochoric process.

The thermodynamic representations of these different possible storage processes are given by the P-V and T-S diagrams of Figure 2.8 where it has been

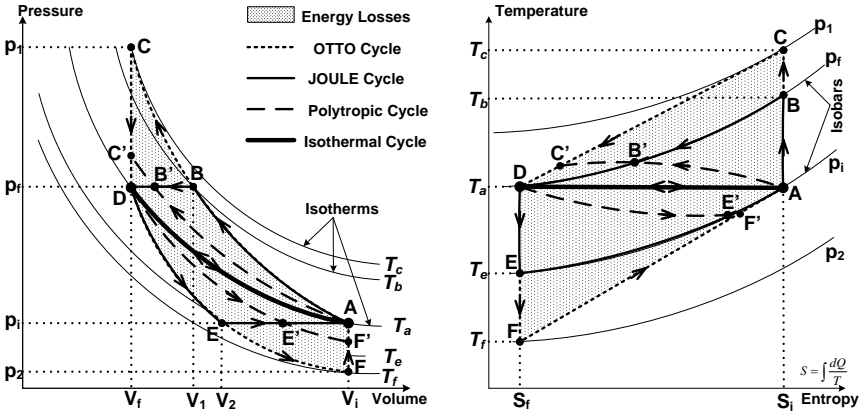


Figure 2.8.: Possible thermodynamic cycles for the pneumatic energy storage process

assumed that the irreversible losses such as friction losses are negligible (Isentropic processes). These diagrams show the behavior of the physical variables during the storage cycle. Combining each storage path with the corresponding discharge path would result in some well-known thermodynamic cycles [59]:

- The Pneumatic Otto Cycle for the first way. This is a combination of the adiabatic and isochoric process defined by the path A-B-C-D-E-F-A.
- The Pneumatic Joule Cycle for the second way. This is a combination of the adiabatic and isobaric process defined by the path A-B-D-E-A.

The dotted area enclosed in each cycle's path represents the energy losses for that cycle. These diagrams clearly show that the isothermal cycle (Path A-D-A) is the best cycle as it generates no losses because of the reversibility of the path. On the other hand, the Otto Cycle (Path A-B-C-D-E-F-A) is the worst cycle because it generates the largest losses area. The Joule Cycle (path A-B-D-E-A) is a little bit more efficient than the OTTO cycle because of the smaller compression ratio. In practice, the storage performs a polytropic cycle which generates the losses area delimited by the path A-B'-D-E'-A or A-B'-C'-D-E'-F'-A. The closer this path to the isothermal path, the smaller

the losses area and the more efficient the storage process. The purpose of the thermodynamic optimization in this project is to set this area<sup>2</sup> as small as possible.

### 2.3.2. Thermodynamic analysis of the process of pneumatic storage

In this analysis, air and the other considered gases are assumed behaving like ideal gases. Therefore, they obey the ideal gas law expressed as:

$$\frac{p}{\rho} = pv = \mathcal{R}T \quad (2.1)$$

where  $p$  denotes the absolute pressure (Pa),  $\rho$  the density of the gas ( $kg/m^3$ ),  $v$  the specific volume ( $m^3/kg$ ),  $T$  the absolute temperature (K) and  $\mathcal{R}$  the gas constant ( $\mathcal{R} = 287J/K.kg$ ).

For a given mass  $m$  ( $kg$ ) of gas occupying a volume  $V$  ( $m^3$ ), Equation 2.1 is written:

$$pV = m\mathcal{R}T \quad (2.2)$$

Each phase of the storage cycle takes place between two well defined states: The initial (subscript “ $i$ ”) state  $A(p_i; V_i; T_a)$  and the final (subscript “ $f$ ”) state  $D(p_f; V_f; T_a)$ , where  $T_a$  denotes the ambient temperature. The two cycles described in the previous section for the considered closed gas cycle will be now analyzed.

#### 2.3.2.1. Pneumatic Joule cycle

During each phase of this cycle, the gas may undergo one of the three main transformations represented in Figure 2.9. As long as no condensation (or evaporation) is involved, these transformations are characterized as follows: [60], [61], [62].

- **For an Isothermal transformation:**

---

<sup>2</sup>In Internal Combustion Engine for example, the cycle’s paths are covered in the reverse direction (clockwise). The dotted area therefore corresponds to the add-up work and the larger that area is, the more efficient the engine.

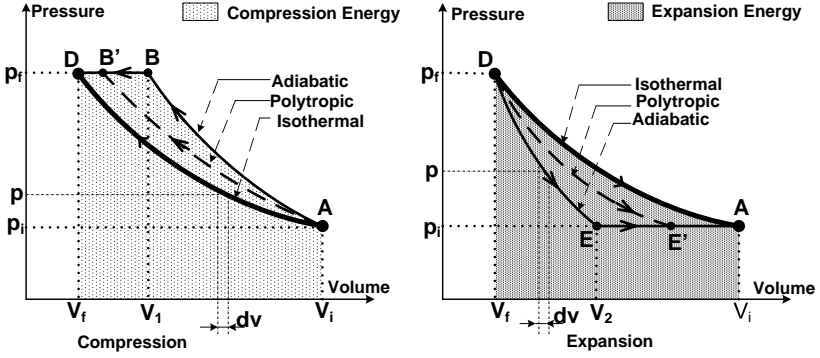


Figure 2.9.: Thermodynamic transformations involved in the process of closed gas cycle pneumatic energy storage

The pressure and volume evolution describes the Mariotte's hyperbola defined by:

$$pV = Constant \quad (2.3)$$

In order to draw up the gas energy balance for a storage cycle, abstraction of the irreversible losses are made again. Therefore, the reversible isothermal compression energy  $W_{Jric}$  received by the gas is represented by the dotted area below the isotherm A-D, and is defined by:

$$W_{Jric} = \int_A^D -pdV \quad (2.4)$$

Substituting Equation 2.3 into Equation 2.4 and integrating from state A( $V_i; p_i; T_a$ ) to state D( $V_f; p_f; T_a$ ) would give:

$$W_{Jric} = \int_A^D -pdV = -p_i V_i \ln \left( \frac{V_f}{V_i} \right) = p_i V_i \ln \left( \frac{p_f}{p_i} \right) = p_i V_i \ln (CR) \quad (2.5)$$

Where  $CR = p_f/p_i$  refers to the compression ratio. The same analysis carried out for the isothermal expansion from state D( $V_f; p_f; T_a$ ) to state A( $V_i; p_i; T_a$ ) would yield the reversible isothermal expansion energy  $W_{Jrie}$  provided by the

gas, which is given by:

$$W_{Jrie} = \int_D^A p dV = p_i V_i \ln \left( \frac{p_f}{p_i} \right) = p_i V_i \ln (CR) = W_{Jric} \quad (2.6)$$

The thermodynamic efficiency of the reversible isothermal cycle  $\eta_{Jri}$  is then equal to:

$$\eta_{Jri} = \frac{W_{rie}}{W_{ric}} = 1 \quad (2.7)$$

This result confirms that the isothermal cycle is the ideal theoretical cycle.

• **For an Adiabatic transformation:**

The pressure and volume evolution describes the Laplace's hyperbola defined by:

$$pV^\gamma = Constant \quad (2.8)$$

With  $\gamma = c_p/c_v$ , where  $c_p$  and  $c_v$  denote the specific heat at constant pressure and constant volume respectively. The value of the isentropic exponent  $\gamma$  for air at 1 standard atmosphere and  $15^\circ C$  is usually taken as 1.40.

The reversible adiabatic compression energy  $W_{Jrac}$  received by the gas is represented by the dotted area below the path A-B-D and defined by:

$$W_{Jrac} = \int_A^B -pdV + p_f (V_1 - V_f) \quad (2.9)$$

A( $V_i; p_i; T_a$ ) and D( $V_f; p_f; T_a$ ) belong to the isotherm ( $T_a$ ); according to Equation 2.3,  $p_i V_i = p_f V_f$ . Substituting Equation 2.8 into Equation 2.9 and integrating from state A( $V_i; p_i$ ) to state B( $V_1; p_f$ ) would give:

$$W_{Jrac} = \frac{\gamma}{\gamma - 1} p_i V_i \left[ \left( \frac{p_f}{p_i} \right)^{\frac{\gamma-1}{\gamma}} - 1 \right] = \frac{\gamma}{\gamma - 1} p_i V_i \left( CR^{\frac{\gamma-1}{\gamma}} - 1 \right) \quad (2.10)$$

The same analysis carried out for the adiabatic expansion considering path D-E-A would yield the reversible adiabatic expansion energy  $W_{Jrae}$  provided by the gas, which is represented by the dotted area below path D-E-A and given by:

$$W_{Jrae} = \int_D^E pdV + p_i (V_i - V_2) \quad (2.11)$$

The result of the integration is:

$$W_{Jrae} = \frac{\gamma}{\gamma - 1} p_f V_f \left[ 1 - \left( \frac{p_i}{p_f} \right)^{\frac{\gamma-1}{\gamma}} \right] = \frac{\gamma}{\gamma - 1} p_f V_f \left( 1 - CR^{\frac{1-\gamma}{\gamma}} \right) \quad (2.12)$$

As seen before,  $p_i V_i = p_f V_f$  since the states A and D belong to the isotherm ( $T_a$ ); therefore, the thermodynamic efficiency of the isentropic or reversible Joule cycle  $\eta_{Jra}$  is:

$$\eta_{Jra} = \frac{W_{Jrae}}{W_{Jrac}} = \frac{1 - CR^{\frac{1-\gamma}{\gamma}}}{CR^{\frac{\gamma-1}{\gamma}} - 1} \quad (2.13)$$

This result shows that the isentropic cycle's efficiency, which is represented in Figure 2.10, depends only upon the compression ratio and the isentropic exponent  $\gamma$ .

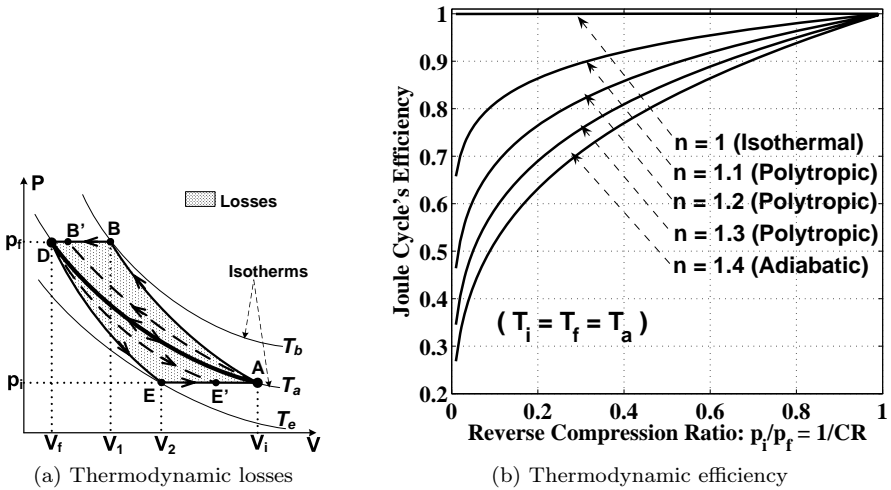


Figure 2.10.: Characteristics of the pneumatic Joule cycle

- **For a polytropic transformation:**

As has been said, isothermal and adiabatic transformations are practically not feasible and the transformations are rather polytropic because there would

always be some temperature change in the gas and some heat exchange with the surroundings. In engineering, this change of temperature is most conveniently indicated by introducing a polytropic exponent  $n$  to the volume  $V$  in the isothermal transformation Equation 2.3, resulting in the hyperbola defined by:

$$pV^n = \text{Constant} \quad (2.14)$$

The value of the exponent  $n$  usually lies between 1.0 and 1.6, depending upon a number of factors, such as the peculiarities of the gas compressed, its specific heats, the degree of heat exchange, the characteristics of the compression/expansion machine, etc. In the literature, there are many more or less accurate formulas for determining by means of some measurements, the polytropic exponent of a given gas undergoing a particular transformation. The most commonly encountered one is the following: [63]

$$n = \frac{\ln(p_f/p_i)}{\ln(p_f/p_i) - \ln(T_f/T_i)} \quad (2.15)$$

Equations 2.3, 2.8 and 2.15 show that isothermal and adiabatic transformations are simply particular cases of the polytropic transformation, where the value of the exponent  $n$  is 1 and  $\gamma$  respectively. The energy evaluation procedure for the polytropic transformations is therefore similar to that for adiabatic transformations. The reversible polytropic compression energy  $W_{Jrpc}$  received by the gas is therefore represented by the dotted area below the path A-B'-D and defined by:

$$W_{Jrpc} = \frac{n}{n-1} p_i V_i \left[ \left( \frac{p_f}{p_i} \right)^{\frac{n-1}{n}} - 1 \right] = \frac{n}{n-1} p_i V_i \left( CR^{\frac{n-1}{n}} - 1 \right) \quad (2.16)$$

A similar evaluation for the polytropic expansion energy from state D( $V_f; p_f; T_a$ ) to state A( $V_i; p_i; T_a$ ) through the path D-E'-A would yield the reversible polytropic expansion energy  $W_{Jrpe}$  provided by the gas, which is defined by:

$$W_{Jrpe} = \frac{n}{n-1} p_f V_f \left[ 1 - \left( \frac{p_i}{p_f} \right)^{\frac{n-1}{n}} \right] = \frac{n}{n-1} p_f V_f \left( 1 - CR^{\frac{1-n}{n}} \right) \quad (2.17)$$

Hence, the thermodynamic efficiency of the reversible polytropic Joule cycle  $\eta_{Jrp}$  is given by:

$$\eta_{Jrp} = \frac{W_{Jrpe}}{W_{Jrpc}} = \frac{1 - CR^{\frac{1-n}{n}}}{CR^{\frac{n-1}{n}} - 1} \quad (2.18)$$



Figure 2.10 depicts the polytropic cycle efficiency with respect to the compression ratio  $CR$ , for values of the polytropic exponent  $n$ , lying between the isothermal transformation ( $n = 1$ ) and the adiabatic transformation for air ( $n = \gamma = 1.4$ ). As can be seen, the smaller the compression ratio the better the efficiency, and the closer to isothermal the transformation is, the better the efficiency.

### 2.3.2.2. Pneumatic Otto cycle

An analogous analysis can be carried on, considering the Otto cycle represented in Figure 2.11. This analysis would give the following results:

- **For an isothermal transformation:**

The results are similar to that of the Joule cycle since the two processes follow the same path A-D.

- **For an adiabatic transformation:**

The compression energy  $W_{Orac}$  obtained through integration along the path A-C-D is:

$$W_{Orac} = \frac{p_i V_i}{\gamma - 1} \left[ \left( \frac{V_f}{V_i} \right)^{1-\gamma} - 1 \right] = \frac{p_i V_i}{\gamma - 1} (CR^{\gamma-1} - 1) \quad (2.19)$$

The expansion energy  $W_{Orae}$  obtained through integration along the path D-F-A is:

$$W_{Orae} = \frac{p_f V_f}{\gamma - 1} \left[ 1 - \left( \frac{V_i}{V_f} \right)^{1-\gamma} \right] = \frac{p_i V_i}{\gamma - 1} (1 - CR^{1-\gamma}) \quad (2.20)$$

The thermodynamic efficiency of the isentropic or reversible adiabatic OTTO cycle  $\eta_{Ora}$  is then:

$$\eta_{Ora} = \frac{W_{Orae}}{W_{Orac}} = \frac{1 - CR^{1-\gamma}}{CR^{\gamma-1} - 1} \quad (2.21)$$

- **For a polytropic transformation:**

The compression energy  $W_{Orpc}$  obtained through integration along the path A-C'-D is:

$$W_{Orpc} = \frac{p_i V_i}{n - 1} \left[ \left( \frac{V_f}{V_i} \right)^{1-n} - 1 \right] = \frac{p_i V_i}{n - 1} (CR^{n-1} - 1) \quad (2.22)$$

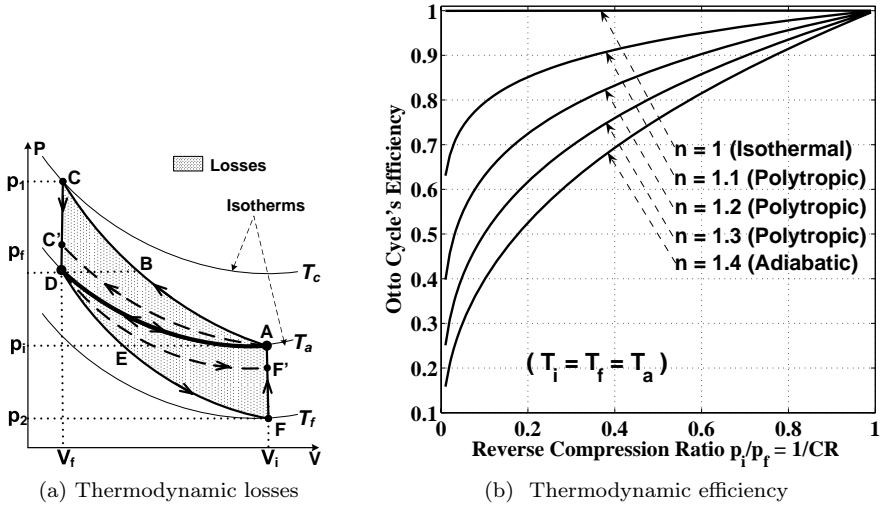


Figure 2.11.: Characteristics of the pneumatic Otto cycle

The expansion energy  $W_{Orpe}$  obtained through integration along the path D-F'-A is:

$$W_{Orpe} = \frac{p_f V_f}{n-1} \left[ 1 - \left( \frac{V_i}{V_f} \right)^{1-n} \right] = \frac{p_i V_i}{n-1} (1 - CR^{1-n}) \quad (2.23)$$

The reversible polytropic efficiency  $\eta_{Orp}$  is then:

$$\eta_{Orp} = \frac{W_{Orpe}}{W_{Orpc}} = \frac{1 - CR^{1-n}}{CR^{n-1} - 1} \quad (2.24)$$

This relation shows that the reversible efficiency represented in Figure 2.11 is, like in the case of Joule cycle, only dependant upon the compression ratio CR and the polytropic exponent.

Figures 2.10 and 2.11 confirm that the pneumatic Joule cycle is more efficient than the pneumatic Otto cycle because of the reduced pressure ratio throughout the cycle. This fact is well illustrated in Figure 2.7 where the

intermediary values of the state variables are indicated for a given mass of air taken at the ambient initial temperature  $T_a = 15^\circ C = 288.15^\circ K$  and a compression ratio  $CR = 2.5$ . In that case ( $1/CR = 0.4$ ), the efficiency curves show that one can expect to recover a maximum of about 77% of the energy expended in compressing the air with the Joule cycle (A-B-D-E-A), whereas this will be reduced to about 69% with the Otto cycle (A-C-D-F-A).

If some heat exchange is allowed with the surroundings, for instance with a polytropic exponent of  $n = 1.1$ , the efficiencies will be improved to about 92% for both cycles (A-B'-D-E'-A) and (A-C'-D-F'A). These figures show the great impact of the pressure ratio  $CR$  and the quality of heat exchange (represented by the polytropic exponent  $n$ ) on the efficiency of pneumatic energy storage.

It should be noted that the efficiencies stated here are based only on the thermodynamic properties of compressed air and therefore do not take into account the imperfections of the pneumatic-to-mechanical energy conversion system. This will be studied in Chapter 3.

### 2.3.2.3. Open gas cycle

In the previous section, only closed systems where the gas mass does not change during the storage cycle have been considered. The compression and expansion processes take place in the storage vessel. This is, for instance, the case of hydraulic accumulators.

In the majority of pneumatic storage applications, the reserve of compressed air is made by stuffing the storage vessel with atmospheric air, generally by means of a positive displacement volumetric machines, until the desired pressure is reached inside the vessel. The basic operation of such a system is similar to that of closed systems as illustrated by Figure 2.7, with however two major modifications: a) The orifices ( or valves) of the hand-pump will be controllable (can be open and closed), and b) A high pressure tank will be inserted at state D, where the compressed air is stored for later use during discharge.

As the cylinder's capacity  $V_{ai}$  of the volumetric machine is limited, the storage and discharge phases are sums of elementary compression and expansion cycles respectively. These elementary cycles are presented by the Clapeyron

P-V diagram of Figure 2.12 where it is assumed that the volumetric machine presents no clearance volume. As it can be seen, they are composed of the same transformations like the Joule cycle in closed systems. During a storage phase, the intermediary final pressure  $p_{fi}$  would vary from the atmospheric pressure  $p_a$  to the final vessel pressure  $p_f$ .

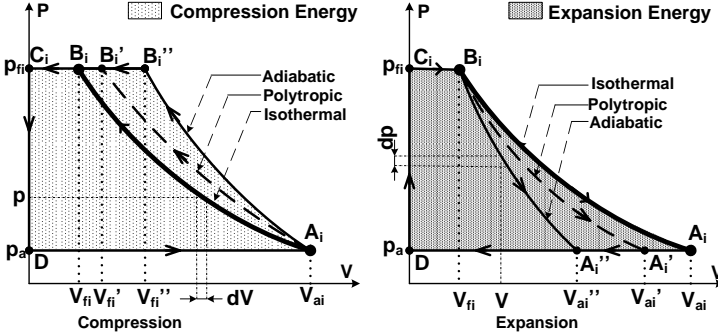


Figure 2.12.: P-V diagram of pneumatic open gas cycle for one volumetric machine's cycle

The energy evaluation is done by integrating along the compression and expansion line for each transformation. The initial compression state is defined as  $A(p_a; V_a; T_a)$  and the initial expansion state as  $B(p_f; V_f; T_a)$ ; where  $V_a$  denotes the total gas volume at atmospheric pressure and  $V_f$  the vessel's volume. This evaluation has led to expressions similar to those obtained with the Joule cycle as presented in Section 2.3.2.1:

The open gas cycle polytropic compression energy  $W_{opc}$  is given by:

$$W_{opc} = \frac{n}{n-1} p_a V_a \left[ \left( \frac{p_f}{p_a} \right)^{\frac{n-1}{n}} - 1 \right] = \frac{n}{n-1} p_a V_a \left( CR^{\frac{n-1}{n}} - 1 \right) \quad (2.25)$$

The open gas cycle polytropic expansion energy  $W_{ope}$  is given by:

$$W_{ope} = \frac{n}{n-1} p_f V_f \left[ 1 - \left( \frac{p_a}{p_f} \right)^{\frac{n-1}{n}} \right] = \frac{n}{n-1} p_f V_f \left( 1 - CR^{\frac{1-n}{n}} \right) \quad (2.26)$$

Therefore, the thermodynamic efficiency of the open gas cycle is given by:

$$\eta_{op} = \frac{W_{ope}}{W_{opc}} = \frac{1 - CR^{\frac{1-n}{n}}}{CR^{\frac{n-1}{n}} - 1} \quad (2.27)$$

Hence, the thermodynamic efficiency of the open gas cycle is equal to that of

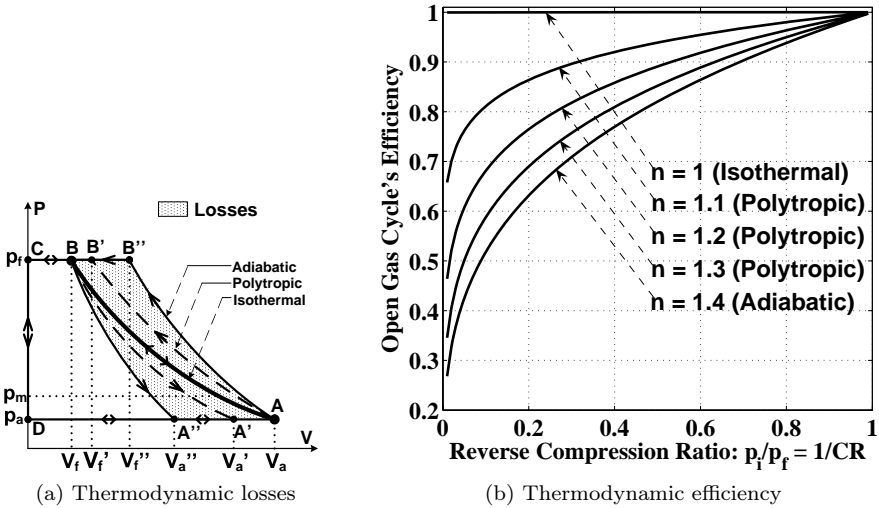


Figure 2.13.: Characteristics of the open gas cycle pneumatic storage

Joule cycle in closed system as presented in Figure 2.13. The main difference between these two cycles relies on the energy density that can be expected from each of them as it will be shown in the next section.

### 2.3.3. Main energy characteristics of pneumatic energy storage

#### 2.3.3.1. Actual storage media in pneumatic energy storage

In this section, it will be once again assumed that air behaves like an ideal gas and that the irreversible losses are negligible. Under that assumptions, the energy conversion in the storage process is done according to the law of

conservation of energy or first law of thermodynamics. Its derivative form is written:

$$dU = dQ + dW \tag{2.28}$$

where  $U$  refers to the internal energy of the gas which depends only on the initial and final states,  $Q$  denotes the Heat and  $W$  the work which depend upon the path followed during the process. For the ideal gas, the change in internal energy  $dU$  is given by:

$$dU = mc_v dT \tag{2.29}$$

It has been stated that in pneumatic energy storage, the initial and final temperatures of the storage<sup>3</sup> process are equal to the ambient temperature; i.e  $\Delta T = T_f - T_i = T_a - T_a = 0$ . Therefore,

$$dU = mc_v dT = mc_v (T_f - T_i) = 0 \tag{2.30}$$

This equation states that a given mass of air possesses no more internal energy at the end of the pneumatic storage process, than what was already in it at the beginning of the process, therefore it contains no part of the work invested in compressing it, seen from the First Law of thermodynamics... Combining Equations 2.28 and 2.30 gives:

$$dQ = -dW \tag{2.31}$$

This equation confirms that all the energy expended in compressing the air has been exported in form of heat to the surroundings. This heat is expected to be recovered during expansion to do useful work, however this depends upon the expansion conditions which can be different from the compression conditions, but also upon the surrounding's conditions, which may change between the two processes. Consequently, the power required to produce compressed air is uniquely unrelated to the power available from it later, in other words, the work done during discharge is not strictly the restoration of the energy expended during storage.

Equation 2.30 may suggest that the compressed air produced by the storage process possesses no work potential, however it is not the case. In fact the first law accounts for the energy balance during the conversion process but

---

<sup>3</sup>This is also true for the discharge process.

does not reflect the quality or grade of the different resultant forms of energy. An exergy evaluation allows figuring out the work potential incurred from the change of gas state during compression. Actually once compressed, air can perform two tasks:

1- *It makes part of its internal energy, that was in it before the compression, usable:*

A stationary, simple compressible closed system only possesses internal energy associated with the random, disordered motion of molecules related to the temperature. The work potential of the air at the compressed state ( $p_f, T_f$ ) is its exergy  $E_f$  which equals the work which could be recovered using reversible transformation until equilibrium with the atmosphere. Considering the atmosphere ( $p_a, T_a$ ) as reference and under the assumptions made at the beginning of this section, the exergy  $E_f$  at the compressed state is given by:

$$E = \Delta U + p_a dV - T_a dS \quad (2.32)$$

$$E_f = mc_v (T_f - T_a) + p_a (V_f - V_a) - mT_a \left( c_v \ln \frac{T_f}{T_a} - \mathcal{R} \ln \left( \frac{p_f}{p_a} \right) \right) \quad (2.33)$$

As the gas is initially at ambient temperature,  $T_f = T_a$  and  $p_f V_f = p_a V_a$ .  $V_f$  and  $V_a$  are the volumes of the considered mass of air respectively at compressed state and atmospheric conditions. Equation 2.33 then becomes:

$$E_f = +p_a V_a \left( \frac{V_f}{V_a} - 1 \right) + m\mathcal{R}T_a \ln \left( \frac{p_f}{p_a} \right) \quad (2.34)$$

Introducing the ideal gas law given by Equation 2.2 finally gives:

$$E_f = p_f V_f \left( \frac{p_a}{p_f} - 1 + \ln \left( \frac{p_f}{p_a} \right) \right) \quad (2.35)$$

This equation shows that compressed air really possesses a useful work potential which is determined the pressure and volume at the compressed state.

2- *It allows the exploitation of the ambient thermal energy:*

The temperature gradient  $\Delta T$  created during the expansion acts like a driven force for heat transfer from the surroundings to the air (assuming the expansion enclosure allows to do so), which in turn can be converted in to useful

through CARNOT cycles. The amount of heat that can be imported is proportional to the temperature difference with the surroundings and therefore to the pressure drop according to the gas equation of state. The imported heat will tend to compensate the temperature drop. If the heat importation is done in such a way that the gas temperature remains constant during the process, then the amount of available work is maximum and equivalent of the heat that has been imported.

In conclusion the work potential of pneumatic storage relies on one hand on the exergy of the air related to its compressed state and, on the other hand on the heat exchange capability of the expansion system with the surroundings. The pneumatic storage technique presents the advantage of needing no heat storage device as it relies on the “infinite-capacity heat source” which is the environment. Consequently, it requires a good heat-conducting interface with the surrounding, which is easier to realize compared to the good heat-insulating interface required by the hybrid thermal and compressed air storage systems.

### 2.3.3.2. Energy density of closed gas cycle pneumatic storage systems

For obvious practical reasons, it is important to determine the energy density of pneumatic storage like for any storage technology. It has just been seen that although the pneumatic storage process results in no increase in the internal energy of the compressed air, there exists a real potential of doing useful work from the gas due to its change in state. However, the actual work that can be done strongly depend on the way the compressed air is brought back to the initial expanded state. Hence, the *energy density* will simply refer to the expectable work or “*transformation-exergy*” from a unit amount of compressed air that undergoes a given reversible expansion process [64].

For systems with a closed gas cycle, the polytropic expansion energy is given by Equation 2.17. In practice, the most relevant parameters are the volume at the expanded state  $V_i$ , which corresponds to the vessel volume and the pressure at the compressed state  $p_f$  that would be nearly the rating pressure of the system. Introducing these two parameters in Equation 2.17 using the Mariotte’s relation given in Equation 2.3 would give a more meaningful expression



of the expansion energy as:

$$W_{rpe} = \frac{np_f V_i}{(n-1)CR} \left(1 - CR^{\frac{1-n}{n}}\right) \quad (2.36)$$

If a unit volume of  $1m^3$  is considered, the volumetric energy density  $w_v$  is given by:

$$w_v = \frac{np_f}{(n-1)CR} \left(1 - CR^{\frac{1-n}{n}}\right) \quad (2.37)$$

Figure 2.14 represents this energy density as a function of the compression

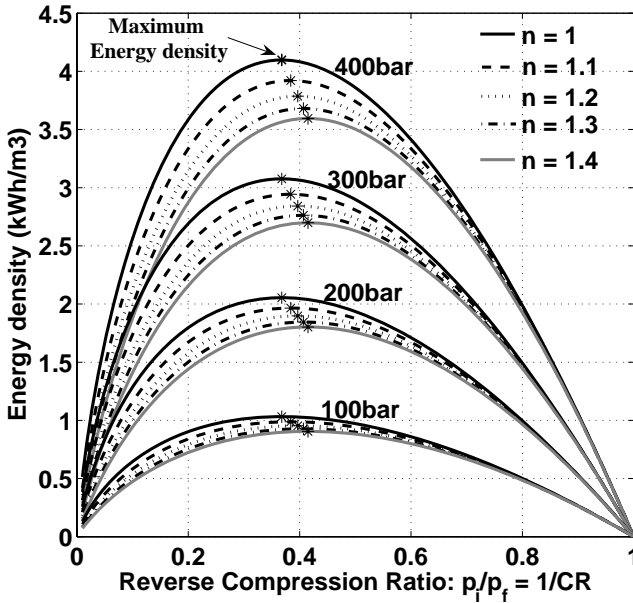


Figure 2.14.: Volumetric energy density for closed gas cycle and different value of maximum pressure  $p_f$

ratio, for different values of the maximum pressure and polytropic exponent. It can be seen that on one end, there is obviously no energy without pressure difference ( $CR = 1$ ). On the other end, the volumetric energy also tends

zero when the compression ratio tends to infinity ( $CR \rightarrow \infty$ ) for, the residual volume of the compressed gas tends to zero ( $V_f = V_i/CR \rightarrow 0$ ). Hence, while the volumetric energy density remains low, there exists for each polytropic exponent an optimal compression ratio that corresponds to its maximum value.

Deriving Equation 2.37 with respect to the compression ratio will result in the expression of the optimal compression ratio  $CR_{opt}$ , defined by:

$$CR_{opt} = \left( \frac{n}{2n-1} \right)^{\frac{n}{1-n}} \quad (2.38)$$

Introducing this result in Equation 2.37 gives the maximum volumetric energy density  $w_{vmx}$  as:

$$w_{vmx} = \frac{np_f}{(n-1)CR_{opt}} \left( 1 - CR_{opt}^{\frac{1-n}{n}} \right) = p_f \left( \frac{n}{2n-1} \right)^{\frac{1-2n}{1-n}} \quad (2.39)$$

Figure 2.15 presents the variation of the optimal compression ratio with regard to the polytropic exponent for compressed air, as well as the corresponding energy density. This figure that can be a helpful tool for a quick sizing of a closed gas cycle storage system, shows that  $CR_{opt}$  lies between 2.72 (for the isothermal transformation) and 2.42 (for the adiabatic one).

Equation 2.37 states that the volumetric energy density is proportional to the maximum pressure  $p_f$ . Therefore, the higher the maximum pressure, the higher the energy density as it can be seen on Figure 2.15. On the other hand, the same figure shows that the maximum energy density will be achieved only if the compression ratio is equal to  $CR_{opt}$ ; which means that the initial pressure  $p_i$  should be about a half of the maximum pressure  $p_f$ . This initial pressure, which is obtained at the expense of some energy, corresponds to a potential energy that can not be exploited because of the limited compression ratio.

If it is assumed that the compressed air could be expanded down to atmospheric pressure  $p_a$ , the unused energy  $w_{uve}$  in a unit volume of compressed air at the initial pressure  $p_i$  would be given by the following expression, similar to that of Equation 2.26

$$w_{uve} = \frac{np_i}{n-1} \left[ 1 - \left( \frac{p_a}{p_i} \right)^{\frac{n-1}{n}} \right] \quad (2.40)$$

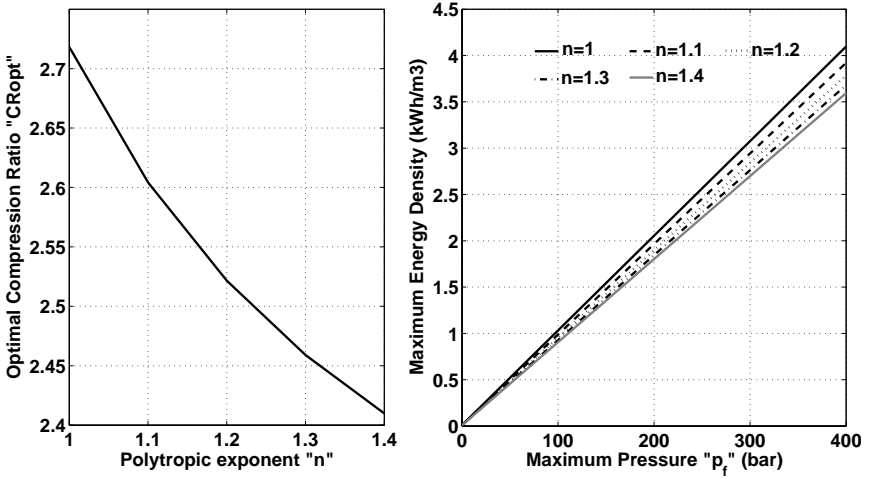


Figure 2.15.: Optimal compression ratio and maximum volumetric energy density for a closed gas cycle

Introducing the maximum pressure  $p_f$  and the optimal compression ratio  $CR_{opt}$  in this equation gives:

$$w_{uve} = \frac{np_f}{(n-1)CR_{opt}} \left[ 1 - \left( \frac{p_f}{p_a \cdot CR_{opt}} \right)^{\frac{1-n}{n}} \right] \quad (2.41)$$

- **The pressure utilization factor**

For a good relative estimation of this unused energy, the *Pressure Utilization Factor* ( $PUF$ ) of the closed gas cycle  $PUF_{cgc}$  can be defined as:

$$PUF_{cgc} = \frac{w_{vmx}}{w_{vmx} + w_{uve}} \quad (2.42)$$

The representations of both  $w_{uve}$  and  $PUF_{cgc}$  are given in Figure 2.16. As can be seen in the optimal compression ratio conditions, when the maximum pressure  $p_f$  is increased to have a higher energy density, so does the initial

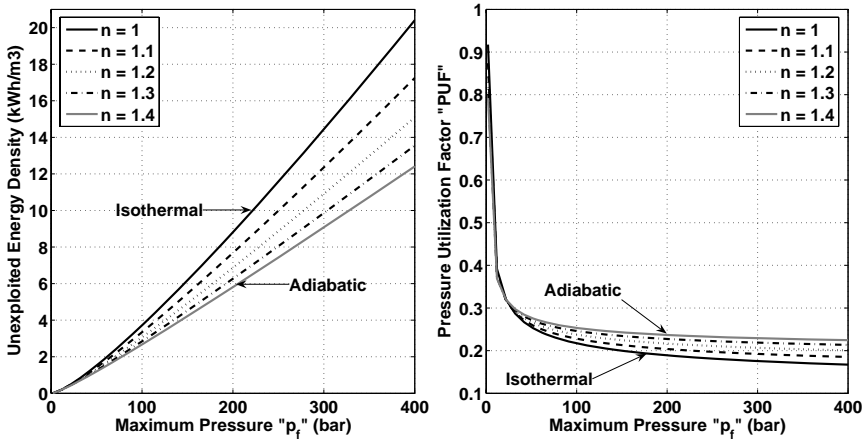


Figure 2.16.: Unused energy and pressure utilization factor of a closed gas cycle pneumatic storage system

pressure  $p_i$  and therefore the unexploited potential energy  $w_{uve}$  related to this initial pressure. In addition, this unusable energy is much higher compared to the available energy presented in Figure 2.15. Consequently, what has been defined as the pressure utilization factor remains very low, around 20%.

This is another reason why the volumetric energy density of closed gas cycle pneumatic energy storage systems is quite low compared to that of other classical energy storage technologies. For those reasons, these systems will be mainly dedicated to stationary applications where the volume and weight are not critical.

• *The energy factor*

Another approach for analyzing the energetic performance of pneumatic storage systems is to consider the maximum energy  $W_{max}$ , defined by the following product: [59]

$$W_{max} = p_f \cdot V_i \tag{2.43}$$

The energy factor or energy quotient  $\beta$  of the storage system will be defined as the ratio of its expansion energy to the maximum energy.  $\beta$  is then equal

to:

$$\beta = \frac{W_{rpe}}{W_{max}} = \frac{n}{(n-1)CR} \left(1 - CR^{\frac{1-n}{n}}\right) \quad (2.44)$$

The graphical representation of  $\beta$  is given by Figure 2.17. The main advantage

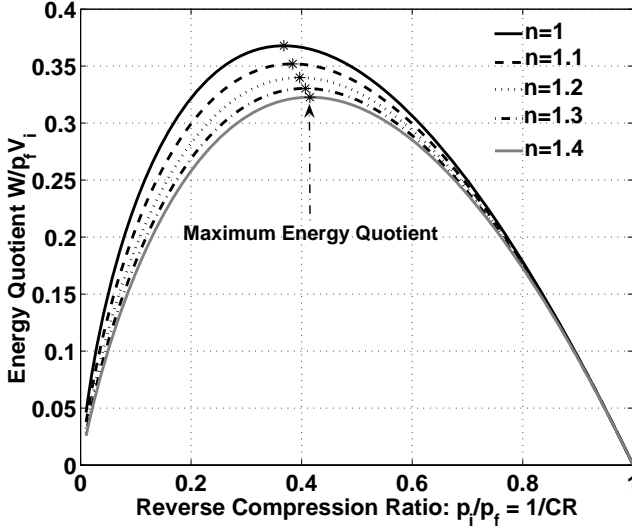


Figure 2.17.: Energy factor of closed gas cycle pneumatic storage systems

of this factor is that it gives an accurate figure of the energetic performance of a system, independently of its size and rating parameters like the pressure. Therefore it can be used to compare different systems simply on the basis of their operating conditions, which are mainly determined by the compression ratio and the polytropic exponent.

### 2.3.3.3. Energy density of closed gas cycle hydro-pneumatic storage systems

Despite their low energy density, the pneumatic storage systems with Closed gas cycle possess a simple and efficient conversion chain because the compression and expansion processes take place in the storage volume as it will be seen

more in detail in the chapter 3. More often, the compression is achieved by injecting a liquid into the storage volume where there is a physical separation between the compressing liquid and the trapped gas. This yields closed gas cycle hydro-pneumatic storage systems with two possible cases:

• **1- Water hydro-pneumatic systems:**

The compressing liquid is water. Such a storage system will be generally installed near a natural source of water like a river or a lake. In that case, the system volume is mostly determined by the gas volume at expanded state and the volumetric energy density is given by Equation 2.36.

• **2- Oil hydro-pneumatic systems:**

The compressing liquid is oil like in the case of the first hydro-pneumatic storage system presented in Section 2.2.3.2. In that case, the system requires an external tank for the storage of that compressing liquid. This external vessel increases the overall system volume and therefore decreases its volumetric energy density.

In the conditions of optimal compression ratio  $CR_{opt}$ , the necessary oil volume  $V_{liq}$  to achieve that compression from an initial gas volume  $V_i$  is equal to:

$$V_{liq} = \left(1 - \frac{1}{CR_{opt}}\right) V_i \quad (2.45)$$

Given the low energy density, in most applications the volume of the conversion unit will always be negligible compared to that of the gas and liquid tanks. The overall system volume  $V_T$  is therefore equal to:

$$V_T = V_i + V_{liq} = \left(2 - \frac{1}{CR_{opt}}\right) V_i \quad (2.46)$$

Hence, for a unit total volume of  $V_{Tu}$ , the initial gas volume is:

$$V_i = \frac{CR_{opt}}{2CR_{opt} - 1} V_{Tu}. \quad (2.47)$$

As a consequence, the effective maximum volumetric energy density for a

hydro-pneumatic storage system  $w_{vhp}$  with closed gas cycle is given by:

$$w_{vhp} = \frac{CR_{opt}}{2CR_{opt} - 1} w_{vmx} = p_f \left( \frac{n}{2n - 1} \right)^{\frac{1-2n}{1-n}} \left( \frac{1}{2 - \left( \frac{n}{2n-1} \right)^{\frac{-n}{1-n}}} \right) \quad (2.48)$$

If an average optimal compression ratio of  $CR_{opt} = 2.5$  is considered, a simplified expression becomes:

$$w_{vhp} \cong 0.625 w_{vmx} \cong 0.625 p_f \left( \frac{n}{2n - 1} \right)^{\frac{1-2n}{1-n}} \quad (2.49)$$

The effective maximum volumetric energy densities for the two categories of

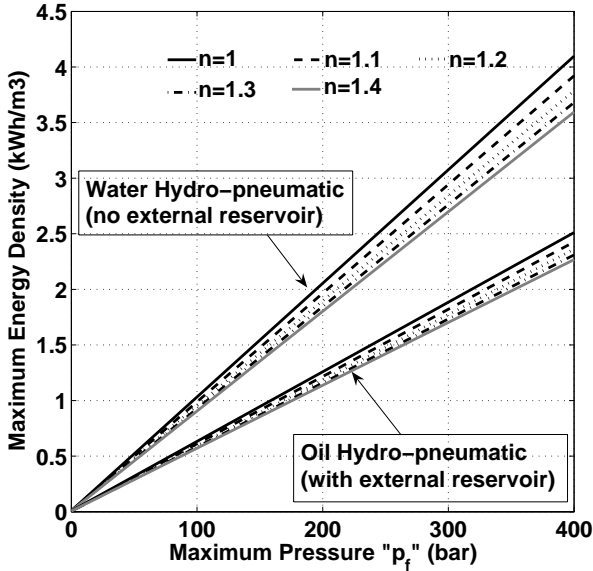


Figure 2.18.: Maximum volumetric energy density of closed gas cycle hydro-pneumatic storage systems

closed gas cycle hydro-pneumatic systems are represented in Figure 2.18. As

it can be seen, when the volume of the compressing liquid's tank is taken into account like for oil hydro-pneumatic systems, the volumetric energy density is much lower than that obtained considering only the gas reservoir volume like for water hydro-pneumatic systems.

#### 2.3.3.4. Energy density of open gas cycle pneumatic storage systems

It has been seen that, the volumetric energy density of closed gas cycle pneumatic storage systems was low because of the partial exploitation of the available pressure range. Open gas cycle systems avoid that limitation by expanding the compressed air from the maximum down to the atmospheric pressure, exploiting thus the whole pressure range. In that case, the available energy in the expanding air is illustrated by the dotted area in Figure 2.19a and corresponds to the expansion energy determined by Equation 2.26.

It should be noticed in that equation that the final volume  $V_f$  corresponds also to the vessel volume. For a unit volume of  $1m^3$ , the volumetric energy density  $w_{ov}$  is therefore given by:

$$w_{ov} = \frac{n}{n-1} p_f \left[ 1 - \left( \frac{p_a}{p_f} \right)^{\frac{n-1}{n}} \right] \quad (2.50)$$

Figure 2.19b represents this energy density as a function of the maximum pressure  $p_f$  for different values of the polytropic exponent. As can be seen, the volumetric energy density for an open cycle is more than 10 times greater than the one of a closed gas cycle.

In practice, there is a minimum vessel pressure  $p_m$  under which the compressed air expansion process is stopped. This is mainly because below that pressure limit, the delivered power becomes so low that the operation of the system is inefficient. The value of  $p_m$  depends on the application. Hence, in case  $p_m$  is greater than the atmospheric pressure  $p_a$ , an unexploited energy  $w_{ouv}$  will remain in the air reservoir. This is illustrated by the lightly dotted area in Figure 2.20a. It can be estimated simply by replacing  $p_f$  by  $p_m$  in Equation 2.51:

$$w_{ouv} = \frac{n}{n-1} p_m \left[ 1 - \left( \frac{p_a}{p_m} \right)^{\frac{n-1}{n}} \right] \quad (2.51)$$



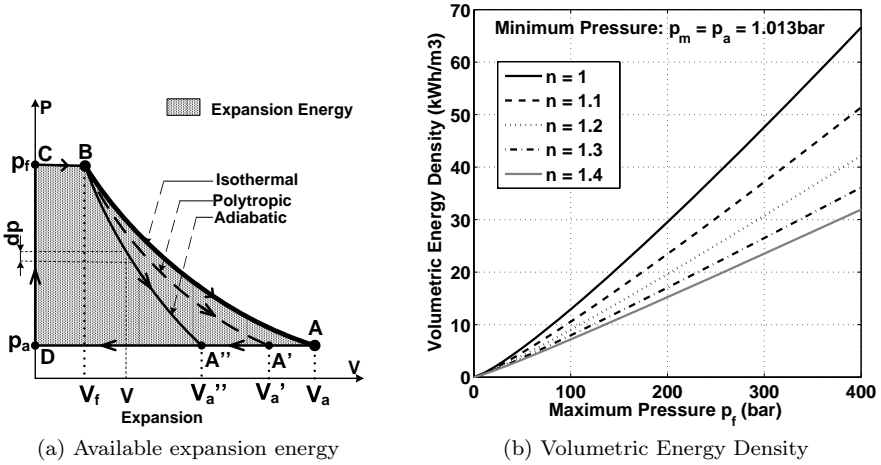


Figure 2.19.: Volumetric energy density of open gas cycle pneumatic energy storage systems

Consequently, the effective energy density  $w_{oev}$  will be reduced and equal to the difference between the available energy density  $w_{ov}$  and the unused energy density  $w_{ouv}$ .

$$w_{oev} = w_{ov} - w_{ouv} \quad (2.52)$$

Figure 2.20b represents this effective energy density as a function of the minimum pressure  $p_m$  for different values of the maximum pressure  $p_f$  and the polytropic exponent. As can be seen, the lower the minimum pressure, the higher the effective energy density.

The pressure utilization factor of the open gas cycle  $PUF_{ogc}$  can also be defined as:

$$PUF_{ogc} = 1 - \frac{w_{ouv}}{w_{ov}} \quad (2.53)$$

It can be deduced from this equation that  $PUF_{ogc} = 1$  when  $p_m = p_a$  and  $PUF_{ogc} = 0$  when  $p_m = p_f$ . In practice, the minimum pressure  $p_m$  will be

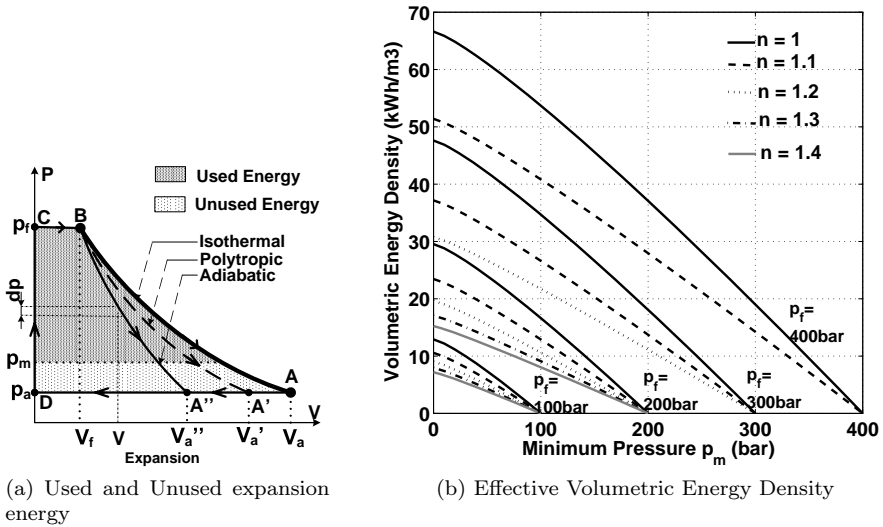


Figure 2.20.: Effect of minimum pressure on the Volumetric Energy Density of Pneumatic storage with Open gas Cycle

much smaller than the maximum pressure  $p_f$  such that the pressure utilization factor will be generally greater than 0.8.

## 2.4. Chapter summary

In this chapter, a short history of the used of compressed air as “energy carrier” has been given and the main modern, compressed air-based energy storage technologies have been briefly described. They can be classified in three main categories:

- The classical CAES systems which derive from the splitting of the normal gas turbine cycle and still rely on the utilization of fossil fuel. Hence, they appear more likely as an economical way of generating electricity from fuel than as a conventional storage system.

- The hybrid compressed air and thermal storage systems that try to store the compression heat, either with the compressed air or in a separated thermal storage unit, and later use it to reheat the air before expansion. This systems present the advantages of being fuel-free and emission-free. Their main drawbacks are the high thermal constraints on the conversion equipments and the important standby losses due to imperfect thermal isolation that limit the storage time and the round-trip efficiency.
- The pure pneumatic storage systems that try to implement isothermal gas processes by exporting the compression heat to the surroundings and later importing it during expansion. The thermal constraints and standby losses are therefore much lower. However, they require a very good heat exchange with the surroundings.

The last category is the object of this thesis and has been further studied more in details. The storage cycle has been described and the related thermodynamic cycles studied. The thermodynamic round-trip efficiencies of these cycles have been evaluated. They mainly depend upon the compression ratio and the polytropic exponent which define the rate of heat exchange with the surroundings.

The energy analysis has shown that the useful work potential of pneumatic storage depends on the exergy of the compressed air and the quality of heat exchange with the atmosphere. A good heat exchange with the external milieu is an essential condition for high energy performances. The volumetric energy density of this storage technique has been also evaluated, for closed gas cycle systems as well as for open gas cycle ones. This evaluation has shown that closed gas cycle storage systems present low volumetric energy densities mainly because of their low pressure utilization factor, whereas open gas cycle storage systems exploit the whole available pressure range which results in high energy densities.

The different means and strategies for efficiently producing compressed air and later recovering the maximum work from its potential energy will be studied in Chapter 3.



### 3. Investigation and Optimization of Pneumatic-to-Mechanical Energy Conversion: Strategies for Maximum Efficiency

Storing/producing electrical energy into/from compressed air is always done through an indirect conversion process with intermediary mechanical energy. For such a multiple-step conversions in energy storage applications, each conversion step shall exhibit the highest possible efficiency in order to expect an acceptable overall efficiency. In this chapter the Pneumatic-to-Mechanical (and vice versa) energy conversion process is investigated and some solutions for its optimization are proposed. For the targeted storage applications' power range, this conversion is mainly achieved by means of volumetric machines, therefore the investigations will be limited to this type of machines. The optimization approach mainly consists in:

- Suppressing all the unnecessary sources of losses.
- Controlling the operation of the conversion unit so as to avoid the lossy operation modes.

A pure pneumatic conversion unit, i.e one using a volumetric air machine will be studied first. An analytical quasi-static model of the conversion system will be proposed, then its conversion performances will be analyzed and some strategies to improve its efficiency proposed. Some simulation results of the implementation of these strategies to a small vane type pneumatic motor will be presented and discussed.

Afterwards, the oil-hydraulic conversion unit will be considered. Unlike air machines, hydraulic machines suffer less from some thermodynamic limitations and therefore exhibit more interesting conversion performances, even though they require an air-to-oil interface which is not always easy to realize. The first hydro-pneumatic storage systems called *Batteries with Oil-hydraulics and Pneumatics, type A (BOP-A)* and introduced in Chapter 2 will be studied and their conversion performances analyzed. The efficiency optimization strategies proposed with pneumatic conversion will be also applied to hydraulic conversion and some simulation results presented.

### 3.1. Investigation and Optimization of purely pneumatic conversion units

Only the Pneumatic-to-Mechanical energy conversion that corresponds to the discharge phase will be considered in this section, however the approach and results are also valid for the reverse conversion during the storage phase.

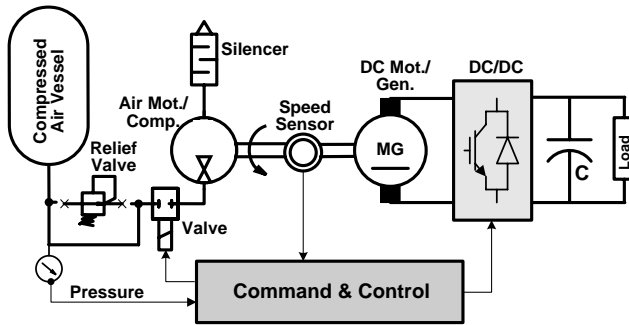


Figure 3.1.: Principle of Pneumatic energy conversion using volumetric air machine

The simplified diagram of the pneumatic-to-electrical energy conversion is shown in Figure 3.1 where the two steps of this process can be clearly identify: Firstly, the production of the intermediary mechanical energy by means of a volumetric air motor; and secondly the mechanical-to-electrical energy

conversion with a classical electrical machine. A small DC motor/generator is used for instance to get rapidly and easily controllable electro-mechanical conversion. A DC-DC converter is used to control the system operation and to obtain the desired output power conditioning. As mentioned above, only the first step is the concern of this chapter.

### 3.1.1. Suppression of the pressure control valve

In Chapter 2, it has been seen that in most pneumatic applications, the maximum storage pressure is chosen as high as possible in order to obtain a high energy density. But most often in practice, the air machine operates at a lower and constant pressure. As the vessel pressure decreases during the discharge, a pressure control valve is used to regulate the motor inlet pressure. Depending upon the operating conditions, this device can be a source of important energy losses. The effect of the use of a pressure relief valve on the potential energy of a compressed air vessel is illustrated in Figure 3.2 [37].

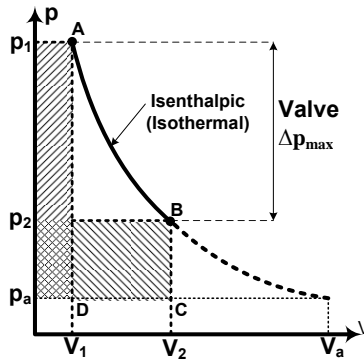


Figure 3.2.: Effects of Relief valve on available pneumatic energy

In a simplistic approach, the pressure regulation process can be viewed as the transfer of the compressed air from the high pressure tank into an imaginary lower pressure one through the relief valve, from where it is used to do work in the air motor. The high pressure tank is considered large enough to maintain the air it contains at ambient temperature during its discharge. The

initial exergy  $E_1$  of the vessel of volume  $V_1$  and maximum pressure  $p_1$  can be illustrated by the shaded area  $p_1ADp_a$ . On the basis of the development carried on in Section 2.3.3.1,  $E_1$  is given by:

$$E_1 = p_1 V_1 \left( \frac{p_a}{p_1} - 1 + \ln \left( \frac{p_1}{p_a} \right) \right) \quad (3.1)$$

where  $p_a$  denotes the atmospheric pressure. Further to the pressure reduction thanks to an “ideal” valve, what is lost in pressure should be normally gained in volume. If the valve is assumed as perfectly isolated and in steady flow conditions, then the air flow can be considered as isenthalpic. For an ideal gas as considered in this study, this yields to an isothermal expansion described by the relation:  $p_1 V_1 = p_2 V_2 = p_a V_a$ . The exergy  $E_2$  of the imaginary lower pressure tank downstream the relief valve is represented by the shaded area  $p_2BCp_a$  and defined by:

$$E_2 = p_2 V_2 \left( \frac{p_a}{p_2} - 1 + \ln \left( \frac{p_2}{p_a} \right) \right) \quad (3.2)$$

where  $p_2$  is the valve outlet pressure and  $V_2$  the total gas volume at pressure  $p_2$ . The exergy efficiency  $\eta_{pre}$  of the pressure regulation process is defined as:

$$\eta_{pre} = \frac{E_2}{E_1} \quad (3.3)$$

The pressure ratio  $PR$  is defined as  $PR = p_2/p_1 = 1 - \Delta p_{max}/p_1$ , where  $\Delta p_{max}$  is the maximum pressure drop across the valve. Introducing these relations in Equation 3.3 gives the final expression of the exergy efficiency of the pressure regulation process:

$$\eta_{pre} = \frac{\frac{p_a}{p_1 PR} - 1 + \ln \left( \frac{p_1 PR}{p_a} \right)}{\frac{p_a}{p_1} - 1 + \ln \left( \frac{p_1}{p_a} \right)} \quad (3.4)$$

Figure 3.3 represents this exergy efficiency with respect to the pressure ratio  $PR$  for different values of the maximum pressure. As can be seen, the exergy efficiency of the pressure regulation process decreases as the pressure drop increases and is lower for low pressure than for high pressure. These curves show that shows that, even when considering an ideal (lossless) valve, the energy



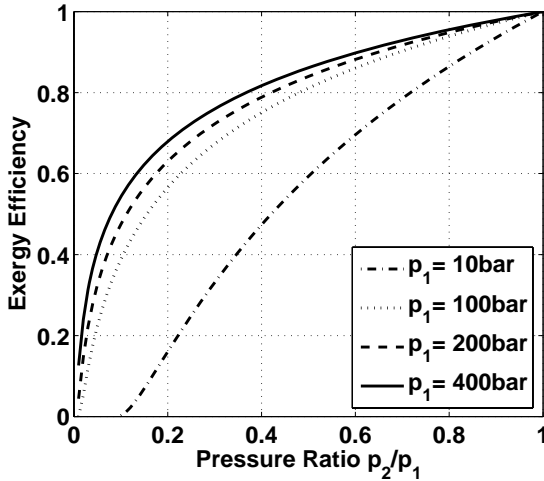


Figure 3.3.: Exergy efficiency of the pressure regulation process

available at the valve outlet is lower than that available in the compressed air tank.

In the case for instance of a compression ratio of 5 ( $PR = 0.2$ ) and for a maximum pressure of 100bar, the losses related to the pressure regulation represent with an ideal valve more than 40% of the total exergy, which is huge. This is the reason why the pressure relief valve has been suppressed from the air circuit. As a consequence, the air motor must be sized for the maximum pressure and must operate at variable inlet pressure. This may have some undesired impacts on its performances, what will be checked in the next section. A valveless system nevertheless presents the advantages of higher exergy, pressure utilization factor and maximum output power.

### 3.1.2. Analytical model for the volumetric air motor

A model of the air motor is necessary to analyze the conversion of pneumatic energy and later simulate and evaluate the optimization strategies. The ideal model should take into consideration all the physical phenomena involved in the energy conversion process, however it is difficult to collect from manufac-

turers all the necessary data to do so, and this approach doesn't fit with the scope of this project. On the other hand, an overview of different manufacturer's catalogues shows that nearly all the volumetric air machines, no matter the technology, exhibit almost the same characteristic curve's shapes. Therefore, an analytical model built on the basis of these curves is sufficient and accurate enough for a generalized description of the behavior and conversion performances of these machines for the targeted objectives.

The air motor used for these investigations is a low power vane type, whose exploded view and cross section are shown in Figure 3.4. This technology presents the advantages of simplicity, safety, lightness and high power density that make it suitable for portable applications [65].

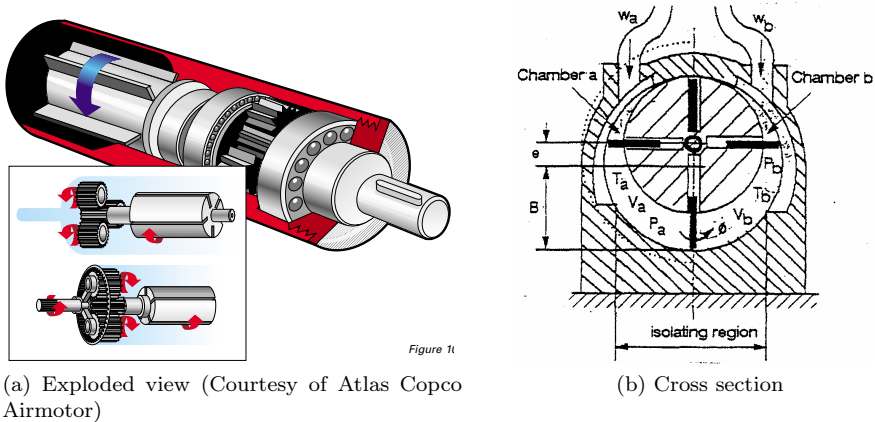


Figure 3.4.: Exploded view and cross-section of a low power vane air motor

### 3.1.2.1. Constant pressure model

The manufacturer characteristic curves for the constant nominal pressure [66] are represented in Figure 3.5a. As can be seen, the motor exhibits a linear torque characteristic that can be modeled by the following first order polyno-

mial function:

$$M_m = M_0 \left( 1 - \frac{N}{N_0} \right) \quad (3.5)$$

$M_m$  denotes the mechanical torque,  $M_0$  the stall torque,  $N$  the rotational speed and  $N_0$  the free speed. For the LBZ14R motor used in these investigations,  $M_0 = 1.2Nm$  and  $N_0 \cong 3200rpm$  for the nominal pressure of 6.3bar. The mechanical power  $\dot{W}_m$  is then given by:

$$\dot{W}_m = \frac{\pi}{30} N \cdot M_m = \frac{\pi}{30} M_0 \left( N - \frac{N^2}{N_0} \right) \quad (3.6)$$

The motor air consumption  $\dot{V}_a$  exhibits a non linear variation with respect to the speed. An analysis of this characteristic has shown that it can be accurately modeled with the following exponential function:

$$\dot{V}_a = 10^{(c_1 N^2 + c_2 N + c_3)} \quad (3.7)$$

where  $c_1$ ,  $c_2$  and  $c_3$  are real constants that are determined from at least three different and distant points of the air consumption characteristic. The representation of the modeled characteristics for the nominal pressure is given in Figure 3.5b. It can be seen that these curves match the manufacturer's curves very well, confirming thus the accuracy of the analytical model.

#### 3.1.2.2. Variable pressure model

Following the suppression of the pressure control valve, the motor will operate at variable pressure. It is therefore important to know and model the effect of the pressure variation on its performances. The variable pressure data provided by the manufacturer show that pressure variation does not modify the shape of the characteristic curves, but mainly their boundary parameters like the stall torque  $M_0$  and the free speed  $N_0$ . The data provided have thus allowed defining some correction functions  $f_t$ ,  $f_n$  and  $f_a$  which describe that effect as follow:

- For the stall torque:  $f_t = c_{t1} \cdot p + c_{t2}$
- For the free speed:  $f_n = c_{n1} \cdot p^2 + c_{n2} \cdot p + c_{n3}$
- For the air consumption:  $f_a = c_{a1} \cdot p + c_{a2}$

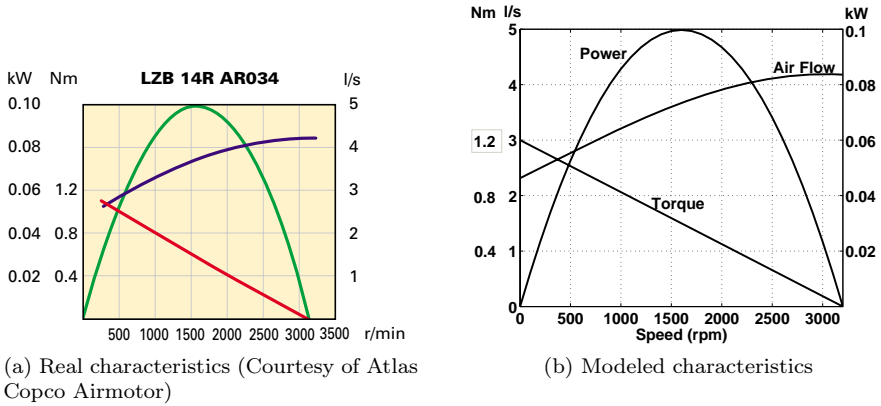


Figure 3.5.: Real and modeled characteristics for the nominal pressure (6.3bar)

$c_{t1}$ ,  $c_{t2}$ ,  $c_{n1}$ ,  $c_{n2}$ ,  $c_{n3}$ ,  $c_{a1}$  and  $c_{a2}$  are constants determined from the manufacturer's data tables. These functions show that the stall torque and the air consumption vary linearly with the pressure, whereas the free speed exhibits a non linear dependence. Introducing these correction functions into Equations 3.5, 3.6 and 3.7 would give the variable pressure characteristics as follow:

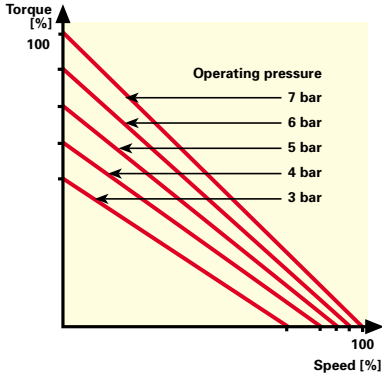
$$M_m = f_t \cdot M_0 \left( 1 - \frac{N}{f_n \cdot N_0} \right) \quad (3.8)$$

$$\dot{W}_m = \frac{\pi}{30} f_t \cdot M_0 \left( N - \frac{N^2}{f_n \cdot N_0} \right) \quad (3.9)$$

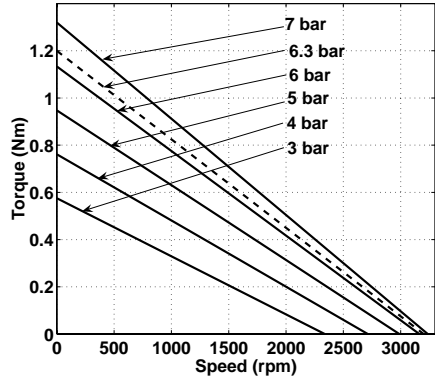
$$\dot{V}_a = f_a \cdot 10^{(c_1 \cdot N^2 + c_2 \cdot N + c_3)} \quad (3.10)$$

The modeled variable pressure characteristics for the experimental motor are represented in Figure 3.6 together with variable pressure torque characteristics provided by the manufacturer. It can be seen that the modeled torque characteristics exhibit the same shape like the manufacturer's ones, proving thus the effectiveness of the correction functions given above.

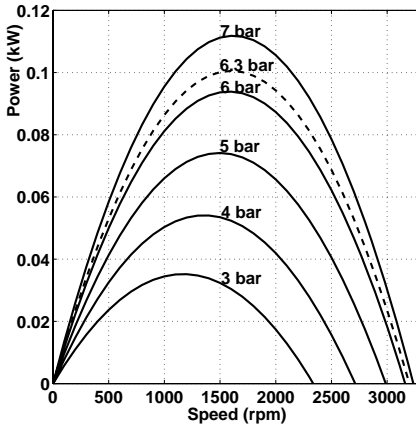
### 3.1. Investigation and Optimization of purely pneumatic conversion units



(a) Data sheet's torque characteristics  
(Courtesy of Atlas Copco Air motor)



(b) Modeled torque characteristics



(c) Modeled power and air consumption characteristics

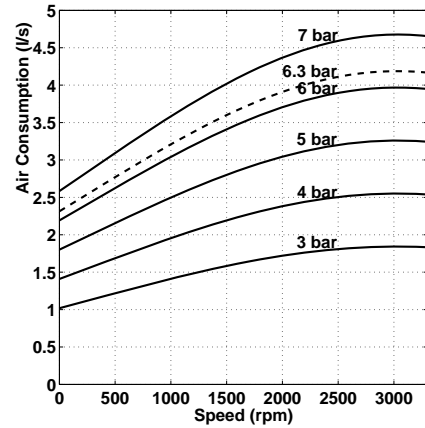


Figure 3.6.: Real and modeled characteristics for variable pressure

### 3.1.3. Evaluation of the pneumatic-to-mechanical conversion efficiency

In order to calculate the efficiency of the pneumatic-to-mechanical conversion, the power available in the compressed air flowing through the air motor must be evaluated first. A simplified diagram of this conversion system is given in Figure 3.7 where the main heat and mass transfers with the corresponding variables are represented. The following simplifying assumptions will be made in this evaluation:

- Air is a perfect gas and its specific heats remain constant.
- Air flow through the air motor, which is modeled as a control volume open system, is steady.
- The changes in kinetic and potential energies are negligible.

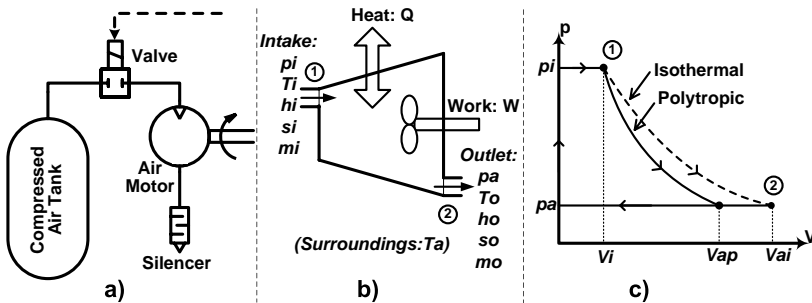


Figure 3.7.: Principle of pneumatic-to-mechanical energy conversion

In those conditions, and according to the first and second laws of thermodynamics applied to this open system, the elementary energy  $\delta w_a$  available in a unity mass of air is given by: [63]

$$\delta w_a \leq -dh + T_a ds \tag{3.11}$$

where  $dh$  and  $ds$  denote the change in specific enthalpy and entropy respectively. Integrating from state 2 at the motor outlet to state 1 at its intake

gives the specific work  $w_a$  as:

$$w_a \leq (h_i - h_o) - T_a(s_i - s_o) \quad (3.12)$$

$h_i$  and  $h_o$  are the specific enthalpy at the inlet and outlet respectively, and  $s_i$  and  $s_o$  are the specific entropy at the intake and outlet respectively. For the ideal gas, the net enthalpy and entropy changes are given by:

$$h_i - h_o = c_p(T_i - T_o) \quad (3.13)$$

$$s_i - s_o = c_p \cdot \ln\left(\frac{T_i}{T_o}\right) - \mathcal{R} \ln\left(\frac{p_i}{p_a}\right) \quad (3.14)$$

Substituting Equations 3.13 and 3.14 into Equation 3.12 gives:

$$w_a \leq \mathcal{R}T_a \left[ \ln\frac{p_i}{p_a} + \frac{\gamma}{\gamma - 1} \left( \frac{T_i - T_o}{T_a} - \ln\frac{T_i}{T_o} \right) \right] \quad (3.15)$$

In practice, the reservoir discharge would generally last for a relatively long time, such that the air expansion it contains can be considered as isothermal. Therefore, air temperature at the motor intake can be assumed equal to the ambient temperature,  $T_i = T_a$ . Introducing this assumption in Equation 3.15 and dropping the inequality sign (assuming an isentropic process) gives the maximum specific energy of compressed air as:

$$w_a = \mathcal{R}T_a \left[ \ln\frac{p_i}{p_a} + \frac{\gamma}{\gamma - 1} \left( 1 - \frac{T_o}{T_a} - \ln\frac{T_o}{T_a} \right) \right] \quad (3.16)$$

The compressed air power  $\dot{W}_a$  is obtained by multiplying the specific energy  $w_a$  by the mass flow rate  $\dot{m}_a$ . The continuity equation applied to the motor gives:

$$\frac{dm_a}{dt} = \dot{m}_a = \rho \dot{V} = \frac{p_i}{\mathcal{R}T_a} \dot{V}_i = \frac{p_a}{\mathcal{R}T_o} \dot{V}_a \quad (3.17)$$

In practice, the volumetric flow rate is measured at the outlet. The mechanical power is then equal to:

$$\dot{W}_a = w_a \dot{m}_a = p_a \dot{V}_a \frac{T_a}{T_o} \left[ \ln\frac{p_i}{p_a} + \frac{\gamma}{\gamma - 1} \left( 1 - \frac{T_o}{T_a} - \ln\frac{T_o}{T_a} \right) \right] \quad (3.18)$$

Given the high motor speed, one can consider that the air expansion is adiabatic. Introducing the isentropic process relation  $\frac{T_a}{T_o} = \left(\frac{p_i}{p_a}\right)^{\frac{\gamma-1}{\gamma}}$  into Equation 3.18 gives the following result:

$$\dot{W}_a = \frac{\gamma}{\gamma-1} p_a \dot{V}_a \left[ \left(\frac{p_i}{p_a}\right)^{\frac{\gamma-1}{\gamma}} - 1 \right] \quad (3.19)$$

Finally, the real time pneumatic-to-mechanical energy conversion efficiency  $\eta_{pm}$  is obtained from Equations 3.9 and 3.19 as:

$$\eta_{pm} = \frac{\dot{W}_m}{\dot{W}_a} = \frac{\frac{\pi}{30} f_t \cdot M_0 \left( N - \frac{N^2}{f_n \cdot N_0} \right)}{\frac{\gamma}{\gamma-1} p_a \dot{V}_a \left[ \left(\frac{p_i}{p_a}\right)^{\frac{\gamma-1}{\gamma}} - 1 \right]} \quad (3.20)$$

It can be seen on Equations 3.20 the the conversion efficiency  $\eta_{pm}$  is a function of speed  $N$  and intake relative pressure  $p_i$ . As  $\dot{W}_m$  is the effective power at the motor shaft, with the assumptions that the air intake temperature is equal to the ambient temperature  $T_i = T_a$  and that the heat exchanges between the motor chambers and the surroundings are negligible (adiabatic expansion),  $\eta_{pm}$  represents then the overall efficiency of the air motor, which includes the thermodynamic efficiency, the volumetric efficiency and the mechanical efficiency. The conversion efficiency curves are represented in Figure 3.8. Two important remarks can be made on these curves which are typical to all volumetric machines:

1. The conversion efficiency increases with decreasing inlet pressure over most of the speed range: As the outlet pressure remains constant (atmospheric pressure), the expansion ratio decreases when the inlet pressure decreases and therefore the thermodynamic efficiency increases as it has been shown in Chapter 2 (Figure 2.10).
2. Like the power, the conversion efficiency exhibits with respect to the speed, a parabolic shape with a maximum efficiency point. Moreover, the optimal speed that corresponds to that maximum efficiency changes with pressure. As the pressure control valve has been removed, the motor will operate at variable pressure. The conversion efficiency would be



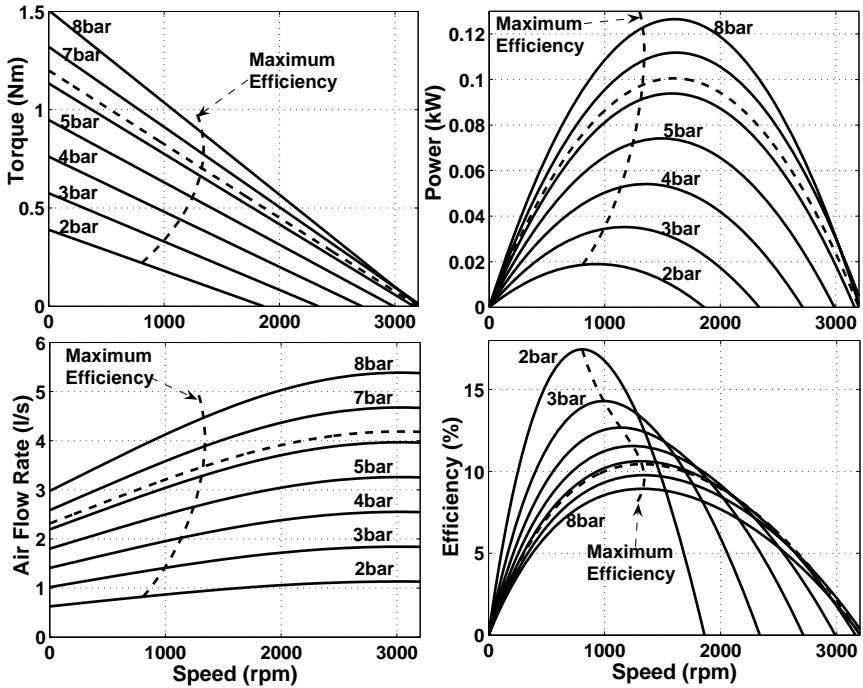


Figure 3.8.: Pneumatic-to-mechanical conversion characteristics

optimized if the speed is controlled so as to always maintain it at the maximum efficiency operating point. This is the purpose of the strategy for Maximum Efficiency Point Tracking (MEPT) presented in Section 3.1.4

### 3.1.4. Strategy for maximum efficiency

#### 3.1.4.1. Principle of maximum efficiency point tracking (MEPT)

A 3D representation of the motor efficiency is given in Figure 3.9 that highlights its variations with regard to pressure and speed. The figure shows that the variation with respect to pressure is non linear and difficult to formalize.

In addition, this variation depends on some peculiarities of the machine that may change from one size and technology to others. Therefore, a real time optimization strategy based only on measurements is necessary. The principle

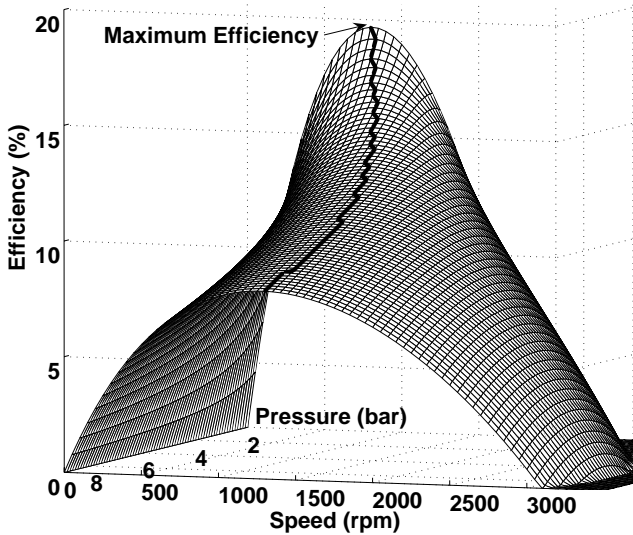
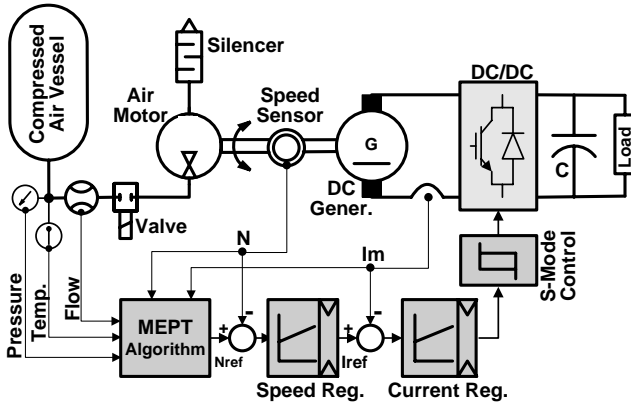


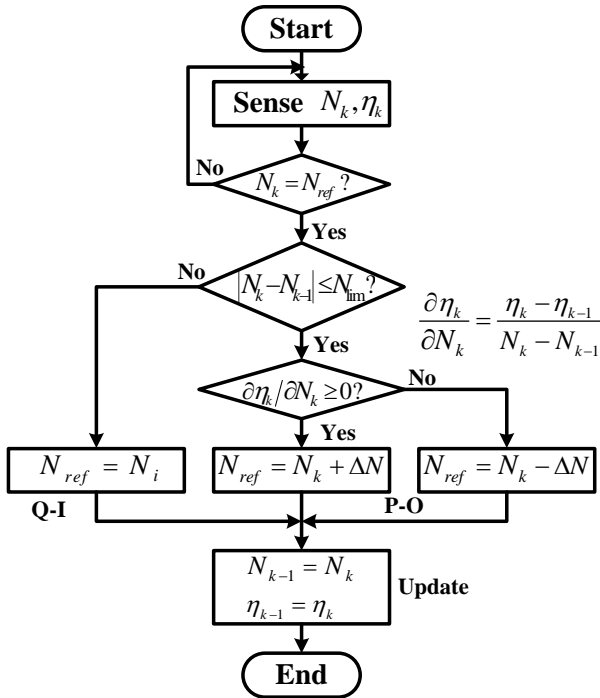
Figure 3.9.: Efficiency surface of the air motor

of this strategy is illustrated in Figure 3.10a. On the basis of various measurements (pressure, flow rate, speed, etc), the MEPT algorithm determines the optimal speed that corresponds to the maximum efficiency. This optimal speed is provided as reference  $N_{ref}$  to the speed control module and is achieved by controlling the electromagnetic torque of the DC generator through the current regulator and the DC/DC converter.

The objective of the MEPT algorithm is to keep the operating point of the air motor always on the bolt line at the top of the efficiency surface of Figure 3.9. This is achieved with the combination of two techniques: **Quadratic Interpolation (Q-I)** and the so-called **Perturbation-Observation (P-O)** techniques.



(a) Schematic diagram of the MEPT principle



(b) Flow diagram of the MEPT algorithm

Figure 3.10.: Schematic representation of the MEPT strategy

- **Quadratic Interpolation** is used at startup to come rapidly and accurately close to the optimal speed. It exploits the quadratic shape of the efficiency with respect to the speed, which can be approximated by a second order polynomial function to predict the initial optimal speed. The interpolated optimal speed  $N_i$  which serves as reference speed  $N_{ref}$  at the present time  $t_k$  is determined from the stall point  $(0;0)$ , the previous efficient and speed measurements at time  $t_{k-1}$ :  $(N_{k-1}; \eta_{k-1})$  and the present ones:  $(N_k; \eta_k)$  as follow:

$$N_{ref} = N_i = \frac{\eta_{k-1} \cdot N_k^2 - \eta_k \cdot N_{k-1}^2}{2(\eta_{k-1} \cdot N_k - \eta_k \cdot N_{k-1})} \quad (3.21)$$

- Once the interpolated optimum is reached, it is tracked using the “**Perturbation-Observation**” technique, well known in solar systems for peak power tracking [67]. This technique consists of periodically incrementing or decrementing the speed and analyzing the resulting change in efficiency. The subsequent change in speed is performed so as to always move in the direction of rising efficiency. This tracking technique presents the advantage of inherently taking into account the variation of the efficiency with regard to the pressure and works well if the dynamic of the pressure is lower than that of the speed.

The flow diagram of Figure 3.10b summarizes this algorithm.  $N_{lim}$  is referred to as the minimum difference between the consecutive speed measurements  $N_k$  and  $N_{k-1}$ , that ensures the convergence of Quadratic Interpolation.  $\Delta N$  denotes the speed increment.

#### 3.1.4.2. Simulation results of the MEPT strategy

Some simulations have been performed using the SIMPLORER program to evaluate the performances of the proposed maximum efficiency tracking algorithm. The irreversible losses in the system are neglected; the switching phenomena in the converter are not taken into account so that it can be modeled with ideal electric sources; the transformation in the compressed air reservoir is assumed isothermal at ambient temperature  $T_a$  and that in the air motor adiabatic. With all these assumptions, the model is not of high physical accuracy, but this simplification has no impact on the operation of the optimization strategy and is a good compromise to simulate the system operation over the whole pressure range in reasonable time.

### 3.1. Investigation and Optimization of purely pneumatic conversion units

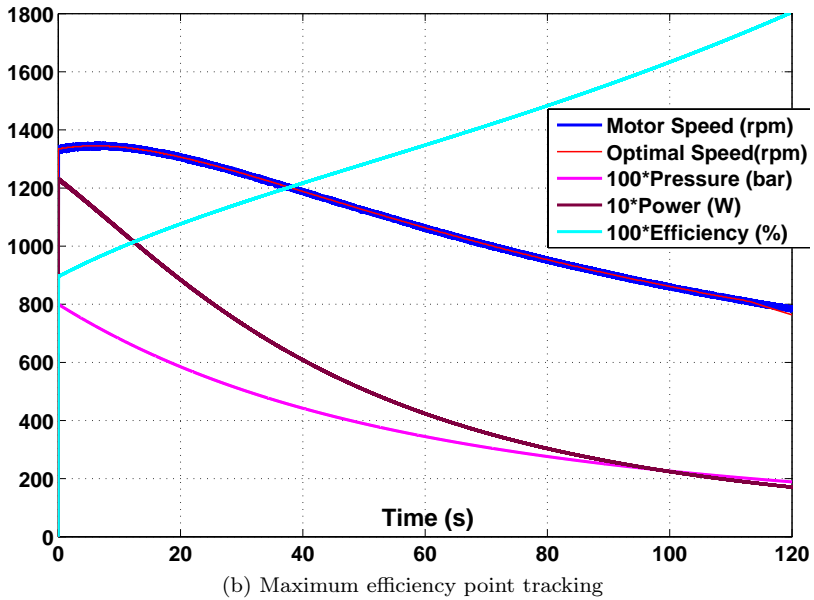
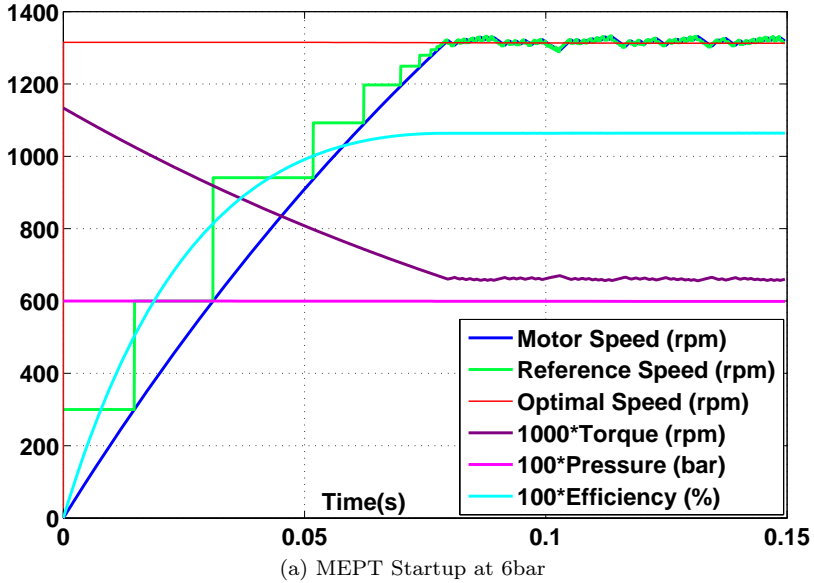


Figure 3.11.: Simulation curves of MEPT operation

The simulation curves of a startup operation at 6bar are shown in Figure 3.11a. The optimal speed  $N_{opt}$  denotes the analytical speed that corresponds to the maximum efficiency. It is obtained by deriving the expression of Equation 3.20 with respect to the speed  $N$ . It should be noted that  $N_{opt}$  is not used by the optimization algorithm, but simply represented with the simulation results in order to evaluate its performances.

The two first reference speeds are imposed at startup because at least two points are necessary to apply Quadratic Interpolation (Q-I). These first reference speeds should be chosen as low as possible to avoid going beyond the optimal speed when starting up at low pressure. As the motor approaches the optimal speed, the Q.I decreases the reference speed increment. When the speed is close to the optimal speed, the efficiency derivative with regard to speed becomes very small and the interpolation can diverge. To prevent this to happen, the algorithm switches to Perturb-and-Observe (P-O) technique when the interpolation speed increment comes below the threshold value  $N_{lim}$ . In the studied case, it has been set to  $N_{lim} = 20rpm$  which is a good compromise between the accuracy of P-O and fastness of Q-I. As can be seen on Figure 3.11a, the initial optimal speed is reached only after a few steps, which shows the accuracy and rapidity of the algorithm at startup.

The simulation curves of the tracking operation are presented in Figure 3.11b where it can be seen that the motor speed and the optimal speed are well superposed, which proves the effectiveness of the proposed tracking algorithm. The motor speed exhibits a ripple around the optimal speed; this is inherent to the P-O technique used for tracking. The amplitude for this speed ripple depends upon the speed increment  $\Delta N$  used by the tracking algorithm. It should be chosen judiciously to ensure an accurate operation of the algorithm and to avoid important mechanical constraints on the rotating parts. The Perturbation-Observation technique would operate efficiently if the smallest speed variation can always cause a perceptible efficiency variation. Around the optimal speed however, the efficiency derivative with respect to speed is almost equal to zero (what is normal for an extremum); and the effect of pressure variation is much less perceptible due the low pressure dynamic. Therefore, a very small value of  $\Delta N$  would cause the algorithm to diverge from the optimum. On the opposite side, a large  $\Delta N$  would cause important oscillations around the optimum that may provoke some mechanical constraints.

With the studied system, a smooth and accurate operation was performed with  $3rpm \leq \Delta N \leq 5rpm$ . Some experimental results recorded from the LBZ14R vane type air motor are presented in chapter 6.

One advantage of the proposed MEPT algorithm is that it is based only on measurements as can be seen on the flow diagram of Figure 3.10b and does not require any particular knowledge of the controlled machine. Hence, it can be generalized for the control of any kind of volumetric machine.

#### 3.1.5. Extension of the MEPT principle to power-controlled operating modes

The efficiency optimization strategy just presented can be easily extended to control the air motor in two power-controlled modes, namely the **Maximum Power Point Tracking (MPPT) operating mode** and the **Variable Power-Controlled operating mode**. It should be noted that these power-controlled modes will be done at the expense of the conversion efficiency: Any power requirement that imposes a different speed reference than that of maximum efficiency would obviously yield to a lower efficiency.

##### 3.1.5.1. Maximum power point tracking (MPPT) operating mode

The power characteristics of the volumetric air machine presented in Figure ?? shows the existence of a maximum power operating point. The need of maximum power can occur in case of temporary peak power demand. The speed of the motor should be therefore controlled so as to deliver the maximum power.

The behavior of the Maximum Power Point (MPP) with respect to the speed and pressure is shown in Figure 3.12 where the Maximum Efficiency Point (MEP) is represented again to ease the comparison of the two operating points. It can be seen that although the two optimums are different, they behave almost similarly. Therefore, the strategy for MEPT can be used for MPPT simply by replacing the efficiency objective function by the power function in the optimization algorithm. The resulting flow diagram is presented in Figure 3.13. The analytical optimal speed  $N_{opt}$  for the maximum power point is easily obtained through the derivation of the mechanical power Equation 3.9.

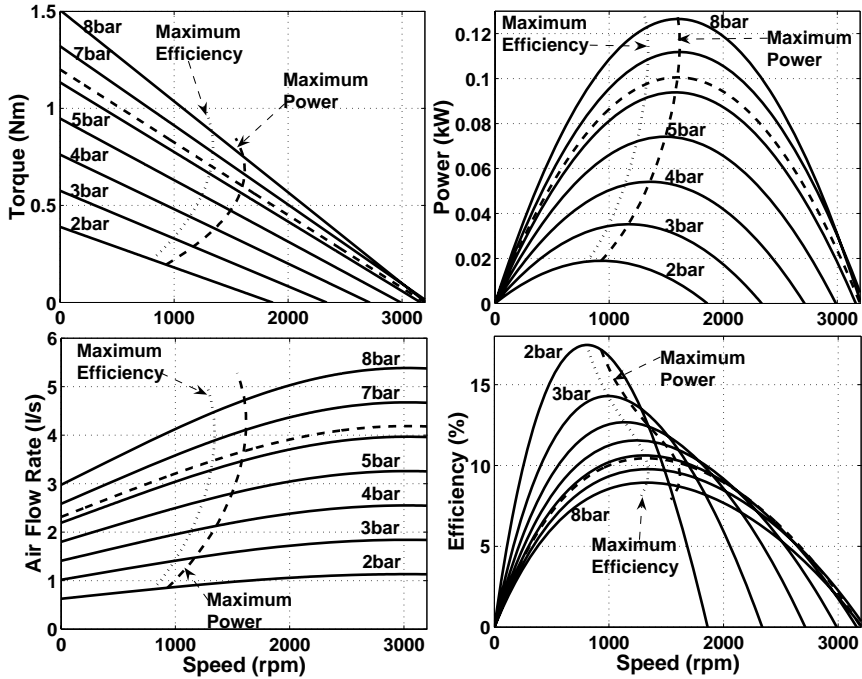


Figure 3.12.: Characteristics of the maximum power operating point

Its expression is:

$$N_{opt} = \frac{f_n N_0}{2} \tag{3.22}$$

$N_{opt}$  is represented with the simulation curves to evaluate the performances of the proposed algorithm.

The simulation results for the startup at 6bar in MPPT mode are presented in Figure 3.14a. As the modeled power expression given by Equation 3.6 is really a second order polynomial function, quadratic-interpolation is very effective in predicting the maximum power point. The reference speed curve shows that the initial optimal power point is reached only after 3 steps. As in the case of MEPT, the two first reference speeds are imposed to acquire



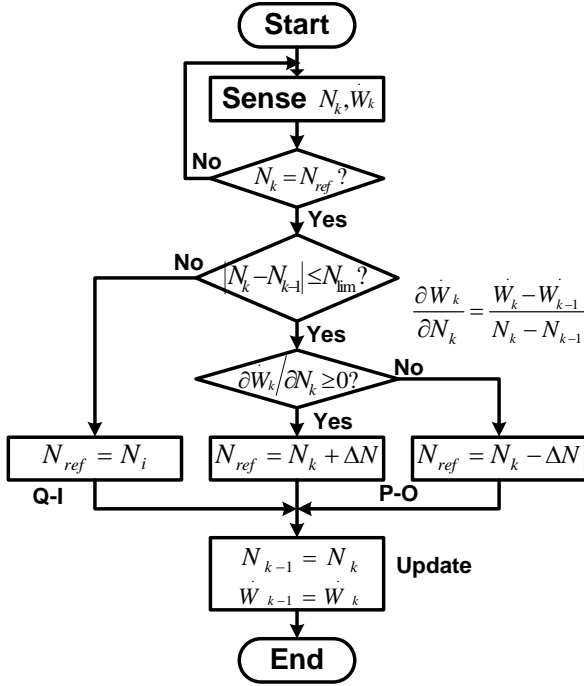
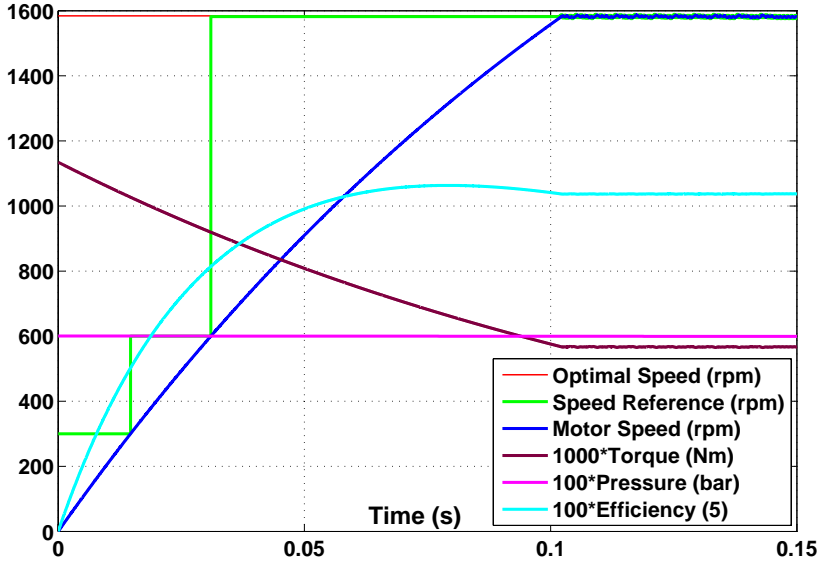


Figure 3.13.: Flow diagram of the MPPT algorithm

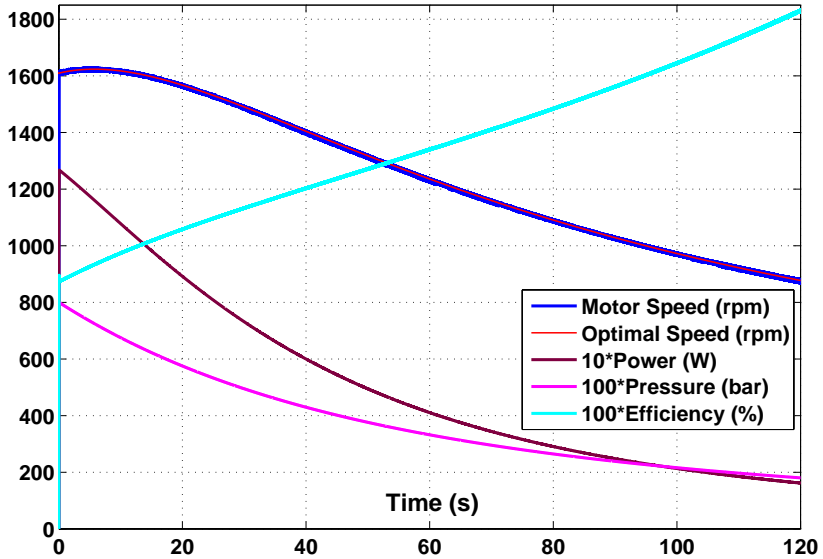
the necessary measurements for the application of interpolation equation. The interpolated reference speed for maximum power is obtained from the  $k^{th}$  and  $(k-1)^{th}$  speed  $N$  and the mechanical power  $\dot{W}m$  measurements with the following equation:

$$N_{ref} = N_i = \frac{\dot{W}m_{k-1} \cdot N_k^2 - \dot{W}m_k \cdot N_{k-1}^2}{2 \left( \dot{W}m_{k-1} \cdot N_k - \dot{W}m_k \cdot N_{k-1} \right)} \quad (3.23)$$

It can be seen on the figure that the efficiency goes through its maximum before the MPP is reached, which confirms that the MPP's efficiency is lower than the maximum efficiency achievable by the conversion system. The simulation



(a) MPPT Startup at 6bar



(b) Maximum power point tracking

Figure 3.14.: Simulation curves of MPPT operation

### 3.1. Investigation and Optimization of purely pneumatic conversion units

curves of the MPPT operation are given in Figure 3.14b. It can be seen that the analytical optimal speed and the simulated motor speed are quite well superposed, confirming the effectiveness and accuracy of the presented MEPT algorithm when used for MPPT.

#### 3.1.5.2. Variable power-controlled operating mode

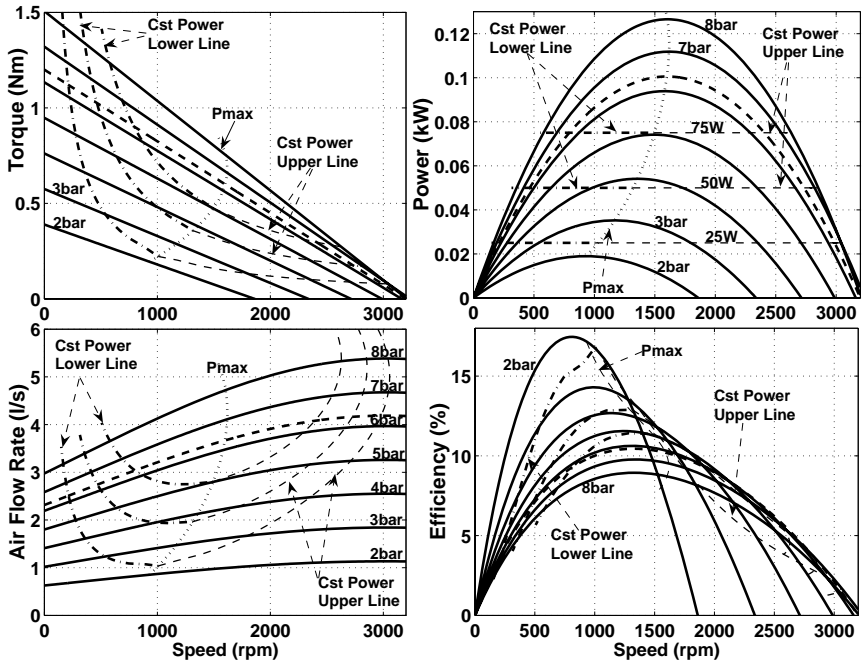


Figure 3.15.: Characteristics of the variable power-controlled operating points

Generally in electric power systems, the power generated must instantaneously balance the load consumption, unless there is an energy storage unit in the system. In autonomous applications without storage device, this requirement must be necessarily satisfied for a proper and safe operation of the system. Such operating conditions have been considered for the conversion

system that is being studied, and means of freely varying the generated power in a certain range analyzed.

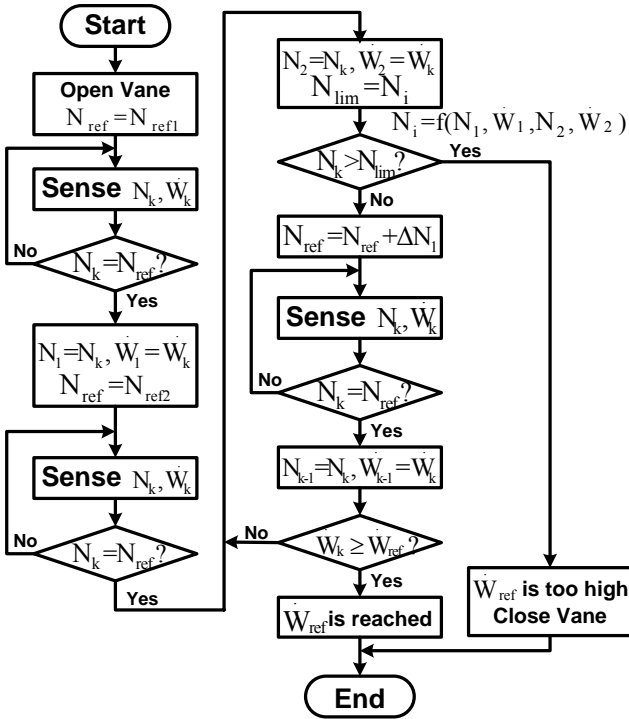


Figure 3.16.: Flow diagram of the variable power-controlled startup algorithm

Figure 3.15 presents the characteristics of three constant-power operating points. Given the quadratic shape of the power characteristic, there exist two possible operating points for each given power, let's say the “lower” and the “upper” operating points. Of both operating points, the lower one possesses the higher energy efficiency because the speed and hence air-consumption are lower; only that point will be considered in this section. As the vessel pressure decreases, the motor speed must vary to produce the same power; this leads

to the constant power operating lines that can be seen in Figure 3.15.

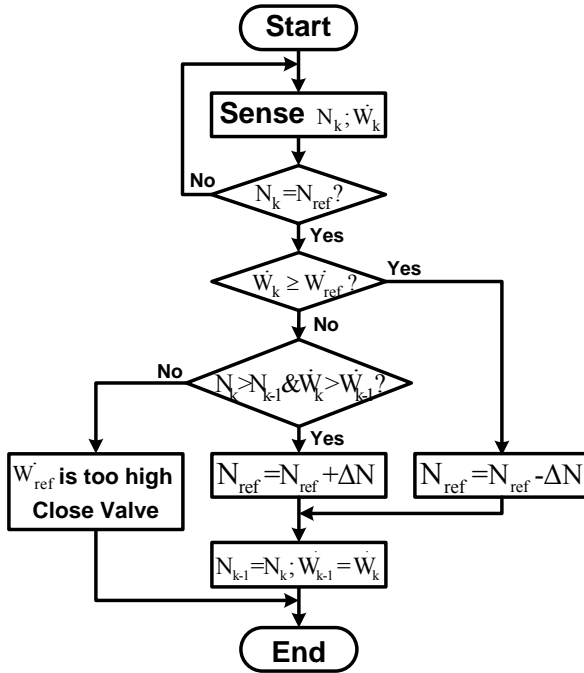


Figure 3.17.: Flow diagram of the variable power-controlled tracking algorithm

The variable power-controlled operation consists in controlling the motor speed so as to instantaneously generate any variable reference power. The flow diagrams of such a control are given in Figure 3.16 for startup and Figure 3.17 for tracking. At turn-on, 2 points are measured in order to determine the maximum power speed with Quadratic-Interpolation as it has been seen in Section 3.1.5.1. This speed is used as a border to make sure that the motor is running in the lower half part of the power characteristic. If this border is reached before the reference power is produced, it means that the desired power is too high to be produced and the system is turned off. When the

reference power is reached before the speed limit, the control switches to the tracking mode. In that mode the maximum power can be easily sensed by checking the sign of the power derivative with regards to the speed.

The simulation curves for the startup operation at 6bar and 75W power reference are given in 3.18a. The speed must be increased slowly in order to avoid going far beyond the desired power and oscillate around it. The first speed increment  $\Delta N_1$  should then be chosen judiciously. With a fixed  $\Delta N_1$ , the startup time is proportional to the startup reference power. As it can be seen, once the reference power is achieved, the speed increment is changed to  $\Delta N$  for power tracking, with  $\Delta N < \Delta N_1$ . The simulation curves for variable power-controlled operation are shown in Figure 3.18b, starting at 8bar and 50W. The figure shows that the variable reference power is well tracked, which proves the effectiveness and accuracy of the proposed algorithm.

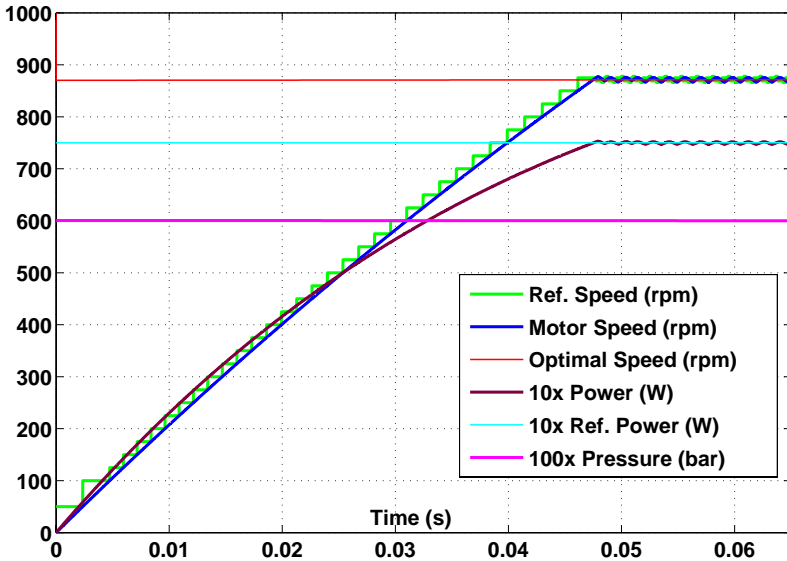
## 3.2. Investigation and optimization of hydro-pneumatic conversion systems

Despite the implementation of the optimization strategy just presented, the performances of pure pneumatic conversion systems remain unsatisfactory for storage applications, for two main reasons:

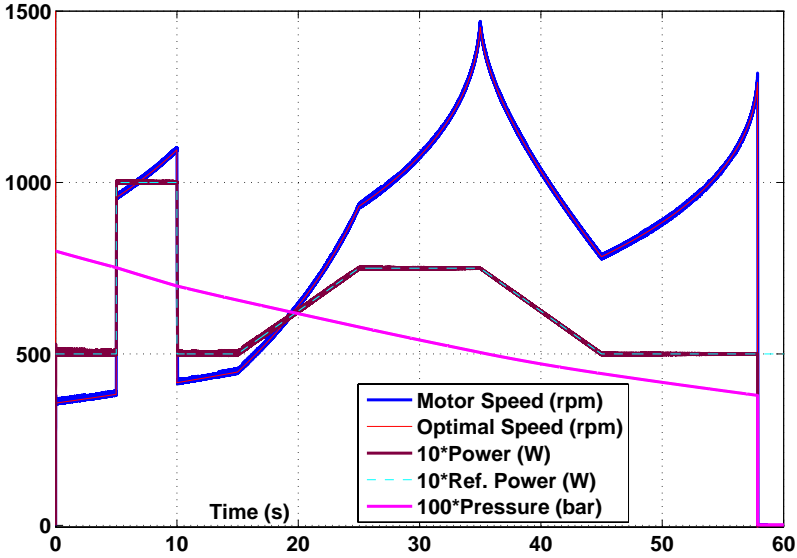
Firstly, in the low and medium power range considered in this study, the pressure ratings of volumetric machines are low (up to a few tens of bars). This pressure limitation does not allow achieving acceptable energy densities as it has been seen in Section 2.3.3.

Secondly, although some technologies of volumetric air machines like twin-screw and scroll exhibit interesting conversion efficiencies (up to 80% adiabatic efficiency), the conversion performances of the most commonly encountered machines in the considered power range remain insufficient (between 20% for low power and 60% for high power machines) for storage applications. This is due to the low thermodynamic efficiency related to non-isothermal processes taking place in these devices, and to the important leakage and friction related to the gaseous nature of air. In fact most of these machines are designed for high power density rather than energy efficiency purposes. Nevertheless with such efficiency values, the overall efficiency of pneumatic storage systems would be prohibitive given the number of conversion steps. An acceptable overall ef-

### 3.2. Investigation and optimization of hydro-pneumatic conversion systems



(a) Variable power-controlled startup at 6bar for 75W



(b) Variable power tracking

Figure 3.18.: Simulation curves of variable power-controlled operation

efficiency requires high individual efficiencies as it will be seen in chapter 4. Therefore, some technological improvements are still necessary to make volumetric air machines efficient enough for pneumatic storage applications. But in the meantime and given the urgent need of more environmentally compatible storage technology, alternative conversion solutions for pneumatic storage have been assessed.

Because of the very low compressibility of oil, hydraulic machines suffer less from the thermodynamic problems mentioned above and therefore exhibit better conversion performance. Hence, they appear as good alternative to air machines. The main difficulty in using hydraulic machines to compress or expand air is to realize an appropriate interface between the two fluids. This can be done in two ways that have led to the two hydro-pneumatic systems introduced in Section 2.2.3.2 and studied in the following sections:

1. The **B**attery with **O**il-hydraulics and **P**neumatics, type **A**: BOP-A
2. The **B**attery with **O**il-hydraulics and **P**neumatics, type **B**: BOP-B

### **3.2.1. Investigation and optimization of the hydro-pneumatic conversion for BOP-A**

#### **3.2.1.1. Principle of BOP-A: A close gas cycle hydro-pneumatic storage system**

Hydraulic accumulators are well known components in industrial applications. They are based on high-pressure steel vessels, where a trapped volume of gas (generally nitrogen) is compressed, up to 350 bars and more, by injecting oil into the shell or body. They possess a physical gas-to-oil separation device that can be a diaphragm, a bladder or a piston. Figure 3.19a shows classical accumulators as can be found from many hydraulics manufacturers. These equipments are generally designed to deliver high instantaneous power and are therefore oversized and expensive for energy storage applications as considered in this study; their design should be reviewed for that purpose.

On the other hand, hydraulic machines are highly interesting devices, because they exhibit exceptional energy conversion performances and are easily reversible (can operate as motor and as pump). In addition, their high pressure



### 3.2. Investigation and optimization of hydro-pneumatic conversion systems

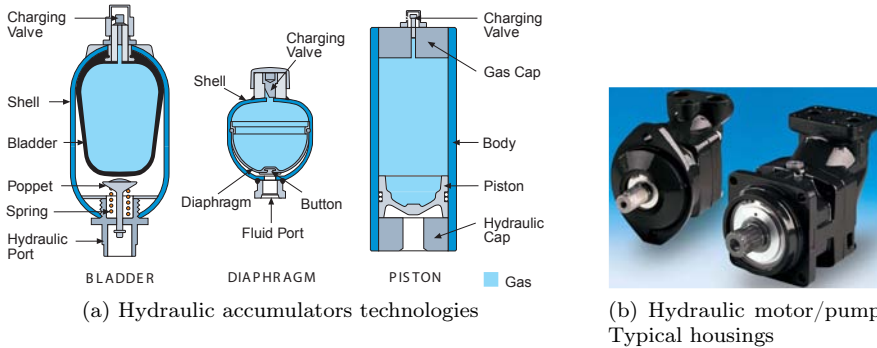


Figure 3.19.: Types of hydraulic devices used in hydro-pneumatic storage systems (Courtesy of Parker Hydraulics)

rating (in the range of several hundreds of bars) would allow reaching energy densities comparable to that of lead acid batteries. Typical housings of such machines are shown in Figure 3.19b; they are very compact device and thus possess high power densities. The efficiency characteristics of the illustrated machines in pump operation is given in Figure 3.20 which confirms their high conversion performances.

Combining these two hydraulic components, a closed gas cycle hydro-pneumatic storage system can be realized, where interesting performance can be achieved regarding energy conversion. The principle of the pneumatic-to-electric energy conversion with such a system is given in Figure 3.21. The compression and expansion processes take place in the storage volume. By operating the system in isothermal cycles as seen in Section 2.3.2, very high thermodynamic efficiencies can be easily obtained. Isothermal processes will be achieved if the “volumetric time constant”  $\tau_v$ <sup>1</sup> is much greater than thermal time constant  $\tau^2$ . In other words, this is achieved when the charging (or discharging) time of the accumulators is much greater than the time needed for the thermal exchange between the gas chamber and the external environment. Typically, photovoltaic generators would charge the accumulator within the 8 daytime hours

<sup>1</sup>The volumetric time constant can be defined as the ratio of the accumulator’s total volume  $V_0$  to the oil volumetric flow rate  $\dot{V}$ :  $\tau_v = V_0/\dot{V}$

<sup>2</sup>See Section 3.2.1.3

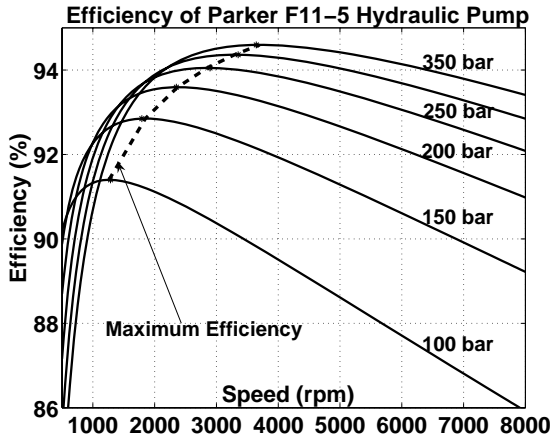


Figure 3.20.: Example of the efficiency characteristic of an oil-hydraulic machine

while the thermal exchange will need tens of minutes.

### 3.2.1.2. Principle of MEPT strategy applied to hydro-pneumatic conversion

It appears obvious from the efficiency curves of Figure 3.20 that the MEPT algorithm previously presented is necessary to achieve optimal efficiency with oil-hydraulic conversion. Figure 3.22 gives the implementation principle of the MEPT strategy on oil-hydraulic systems. As can be seen, it is similar to that of the pneumatic conversion. Given the high power necessary for the higher pressure and speed, a 3-phase electric machine would be more effective for the electric drive system.

### 3.2.1.3. Modeling the closed gas cycle hydro-pneumatic storage process

- *The gas process*

The non-flow gas processes in the hydraulic accumulator can be adequately modeled using the “Thermal Time Constant” theory introduced by Otis D. R. in 1973 [68]. The thermal time constant model is based on simple thermody-

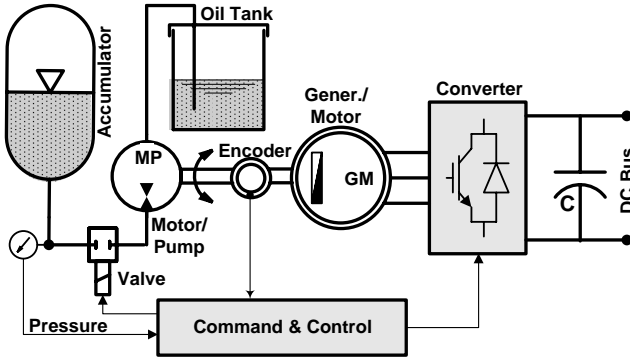


Figure 3.21.: Principle of pneumatic-to-electric energy conversion for BOP-A

dynamic and heat transfer physics. The energy equation for a closed system is given by:

$$m \frac{du}{dt} = \frac{dQ}{dt} + \frac{dW}{dt} \quad (3.24)$$

where  $m$  and  $u$  are the mass and the specific internal energy of the gas respectively. When oil is pumped into or withdrawn from the accumulator, the rate of work is given by:

$$\frac{dW}{dt} = -p \frac{dV}{dt} \quad (3.25)$$

where  $p$  and  $V$  are the gas pressure and volume, and  $dV/dt$  is the outgoing oil volumetric flow rate. The Heat transfer of the system is given by:

$$\frac{dQ}{dt} = hA_w (T_w - T) \quad (3.26)$$

where  $h$  is the convection heat transfer coefficient,  $A_w$  denotes the effective area of the accumulator for heat convection,  $T_w$  refers the accumulator wall temperature and  $T$  is the gas temperature. From Maxwell's thermodynamic relations [69]:

$$du = c_v dT + \left[ T \left( \frac{\partial p}{\partial T} \right)_v - p \right] dv \quad (3.27)$$

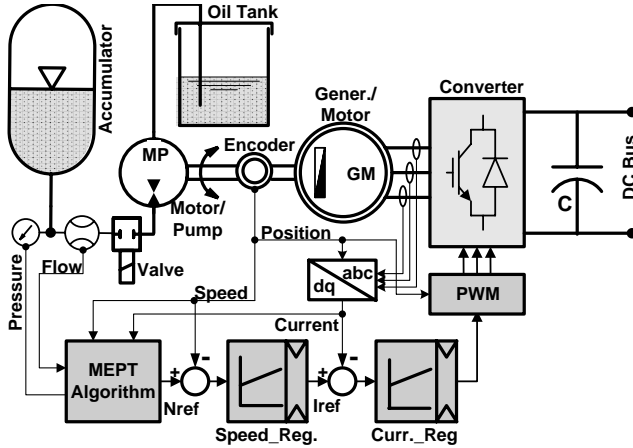


Figure 3.22.: Principle of the MEPT strategy for BOP-A

where  $v$  is the specific volume of the charged gas and  $c_v$  is the constant volume specific heat of nitrogen. Substituting equations 3.25, 3.26 and 3.27 into the energy equation 3.24 yields:

$$\frac{dT}{dt} = \frac{T_w - T}{\tau} - \frac{T}{c_v} \left( \frac{\partial p}{\partial T} \right)_v \frac{dv}{dt} \quad (3.28)$$

where  $\tau$  is the thermal time constant defined as:

$$\tau = \frac{mc_v}{hA_w} \quad (3.29)$$

$\tau$  must be determined for each particular accumulator and range of operation, either by experiments as described in [70] or by empirical analytical correlation as suggested by [70], [71] and [59]. The following correlations proposed in [59] were used in these investigations for the first estimation of  $\tau$  which was adjusted afterwards with experimental measurements:

### 3.2. Investigation and optimization of hydro-pneumatic conversion systems

---

$$\tau_0 = 1.338p_0V_0^{0.313} \quad \text{For bladder accumulators}$$

$$\tau_0 = 4.26p_0V_0^{0.56} \quad \text{For membrane accumulators}$$

$$\tau_0 = 0.3p_0V_0^{0.22} + 86.2V_0^{0.49} \quad \text{For piston accumulators}$$

where  $\tau_0(s)$ ,  $p_0(\text{bar})$  and  $V_0(m^3)$  are the thermal time constant, the initial gas pressure and gas volume at  $20^\circ\text{C}$ . The thermal time constant  $\tau$  for any initial temperature  $T_i(^\circ\text{K})$  can be derived from  $\tau_0$  with the following extrapolation:

$$\tau = \tau_0 \frac{293}{T_i}$$

The thermal time constant  $\tau$  is not really a constant, since both the convection heat transfer coefficient  $h$  and the effective area for heat transfer  $A_w$  change during the process. If a high accuracy is necessary, a new value of  $\tau$  should be computed at each simulation step; however as shown in the referenced literature, for the majority of practical cases a constant value for  $\tau$  gives satisfactory results. Therefore  $\tau$  will be considered constant in this study.

Given the high level and wide range of the operating pressure, the gas behavior is far from that of an ideal gas and the ideal gas assumption can be no more considered in this situation. Rather, the Benedict-Webb-Rubin (BWR) equation is employed to represent the p-v-T relationship [72]:

$$p = \frac{\mathcal{R}T}{v} + \left( B_o \mathcal{R}T - A_o - \frac{C_o}{T^2} \right) \frac{1}{v^2} + \frac{b \mathcal{R}T - a}{v^3} + \frac{a \alpha}{v^6} + \left[ c \left( 1 + \frac{\gamma}{v^2} \right) e^{-\gamma/v^2} \right] \frac{1}{v^3 T^2} \quad (3.30)$$

The BWR equation of state is more accurate than the common  $pV = m\mathcal{R}T$  equation for an ideal gas due to the inclusion of the 8 empirical constants  $a$ ,  $A_o$ ,  $b$ ,  $B_o$ ,  $c$ ,  $C_o$ ,  $\alpha$  and  $\gamma$ . The value of which can be found in [73]. For nitrogen in the SI unit system:  $a = 0.15703387$ ,  $A_o = 136.0474619$ ,  $b = 2.96625e - 6$ ,  $B_o = 0.001454417$ ,  $c = 7.3806143e - 5$ ,  $C_o = 1.0405873e - 6$ ,  $\alpha = 5.7863972e - 9$  and  $\gamma = 6.7539311e - 6$ .

Differentiating Equation 3.30 with respect to  $T$  and combining with Equa-

tion 3.28 gives:

$$\begin{aligned} \frac{dT}{dt} = & \frac{T_w - T}{\tau} - \frac{1}{c_v} \left[ \frac{\mathcal{R}T}{v} \left( 1 + \frac{b}{v^2} \right) + \frac{1}{v^2} \left( B_o \mathcal{R}T + \frac{2C_o}{T^2} \right) \right] \frac{dv}{dt} \\ & + \frac{1}{c_v} \left[ \frac{2c}{v^3 T^2} \left( 1 + \frac{\gamma}{v^2} \right) e^{-\gamma/v^2} \right] \frac{dv}{dt} \end{aligned} \quad (3.31)$$

The specific heat  $c_v$  at any pressure can be computed from a known value at low pressure by using the relation [69]:

$$c_v = c_v^0 + \int_{\text{inf}}^v T \left( \frac{\partial^2 p}{\partial T^2} \right)_v dv \quad (3.32)$$

The integrand is evaluated using the BWR equation of state with the following result:

$$c_v = c_v^0 + \frac{6}{T^3} \left( \frac{C_o}{c} - \frac{c}{\gamma} \right) + \frac{3c}{T^3} \left( \frac{2}{\gamma} + \frac{1}{v^2} \right) e^{-\gamma/v^2} \quad (3.33)$$

where  $c_v^0$  is the ideal gas specific heat whose temperature dependence can be accurately approximated by [72]:

$$c_v^0 = \mathcal{R} \left( \frac{N_1}{T^3} + \frac{N_2}{T^2} + \frac{N_3}{T} + (N_4 - 1) + N_5 T + N_6 T^2 + N_7 T^3 + \frac{N_8 y^2 e^y}{(e^y - 1)^2} \right) \quad (3.34)$$

with  $y = N_9/T$  and  $N_1$  to  $N_9$  are constants whose values can be found in [74]. For nitrogen:  $N_1 = -735.210$ ,  $N_2 = 34.224$ ,  $N_3 = -0.557648$ ,  $N_4 = 3.5040$ ,  $N_5 = -1.7339e - 5$ ,  $N_6 = 1.7465e - 8$ ,  $N_7 = -3.5689e - 12$ ,  $N_8 = 1.0054$ , and  $N_9 = 3353.4061$  with  $T$  in Kelvin.

It was found that for the pressure range considered in this study,  $c_v$  and  $c_v^0$  differ by less than 0.001%; therefore the pressure correction made by Equation 3.33 can be neglected. Equation 3.31 is the energy equation of nitrogen and can be numerically integrated to give the temperature history of the process. Substituting  $T$  and  $v$  into Equation 3.30 will give the pressure history of the same process. This method of modeling is proven to be much more accurate than the polytropic model  $PV^n = \text{constant}$ .

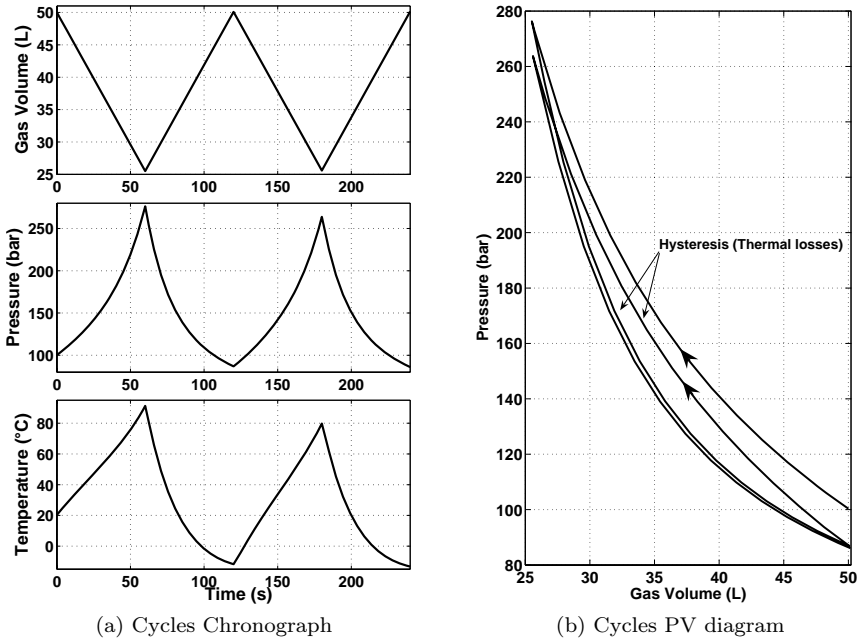


Figure 3.23.: Simulation curves of a bladder accumulator's charge-discharge cycle

The model requires only one input, the oil flow rate, while the gas pressure and temperature are the two outputs. It was implemented with Matlab/Simulink simulation tools and Figure 3.23 displays the simulation results of some constant flow rate charge-discharge cycles, for a bladder accumulator from the initial condition defined by:  $V_0 = 50L$ ,  $p_0 = 100bar$  and  $T_0 = 20^\circ C$ . The “hysteresis” behavior that illustrates the thermal losses can be easily seen on the cycle's PV-diagram, a phenomenon that the ideal gas models are unable to show.

- *The oil-hydraulic machine*

The hydraulic machine is the key element of the pneumatic-to-mechanical energy conversion process. As the simulations aim to evaluate the effectiveness

of the MEPT strategy for the optimization of that conversion, the hydraulic machine's model should allow computing its efficiency so as to implement that optimization strategy. The model's two input variables are the pressure  $p$  and the speed  $N$ , while the two main outputs are the mechanical torque  $M_m$  and the oil flow rate  $\dot{V}$ . In motor operation, the mechanical torque  $M_{mm}$  generated is given by [75], [62]:

$$M_{mm} = \eta_{hm} \frac{pCyl}{2\pi} \quad (3.35)$$

where  $\eta_{hm}$  denotes the hydro-mechanical efficiency, and  $Cyl$  the displacement. The oil volumetric flow rate  $\dot{V}_m$  is given by:

$$\dot{V}_m = \frac{NCyl}{\eta_{vol}} \quad (3.36)$$

where  $\eta_{vol}$  is the volumetric efficiency. Finally the motor mechanical power  $\dot{W}_{mm}$  is defined by:

$$\dot{W}_{mm} = M_{mm}\omega = \eta_m p \dot{V}_m \quad (3.37)$$

where  $\omega$  is the angular velocity (rad/s) and  $\eta_m$  is the total motor efficiency.

The main difficulty in building the model is to obtain all the data necessary to determine the various efficiencies, which depend upon pressure, speed and motor's technology. Finally the same approach like in the case of the air motor was adopted and the hydraulic machine's quasi-static model was built on the basis of the experimental measurements provided by the manufacturer [76]. For the experimental machine, the following correlations were obtained for the mechanical torque  $M_{mm}$  and oil flow rate  $\dot{V}_m$  in motor operation, as well as in pump operation,  $M_{mp}$  and  $\dot{V}_p$  respectively:

### For motor operation

$$M_{mm} = c_{mm1}N + c_{mm2} \quad (3.38)$$

$$c_{mm1} = k_{mm11}p + k_{mm12}$$

$$c_{mm2} = k_{mm21}p + k_{mm22}$$

$$\dot{V}_m = c_{vm1}N + c_{vm2} \quad (3.39)$$

$$c_{vm1} = k_{vm11}p + k_{vm12}$$

$$c_{vm2} = k_{vm21}p + k_{vm22}$$



The efficiency  $\eta_m$  for motor operation is therefore given by:

$$\eta_m = \frac{2\pi N M_{mm}}{p \dot{V}_m} \quad (3.40)$$

#### For pump operation

$$M_{mp} = c_{mp1}N + c_{mp2} \quad (3.41)$$

$$c_{mp1} = k_{mp11}p + k_{mp12}$$

$$c_{mp2} = k_{mp21}p + k_{mp22}$$

$$\dot{V}_p = c_{vp1}N + c_{vp2} \quad (3.42)$$

$$c_{vp1} = k_{vp11}p + k_{vp12}$$

$$c_{vp2} = k_{vp21}p + k_{vp22}$$

The efficiency  $\eta_p$  for pump operation is therefore given by:

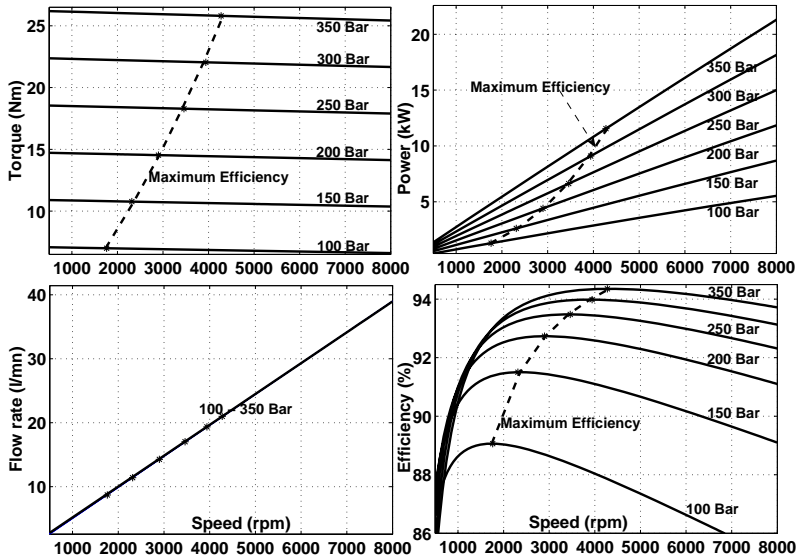
$$\eta_p = \frac{p \dot{V}_p}{2\pi N M_{mp}} \quad (3.43)$$

The constants  $k_{xnn}$  in Equation 3.38 to 3.42 describe the pressure dependence of the characteristics while the constants  $c_{xnn}$  describe their speed dependence. These constants are obtained by polynomial interpolation of the measurements.

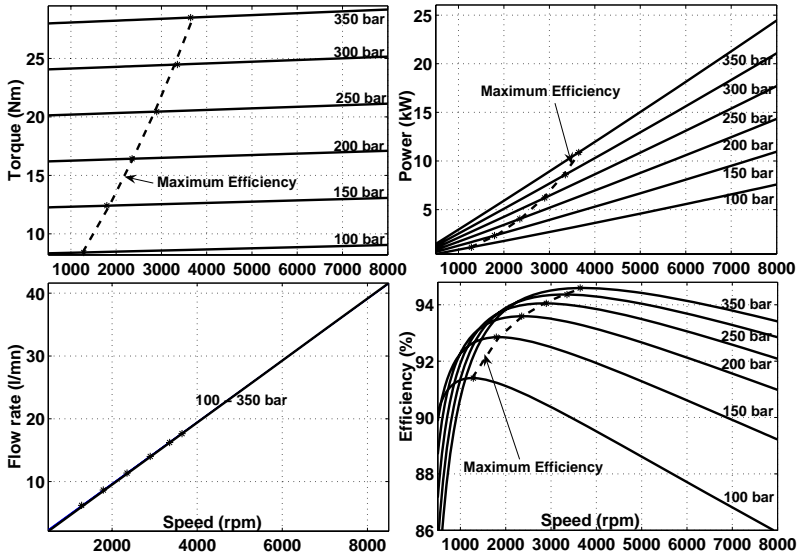
The representation of these characteristics is given in Figure 3.24. It can be seen that the flow rate is almost independent of the pressure as, oil is a nearly incompressible fluid; the pressure dependence of the flow rate can therefore be ignored.

- **The AC electrical drive system**

A simplified model of the electrical drive system composed of speed and current regulators, an ideal 3-phase 2-level IGBT frequency converter and a permanent magnet synchronous (PMS) machine is built using the “SimPowerSystems” and “PLECS” toolboxes of Matlab/Simulink. The losses and switching phenomena in the drive system are not taken into account because a detailed model of this system is not necessary at this point. The issue is to be able to control the speed of the hydraulic machine through the electric drive



(a) F11-5 characteristics in motor operation



(b) F11-5 characteristics in pump operation

Figure 3.24.: Characteristics of the Parker F11-5 oil-hydraulic motor/pump

system. Basic principles of the control method used for the PMS machine are given in Annexe A.

- ***The MEPT algorithm***

The MEPT algorithm is similar to the one of the purely pneumatic system described by the flow diagram of Figure 3.10b. As explained in Section 3.1.4.1, the MEPT algorithm aims at controlling the hydraulic machine's speed so as to keep it on the "maximum efficiency line" represented on Figure 3.24 during the variable pressure operation. The MEPT flow diagram is implemented in Matlab/Simulink using the "StateFlow" toolbox.

### 3.2.1.4. Simulation results of MEPT strategy applied to hydro-pneumatic conversion

Figure 3.25 presents the simulation curves for a charge-discharge cycle of a bladder accumulator in MEPT conditions, from the initial pressure of 100bar to the final pressure 200bar. The analytical optimal speed (dash line) is again represented to ease the appreciation of the MEPT algorithm performances; it is not used by the algorithm.

The startup speeds graph on the left show that the initial optimal speed is reached only after a few steps like in the case of volumetric air machine. The tracking graphs on the right show that the real and analytical optimal speeds are well superposed, which confirms the effectiveness and accuracy of the MEPT algorithm with oil-hydraulic conversion too.

It can be noticed that by the end of the storage phase, the speed ripple becomes more important. This is due to the higher pressure dynamics related to the exponential increase of the gas pressure. At that time, the efficiency change due to a pressure change becomes more important than that due to the speed increment and the algorithm needs more speed increments in each direction to detect the maximum efficiency. It should be noted that such a situation does not occur in normal operation since the processes are more likely isothermal and under such conditions the pressure dynamics are much lower. It was just simulated to see the limits of the proposed algorithm.

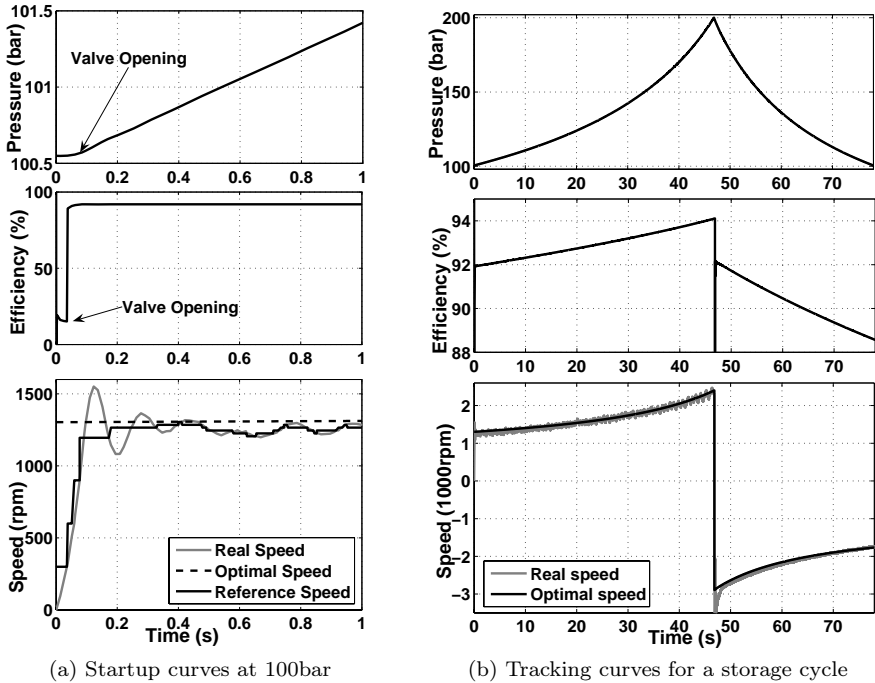


Figure 3.25.: Simulation curves for MEPT strategy applied to BOP-A

### 3.2.1.5. Limitations of BOP-A

The main advantages of BOP-A are the high efficiency of the conversion unit and the simplicity of the air-oil interface. However, the closed nitrogen cycle together with the large external vessel needed for the storage of the compressing oil lead to a very low energy density as it as be demonstrated in Section 2.3.3.2 (about  $2.5kWh/m^3$  with a maximum pressure of 400bar, see Figure 2.18). Because of this low energy density, the BOP-A system is more suitable for low energy capacity applications or stationary applications where volume and weight are not critical.

It has been stated in Section 2.3.3.4 that an open gas cycle and a high pres-

sure are necessary to obtain high energy density, and the study of BOP-A has shown that hydraulic machines are the key element to achieve high conversion efficiencies. A storage system fulfilling these two requirements would be quite interesting from an energy density point of view as well from an efficiency one. Such a system called BOP-B, is described in Section 3.2.2, as well as in [35] and [36].

### 3.2.2. Principle of BOP-B: An open gas cycle hydro-pneumatic storage system

The BOP-B system aims at compressing and later expanding fresh air from outside by means of an oil-hydraulic system using a very reduced amount of oil. In this system, the compression and expansion processes take place in reciprocating “liquid-piston” working chambers. Almost isothermal processes necessary for high thermodynamic efficiencies are achieved by integrating heat exchangers in these working-chambers. The working principle of such a converter is shown in Figure 3.26 in a simplified manner in order to explain the sequences of one cycle.

During discharge (expansion), the compressed air enters through the opened valve (D), the work-chamber (1R) of the right cylinder comprising the liquid piston (2R); the said valve (D) being controlled so as to admit exactly the quantity of compressed air which, once expanded, will reach the atmospheric pressure. The pressure established in the right cylinder is transmitted through the exchanger coil (3R) to the hydrostatics (4), passing through the four-way-valve (5). This valve remains in position (b) and thus activates the motor port. This leads to the expulsion of the air in the work-chamber (1L) by the return flow of (4), which enters the muffler (6) through the opened valve (B). The air in the right-hand work-chamber (1R) squeezes into the tight spaces between metal plates when expanding; these metal plates just emerge from the thermally stabilized liquid, so any cooling down of the air is strongly limited (the same would happen during compression, where a temperature rise would be limited, as the external exchanger (3R) always tends towards the surrounding temperature of the fan air flow). As the stroke ends, the 4-Way Valve (5) inverts the flow by switching to the position (a) without changing the rotational direction of the hydraulic motor, the inertia of the liquid pistons being negligible.

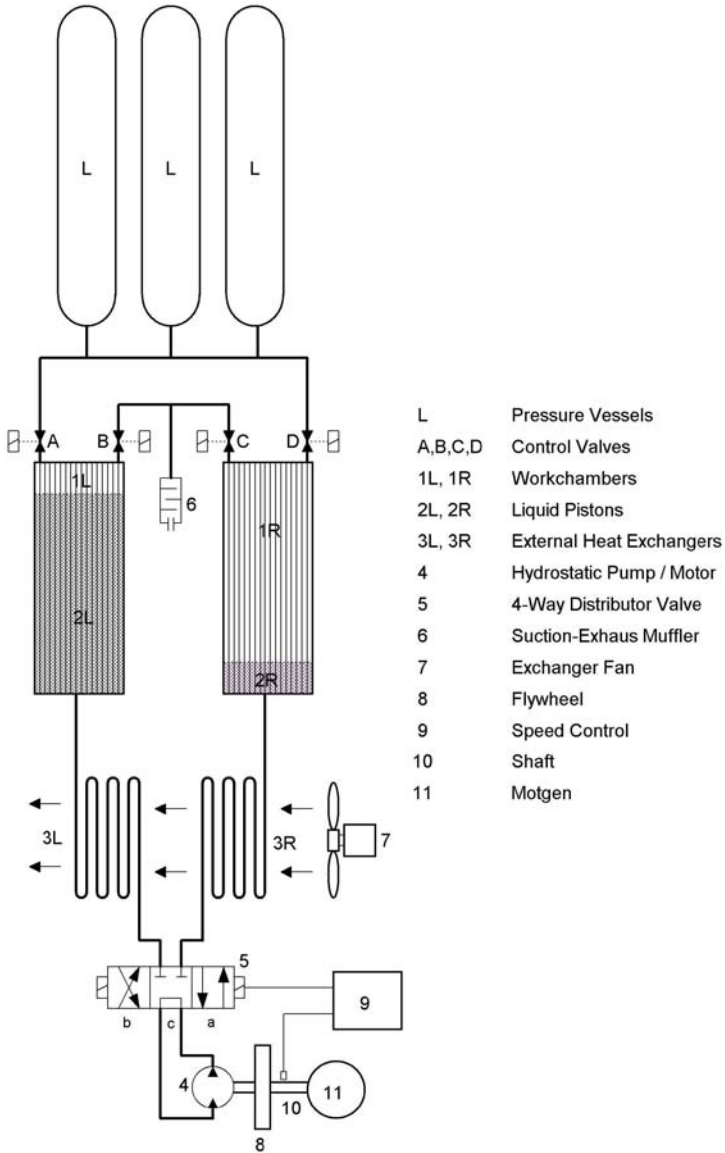


Figure 3.26.: Layout of “BOP-B”: open gas cycle hydro-pneumatic storage system (Courtesy of Cyphelly & Cie)

The system works the same way in both direction (i.e during storage or compression). The operation mode can be reversed without changing the rotational direction of the drive train, thanks to the 4-way distributor valve (5) and the control valve (A, B, C, D). The open-gas cycle together with the reduced amount of oil yield volumetric energy density of about 30Wh/l for a maximum pressure of 250bar (See Figure 2.19b) and a specific energy from 20Wh/kg for steel vessels to 50Wh/kg Carbon fiber wounded vessels, which is competitive with lead acid batteries.

The BOP-B appears as the final configuration of hydro-pneumatic storage systems investigated in this project because of its high energetic and conversion performances. But its detailed study is out of the scope of this thesis because of the necessary deep thermal and thermodynamics analysis. However, at the moment this report is written, theoretical studies are being carried on, in the fields of thermodynamics, heat & mass transfer, and power electronics & control, to optimize the design, simulate and evaluate the performances of pneumatic-to-mechanical conversion based on liquid-piston with integrated heat exchanger. Some experiments have started to characterize the appropriate liquid to be used in the liquid-piston units. This is a multidisciplinary project in which three laboratories of the Energy Sciences Institute of EPFL are involved: The Laboratory for Industrial Energy System (LENI) for thermodynamic analysis, the Heat & Mass transfer Laboratory (LICM) for heat transfer analysis, and the Industrial Electronics Laboratory (LEI) for energy conversion and system control. The results of this joint-venture study will be presented in further contributions.

### 3.3. Chapter summary

In this chapter, a pneumatic-to-mechanical energy conversion system based on a volumetric air machine has been investigated and some efficiency optimization strategies proposed. Firstly, the pressure regulator valve has been suppressed to avoid the important losses in these devices. Secondly, the analysis of the efficiency characteristics of an air machine has shown the existence of a pressure-dependent optimal speed that corresponds to the maximum efficiency. A maximum Efficiency Point Tracking (MEPT) strategy has been proposed to optimize the conversion efficiency through speed variation. Simulation results have proved the effectiveness and accuracy of this MEPT strategy that

has been extended to control the volumetric machine in two power-controlled modes.

Despite the proposed optimization strategies, the conversion efficiency of most volumetric machines remains low, what is inherent to their design and the gaseous nature of air. Hydraulic machines have appeared as good alternatives as they exhibit very high conversion efficiency. A hydro-pneumatic storage system called “BOP-A” and based on classical hydraulic accumulators and machines has been presented and studied. The analysis of the efficiency characteristic of these machines has shown a shape similar to that of air machines. Hence, the MEPT strategy has been applied to oil-hydraulic conversion and the simulation results have confirmed its effectiveness in that context too. Thus, the proposed strategy is universal for the optimization of the operation of any kind of volumetric machine.

The main limitation of BOP-A is the low energy density due to the closed gas cycle. A more promising hydro-pneumatic system called BOP-B, that combines an open gas cycle and an oil-hydraulic conversion system for high energy density and high conversion efficiency has been introduced. A detailed study of this system is still going on and will be presented in further contributions.

The MEPT strategy proposed in this chapter imposes the level of the generated or stored power, which may not be compatible with the source or load powers. The means of circumventing this constraint have led to the hybrid energy storage concept that is studied in Chapter 4.



## 4. Principle of Hybrid Energy Storage Systems based on Pneumatics and Supercapacitors

By imposing the rotational speed of volumetric machine, the MEPT algorithm imposes the level of the converted power, which may not always balance the source and load powers. The available source power may depend upon uncontrollable factors like weather in the case of renewable sources or daytime in the case of grid connected storage systems. As for the load power, it would depend upon the users activity and may exhibit strong dynamics. Therefore the storage system must possess a certain power flexibility to be able to fulfill the application requirements.

In this chapter, the concept of hybrid energy storage that allows achieving the necessary power flexibility is presented and the strategy to vary the output power is analyzed. The hybridization of the storage leads to a more complex topology. This is the reason why the overall system efficiency is calculated and analyzed to evaluate the effect of this topology complexity on the system performances. Finally, different topologies of the hybrid storage systems for various application contexts are proposed and commented.

## 4.1. Concept of hybrid compressed air and supercapacitor energy storage (CASCES)

### 4.1.1. Principle of hybrid CASCES system

The idea of associating a “high capacity energy storage media” (compressed air) and a high power density storage device (Supercapacitors) was first implemented in the context of an off-line UPS system whose principle is given in Figure 4.1. This system was used for the first investigations on CASCES technology, even though the energy efficiency of the volumetric air machine was known to be very low (See Figure 3.8). The main goal of these investigations was to develop methods for operating that family of pneumatic energy converters at their optimal efficiency conditions, as it has been presented in Chapter 3.

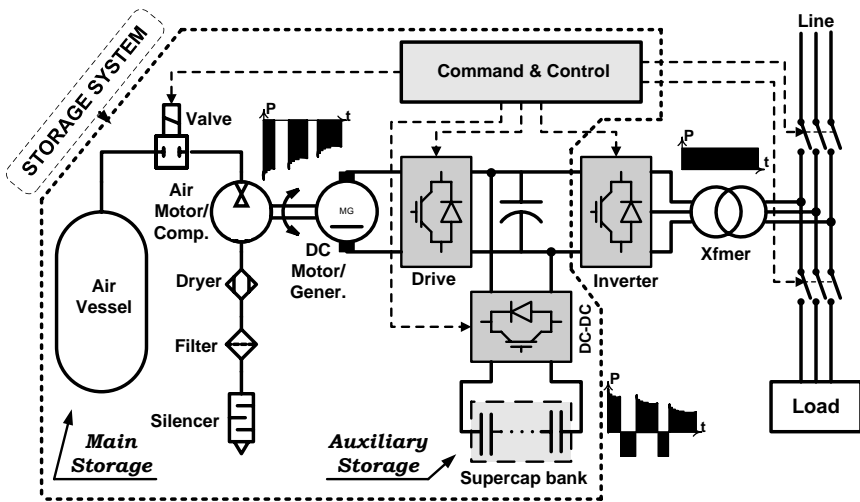


Figure 4.1.: Principle of CASCES system

All the devices of the system are assumed to be reversible. During the storage process, the electric machine works as a motor and drives the pneumatic machine, which operates as a compressor to fill the vessel with pressurized

air. During the discharge process, the compressed air is directly expanded in the pneumatic machine, which operates as a motor to power the DC generator. The following technical solutions, presented in Chapter 3, have been implemented to improve the efficiency of the pneumatic energy conversion:

- There is no pressure regulation device between the air tank and the air machine in order to avoid the additional losses in such a device as shown in Section 3.1.1. The motor inlet pressure therefore varies continuously.
- The MEPT strategy presented in Section 3.1.4 is used to control the volumetric air machine through variable speed, so as to always keep it at the maximum efficiency operating point.

The consequence of the implementation of these efficiency optimization strategies is the loss of the possibility of freely varying the converted power. To circumvent this limitation, the following technical solutions have been adopted:

- An intermittent time-modulated operation is applied to pneumatic-to-electric conversion subsystem to modulate the converted power in function of the source and load powers. The result is a pulsating power whose mean value is equal to the sum of the source and load powers.
- A supercapacitive auxiliary storage is then added to the pneumatic storage which serves as a filter to obtain a smoothly variable, high quality output power. This results in the hybrid CASCES system.

The operation of the system during discharge is well illustrated by the “black” power profiles represented in Figure 4.1. The strategy to provide it with power flexibility is presented in detail in Section 4.1.2.

## 4.1.2. Strategy for output power variation

### 4.1.2.1. Principle of power variation

The strategy of output power variation is described considering only the discharge process, but the approach is identical for the storage process. As explained in Section 4.1.1, the variation of load power  $P_{ld}$  is based on the intermittent, time-modulated operation of the pneumatic-to-electric conversion chain. The excess of the converted power  $P_{cv}$  is stored in the supercapacitors and later used to supply the load during the stop-time of the said conversion

chain, or as power-assistance during peak power demand. The control scheme of the power variation strategy is presented in Figure 4.2.

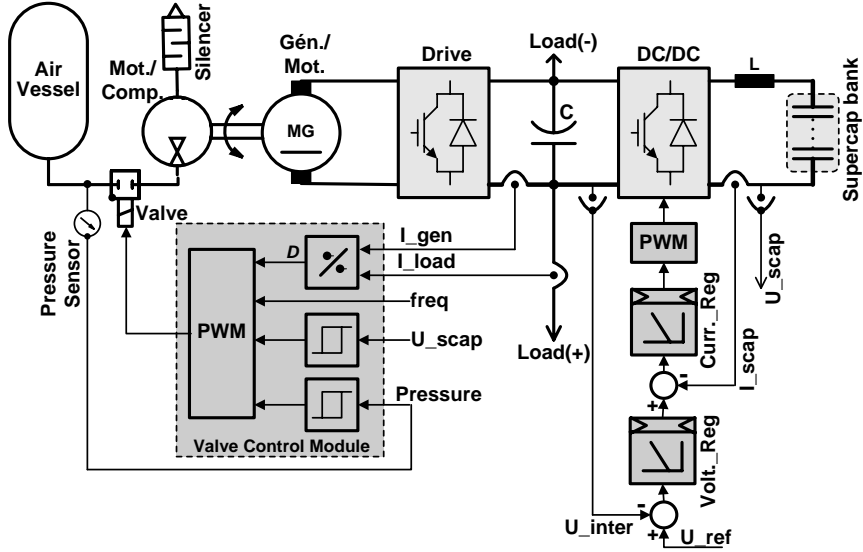


Figure 4.2.: Principle of output power variation

By maintaining the intermediary DC bus voltage  $U_{inter}$  constant, the voltage regulator automatically compensates the lack or excess of the generated power, allowing thus the output power to vary freely. The time-modulated on-off operation of the pneumatic energy conversion is achieved thanks to the electrovalve control module. There are two possible power modulation modes:

- The Fixed-frequency power modulation mode.
- The Free-oscillating power modulation mode.

#### 4.1.2.2. Fixed-frequency power modulation mode

In this mode, the on-off cycle period  $T$  is constant. The converted energy  $W_{cv}$  is then proportional to the duty cycle ratio  $D$  as shown in Figure 4.3.

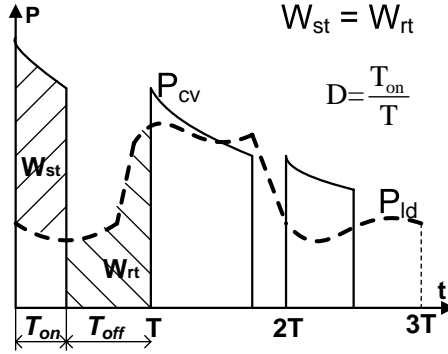


Figure 4.3.: Principle of power modulation

As the reservoir pressure drops, the converted power  $P_{cv}$  decreases. If the auxiliary storage is assumed lossless and the system suitably controlled, the energy  $W_{st}$  stored during the running time  $T_{on}$  would be equal to the energy  $W_{rt}$  restored to the load during the stop time  $T_{off}$ .

$$W_{st} = W_{rt} \Leftrightarrow \int_0^{D \cdot T} P_{cv} dt = \int_0^T P_{ld} dt \quad (4.1)$$

For simplification, the produced power  $P_{cv}$  and the load power  $P_{ld}$  are assumed constant during the on-off cycle  $T$ . Therefore, the duty cycle can be deduced from equation 4.1 as:

$$D = \frac{P_{ld}}{P_{cv}} \quad (4.2)$$

Since it is not possible to predict the behavior of the load power,  $D$  is determined once at the beginning of each cycle using equation 4.2. This approach is effective only if the cycle period  $T$  is small enough compared to the "power variations time constant". It may however happen that the load power increases strongly within a cycle in such a way that the stored energy  $W_{st}$  becomes insufficient to supply the load. In that case, the pneumatic energy conversion chain is turned on as soon as the minimum allowable value  $U_{min}$  of the supercapacitive bank voltage  $U_{scap}$  is reached. It is also turned off at its maximum value  $U_{max}$  and at the minimum operating pressure  $p_{min}$  as can be

seen on Figure 4.2.

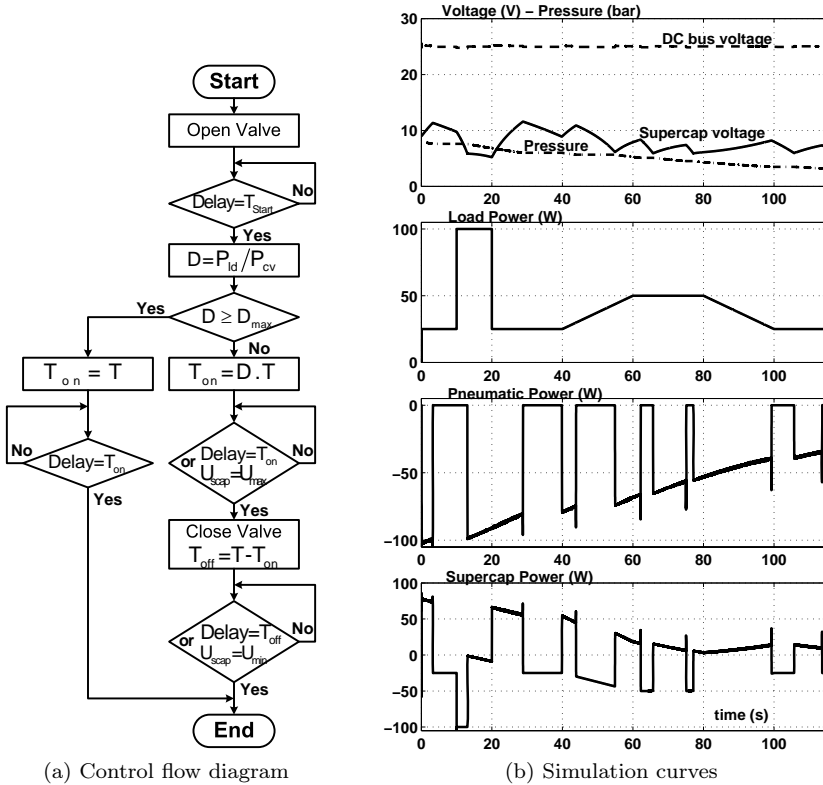


Figure 4.4.: Control and simulation of fixed-frequency power modulation mode

The control of this modulation mode is summarized in the flow diagram of Figure 4.4a. A delay time  $T_{start}$  must be observed after the valve opening to allow the establishment of steady conditions before the duty cycle ratio can be measured. For proper operation, a minimum off-time  $T_{off}$  must pass after the valve closing before the pneumatic conversion chain can be turned on again. This minimum time corresponds to a maximum duty cycle  $D_{max}$ . When the

measured duty cycle  $D$  is greater than  $D_{max}$ , the conversion chain is kept running for the whole cycle period  $T$  and a new cycle is started without turning it off.

The simulation results are presented in Figure 4.4b. As it can be seen, the cycle period is not always constant, particularly when the load power is high and the supercapacitive bank discharged.

#### 4.1.2.3. Free-oscillating power modulation mode

In this mode, the on-off cycle period is never constant. The only control parameter is the supercapacitive bank voltage  $U_{scap}$ . When it reaches the minimum value  $U_{min}$ , the pneumatic energy conversion chain is turned on and when it reaches the maximum value  $U_{max}$ , it is turned off. As the intermediary voltage is held constant, the cycle period and duty cycle are automatically fitted to the ratio  $P_{ld}/P_{cv}$ . This control strategy which is the simplest way to modulate the produced power, is summarized in the flow diagram of Figure 4.5a.

The simulation curves of this power modulation mode are presented in Figure 4.5b. It can be seen that, for the same load power profile, the number of switchings of the pneumatic conversion chain is lower than that of the fixed-frequency mode.

### 4.1.3. Principle of hybrid energy storage system based on hydro-pneumatics and supercapacitors

Purely pneumatic storage systems (i.e with air machine) have been the basis of the study and development of optimization and control strategies presented so far, mainly because of their simplicity. However, their low efficiency makes them inappropriate for any practical storage application. For that reason further investigations will be focused on hydro-pneumatic systems, for which higher practical potentials exist.

The concept of associating compressed air and supercapacitors can obviously also be applied to the two hydro-pneumatic storage systems studied in chapter 3. This association will lead to the two hybrid storage systems whose

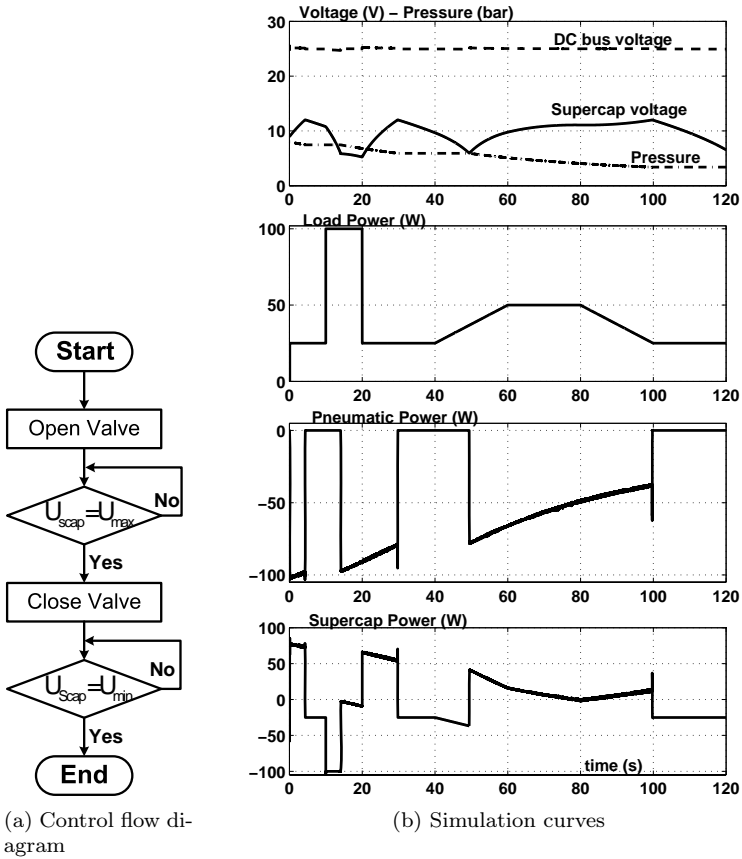
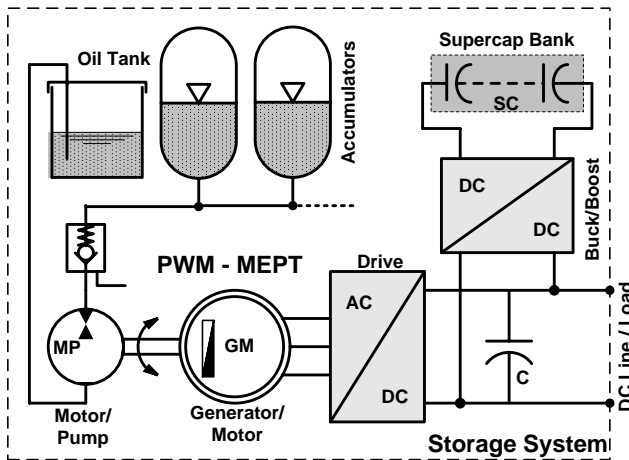


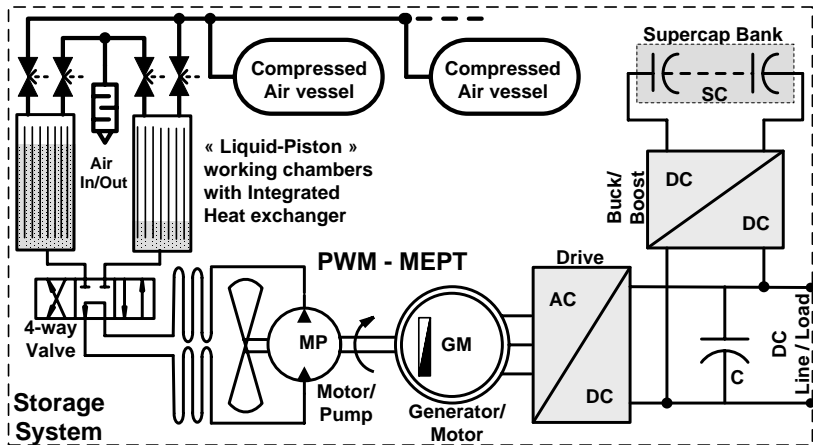
Figure 4.5.: Control and simulation of free-oscillating power modulation mode



4.1. Concept of hybrid compressed air and supercapacitor energy storage (CASCES)



(a) hybrid, closed gas cycle hydro-pneumatics and Supercapacitors storage system



(b) hybrid, open gas cycle hydro-pneumatics and Supercapacitors storage system

Figure 4.6.: Schematic diagrams of hybrid, hydro-pneumatics and supercapacitors storage systems

simplified diagrams are depicted in Figure 4.6.

The supercapacitive auxiliary storage will play the same role like in the CASCES system, i.e filtering the pulsating converted power to provide a smoothly variable high quality output power. Moreover in this case of hydro-pneumatic systems, it will also play the important role of “*Power adapter*”. In fact, the pressure rating is much higher than for the purely pneumatic systems; the power required for the optimal operation will therefore be also higher. On the other hand, particularly for renewable energy applications, the source and load power level would be, at least at certain times, much lower than the required or generated pneumatic power. The auxiliary storage is therefore necessary to “*boost*” the power during the storage phase and to “*attenuate*” it during the discharge phase.

## 4.2. Evaluation and analysis of the cycle efficiency for the global hybrid storage system

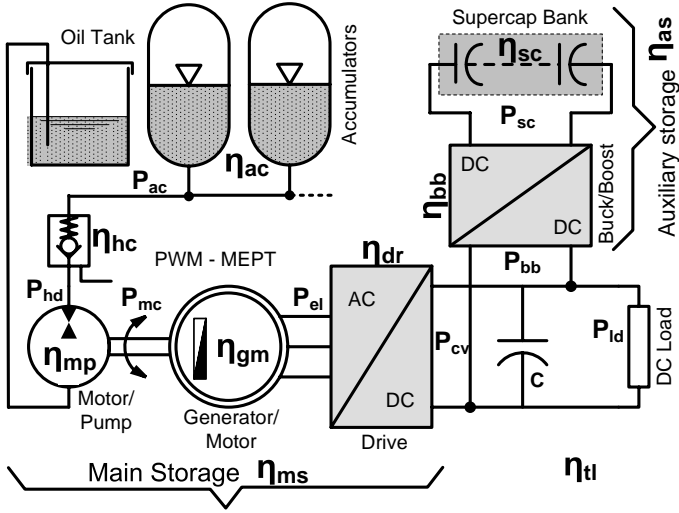
The operation of the hybrid storage system implies energy passing several times through different types of lossy converters. Knowing the effects of the topology and the main design parameters on the overall efficiency of the system can help optimizing these aspects.

### 4.2.1. Expression of the overall system cycle efficiency

The evaluation of the overall system efficiency will be based on the hybrid closed gas cycle hydro-pneumatic storage system presented in Figure 4.6a. Only the discharge (expansion) phase will be considered, but the analysis is identical for the storage phase. The power and efficiency variables that determine the system efficiency are presented in Figure 4.7.

Simplified power profiles for 3 on-off periods during the discharge operation is illustrated in Figure 4.8. This illustration considers a constant load power  $P_{ld}$  and the free-oscillating power modulation mode. Remember that in this mode, the time  $T_{on}$  is controlled by the “Depth Of Discharge (DOD)” of the

4.2. Evaluation and analysis of the cycle efficiency for the global hybrid storage system



(a) Power and efficiency variables

$\eta_{ac}$ : Accumulators Efficiency	$P_{ac}$ : Accumulators Power
$\eta_{hc}$ : Hydraulic Circuit Efficiency	$P_{hd}$ : Hydraulic Power
$\eta_{mp}$ : Motor/Pump Efficiency	$P_{mc}$ : Mechanical Power
$\eta_{gm}$ : Generator/Motor Efficiency	$P_{el}$ : Electric AC Power
$\eta_{dr}$ : Drive Converter Efficiency	$P_{cv}$ : Converted DC Power
$\eta_{ms}$ : Main Storage Efficiency	$P_{bb}$ : Buck/Boost Power
$\eta_{bb}$ : Buck/Boost Efficiency	$P_{sc}$ : Supercap Power
$\eta_{sc}$ : Supercap Bank Efficiency	$P_{ld}$ : Load Power
$\eta_{as}$ : Auxiliary Storage Efficiency	$\eta_{tl}$ : Total Efficiency (1 way)

(b) Nomenclature

Figure 4.7.: Main variables for the hybrid storage system's overall efficiency evaluations

supercapacitors bank; the frequency is therefore not constant.

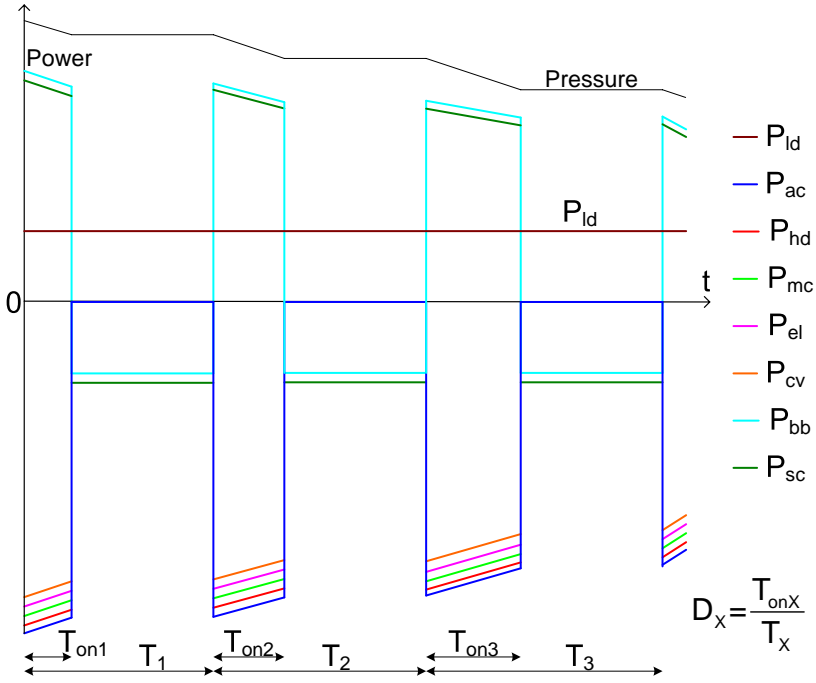


Figure 4.8.: Simplified power profiles during the discharge operation mode

The system efficiency is evaluated for 1 on-off period  $T$ . All the units are assumed perfectly reversible, i.e the efficiency is independent of the power flow direction. The total efficiency  $\eta_{tl}$  is defined as:

$$\eta_{tl} = \frac{W_{ld}}{W_{rie}} = \frac{\int_0^T P_{ld} dt}{\int_0^{T_{on}} \dot{W}_{rie} dt} \quad (4.3)$$

where  $W_{ld}$  denotes the load energy during the period  $T$  and  $W_{rie}$  is the pneumatic energy available in the accumulators. The later corresponds to the

reversible isothermal expansion energy whose expression is given by Equation 2.6. The accumulator efficiency  $\eta_{ac}$  can be simply defined as:

$$\eta_{ac} = \frac{W_{ac}}{W_{rie}} = \frac{\int_0^{T_{on}} P_{ac} dt}{\int_0^{T_{on}} \dot{W}_{rie} dt} \quad (4.4)$$

where  $W_{ac}$  refers to as the hydraulic energy at the accumulators output.  $\eta_{hc}$  is relevant of the energy losses in the hydraulic circuit, which includes the electro-valve, the filter and the pipes.  $\eta_{mp}$ ,  $\eta_{gm}$  and  $\eta_{dr}$  represent the energy efficiency of the hydraulic machine, the electric machine and drive converter respectively. They are defined similarly as  $\eta_{ac}$ . Further, the main storage subsystem's efficiency  $\eta_{ms}$  is defined as:

$$\begin{aligned} \eta_{ms} &= \frac{W_{cv}}{W_{rie}} = \frac{W_{ac}}{W_{rie}} \frac{W_{hd}}{W_{ac}} \frac{W_{mc}}{W_{hd}} \frac{W_{el}}{W_{mc}} \frac{W_{cv}}{W_{el}} \\ &= \eta_{ac} \eta_{hc} \eta_{mp} \eta_{gm} \eta_{dr} \end{aligned} \quad (4.5)$$

where  $W_{cv}$ ,  $W_{el}$ ,  $W_{mc}$ ,  $W_{hd}$  denote respectively the converted dc electric energy, the generated ac electric energy, the mechanical energy and the hydraulic energy at the hydraulic motor's inlet port. The load energy  $W_{ld}$  during the whole period  $T$  can be written as:

$$W_{ld} = \int_0^{T_{on}} P_{ld} dt + \int_{T_{on}}^T P_{ld} dt = W_{ld_{Ton}} + W_{ld_{Toff}} \quad (4.6)$$

where  $W_{ld_{Ton}}$  and  $W_{ld_{Toff}}$  denote the load energies during the periods  $T_{on}$  and  $T_{off}$  respectively. During the time  $T_{on}$ , the excess  $W_{st}$  of the converted energy  $W_{cv}$  is stored in the auxiliary storage device and restored as  $W_{rt}$  during the time  $T_{off}$  to feed the load. These energies are then defined as:

$$W_{st} = W_{cv} - W_{ld_{Ton}} = \eta_{ms} W_{rie} - W_{ld_{Ton}} \quad (4.7)$$

$$W_{rt} = W_{ld_{Toff}} \quad (4.8)$$

In the considered power modulation mode, the supercapacitors bank's voltage varies in the same range ( $U_{min}$ ,  $U_{max}$ ) during the charge and discharge of the bank; therefore the energy effectively stored in the supercapacitors cells during the charge is totally restored during the discharge. This leads to the following relationship:

$$\eta_{bb} \eta_{sc} W_{st} = \frac{W_{rt}}{\eta_{bb} \eta_{sc}} \iff \eta_{as} W_{st} = \frac{W_{rt}}{\eta_{as}} \implies W_{rt} = \eta_{as}^2 W_{st} \quad (4.9)$$

where the auxiliary storage subsystem's efficiency  $\eta_{as}$  is defined as :

$$\eta_{as} = \eta_{bb}\eta_{sc} \quad (4.10)$$

$\eta_{bb}$  and  $\eta_{sc}$  are respectively the buck-boost converter's efficiency and the the supercapacitors bank's efficiency. Introducing Equations 4.9 and 4.7 into Equation 4.6 would give:

$$W_{ld} = \eta_{ms}W_{rie} + \frac{\eta_{as}^2 - 1}{\eta_{as}^2}W_{ld_{T_{off}}} \quad (4.11)$$

For simplification, the proportionality relation of Equation 4.12 is assumed valid. This relation is true in the case of a constant load power  $P_{ld}$  as represented in Figure 4.8. It will induce negligible error in the more often encountered case where the cycle period  $T$  is small enough compared to the "load power variation's time constant".

$$\frac{W_{ld}}{T} = \frac{W_{ld_{T_{on}}}}{T_{on}} = \frac{W_{ld_{T_{off}}}}{T_{off}} = P_{ld} \quad (4.12)$$

From this relation,  $W_{ld_{T_{on}}}$  and  $W_{ld_{T_{off}}}$  can be expressed in function of  $W_{ld}$  as:

$$W_{ld_{T_{on}}} = DW_{ld} \quad (4.13)$$

$$W_{ld_{T_{off}}} = (1 - D)W_{ld} \quad (4.14)$$

where  $D$  is the duty cycle as defined in Section 4.1.2.2. Replacing  $W_{ld_{T_{off}}}$  in Equation 4.11 would result in the final expression of the global system efficiency:

$$\eta_{tl} = \frac{W_{ld}}{W_{rie}} = \frac{\eta_{ms}\eta_{as}^2}{1 + D(\eta_{as}^2 - 1)} = \frac{\eta_{ac}\eta_{hc}\eta_{mp}\eta_{gm}\eta_{dr}(\eta_{bb}\eta_{sc})^2}{1 + D[(\eta_{bb}\eta_{sc})^2 - 1]} \quad (4.15)$$

## 4.2.2. Analysis of the global system efficiency

The expression 4.15 shows that the global system efficiency  $\eta_{tl}$  is proportional to the main storage efficiency  $\eta_{ms}$  and to the square of the auxiliary storage efficiency  $\eta_{as}$ . This "square" relation is due to the fact that the auxiliary storage is charged and discharged during each on-off period  $T$ . Hence,  $\eta_{as}$  would

appear to the “power 4” in the round trip efficiency expression. An optimal design and operation of the auxiliary storage is therefore crucial for a high global system efficiency.

It can be seen from Equation 4.5 that  $\eta_{ms}$  is the product of 5 individual efficiencies of the different units of the main storage subsystem. Similarly, Equation 4.10 shows that  $\eta_{as}$  is the product of the efficiency of the 2 units of the auxiliary storage. The number of units of each subsystem should be therefore reduced to the strict minimum depending upon the application requirements, and each unit should exhibit the highest possible efficiency to expect an acceptable value for  $\eta_{tl}$ .

To estimate the order of magnitude of  $\eta_{tl}$  for the topology considered in this analysis, it is assumed that all the units exhibit a 95% efficiency 1 way. This assumption is pessimistic of some units like the accumulators and hydraulic circuit that would exhibit higher efficiency if well sized. It is realistic for other units like hydraulic machine and power electronics, and is a bit optimistic for some other units like electric machine that would require some R&D improvements to guaranty such a value. Under this assumption, the total efficiency is given by:

$$\eta_{tl} = \frac{0.95^9}{1 + D(0.95^4 - 1)} = \frac{0.63025}{1 - 0.1855 * D} \quad (4.16)$$

The duty cycle  $D = T_{on}/T$  can vary in the range  $[0, 1]$ . The value  $D = 0$  (i.e  $T_{on} = 0$ ) would correspond to the improbable case where the load is supplied from the auxiliary storage during the whole cycle period  $T$ . The value  $D = 1$  (i.e  $T_{on} = T$ ) would correspond to the case where the auxiliary storage is not used and the load feeded from the main storage during the whole period  $T$ . Thus,  $D$  is relevant of the “degree of solicitation” of the auxiliary storage.

With the assumption that all the unit’s efficiencies are independent of the power flow direction, the on-off round-trip efficiency  $\eta_{rt}$  would be obtained simply by squaring  $\eta_{tl}$ . An estimation of  $\eta_{rt}$  in the same conditions as for  $\eta_{tl}$  is then equal to:

$$\eta_{rt} = \eta_{tl}^2 = \left[ \frac{0.95^9}{1 + D(0.95^4 - 1)} \right]^2 = \frac{0.3972}{(1 - 0.1855 * D)^2} \quad (4.17)$$

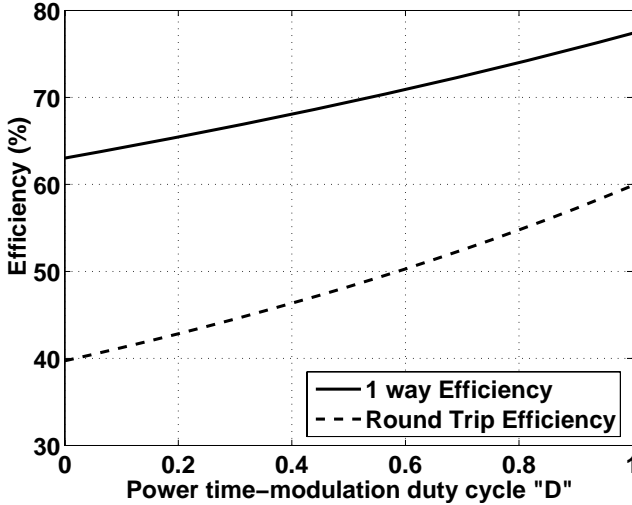


Figure 4.9.: Estimated global efficiency of hybrid BOP-A with supercapacitors storage system

From Figure 4.9, it can be seen that  $\eta_{tl}$  would lay between 63% and 77% while  $\eta_{rt}$  would lay between 40% and 60%. With the assumption made in Section 4.1.2.2,  $D$  can be also approximated by the ratio  $D = P_{ld}/P_{cv}$ . In the case of a constant load power  $P_{ld}$ ,  $D$  depends mainly on the converted power  $P_{cv}$  which in turn is determined by the pressure and the speed in the main storage subsystem. This means that during the discharge phase for instance,  $D$  would vary in the range  $D_{min} = P_{ld}/P_{cv_{max}}$  for the maximum pressure and  $D_{max} = P_{ld}/P_{cv_{min}}$  for the minimum pressure. The effective total 1 way energy efficiency  $\eta_{e1w}$  would be therefore the integral mean-value of the on-off period efficiency during the whole charge or discharge period  $T_{1way}$ :

$$\eta_{e1w} = \frac{\int_{D_{min}}^{D_{max}} \eta_{tl} dT}{T_{1way}} \quad (4.18)$$

It should be noted that the efficiency of some components depends strongly upon their operating point which may vary enough within one on-off period  $T$



or the 1-way period  $T_{1way}$ . Therefore, real efficiency would be obtained only by measurements.

### 4.3. Possible layouts of the hybrid hydro-pneumatic and supercapacitor storage system

The analysis carried out in Section 4.2.2 has highlighted the impacts of the system's topology, characterized by the number of conversion units and their arrangement, on its efficiency. Beside the efficiency constraint, the load requirements and source characteristics are other criteria that should be taken into considerations when designing the storage system. In this section, some possible layouts of the hybrid storage system will be presented and briefly commented. For simplicity, the layouts are presented with the closed gas cycle hydro-pneumatic system (BOP-A), but are also applicable to the open gas cycle hydro-pneumatic system (BOP-B).

#### 4.3.1. Layout A

*Direct coupling of hydraulic and electric machines with optional power electronic converters.*

- **Description**

A simplified diagram of this configuration is given in Figure 4.10. There is no auxiliary storage device. The electric machine must be sized for hydraulic peak power.

- **Power features**

There would be no power flexibility without the power electronic converters: the speed is imposed by the line/load frequency and the power by the pressure. With the power electronic converters, it is possible to vary the output power in a limited range

Typical power range: From kilowatts (kW) to several Megawatts (MW).

- **Efficiency features**

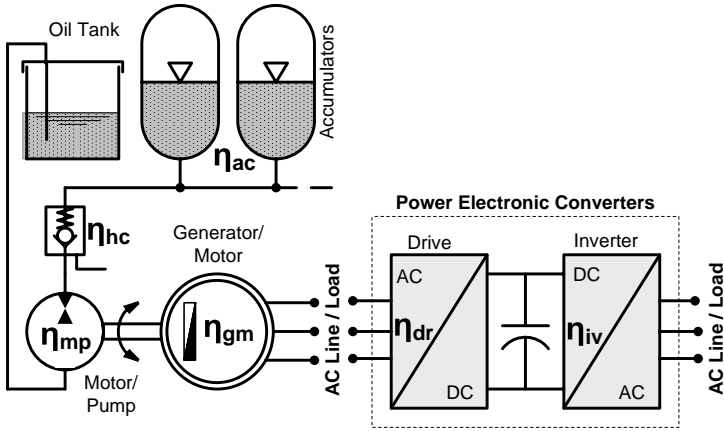


Figure 4.10.: Simplified diagram for layout A

The expression of the total efficiency for 1-way operation is:

$$\eta_{tA} = \eta_{ac}\eta_{hc}\eta_{mp}\eta_{gm}\eta_{dr}\eta_{iv} \quad (4.19)$$

The system would exhibit high efficiency due to the reduced number of components.

- **Typical applications**

Layout A would be well adapted mainly to grid applications, typically for *Grid Boost* and *Peak Power Shaving*.

### 4.3.2. Layout B

*Direct coupling of the electric machine to a variable displacement hydraulic machine.*

- **Description**

A simplified diagram of this configuration is given in Figure 4.11. There is no auxiliary storage device too and the electric machine must be sized again

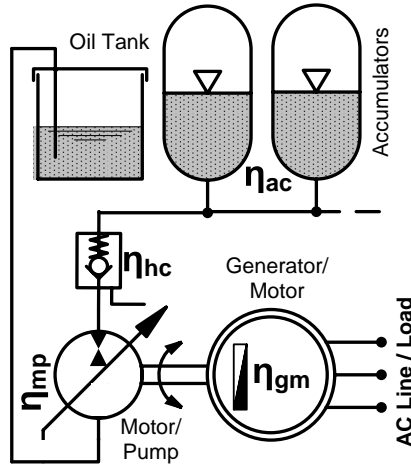


Figure 4.11.: Simplified diagram for layout B

for hydraulic peak power.

- **Power features**

The system presents a high power flexibility thanks to the variable displacement hydraulic machine, which plays the role of the power electronic converters in layout A, in a wider power range.

Typical power range: From kilowatts (kW) to several Megawatts (MW).

- **Efficiency features**

The expression of the total efficiency for 1-way operation is:

$$\eta_{tl_B} = \eta_{ac}\eta_{hc}\eta_{mp}\eta_{gm} \quad (4.20)$$

The system would exhibit high efficiency due to the reduced number of units. However, this efficiency will decrease at low power (speed) because of the low efficiency of the variable displacement hydraulic machine in that condition.

- **Typical applications**

Grid injection of renewable energies and grid power quality.

### 4.3.3. Layout C

Direct coupling of hydraulic and electric machines, and interfaced supercapacitive auxiliary storage.

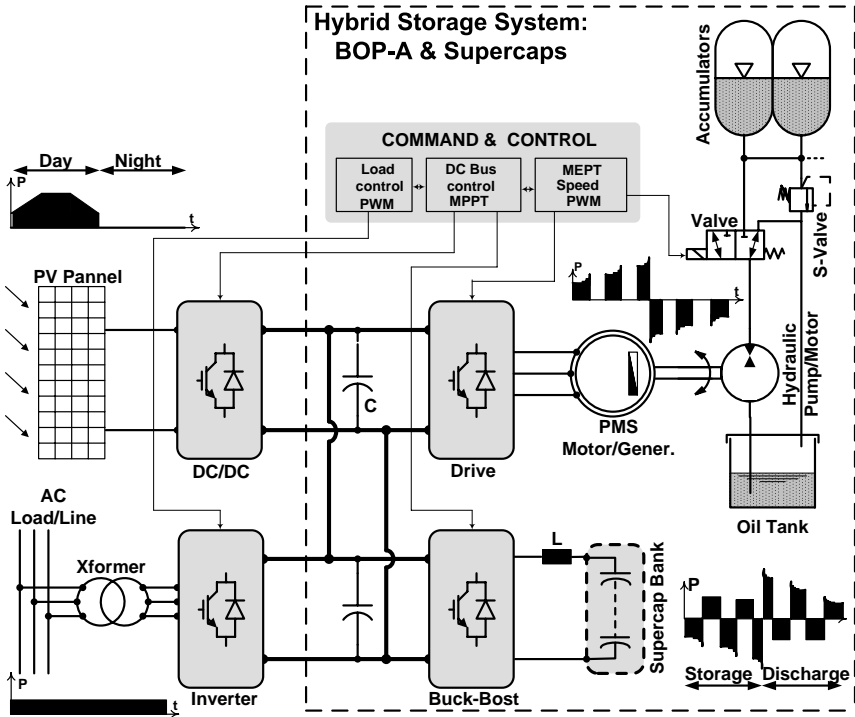


Figure 4.12.: Simplified diagram for layout C in the context of a PV application

• *Description*

A simplified diagram of this configuration is given in Figure 4.12 in a possible configuration for a stand alone or grid connected photovoltaic application. The power profiles (in black) illustrate the operation of the system, that can be controlled by a single DSP-based command & control module. Practical

results of the operation of this storage system are presented in Chapter 6.

This system possesses a supercapacitive downstream auxiliary storage system interfaced with a DC-DC converter to the DC bus. The electric machine must be sized for the hydraulic peak power as it is directly coupled to the hydraulic machine.

- ***Power features***

As seen in Section 4.1.2, the system presents a high power quality and flexibility thanks to the PWM operation and interfaced auxiliary storage which maintains the DC Bus voltage constant.

Typical power range: From a few to several hundreds kilowatts (kW).

- ***Efficiency features***

The expression of the total efficiency for 1-way operation is given by Equation 4.15 as:

$$\eta_{tl_C} = \frac{\eta_{ac}\eta_{hc}\eta_{mp}\eta_{gm}\eta_{dr}(\eta_{bb}\eta_{sc})^2}{1 + D \left[ (\eta_{bb}\eta_{sc})^2 - 1 \right]} \quad (4.21)$$

The efficiency is optimized with the MEPT algorithm and the system presents high no-load efficiency because the main storage subsystem would be operated only for very short time.

- ***Typical applications***

This Layout exhibits constant output DC voltage; it will be appropriated for high power quality DC applications.

#### 4.3.4. Layout D

*Direct coupling of hydraulic and electric machines, and non-interfaced supercapacitive auxiliary storage.*

- ***Description***

A simplified diagram of this configuration is given in Figure 4.13. As it can be seen, it is similar to that of Layout C except that the supercapacitors bank is directly inserted in the DC bus, saving thus the cost and losses of a DC-DC

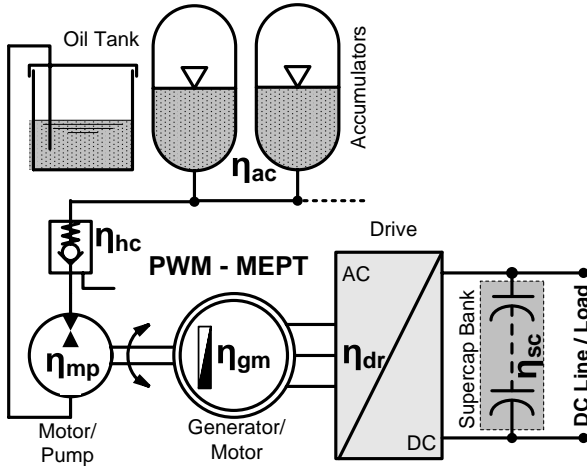


Figure 4.13.: Simplified diagram for layout D

converter.

- **Power features**

The system presents a high power flexibility as well as Layout C, thanks to the PWM operation and auxiliary storage. However the power quality is not as good because the DC bus voltage fluctuates.

Typical power range: From few to several hundreds kilowatts (kW).

- **Efficiency features**

The expression of the total efficiency for 1-way operation is:

$$\eta_{tlD} = \frac{\eta_{ac}\eta_{hc}\eta_{mp}\eta_{gm}\eta_{dr}\eta_{sc}^2}{1 + D(\eta_{sc}^2 - 1)} \quad (4.22)$$

$\eta_{tlD}$  is higher than  $\eta_{tlC}$  for, the term  $\eta_{bb}$  has been removed. The efficiency is optimized with the MEPT algorithm and the standby efficiency is high as the main storage subsystem would be operated only for very short time too.

- **Typical applications**

Typical applications would be low voltage DC applications that allow at least 10% voltage fluctuation. For instance, such a system would easily replace batteries in PV applications.

### 4.3.5. Layout E

*Indirect coupling of the electric machine to hydraulic machine through flywheel and clutch.*

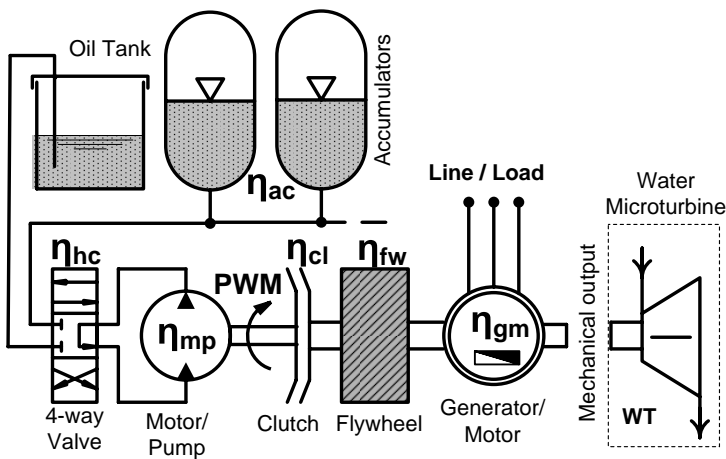


Figure 4.14.: Simplified diagram for Layout E in the context of a mini water hydraulic application

- **Description**

A simplified diagram of this topology is given in Figure 4.14. As can be seen this layout can provide a mechanical output for a turbine or any other mechanical application. It possesses a flywheel upstream auxiliary storage. As the the electric machine is not directly coupled to the hydraulic machine, it is sized for the output peak power, which may substantially reduce its size.

- **Power features**

The system presents a high power flexibility thanks to the PWM operation and auxiliary storage.

Typical power range: From a few to several hundreds kilowatts (kW).

- **Efficiency features**

The expression of the total efficiency for 1-way operation is:

$$\eta_{tl_E} = \frac{\eta_{ac}\eta_{hc}\eta_{mp}\eta_{cl}\eta_{gm}\eta_{fw}^2}{1 + D(\eta_{fw} - 1)} \tag{4.23}$$

This layout would exhibit low standby efficiency due to the always rotating parts.

- **Typical applications**

Typical applications would be low power water hydraulic (Mini-Pelton).

### 4.3.6. Layout F

*Indirect coupling of the electric machine to hydraulic machine through flywheel, and non-interfaced supercapacitive auxiliary storage.*

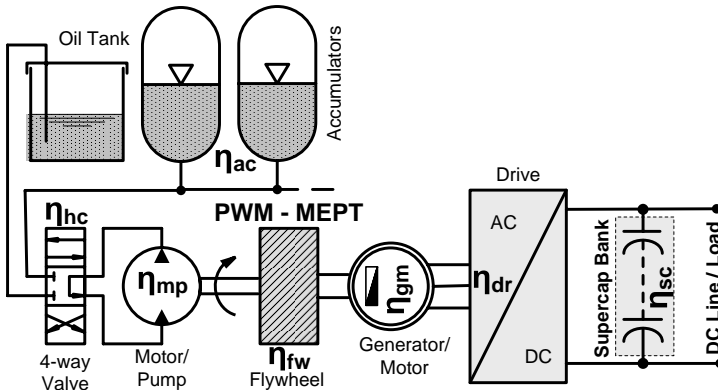


Figure 4.15.: Simplified diagram for Layout F



- **Description**

A simplified diagram of this configuration is given in Figure 4.15. The system possesses a flywheel upstream auxiliary storage and a downstream supercapacitive auxiliary storage directly inserted in the DC bus. The indirect coupling allows sizing the electric machine for the output power which is much lower than the hydraulic power. The supercapacitors allow stopping the rotating machines when they are not fully used, thus the standby losses present in layout E are completely avoided and the efficiency increased.

- **Power features**

The system presents a high power flexibility thanks to the PWM operation and auxiliary storage.

Typical power range: From a few to several hundreds kilowatts (kW).

- **Efficiency features**

The expression of the total efficiency for 1-way operation is:

$$\eta_{tl_F} = \frac{\eta_{ac}\eta_{hc}\eta_{mp}\eta_{fw}\eta_{gm}\eta_{dr}\eta_{sc}^2}{1 + D(\eta_{sc}^2 - 1)} \quad (4.24)$$

The efficiency is optimized with the MEPT algorithm and the standby efficiency is high since the main storage subsystem would be turned off for long period.

- **Typical applications**

Typical applications would be low voltage DC applications that allow at least 10% voltage fluctuation.

### 4.3.7. Layouts comparison

Layouts A and B are non-hybrid layouts since they possess no auxiliary storage systems unlike the 4 other topologies. They are presented simply to illustrate the important possibilities offered by the hydro-pneumatic storage technology for electrical energy applications.

Tables 4.1 and 4.2 summarize the main characteristics of the 4 hybrid topologies just presented to ease their comparison.

Layout	Description	Power features	Efficiency features	Typical Applications
<b>C</b>	<p>Direct coupling of hydraulic and electric machines</p> <ul style="list-style-type: none"> <li>• Downstream interfaced supercapacitive auxiliary storage</li> <li>• Electric machine sized for hydraulic power</li> </ul>	<ul style="list-style-type: none"> <li>• High power flexibility thanks to PWM operation and auxiliary storage</li> <li>• High power quality thanks to constant DC Bus voltage</li> <li>• Typical range: Several kW</li> </ul>	<ul style="list-style-type: none"> <li>• Equation 4.21</li> <li>• High efficiency at no-load</li> <li>• Efficiency optimization thanks to MEPT algorithm</li> </ul>	<ul style="list-style-type: none"> <li>• DC Applications with high power quality requirements (low output voltage ripple)</li> </ul>
<b>D</b>	<p>Direct coupling of hydraulic and electric machines</p> <ul style="list-style-type: none"> <li>• Downstream non-interfaced supercapacitive auxiliary storage</li> <li>• Electric machine sized for hydraulic power</li> </ul>	<ul style="list-style-type: none"> <li>• High power flexibility thanks to PWM operation and auxiliary storage</li> <li>• Lower power quality due to fluctuating DC Bus voltage</li> <li>• Typical range: Several kW</li> </ul>	<ul style="list-style-type: none"> <li>• Equation 4.22</li> <li>• High efficiency at no-load</li> <li>• Efficiency optimization thanks to MEPT algorithm</li> <li>• Higher efficiency &amp; lower cost compared to Layout C</li> </ul>	<ul style="list-style-type: none"> <li>• Low voltage DC applications that allow +/- 10% voltage fluctuation</li> <li>• PV applications</li> </ul>

Table 4.1.: Summary of the main characteristics of the hybrid topologies C and D

### 4.3. Possible layouts of the hybrid hydro-pneumatic and supercapacitor storage system

Layout	Description	Power features	Efficiency features	Typical Applications
E	<p>Indirect coupling of electric machine to hydraulic machine through flywheel and clutch</p> <ul style="list-style-type: none"> <li>• Possible mechanical output for turbine or mechanical application</li> <li>• Upstream auxiliary storage in Flywheel</li> <li>• Electric machine sized for output power</li> </ul>	<p>High power flexibility thanks to PWM operation and auxiliary storage</p> <ul style="list-style-type: none"> <li>• Typical range: Several kW</li> </ul>	<p>Equation 4.23</p> <ul style="list-style-type: none"> <li>• Low efficiency at no-load due to rotating parts</li> </ul>	<p>Low power water hydraulic (Mini-Pelton)</p>
F	<p>Indirect coupling of electric machine to hydraulic machine through flywheel</p> <ul style="list-style-type: none"> <li>• Downstream non-interfaced supercapacitive auxiliary storage</li> <li>• Upstream auxiliary storage in Flywheel</li> <li>• Electric machine sized for output power</li> </ul>	<p>High power flexibility thanks to PWM operation and auxiliary storage</p> <ul style="list-style-type: none"> <li>• Typical range: Several kW</li> </ul>	<p>Equation 4.24</p> <ul style="list-style-type: none"> <li>• High efficiency at no-load</li> <li>• Efficiency optimization thanks to MEPT algorithm</li> </ul>	<p>Low voltage DC applications that allow +/- 10% voltage fluctuation</p>

Table 4-2.: Summary of the main characteristics of the hybrid topologies E and F

An estimation of the efficiencies of the presented layouts can be made on the basis of the assumptions stated in Section 4.2.2, i.e considering that all the units exhibit a 95% 1-way efficiency. The resulting expressions are:

$$\begin{aligned}
 \eta_{tl_A} &= 0.95^6 = 0.7351 \\
 \eta_{tl_B} &= 0.95^4 = 0.8145 \\
 \eta_{tl_C} &= \frac{0.95^9}{1 + D(0.95^4 - 1)} = \frac{0.63025}{1 - 0.1855 * D} \\
 \eta_{tl_D} &= \frac{0.95^7}{1 + D(0.95^2 - 1)} = \frac{0.6983}{1 - 0.0975 * D} \\
 \eta_{tl_E} &= \frac{0.95^7}{1 + D(0.95 - 1)} = \frac{0.6983}{1 - 0.05 * D} \\
 \eta_{tl_F} &= \frac{0.95^8}{1 + D(0.95^2 - 1)} = \frac{0.6634}{1 - 0.0975 * D}
 \end{aligned}$$

The representations of these efficiencies as functions of the duty cycle  $D$  are given in Figure 4.16. This figure shows how the constitution and topology of each hybrid storage system determines the range (i.e maximum and minimum values) of its efficiency. The more complex the layout, the higher the number of units and the lower the minimum efficiency. The effect of the topology is more pronounced when it concerns the auxiliary storage as it has been seen in Section 4.2.2. The evidence of this statement is found in the comparison of the efficiencies of Layouts C and D: By inserting the supercapacitors bank directly in the DC bus (Suppressing thus the DC-DC converter), the minimum efficiency is increased by 7 points for Layout D. This gain in efficiency is however counterbalanced by a decrease in the power quality (Fluctuating DC bus voltage).

The efficiencies of Layout A and B are independent of the duty cycle  $D$  because these aren't hybrid systems, but possible simple ways of exploiting hydro-pneumatics for large scale energy storage. The lack of auxiliary storage increases their efficiency as the number of units is reduced, but limits their power flexibility.

The presented layout's list is not exhaustive, many other configurations can be imagined depending upon each application's context.

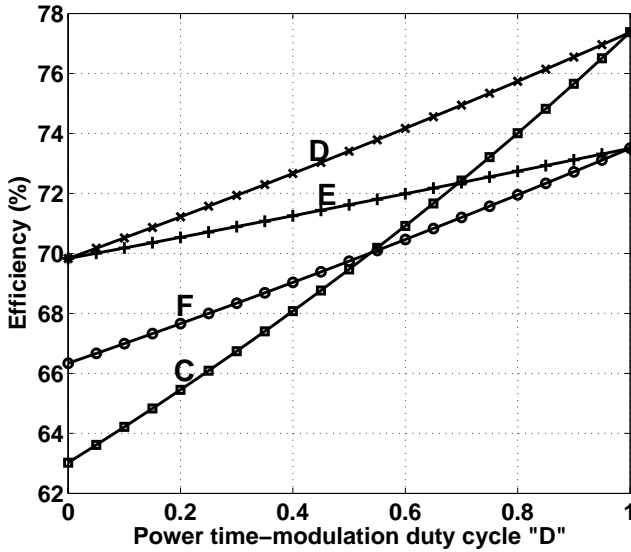


Figure 4.16.: Estimated overall 1-way Efficiency for the 4 presented hybrid layouts

## 4.4. Chapter summary

In this chapter, the concept of hybrid energy storage that combines pneumatics or hydro-pneumatics and supercapacitors to provide the storage system with more power flexibility and quality has been presented. The subsequent strategy to vary the output power has been studied, and two power-modulation techniques have been proposed, namely the fixed-frequency power modulation mode and the free-oscillating power-modulation mode. The free-oscillating power-modulation mode has appeared as the simpler and more effective modulation technique.

Afterwards, the global hybrid storage system's efficiency has been evaluated and analyzed. This analysis has shown that the system composition and topology have an important impact on its efficiency, and that this impact is greater for the auxiliary storage subsystem. Several layouts of the storage

system for different application contexts have been proposed and briefly commented. Their global 1-way efficiencies have been estimated under the realistic assumption that all the units exhibit 95% 1-way efficiency. The comparison of these efficiencies has confirmed the great impact their composition and topology on their performances. It has shown that a complex layout would provide more power flexibility and quality to the hybrid storage system, but would lower its overall efficiency. The design choices would be application dependent and should be a tradeoff between the cost and efficiency constraints on one hand, and the source and load requirements on the other.

It has been seen in Section 4.2.2 that the auxiliary storage subsystem performances are strongly determinant for the overall system performances as, its efficiency  $\eta_{as}$  appears raised to the “power 4” in the expression of the overall system round-trip efficiency. Means for optimizing the design and operation of the auxiliary storage subsystem will be investigated in Chapter 5.

# 5. Design and Optimization of the Supercapacitive Auxiliary Storage Subsystem

The analysis carried out in Section 4.2 has shown the great impact of the performances of the auxiliary storage subsystem on the one of the global system, as the efficiency of the later depends upon the “square” of the one of the previous. The auxiliary storage subsystem should therefore exhibit the highest possible efficiency in order to limit the effect of that square dependence.

In this chapter, the auxiliary storage subsystem composed of the supercapacitor bank and its interfacing DC-DC converter will be studied and some strategies of improving its performances will be proposed. The supercapacitor bank will be considered first; a formal method for optimally designing and sizing the bank in the context of pneumatic storage will be proposed. The DC-DC converter will be studied afterwards; different converter topologies will be analyzed and their efficiency evaluated. Some design and control techniques to obtain a high efficiency over the whole power range will be presented.

## 5.1. Description of the auxiliary storage subsystem

A simplified diagram of the auxiliary storage subsystem is given in Figure 5.1. In addition to its two main units that are the supercapacitor bank and the DC-DC converter, the three other subsystems connected together through the common DC bus are represented by three current sources so that their individual dynamic behaviors can be modeled easily. The command and control module, made of cascaded voltage and current regulators and a PWM gener-

ator is also represented.

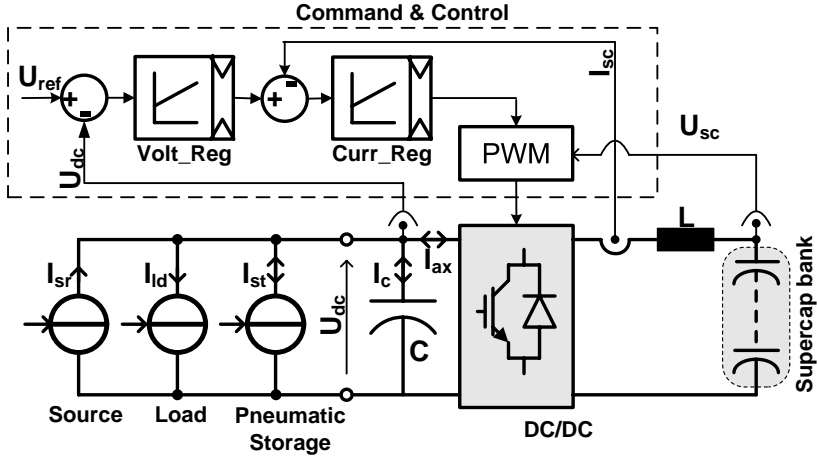


Figure 5.1.: Bloc diagram of the auxiliary storage subsystem

It has been seen in Chapter 3 that the power and the current  $I_{st}$  in the hydro-pneumatic storage subsystem are imposed by the maximum efficiency operating conditions. Similarly, the power and the current  $I_{sr}$  of the source will depend upon external parameters, for instance the weather in the case of renewable sources; it is therefore beyond the control of the system. Finally the current  $I_{ld}$  in the load will depend on the needs of the users which are unpredictable. Without the auxiliary storage, an unbalance of these current sources will force, according to the Kirchoff law, the DC bus voltage  $U_{dc}$  to vary. By regulating this voltage through the current  $I_{ax}$ , the command and control module would allow the current sources to vary freely. The range of the power flexibility thus obtained will depend mainly on the energy capacity of the supercapacitors bank and the power capability of the DC-DC converter. Nevertheless, many other constraints should be taken into account as it will be shown in Section 5.2



## 5.2. Design and optimization of the supercapacitor bank

### 5.2.1. Modeling the supercapacitors bank

A model of the supercapacitor bank is necessary to study its dynamic behavior and evaluate its energetic performances. The model of the bank is built on the basis of the one of its elementary component: The supercapacitor cell.

#### 5.2.1.1. Supercapacitor Cell

Many models for the supercapacitor cell are proposed in the specialized literature, with different modeling approaches [77], [78], [79]. A detailed model proposed by [80] is presented in Figure 5.2a where  $R_s$  is the series resistance (ESR) and the main source of losses in the cell.  $R_l$  is the leakage resistance,  $C_0$  the constant capacitance in parallel with  $C_u$  which has a linear dependence on the voltage:  $C_u = Ku$ . The  $n$  parallel  $RC$  circuits with different time constants represent the “relaxation phenomenon” which is a time related phenomenon observed at the end of the cell charge. An ideal supercapacitor model should possess an infinite number of these  $RC$  branches. For the application and analysis considered in this chapter, such a detailed model is unnecessary because many of the phenomena described above are marginal on one hand, and difficult to quantify on the other hand. The simplified model presented in figure 5.2b where only the series resistance and the constant capacitance are considered, is rather used.

#### 5.2.1.2. Supercapacitor bank

The nominal voltage of a supercapacitor cell is low (typically 2.5V) because of the low rating voltage of the organic electrolyte generally used in this device. Consequently, for medium and high power applications, supercapacitors are used in stacks where many cells are connected in series to obtain acceptable voltages. On the other hand, the energy capacity of a stack may not meet the requirement of the applications; many stacks should therefore be associated to form what is called here a “supercapacitor bank”. Many configurations of the bank can be imagined, however a simple topology capable of fulfilling any voltage and energy requirement is presented in Figure 5.3a. It is made of  $Np$  identical parallel branches comprising  $Ns$  series connected cells, and one

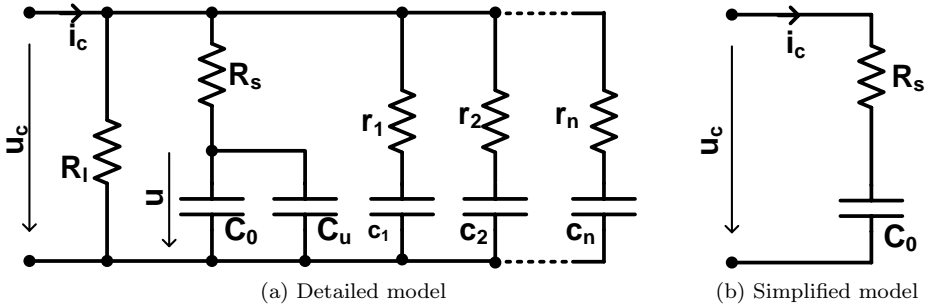


Figure 5.2.: Detailed and simplified models of a supercapacitor cell

extra incomplete branch with  $Ne$  series connected cells ( $0 \leq Ne \leq Ns$ ). One advantage of the presented topology would be its fault tolerance; in fact the bank can still operate with some cells short-circuited or open-circuited. In that case, its energy capacity will obviously be reduced. The main limitation with this dissymmetric topology would be the different voltage dynamics due to the current difference between the lower  $Ne$  rows and the upper  $Ns - Ne$  ones. The mean of circumventing this limitation is presented in Section 5.2.1.3.

On the basis of the simplified model adopted above for the supercapacitor cell, the supercapacitors bank will be modeled with a first order  $RC$  circuit as shown in Figure 5.3b.  $R_{sT}$  and  $C_T$  are the equivalent series resistance and the equivalent capacitance of the bank respectively. Assuming that all the cells have the same nominal characteristics, simple circuit calculation will give the following expressions:

$$R_{sT} = \frac{R_s}{Np} \left( Ns - \frac{Ne}{Np + 1} \right) \quad (5.1)$$

$$C_T = \frac{Np(Np + 1)}{Ns(Np + 1) - Ne} C_0 \quad (5.2)$$

where  $R_s$  and  $C_0$  are the nominal cell's electrical series resistance (ESR) and capacitance respectively. The total number  $N_T$  of supercapacitors is then equal to:

$$N_T = NsNp + Ne \quad (5.3)$$

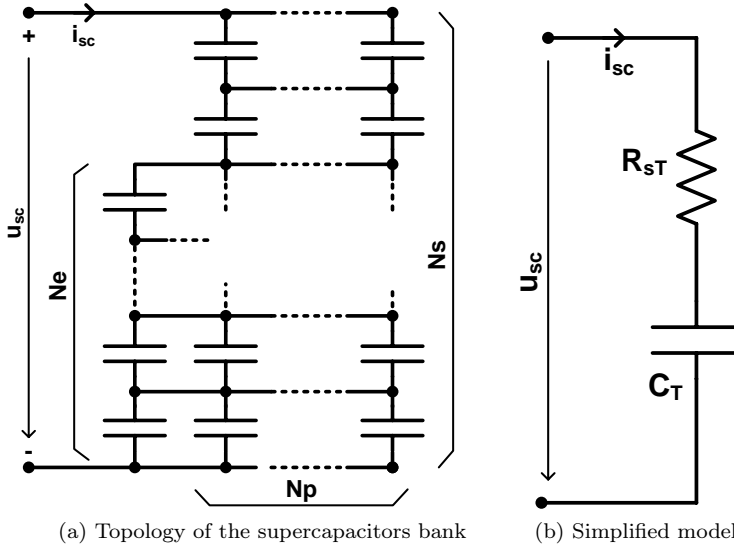


Figure 5.3.: Schematic diagram and simplified model of a supercapacitor bank

### 5.2.1.3. Cell voltage balance

An important issue when connecting many supercapacitor cells in series is the “voltage equalization” during the charge of the bank. Because of the disparities among the cell’s parameters, they won’t exhibit the same charging dynamic and, at the end, some cells may present over-voltage while some others are insufficiently charged. This voltage dynamic difference will be more important with dissymmetric topology like that of Figure 5.3a. This situation may damage overcharged cells or at least accelerate their aging.

To avoid unbalance cell voltages, voltage “sharing” or “equalizing” devices ( $E_q$  in Figure 5.4), connected in parallel with each stage as shown in Figure 5.4, are used to balance the cell voltages. The principle is to provide an alternative way for the current going through an overcharged stage. Passive or active voltage sharing devices can be used, depending on the operating constraints. An example of active equalizing device is described in [81], [82]. The voltage sharing system will induce some cost and losses proportionally to

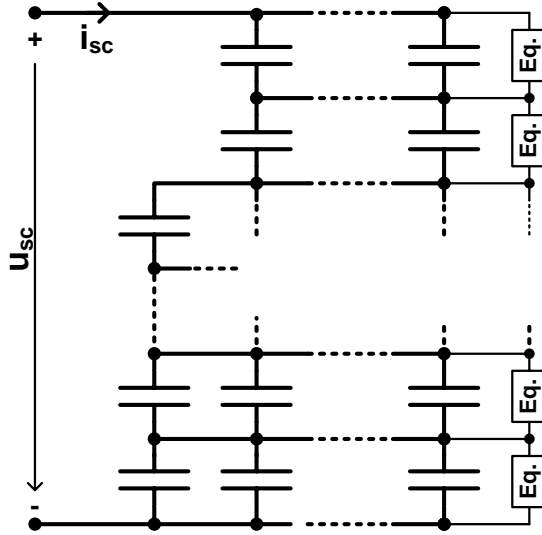


Figure 5.4.: Principle of cell's voltage equalization

the number  $N_s$  of series connected cells in a stack. In this study, the losses related to these devices are not taken into account.

## 5.2.2. Sizing of the supercapacitor bank

### 5.2.2.1. Determination of the number of supercapacitors

As for any capacitor, the maximum energy  $W_{scM}$  that can be stored in the supercapacitor bank of capacitance  $C_T$  is given by:

$$W_{scM} = \frac{1}{2} C_T U_{scM}^2 \quad (5.4)$$

$U_{scM}$  is the maximum supercapacitors bank's voltage. It is not possible to withdraw all this energy for, the current in the supercapacitors and the interfacing converter would become infinite when the voltage reaches zero. In practice, a minimum allowable discharge voltage  $U_{scm}$  is fixed that limits the

available energy. The discharge voltage ratio  $d$  (in %) of the supercapacitors bank is defined as: [80]

$$d = 100 \frac{U_{scm}}{U_{scM}} \quad (5.5)$$

The ‘‘Depth Of Discharge’’  $DOD$  (in %) is then equal to:

$$DOD = 100 - d = 100 \left( 1 - \frac{U_{scm}}{U_{scM}} \right) \quad (5.6)$$

**Power limitation** When performing the DC bus voltage regulation, the auxiliary storage subsystem mainly operates in a power-controlled mode, where the power is imposed by the unbalance of the three other subsystems powers. The supercapacitor bank mainly behaves like a voltage source; the maximum deliverable power during the discharge operation is limited by the ‘‘power adaptation’’ point [83]. The power adaptation point is reached when the output voltage is equal to the voltage drop across the internal series resistance  $R_{sT}$ . The maximum deliverable power  $P_{D_M}$  for given initial voltage  $U_{scM}$  is given by :

$$P_{D_M} = \frac{U_{scM}^2}{4R_{sT}} \quad (5.7)$$

The minimum discharge output voltage  $U_{scm}$  that guaranties the power-controlled operation for a given discharge  $P_D$  power is then given by:

$$U_{scm} = R_{sT} i_{scD} = \sqrt{R_{sT} P_D} \quad (5.8)$$

This condition therefore limits the minimum discharge voltage ratio  $d_{min}$  defined by:

$$d_{min} = 100 \frac{2\sqrt{R_{sT} P_D}}{U_{scM}} \quad (5.9)$$

The sizing of the supercapacitor bank must meet this condition, otherwise the power-controlled operation won’t be always possible.

Under that limited voltage range, the useful energy that the supercapacitors bank can provide is defined by:

$$W_{scu} = W_{scM} \left[ 1 - \left( \frac{d}{100} \right)^2 \right] \quad (5.10)$$

Equation 5.10 shows that, for a 50% *DOD*, the useful energy represents 75% of the maximum energy. Hence, in practice it will be inefficient to discharge the bank below 50% of its maximum voltage because the remaining energy is not so important and, for a given power, the high current due to the low voltage will induce important losses. The total capacitance  $C_T$  of the supercapacitors bank can be derived from Equations 5.10 and 5.4 as:

$$C_T = \frac{2W_{scu}}{U_{scM}^2 \left[ 1 - \left( \frac{d}{100} \right)^2 \right]} \quad (5.11)$$

Part of the useful energy  $W_{scu}$  is lost in the supercapacitors and the interfacing DC-DC converter; a more accurate sizing should take those losses into account. This can be done through the auxiliary storage efficiency  $\eta_{as} = \eta_{bb}\eta_{sc}$  as defined in Chapter 4. A more accurate expression of  $C_T$  would be:

$$C_T = \frac{2W_{scu}}{\eta_{as}U_{scM}^2 \left[ 1 - \left( \frac{d}{100} \right)^2 \right]} \quad (5.12)$$

In general, the number  $N_s$  of series connected cells in one branch is imposed by the stack's maximum voltage. The typical cell voltage  $U_{cel}$  is about 2.5V.  $N_s$  is then given by:

$$N_s = \frac{U_{scM}}{U_{cel}} \quad (5.13)$$

If there were not an extra incomplete branch, the total capacitance  $C_T$  of the bank would be given by  $C_T = C_0 N_p / N_s$ . The additional branch increases the total capacitance for a value less than a branch capacitance which is equal to  $C_0 / N_s$ .  $N_p$  is therefore equal to at least "1" ( $N_p \geq 1$ ) and at most the nearest integer less or equal to:

$$N_p = RoundDown \left( \frac{C_T}{C_0} N_s \right) \quad (5.14)$$

The number  $N_e$  of supercapacitors in the incomplete branch can be then extract from Equation 5.2 and rounded to the nearest integer greater or equal to:

$$N_e = RoundUp \left[ (N_p + 1) \left( N_s - \frac{C_0}{C_T} N_p \right) \right] \quad (5.15)$$

In conclusion, three main parameters are necessary to properly size the supercapacitor bank: The useful energy  $W_{scu}$ , the maximum voltage  $U_{scM}$  and the depth of discharge  $DOD$  or, in other words, the discharge voltage ratio  $d$ . The determination of these parameters will be discussed in the following sections.

### 5.2.2.2. Implications of the dissymmetric topology for the voltage balancing system

With the proposed dissymmetric topology represented in Figure 5.4, the  $N_s - N_e$  upper balancing cells must support the higher current than the  $N_e$  lower ones. The most critical case is that with only one complete stack ( $N_p = 1$ ). The upper balancing cells would support twice more current than the lower ones, which may result in higher cost and losses. In such a case it might be more interesting both in terms of cost and efficiency to turn the topology into a symmetric one by filling the incomplete stack, particularly if the voltage and energy requirements are not very constraining.

The dissymmetric topology is interesting in case of high number  $N_s$  of series connected cells in a stack and several complete stacks in parallel. In that case the dissymmetry caused by the incomplete branch won't have an important consequence on the balancing system and the topology can work well.

### 5.2.2.3. Determination of the useful energy

The useful energy is determined from the power profile of the auxiliary storage. Such a profile during discharge is sketched in Figure 4.8 for the simplistic case where the source and load powers are constant. In reality they aren't; however they remain low compared to the hydro-pneumatic power. Thus, for the auxiliary storage subsystem, the most power demanding unit is the hydro-pneumatic storage subsystem. Hence the supercapacitors bank should be sized so as to provide or absorb the energy converted by the hydro-pneumatic storage during one operation stroke.

It can be seen from Figure 4.8 that the two important parameters needed to determine the useful energy are the hydro-pneumatic power and the on-off cycle period  $T$ . The hydro-pneumatic power is determined by the pressure and the oil flow rate. The maximum pressure will be mainly imposed by the energy

requirements whereas the flow rate will be imposed by the MEPT conditions. Knowing the power, the useful energy will depend on the stroke period  $T$ .

For a given power, a small value for  $T$  will yield a small amount of useful energy and therefore a reduced number of supercapacitors; but it will also induce high switching frequencies for the hydro-pneumatic subsystem. This must be avoided because switching operations are lossy due the constraining transient conditions for many devices and the masses acceleration energy that cannot be completely recovered during turn-off. On another hand, a long stroke period  $T$  would lead to high number of supercapacitors and therefore high cost. In the case of the free-oscillating power modulation mode studied in Chapter 4, high value of  $T$  would also evolve for the closed gas cycle systems, long compression/expansion strokes and therefore high temperature change in the storage volume. This would prevent achieving the isothermal conditions necessary to obtain high thermodynamic efficiencies.

Depending on the DC-DC converter type, the optimal operating conditions would impose the supercapacitors bank voltage and therefore the number  $N_s$  of the cells in series. This number can be used as a basis for the design of the system. In any case, the determination of the useful energy and therefore the sizing the supercapacitors bank is an optimization process that requires the analysis of the operation of the global storage system.

### 5.2.3. Evaluation and analysis of the supercapacitor bank's efficiency

#### 5.2.3.1. Charge-discharge cycle's efficiency evaluation

It has been stated that the auxiliary storage subsystem mainly operates in a power-controlled mode; it is therefore more relevant to analyze its efficiency with regards to the power. The equivalent circuits of such an operation for the charge and the discharge processes of the supercapacitors bank are given in Figure 5.5 [84].

- **Charge efficiency:**

From that simplified circuit, the charge current  $i_{scC}$  is given by:

$$i_{scC} = C_T \frac{du}{dt} = \frac{P_C}{u_{sc}} \quad (5.16)$$



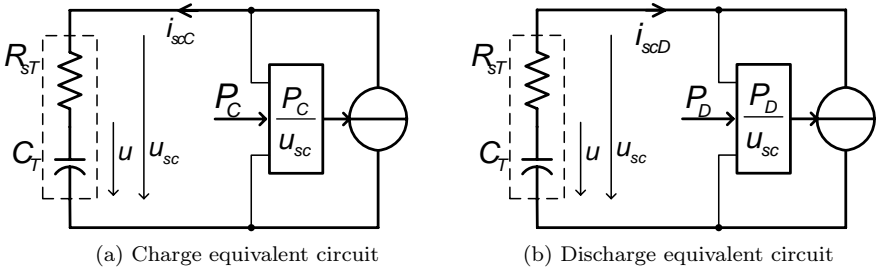


Figure 5.5.: Equivalent circuits for power-controlled charge and discharge operations

The voltage  $u$  across the ideal supercapacitor bank of total capacitance  $C_T$  is equal to:

$$u = u_{sc} - R_{sT}i_{sc}C = u_{sc} - R_{sT}\frac{P_C}{u_{sc}} \quad (5.17)$$

From Equation 5.17, the differential form of the voltage can be written as:

$$du = du_{sc} \left( 1 + \frac{R_{sT}P_C}{u_{sc}^2} \right) \quad (5.18)$$

Combining Equations 5.16 and 5.18 gives:

$$P_C dt = u_{sc} C_T \left( 1 + \frac{R_{sT}P_C}{u_{sc}^2} \right) du_{sc} \quad (5.19)$$

Integrating Equation 5.19 from the minimum voltage  $U_{scm}$  to the maximum one  $U_{scM}$  within the charge time  $T_C$  would give the charge energy  $W_C$  expressed as:

$$W_C = P_C T_C = \frac{(1-d^2)C_T U_{scM}^2}{2} - R_{sT} C_T P_C \ln(d) \quad (5.20)$$

Remember that  $d$  is the voltage ratio defined such that  $U_{scm} = (1-DOD)U_{scM} = dU_{scM}$  with  $0 \leq d \leq 1$ . The effective energy  $W_{scC}$  that is stored in the equivalent capacitance  $C_T$  is given by:

$$W_{scC} = \int_0^{T_C} u i_{sc} C dt = \int_{U_{scm}}^{U_{scM}} C_T u_{sc} C du_{sc} \quad (5.21)$$

Substituting Equation 5.18 followed by integration will result in:

$$\begin{aligned} W_{scC} &= \int_{U_{scm}}^{U_{scM}} \left( u_{sc} - \frac{R_{sT}P_C}{u_{sc}} \right) \left( 1 + \frac{R_{sT}P_C}{u_{sc}^2} \right) du_{sc} \\ &= \frac{(1-d^2)C_T U_{scM}^2}{2} \left( 1 - \frac{R_{sT}^2 P_C^2}{d^2 U_{scM}^4} \right) \end{aligned} \quad (5.22)$$

Combining Equations 5.22 and 5.20, the energy efficiency  $\eta_{scC}$  of the constant power  $P_C$  charge process is given by:

$$\eta_{scC} = \frac{W_{scC}}{W_C} = \left( 1 - \frac{R_{sT}^2 P_C^2}{d^2 U_{scM}^4} \right) \left( 1 - \frac{2R_{sT}P_C \ln(d)}{(1-d^2)U_{scM}^2} \right)^{-1} \quad (5.23)$$

• **Discharge efficiency:**

The same analysis can be carried out for the discharge process on the basis of the simplified equivalent circuit given in Figure 5.5b. In that case, the voltage  $u$  across the ideal supercapacitor bank of total capacitance  $C_T$  is equal to:

$$u = u_{sc} + R_{sT}i_{scD} = u_{sc} + R_{sT} \frac{P_D}{u_{sc}} \quad (5.24)$$

Its differential form will be:

$$du = du_{sc} \left( 1 + \frac{R_{sT}P_C}{u_{sc}^2} \right) \quad (5.25)$$

The same development as for the charge process will result in the expression of the discharge energy  $W_D$  received at the bank's output during the discharge time  $T_D$  as:

$$W_D = P_D T_D = -\frac{(1-d^2)C_T U_{scM}^2}{2} + R_{sT} C_T P_D \ln(d) \quad (5.26)$$

The theoretically available energy  $W_{scD}$  in the supercapacitors bank is equal to:

$$W_{scD} = \frac{(1-d^2)C_T U_{scM}^2}{2} \quad (5.27)$$

The discharge efficiency  $\eta_{scD}$  is therefore equal to:

$$\eta_{scD} = \frac{W_D}{W_{scD}} = 1 + \frac{2R_{sT}P_D \ln(d)}{(1-d^2)U_{scM}^2} \quad (5.28)$$

- **Charge-discharge cycle efficiency:**

The charge-discharge cycle efficiency  $\eta_{sc}$  is therefore the product of the efficiencies of the two phases:

$$\begin{aligned} \eta_{sc} &= \eta_{scC} \cdot \eta_{scD} \\ &= \left(1 - \frac{R_{sT}^2 P_C^2}{d^2 U_{scM}^4}\right) \left(1 - \frac{2R_{sT} P_C \ln(d)}{(1-d^2) U_{scM}^2}\right)^{-1} \left(1 + \frac{2R_{sT} P_D \ln(d)}{(1-d^2) U_{scM}^2}\right) \end{aligned} \quad (5.29)$$

### 5.2.3.2. Analysis of the charge-discharge cycle's efficiency

Equation 5.29 shows that the supercapacitor bank's efficiency depends mainly on the equivalent series resistance  $R_{sT}$ , the maximum voltage  $U_{scM}$ , the depth of discharge through  $d$ , and the charge and discharge powers,  $P_C$  and  $P_D$  respectively. In normal operation, the two powers are not automatically equal. During the discharge of the main storage subsystem for instance,  $P_C$  is mainly imposed by the MEPT conditions whereas  $P_D$  depends mainly on the load power demand. As the bank's "depth of charge" and "depth of discharge" are equal, the charge and discharge average powers for the whole charge-discharge cycle are also equal and will be considered for the efficiency analysis:  $P_C = P_D$ .

The impact of the above listed parameters on the cycle efficiency will be well illustrated with the study of a practical storage system. The main characteristics of the studied case are set as following: DC bus voltage:  $U_{dc} = 315V$ . This value presents the advantage of been directly compatible with 220V single-phase AC grid connected applications. A value of  $U_{dc} = 540V$  would have been suited for three-phase applications. Usable energy:  $W_{scu} = 824.5kJ$ . Power range:  $0 \leq P \leq 30kW$ . A state-of-the-art supercapacitor cell is chosen, the BCAP2600-P270 cell of *Maxwell Technologies*, characterized by: nominal capacitance  $C_0 = 2600F$ ; series resistance  $R_s = 0.31m\Omega$ ; operating voltage  $U_c = 2.7V$ .

Three values of the maximum voltage  $U_{scM}$  and two values of the depth of discharge  $DOD$  are considered, which have lead to the six configurations described in Tables 5.2 and 5.1. The different values are calculated tanks to the equations given in Section 5.2.2.1.

$U_{dc} = 315V$ ; **DOD = 25%** ( $d = 0.75$ );  $W_{scu-ref} = 824.5kJ$ ;  $P_{max} = 30kW$

Maximum voltage: $U_{scM}$ (V)	<b>313</b>	<b>235</b>	<b>156</b>
Minimum voltage: $U_{scm}$ (V)	235	176.17	117.45
Maximum current ( $P_{max}/U_{scm}$ ): $I_{scM}$ (A)	<b>128</b>	<b>170.28</b>	<b>255.42</b>
Number of series connected cells: $N_s$	116	87	58
Number of parallel stacks with $N_s$ cells: $N_p$	1	2	3
Number of cell in the incomplete stack: $N_e$	97	33	29
Total number of cell in the bank: $N_T$	<b>213</b>	<b>207</b>	<b>203</b>
Total cost of the cells (26€/cell) (€)	<b>5'538</b>	<b>5'382</b>	<b>5'278</b>
Effective total capacitance: $C_T$ (F)	<b>38.51</b>	<b>68.42</b>	<b>153.69</b>
Equivalent series resistance: $R_{sT}$ (mΩ)	<b>20.92</b>	<b>11.78</b>	<b>5.24</b>
Effective useful energy: $W_{scu}$ (kJ)	826.35	825.84	824.47
Maximum deliverable power: $P_{DM}$ (kW)	660	659	658

Table 5.1.: Supercapacitor bank characteristics for configuration 1

These tables show that for a given energy requirement, the total number of supercapacitor cells, and therefore the cost of the bank, does not necessarily increase when the maximum voltage decreases. However, it automatically increases with a decreasing depth of discharge.

The supercapacitor bank's cycle efficiency characteristic for the situations described in the above given tables are represented in Figure 5.6. The figure shows that, for a given energy constraint and depth of discharge, the efficiency is independent of the maximum voltage of the supercapacitor bank. This is due to the fact that the voltage change is compensated by equivalent changes in series resistance and current so that, for the given power, the losses remain unchanged. Nevertheless, the higher current related to the lower voltage might induce higher losses in the interfacing converter. That figure also shows that for a given energy and maximum voltage requirements, the efficiency decreases with increasing depth of discharge. Low *DOD* would lead to higher voltages and lower currents as can be seen in the tables, and therefore lower losses. Given that the same current flows through the DC-DC converter, low *DOD* will also benefit the converter as it will be seen in Section 5.3.2.

In conclusion choosing a high maximum voltage and a low depth of dis-

$$U_{dc} = 315V; \text{DOD} = 50\% (d = 0.5); W_{scu-ref} = 824.5kJ; P_{max} = 30kW$$

Maximum voltage: $U_{scM}$ (V)	<b>313</b>	<b>235</b>	<b>156</b>
Minimum voltage: $U_{scm}$ (V)	156	117.5	78
Maximum current ( $P_{max}/U_{scm}$ ): $I_{scM}$ (A)	<b>192</b>	<b>255.42</b>	<b>383.21</b>
Number of series connected cells: $N_s$	116	87	58
Number of parallel stacks with $N_s$ cells: $N_p$	1	1	2
Number of cell in the incomplete stack: $N_e$	0	44	0
Total number of cell in the bank: $N_T$	<b>116</b>	<b>131</b>	<b>116</b>
Total cost of the cells (26 €/cell) (€)	<b>3'016</b>	<b>3'406</b>	<b>3'016</b>
Effective total capacitance: $C_T$ (F)	<b>22.41</b>	<b>40</b>	<b>89.65</b>
Equivalent series resistance: $R_{sT}$ (mΩ)	<b>39.96</b>	<b>20.15</b>	<b>8.99</b>
Effective useful energy: $W_{scu}$ (kJ)	824.5	827.67	824.5
Maximum deliverable power: $P_{DM}$ (kW)	152	171	169

Table 5.2.: Supercapacitor bank characteristics for configuration 2

charge for the supercapacitor bank will be, from an efficiency point of view, more beneficial for both the supercapacitor bank and the DC-DC converter. However, low  $DOD$  would require higher number of supercapacitor cells to fulfill the energy requirement, and therefore induce higher cost.

## 5.3. Design and optimization of the DC-DC converter

### 5.3.1. Analysis of possible topologies and design parameters

#### 5.3.1.1. Converter's topology

To insure the bidirectional energy flow between the two unipolar voltage sources that are the supercapacitor bank and the DC bus, a two-quadrant DC-DC converter is necessary. Beside the classical single phase-leg converter [85], [86], two other main categories of DC-DC converters can be envisaged for this task: Isolated converters and non-isolated multi-phase converters.

- *Isolated DC-DC converters*

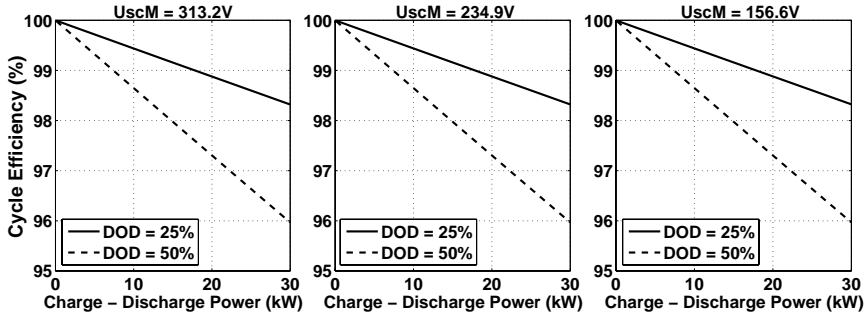


Figure 5.6.: Cycle efficiency for a useful energy  $W_{scu} = 824.5kJ$  and different values of maximum voltage and  $DOD$

Simplified topologies for isolated bidirectional DC-DC converters are sketched in Figure 5.7. These converters are mainly characterized by the use of a medium frequency transformer between the low and the high voltage sides. Dual full-bridge, dual Half-bridge and even mixed configurations are possible depending on the application requirements and operation conditions; the implementation of soft-switching techniques is also possible. Many design and control strategies for these topologies are proposed in literature [87], [88]. The types of active switches will mainly depend on the application's current and voltage ratings; generally power MOSFET in low voltage side (supercapacitors) and IGBT or MOSFET in high voltage side (DC bus).

The main advantages of the isolated topologies are obviously the galvanic isolation that improves in some cases the system security, but mainly the high voltage adaptation capability thanks again to the transformer. The low profile of the high frequency transformer also increases the power density of these converters, reducing thus their size and making them suitable for portable applications. Finally the soft-switching techniques allow reducing the switching losses. Some designs have been proposed for fuel cell and transportation applications [89], [90].

An uncount evaluation would show that theses topologies will be more suited to interface the supercapacitors with high voltage DC bus, in the range of kilovolts. For DC bus of few hundreds volts has considered in this study, su-

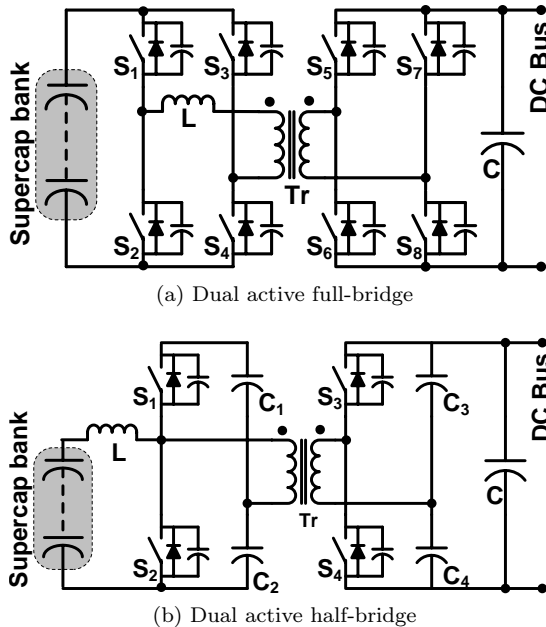


Figure 5.7.: Main topologies of isolated bidirectional DC-DC converters

percapacitor banks of almost the same voltage range can be realized efficiently as it has been seen in Section 5.2.2; high voltage adaptation factors would be therefore unnecessary. The transformer and the high number of components would also induce important losses and high cost. Hence, the second category of converters is preferred in this study.

### *Non-isolated multi-phase bidirectional converters*

Multi-phase DC-DC converters are well known in the field of Switched Mode Power Supplies (SMPS), mainly in low voltage high current applications like CPU core power supplies. The main topology of these converters is very simple as it can be seen on Figure 5.8. The key principle of multi-phase converters is the output current sharing among several interleaved parallel channels. As the conduction losses in resistive elements like power MOSFET and inductors are proportional to the “square” of the current, reducing the channel’s current by

increasing the number of channels would be more efficient to reduce the losses than over-sizing the channel. However, increasing the number of channels may also increase the cost, therefore the design is a trade off between the efficiency and the cost. Another positive point is the phase angle-shift between channel's currents that results in a very low ripple of the total output current [91], [92], [93].

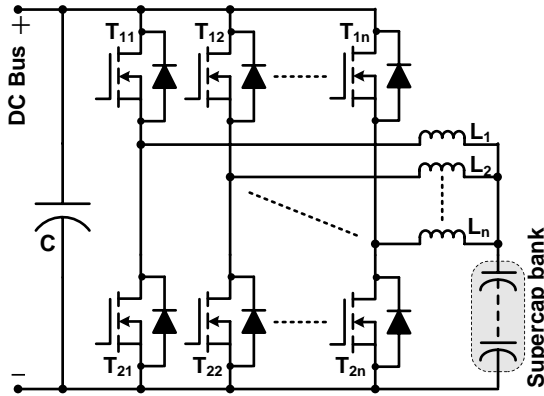


Figure 5.8.: Main topology of Non-isolated bidirectional multi-phase DC-DC Converter

For the voltage and current ranges considered in this study, power MOSFETs are the appropriate switches. They can perform fast switchings and possess a reverse body diode so that an external antiparallel diode for the freewheeling operation is unnecessary. More over, the channel's reverse conduction capability can be exploited instead of the body diode to reduce the conduction losses in the freewheeling mode, resulting thus in a synchronous converter [94], [95]. The converter's performances and efficiency depend upon various design parameters like the inductance value, the switching frequency and the number of channels. These issues will be discussed in the following paragraph.



### 5.3.1.2. Phase inductance value

For given switching frequency  $f_{sw}$  and duty cycle  $D$ , the amplitude of the phase and output current ripples are mainly determined by the phase inductance. The phase inductance  $L_p$  is related to the phase current ripple  $\Delta I_p$  by the following equation [96], [97]:

$$\Delta I_p = \frac{(U_{dc} - U_{sc}) U_{sc}}{U_{dc} f_{sw} L_p} = \frac{(1 - D) D U_{dc}}{f_{sw} L_p} \quad (5.30)$$

This equation shows that a large inductance value will cause a low current ripple and conversely a small inductance value will lead to large current ripple. The maximum phase current ripple  $\Delta I_{p_{max}}$  is obtained for  $D = 0.5$  and is given by:

$$\Delta I_{p_{max}} = \frac{U_{dc}}{4 f_{sw} L_p} \quad (5.31)$$

From this critical situation, the minimum value of the inductance for a given current ripple can be derived from Equation 5.31. Idealized phase and high side transistor currents' shapes for two different inductance values are sketched in Figure 5.9. The effects of these shapes on the converter's efficiency are evaluated below.

The conduction losses in the MOSFET transistors and the copper losses in the inductors are proportional to the “square” of the root means square current. For the trapezoidal waveform like that of the high side transistor current  $I_{TH}$  shown in Figure 5.9b, the expression of the root means square value  $I_{TH_{rms}}$  is given by:

$$I_{TH_{rms}} = \left[ \frac{(I_{p_{max}}^2 + I_{p_{max}} I_{p_{min}} + I_{p_{min}}^2) D}{3} \right]^{1/2} \quad (5.32)$$

where  $I_{max}$  and  $I_{min}$  are the maximum and minimum values of the phase current respectively. These two values also define the following important characteristics for the current shape:

- The current shape squareness  $K$  as:

$$K = \frac{I_{p_{min}}}{I_{p_{max}}} \quad (5.33)$$

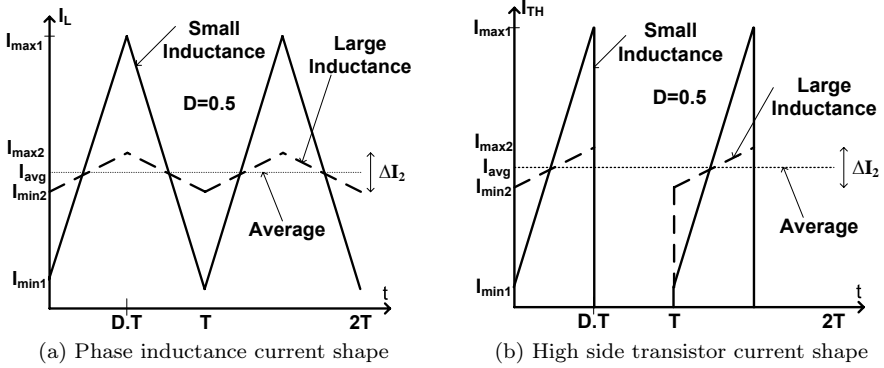


Figure 5.9.: Current shapes for different value of the phase inductance in buck operation

It can be seen that  $K = 0$  for triangular shape and  $K = 1$  for rectangular shape.

- The phase average current  $I_{avg}$  as:

$$I_{p_{avg}} = \frac{I_{sc}}{N_{ph}} = \frac{I_{p_{max}} + I_{p_{min}}}{2} \quad (5.34)$$

where  $I_{sc}$  is the average total output current (in the supercapacitors bank) and  $N_{ph}$  the number of phases.

- The phase current ripple  $\Delta I_p$  as:

$$\Delta I_p = I_{p_{max}} - I_{p_{min}} = \frac{2(1-K)}{1+K} I_{p_{avg}} = \alpha I_{p_{avg}} \quad (5.35)$$

Introducing these parameters in Equation 5.32 and extending the result to the other components would give:

- The high side transistor root means square current  $I_{TH_{rms}}$ :

$$\begin{aligned}
 I_{TH_{rms}} &= \left[ \left( I_{p_{avg}}^2 + \frac{\Delta I_p^2}{12} \right) D \right]^{1/2} \\
 &= 2I_{p_{avg}} D^{1/2} \left( \frac{1 + K + K^2}{3(K + 1)^2} \right)^{1/2}
 \end{aligned} \tag{5.36}$$

- The low side transistor root means square current  $I_{TL_{rms}}$ :

$$\begin{aligned}
 I_{TL_{rms}} &= \left[ \left( I_{p_{avg}}^2 + \frac{\Delta I_p^2}{12} \right) (1 - D) \right]^{1/2} \\
 &= 2I_{p_{avg}} (1 - D)^{1/2} \left( \frac{1 + K + K^2}{3(K + 1)^2} \right)^{1/2}
 \end{aligned} \tag{5.37}$$

- The phase inductance root means square current  $I_{p_{rms}}$ :

$$I_{p_{rms}} = \left( I_{p_{avg}}^2 + \frac{\Delta I_p^2}{12} \right)^{1/2} = 2I_{p_{avg}} \left( \frac{1 + K + K^2}{3(K + 1)^2} \right)^{1/2} \tag{5.38}$$

For constant average current  $I_{p_{avg}}$  and duty cycle  $D$ , the normalized root means square current  $i_{p_{rms}}$  defined such that  $i_{p_{rms}} = 1$  for  $K = 1$  is given by:

$$i_{p_{rms}} = 2 \left( \frac{1 + K + K^2}{3(K + 1)^2} \right)^{1/2} \tag{5.39}$$

From Equation 5.35, the normalized current ripple amplitude  $\Delta i_p$  can be defined as:

$$\Delta i_p = \frac{\Delta I_p}{I_{p_{avg}}} = \frac{2(1 - K)}{1 + K} = \alpha \tag{5.40}$$

The combination of Equations 5.31 and 5.35 yields the minimum phase inductance  $L_p$  for given phase average current and ripple amplitude:

$$L_p = \frac{U_{dc}}{4f_{sw}\Delta I_p} = \frac{U_{dc}}{4f_{sw}\alpha I_{p_{avg}}} = \frac{L_c}{\alpha} \tag{5.41}$$

$L_c$  is the critical phase inductance for given DC bus voltage, average phase current and switching frequency. It is given by:

$$L_c = \frac{U_{dc}}{4f_{sw}I_{p_{avg}}} \tag{5.42}$$

The normalized phase inductance  $L_n$  can therefore be defined as the ratio:

$$L_n = \frac{L_p}{L_c} = \frac{1}{\alpha} = \frac{1 + K}{2(1 - K)} \tag{5.43}$$

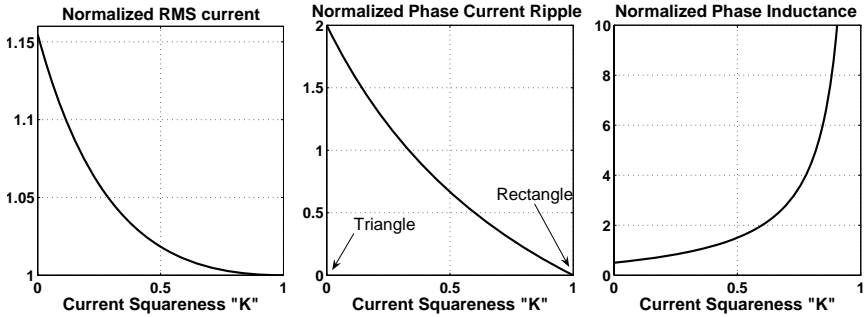


Figure 5.10.: Effect of the phase inductance on the converter’s performances

Figure 5.10 represents the variation of  $i_{p_{rms}}$ ,  $\Delta i_p$  and  $L_n$  as a function of the squareness  $K$  of the phase current. The first graph shows that, the conduction losses  $RI_{p_{rms}}^2$  are 32% higher for a triangular shape than for a rectangular one. Hence, low inductance will produce high current ripples and therefore higher conduction losses.

The current shape also influences the switching losses. The switching losses of the low side transistor in buck operation (or high side transistor in boost operation) are negligible because the transistor always switches when its antiparallel body diode is conducting, that is in almost zero voltage conditions (ZVS). It can be seen from Figure 5.9 that decreasing the current squareness by decreasing the inductance value will decrease the turn-on current of the

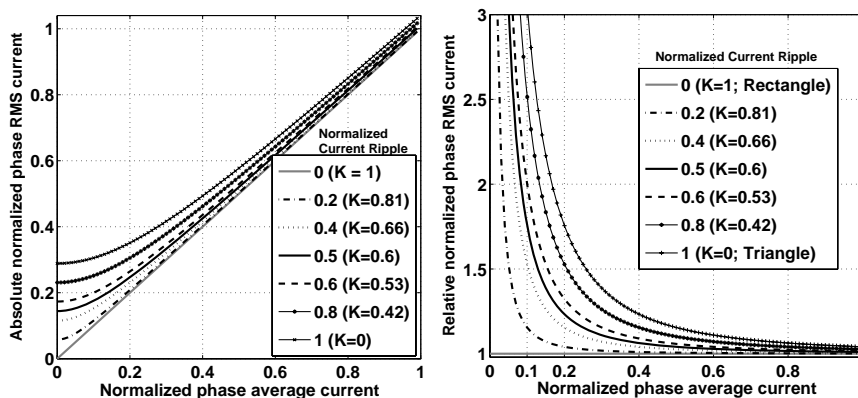


Figure 5.11.: Phase RMS current versus phase average current

high side transistor (or low side one in boost operation) and increase the turn-off current. This can even lead to zero current turn-on (ZCS) like in the case of discontinuous conduction mode converters [98]. As the switching losses are proportional to the switching current, the turn-on losses will decrease while the turn-off losses increase. Since the turn-off losses tend to be larger than the turn-on losses in some cases, decreasing the inductance value may result in an increase of the total switching losses.

One advantage in reducing the inductance value is the reduction of the converter's weight and size, which are important issues in portable applications. However, in stationary applications like those targeted in this study, the converter's weight and size will remain a marginal part of the global system's ones. From all those facts, low inductance does not present any important advantage for the studied cases and should be avoided.

It is apparent from Figure 5.10 that, for  $K > 0.6$  which means for  $\Delta i_p < 0.5$  or  $L_n > 2$ , the maximum "conduction efficiency" improvement incurred by increasing the inductance value is only 2% ( $i_{p,rms} = 1.01$ ). So, from the efficiency point of view, the phase inductance  $L_p$  does not need to be larger than twice the critical inductance  $L_c$ . The main limitation to this design crite-

ria, particularly in the case of bi-directional current DC-DC converter, is the partial load operation. When the average phase current is very low, its AC component and therefore RMS value becomes higher than the average value and the incurred conduction losses represents the major part of the power flow.

The variation of the RMS value of the normalized phase current is represented in Figure 5.11 versus the normalized phase average current, for different value of the normalized ripple current amplitude, from the rectangular shape to the triangular one. It can be seen on the right graph that, for the aforementioned case where the current ripple representing 50% of the nominal phase average current (i.e  $L_p = 2L_c$ ), when the phase current equals 10% of the nominal current, the conduction losses is  $1.8^2/1.15^2 = 3.24/1.32 = 2.45$  times greater than that of the case where the ripple current represents 20% of the nominal current, which substantially reduces the converter's efficiency. For that reason, the phase inductance is generally sized so that the current ripple remains lesser than 20% of the nominal current, unless the converter always operates at nominal conditions.

### 5.3.1.3. Switching Frequency

It can be seen from Equation 5.30 that the current ripple is inversely proportional to the switching frequency  $f_{sw}$ . It is also obvious that the switching losses are proportional to the switching frequency as it will be seen in Section 5.3.2.1. So, increasing the switching frequency will reduce current ripple and therefore the conduction losses but will increase the switching losses much more.

It appears from Equation 5.30 that, for a constant  $L_p \cdot f_{sw}$  product, the current ripple remains constant. Increasing the frequency can be a way of reducing the inductance without changing the current ripple. This approach is generally used in power supplies of very compact electronic systems like CPU cores where very high switching frequencies are implemented .

The converter's operating context is also an important point. The auxiliary storage subsystem studied in this chapter is part of the greater system and, it will be cost effective if the whole system is controlled by a single unit. For that purpose, the switching frequency of the converters should be chosen so

as to be compatible with the central control unit, taking into account all the others controlled processes.

In conclusion, choosing a high frequency does not appear as an efficient way of improving the converter's efficiency, but an effective mean of reducing its size, which is not an important issue in the context of the studied systems. The frequency of the central control unit seems to be a more constraining criteria for the choice of the converter's switching frequency.

### 5.3.2. Evaluation and optimization of the Converter's efficiency

The converter's efficiency is evaluated and analyzed with regards to the output power  $P_{out}$  and the phase number, in order to optimize its operation and the number of phases. The maximum value of the output power and the DC bus voltage are maintained at  $P_{max} = 30kW$  and  $U_{dc} = 315V$  respectively like for study of the supercapacitor bank. The first two configurations of the bank described in Tables 5.1 and 5.2 are considered. They are mainly characterized by the same maximum voltage  $U_{scM} = 313.2V$  and depths of discharge  $DOD = 25\%$  and  $DOD = 50\%$  respectively. The evaluation carried out for the most lossy output condition which corresponds to the minimum supercapacitor bank voltage  $U_{scm}$ . The corresponding converter's rating parameters are summarized in Table 5.3

Configuration number:	1	2
Maximum output Power: $P_{max}$ (kW)	30	30
DC Bus voltage: $U_{dc}$ (V)	315	315
Maximum supercapacitors bank voltage: $U_{scM}$ (V)	313.2	313.2
Depth of Discharge: $DOD$ (%)	<b>25</b>	<b>50</b>
Minimum supercapacitors bank voltage: $U_{scm}$ (V)	<b>235</b>	<b>156</b>
Minimum Duty cycle: $D_{min} = U_{scm}/U_{dc}$	<b>0.746</b>	<b>0.495</b>
Maximum output average current: $I_{scM}$ (A)	<b>128</b>	<b>192</b>
Switching frequency $f_{sw}$ (kHz)	20	20

Table 5.3.: Rating parameters for efficiency evaluation

For each configuration, the efficiency is evaluated for several values of number  $N_{ph}$  of converter's phases. Changing the number of phase will change the rating parameters of components, as it can be seen on Tables 5.4 and 5.6. A cost effective design requires therefore that appropriate components be chosen for each phase number. For an objective analysis mainly focused on the converter's topology, components of the same technology and manufacturer are selected for the two configurations as suggested in Tables 5.5 and 5.7. The power MOSFET are chosen to support the rating current at high temperature. This has led to almost doubling the current ratings at normal temperature.

$$P_{max} = 30kW; U_{dc} = 315V; U_{scM} = 313.2V; DOD = 25\%; I_{scM} = 128A$$

Number of phases: $N_{ph}$	1	3	6	9
Max phase average current: $I_{p_{avgM}}$ (A)	128	42.66	21.33	14.22
Desired current ripple (20%): $\Delta I_p$ (A)	25.6	8.5	4.2	2.8
Critical inductance: $2 \cdot L_c$ ( $\mu H$ )	61.6	184.8	369.6	554.4
Inductance for Desired ripple: $L_p$ ( $\mu H$ )	115.6	347	694	1041
Max peak current: $I_{p_{pkM}}$ (A)	140.5	46.8	23.4	15.6
Min peak current: $I_{p_{pkm}}$ (A)	114.9	38.3	19.5	12.7

Table 5.4.: Converter's rating characteristics for Configuration 1

Selected Components

Number of phases: $N_{ph}$	1	3	6	9
MOSFET reference: APTM50..	AM17F	M38JL	10BLL	16BLL
Manufacturer:	A.P.T	A.P.T	A.P.T	A.P.T
Drain-source voltage: $V_{DSS}$ (V)	500	500	500	500
Drain current at 25°C: $I_D$ (A)	180	88	46	30
On-state resistance: $R_{DSon}$ ( $m\Omega$ )	17	38	100	160
Inductance: $L_p$ ( $\mu H$ )	120	360	720	1080
DC resistance: $R_{Ldc}$ ( $m\Omega$ )	10	20	40	60

**A.P.T:** Advanced Power Technology

Table 5.5.: Converter's components for Configuration 1 and their nominal characteristics



$$P_{max} = 30kW; U_{dc} = 315V; U_{scM} = 313.2V; DOD = 50\%; U_{scm} = 156V; I_{scM} = 192A$$

Number of phases: $N_{ph}$	1	3	6	9	12
$I_{p_{avgM}}$ (A)	192	64	32	21.33	16
$\Delta I_p$ (A)(20%)	34.4	12.8	6.4	4.2	3.2
$2 \cdot L_c$ ( $\mu H$ )	20.5	61.5	123	184.5	246
$L_p$ ( $\mu H$ )	102.5	307.6	615.2	922.8	1230.5
$I_{p_{pkM}}$ (A)	211.2	70.4	35.2	23.5	17.6
$I_{p_{pkm}}$ (A)	172.8	57.6	28.2	19.2	14.4

Table 5.6.: Converter's rating characteristics for Configuration 2

Selected Components					
$N_{ph}$	1	3	6	9	12
MOSFET: APT50..	UM09F	AM25FT	M50JLL	10B2LL	14BLL
Manufacturer:	A.P.T	A.P.T	A.P.T	A.P.T	A.P.T
$V_{DSS}$ (V)	500	500	500	500	500
$I_D$ at $25^\circ C$ : (A)	497	149	71	45	35
$R_{Dson}$ ( $m\Omega$ )	9	25	50	100	140
$L_p$ ( $\mu H$ )	100	300	600	900	1200
$R_{Ldc}$ ( $m\Omega$ )	10	20	40	60	80

**A.P.T:** Advanced Power Technology

Table 5.7.: Converter's components for Configuration 2 and their nominal characteristics

### 5.3.2.1. Efficiency evaluation

The efficiency is evaluated for the buck operation, but the results is applicable to boost operation. As all the phases are identical, the losses are calculated for one phase and the result is multiplied by the number of phase to obtain the total losses. Two main kinds of losses are considered: The conduction losses and the switching losses which include the gate drive losses. The losses are evaluated for a junction temperature  $T_J = 125^\circ C$ .

- **Conduction losses:**

◇ The high side MOSFET conduction losses is given by:

$$P_{TH_{cd}} = R_{DSon_{125}} \cdot I_{TH_{rms}}^2 \quad (5.44)$$

$I_{TH_{rms}}$  is the high side transistor RMS current defined in Equation 5.36.  $R_{DSon_{125}}$  is the on-state resistance of the transistor at  $T_J = 125^\circ C$ .  $R_{DSon}$  found in data sheets is generally given for  $T_J = 25^\circ C$ . Its temperature dependence characteristics is generally also available. For the selected MOSFET  $R_{DSon_{125}} \cong 2 \cdot R_{DSon_{25}}$ .

◇ The low side MOSFET conduction losses is given by:

$$P_{TL_{cd}} = R_{DSon_{125}} \cdot I_{TL_{rms}}^2 \quad (5.45)$$

$I_{TL_{rms}}$  is defined in Equation 5.37.

◇ The phase inductor's cooper losses is given by:

$$P_{L_{cd}} = R_{Ldc} \cdot I_{prms}^2 \quad (5.46)$$

$I_{prms}$  is given in Equation 5.38. As the current ripple is low, the inductance core losses are negligible and are neglected.

◇ The phase inductance current continuity during the two dead times  $t_{dd}$  of each switching period is ensured by the body diode of the low side transistor. During the dead time preceding the high side transistor's turn-on, the current is approximatively equal to the minimum peak current  $I_{pmin} = 0.9I_{pavg}$ . During the dead time following the high side transistor's turn-off, the current is approximatively equal to the maximum peak current  $I_{pmax} = 1.1I_{pavg}$ . The incurred conduction losses in the diode are then given by:

$$P_{D_{cd}} = V_{SD} \cdot f_{sw} \cdot t_{dd} (I_{pmax} + I_{pmin}) = 2 \cdot V_{SD} \cdot f_{sw} \cdot t_{dd} \cdot I_{pavg} \quad (5.47)$$

$V_{SD}$  is the forward voltage drop of the transistor's body diode.  $t_{dd}$  should include the turn-on and turn-off delay times  $t_{don}$  and  $t_{dof}$  respectively.

The total conduction losses  $P_{tot_{cd}}$  for  $N_{ph}$  phases is then equal to:

$$P_{tot_{cd}} = N_{ph} (P_{TH_{cd}} + P_{TL_{cd}} + P_{L_{cd}} + P_{D_{cd}}) \quad (5.48)$$

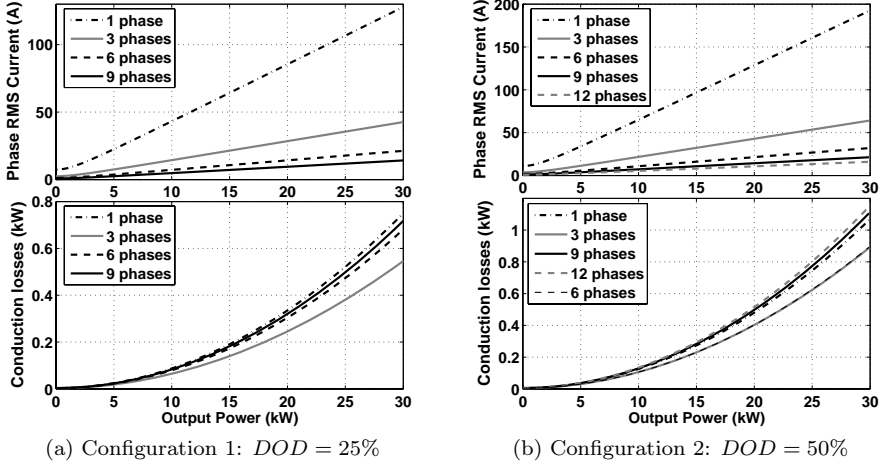


Figure 5.12.: Total conduction losses for the two configurations and different numbers of phase

The variations of the total conduction losses with respect to output power for different values of phase number and the two configurations are shown in Figure 5.12. While the square shape is obvious, it can be seen that the total conduction losses does not necessarily decrease when the phase current decreases (or the number of phase increases). In the first configuration for instance, the single-phase converter is the most lossy whereas in the second configuration it is the 12-phase one. This figure points out the importance of the component's characteristics on the converter's performances.

Let's consider two multi-phase converters with  $N_{ph1}$  and  $N_{ph2}$  phases respectively such that  $N_{ph2} > N_{ph1}$ . The on-state resistances of the MOSFET transistors and DC resistances of the phase inductors are  $R_{DSon1}$ ,  $R_{Ldc1}$  and  $R_{DSon2}$ ,  $R_{Ldc2}$  respectively. As  $N_{ph2} > N_{ph1}$ , the phase current rating of the second converter is lower and logically for the same MOSFET technology,  $R_{DSon2} > R_{DSon1}$ . Under the same power conditions, the total transistors conduction losses are  $P_{T_{cd1}} = R_{DSon1} \cdot I_{p_{rms}}^2 / N_{ph1}$  and  $P_{T_{cd2}} = R_{DSon2} \cdot I_{p_{rms}}^2 / N_{ph2}$

respectively. The total conduction losses  $P_{T_{cd2}}$  in the second converter will be lower than that  $P_{T_{cd1}}$  in the first converter only if its on-state resistance fulfills the following condition:

$$P_{T_{cd2}} < P_{T_{cd1}} \quad \Rightarrow \quad R_{DSon2} < \frac{N_{ph2}}{N_{ph1}} R_{DSon1} \quad (5.49)$$

This condition is also valid for the inductors resistances and should be simultaneously fulfilled to achieve a reduction of the conduction losses through the increase of the phase number. It can be noticed on Figure 5.12 that the 3-phase and 6-phase topologies of the second configuration present the same conduction losses, which means that the condition of Equation 5.49 isn't fulfilled. In fact, the MOSFET's on-state resistances and the inductor's DC resistances of these two topologies vary in the same proportion like the phase current, as it can be seen on Tables 5.6 and 5.7, which cancels the effect of the phase number's increase. The component's resistances have a great impact on the conduction losses. It should be noted that choosing the components so as to have a low on-state resistance could lead to an oversized and therefore costly design of the converter.

• **Switching losses:**

◊ High side MOSFET

The main switching losses occur in the high side transistor that undergoes hard switching conditions. An accurate evaluation of the switching losses is difficult because the necessary dynamic characteristics of the transistor, when they can be found in data sheets, strongly depend on the operating conditions, which may vary and are rarely those specified in data sheets. An estimation will be done on the basis of the switching circuit parameters and simplified waveforms presented in Figure 5.13.

From the curves of Figure 5.13b and omitting at a first step the reverse recovery effects of the low side transistor's body diode, the high side transistor turn-on losses  $P_{TH_{on}}$  can be estimated by:

$$P_{TH_{on}} = \frac{U_{dc} \cdot I_{pmin}}{2} (t_{ri} + t_{fv}) f_{sw} = \frac{U_{dc} \cdot I_{pmin}}{2} \cdot t_{SWon} \cdot f_{sw} \quad (5.50)$$

$t_{ri}$  is the rise time of the drain current and  $t_{fv}$  is the fall time of the drain-source voltage. In the same way, the high side transistor turn-off losses  $P_{TH_{of}}$

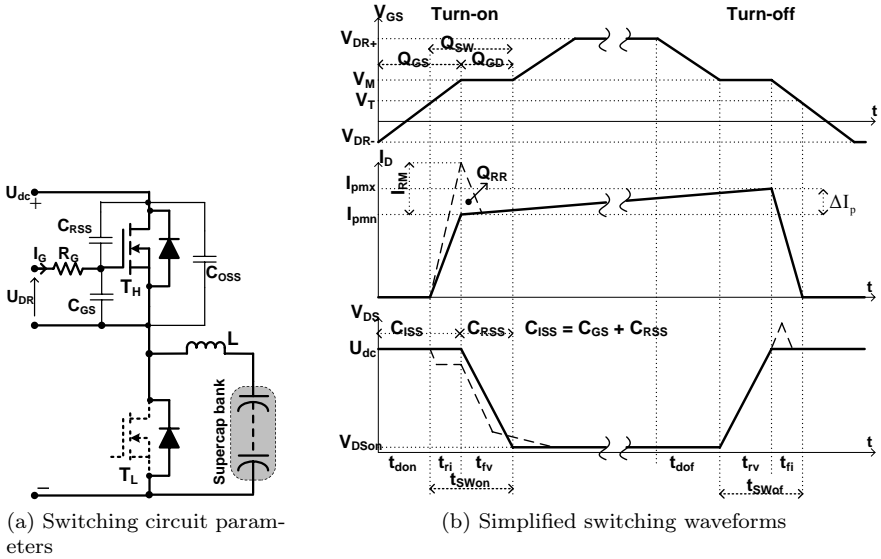


Figure 5.13.: High side MOSFET switching parameters and simplified waveforms

can be estimated by:

$$P_{THof} = \frac{U_{dc} \cdot I_{pmax}}{2} (t_{rv} + t_{fi}) f_{sw} = \frac{U_{dc} \cdot I_{pmax}}{2} \cdot t_{SWof} \cdot f_{sw} \quad (5.51)$$

$t_{rv}$  is the rise time of the drain-source voltage and  $t_{fi}$  is the fall time of the drain current. The rise and fall time must be determined now. They depend mainly on the gate drive circuit. Accurate formulas to evaluate these times are proposed in specialized literature [99], [100]. The main barrier in using these formulas is to find the necessary parameters in data sheets. Generally, these documents provide the gate capacitances  $C_{GD}$  and  $C_{RSS}$  and the gate charges  $Q_{GS}$  and  $Q_{GD}$ . From the capacitances, the different times can be approximated as follow: [101]

$$t_{ri} = R_G \cdot C_{ISS} \cdot \ln \left[ \frac{g_m \cdot V_{DR+}}{g_m (V_{DR+} - V_T) - I_{pmin}} \right] \quad (5.52)$$

$$t_{fv} = \frac{(U_{dc} - V_{DSon}) R_G \cdot C_{RSS}}{V_{DR+} - (V_T - I_{pmin}/g_m)} \quad (5.53)$$

$$t_{rv} = \frac{(U_{dc} - V_{DSon}) g_m \cdot R_G \cdot C_{RSS}}{I_{pmax} + g_m \cdot V_T} \quad (5.54)$$

$$t_{fi} = R_G \cdot C_{ISS} \cdot \ln \left[ \frac{I_{pmax} + g_m \cdot V_T}{g_m \cdot V_T} \right] \quad (5.55)$$

$V_T$  is the typical threshold voltage,  $V_{DR+}$  and  $V_{DR-}$  are the high and low levels of the gate driver's output respectively,  $R_G$  is the gate resistance and  $g_m$  is the MOSFET's transconductance. In case  $g_m$  is not given in the data sheet, it can be estimated from the MOSFET's output characteristic or the transfer characteristic, for the mean value of the drain current  $I_D$  by:

$$g_m = \left[ \frac{\Delta I_D}{\Delta V_{GS}} \right]_{V_{DS}} \quad (5.56)$$

The switching times can be also estimated from the corresponding gate charge  $Q_{SW}$  by: [102]

$$t_{SWon} = \frac{Q_{SW}}{I_{Gon}} \quad (5.57)$$

$$t_{SWof} = \frac{Q_{SW}}{I_{Gof}} \quad (5.58)$$

$I_{Gon}$  and  $I_{Gof}$  are the turn-on and turn-off gate currents respectively. If the switching gate charge  $Q_{SW}$  is not available in the data sheets, it can be approximated by:

$$Q_{SW} \cong Q_{GD} + \frac{Q_{GS}}{2} \quad (5.59)$$

Since the major part of the switching time is spent during the "Miller effect", the gate-source voltage can be assumed constant and equal to the Miller voltage  $V_M$  given by:

$$V_{Mon} \cong V_T + \frac{I_{pmin}}{g_m} \quad (5.60)$$

$$V_{Mof} \cong V_T + \frac{I_{pmax}}{g_m} \quad (5.61)$$

The turn-on and turn-off gate currents will be therefore given by:

$$I_{Gon} \cong \frac{V_{DR+} - V_{Mon}}{R_G} \quad (5.62)$$

$$I_{Gof} \cong \frac{V_{Mof} - V_{DR-}}{R_G} \quad (5.63)$$

Some manufacturers provide the turn-on and turn-off energies  $E_{on}$  and  $E_{of}$  in function of the drain current  $I_D$  for inductive switching. The switching power losses can be simply determined from these energies as follow:

$$P_{TH_{on}} = E_{on} \cdot f_{sw} \quad (5.64)$$

$$P_{TH_{of}} = E_{of} \cdot f_{sw} \quad (5.65)$$

There are several additional losses that are typically much smaller than the aforementioned losses:

The power  $P_{TH_G}$  to charge the gate:

$$P_{TH_G} = Q_G \cdot f_{sw} (V_{DR+} - V_{DR-}) \quad (5.66)$$

The losses  $P_{TH_{Rg}}$  in the gate resistance:

$$P_{TH_{Rg}} = R_G \cdot f_{sw} (t_{SW_{on}} \cdot I_{G_{on}}^2 + t_{SW_{of}} \cdot I_{G_{of}}^2) \quad (5.67)$$

The power  $P_{TH_{Cos}}$  to charge the MOSFET's output capacitance  $C_{OSS}$ :

$$P_{TH_{Cos}} = \frac{C_{OSS} \cdot f_{sw} \cdot U_{dc}^2}{2} \quad (5.68)$$

The reverse recovery power  $P_{TH_{Qrr}}$  of the low side transistor's body diode:

$$P_{TH_{Qrr}} = Q_{RR} \cdot f_{sw} \cdot U_{dc} \quad (5.69)$$

Finally the total switching losses for the high side MOSFET is equal to:

$$P_{TH_{sw}} = P_{TH_{on}} + P_{TH_{of}} + P_{TH_G} + P_{TH_{Rg}} + P_{TH_{Cos}} + P_{TH_{Qrr}} \quad (5.70)$$

◇ Low side MOSFET

The low side transistor always turns on and off while its body diode is conducting current as it can be seen on the simplified switching waveforms of Figure 5.14. The voltage across the transistor at that time is the diode forward voltage and is therefore very low, about 1V (i.e almost Zero Voltage Switching); hence, the low side transistor switching losses are also very low. The switching losses can be determined by replacing the DC bus voltage  $U_{dc}$  by the diode forward voltage  $V_{SD}$  in Equations 5.50 and 5.51:

$$P_{TL_{on}} = \frac{U_{SD} \cdot I_{pmax}}{2} (t_{ri} + t_{fv}) f_{sw} = \frac{U_{SD} \cdot I_{pmax}}{2} \cdot t_{SW_{on}} \cdot f_{sw} \quad (5.71)$$

$$P_{TL_{of}} = \frac{U_{SD} \cdot I_{pmin}}{2} (t_{rv} + t_{fi}) f_{sw} = \frac{U_{SD} \cdot I_{pmin}}{2} \cdot t_{SW_{of}} \cdot f_{sw} \quad (5.72)$$

The switching time for low side transistor can be determined in a similar way as for the high side one, even though there is almost no Miller effect for low side MOSFET because the voltage increases (becomes less negative) when the device is turned on [102]. The incurred error is negligible as the voltage remains anyway very low. Otherwise, the switching times can be determined on the basis of the exponential voltage curves of the gate capacitance. The additional losses can be calculated in the similar way as for the high side transistor, using the diode forward voltage  $V_{SD}$  instead of the DC bus voltage  $U_{dc}$  except for the reverse recovery losses. The total switching losses for the low side transistor is then:

$$P_{TL_{sw}} = P_{TL_{on}} + P_{TL_{of}} + P_{TL_G} + P_{TL_{Rg}} + P_{TL_{Cos}} + P_{TL_{Qrr}} \quad (5.73)$$



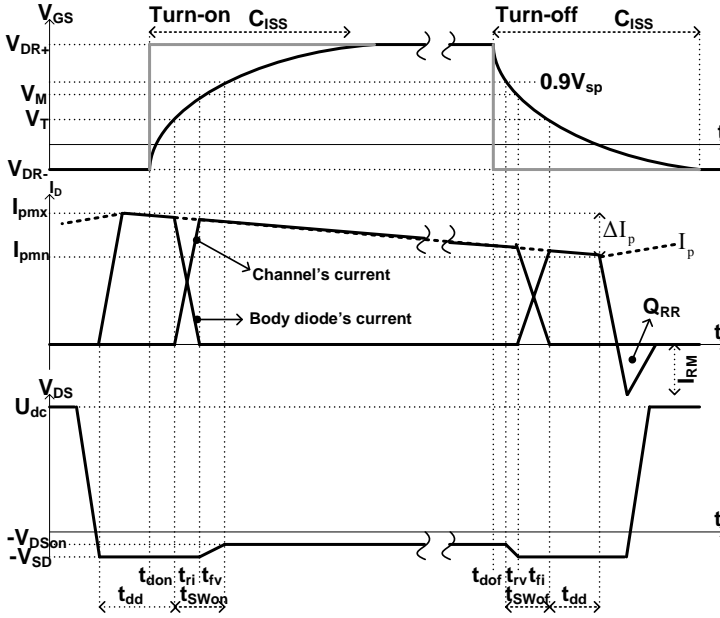
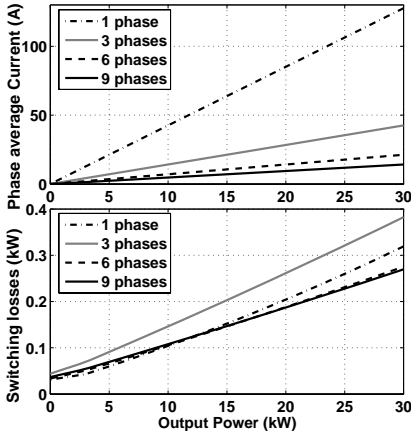


Figure 5.14.: Low side MOSFET simplified switching waveforms

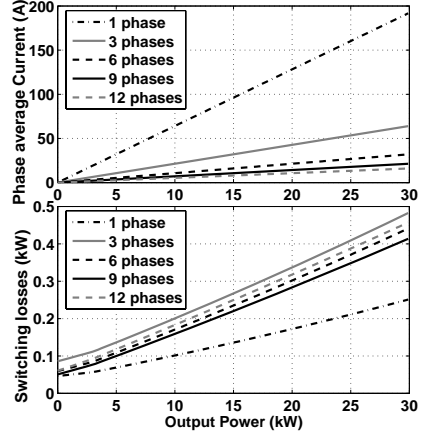
The total switching losses  $P_{tot_{sw}}$  for  $N_{ph}$  phases is the equal to:

$$P_{tot_{sw}} = N_{ph} (P_{TH_{sw}} + P_{TL_{sw}}) \quad (5.74)$$

The variations of the total switching losses with respect to the output power, again for different values of phase number and the two aforementioned configurations are given in Figure 5.15. These switching losses were evaluated on the basis of the switching energy characteristics provided by the manufacturer and thanks to the Equations 5.64 and 5.65. These characteristics appear in fact more accurate to evaluate the switching losses than the methods based on the estimation of the switching times. These methods tend to underestimate the



(a) Configuration 1:  $DOD = 25\%$



(b) Configuration 2:  $DOD = 50\%$

Figure 5.15.: Total switching losses for the two configurations and different numbers of phase

switching losses, what may be due to the important simplifications made on the waveforms. Unfortunately, the switching energy characteristics are rarely available in data sheets. In any case, the efficiency evaluation must be validated with experimental measurements.

The switching losses tend to vary almost linearly with the power or average current. It can be noticed like for the conduction losses that, increasing the number of phase does not automatically lead to a reduction of the switching losses, which confirm the great impact of the component's characteristics. In both configuration, the 3-phase converter is the lossiest.

The converter's efficiency for one way operation (Buck or Boost)  $\eta_{bb_{1w}}$  can be now derived from the losses estimation as follow:

$$\eta_{bb_{1w}} = \frac{P_{out}}{P_{out} + P_{tot_{cd}} + P_{tot_{sw}}} = \frac{P_{out}}{P_{out} + P_{loss}} \quad (5.75)$$

where  $P_{loss} = P_{tot_{cd}} + P_{tot_{sw}}$  is the total power losses.

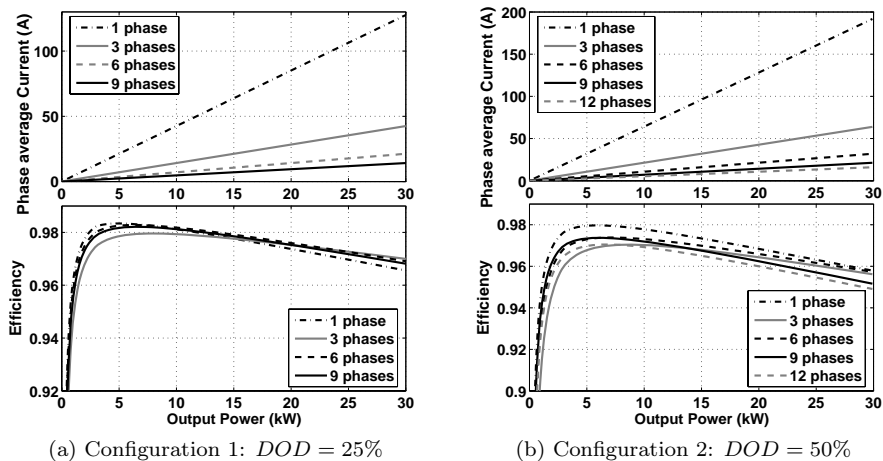


Figure 5.16.: Converter's efficiency for the two configurations and different numbers of phase

Figure 5.16 represents the converter's 1-way efficiency versus the output power for the two studied configurations and different values of phase number. For the first configuration, there is almost no difference between the efficiency curves of the 6-phase and the 9-phase converters, therefore the 6-phase one would be preferred for cost reasons. For the second configuration, the single-phase converter exhibits the best efficiency characteristic no matter the high current. This is mainly due to the interesting characteristics of the selected power MOSFET module. In conclusion, it is difficult to establish a formal rule for the determination of the appropriate number of phase. This is mainly because for each number of phase, different components should be used and their particular characteristics will greatly impact on the converter's performances.

The differences between the various efficiency characteristics are small, for instance about 1% between the single-phase and the 12-phase converters' efficiency characteristics, and even less among the others. Consequently, efficiency cannot be considered as the most important converter's design criterium; other

criteria like cost and reliability should be taken into account. Finally the design must be one more a tradeoff between the performances and cost.

### 5.3.2.2. Standby operation's efficiency improvement: Principle of "Power-controlled variation of the number of active phases"

In the previous sections, the design's effects on the multi-phase DC-DC converter's performances have been discussed. In this section, means of optimizing these performances through the operation control will be investigated. For that purpose the 6-phase converter for the first configuration studied in Section 5.3.2 will be considered.

The main issue is the partial load operation very common in power supply systems, where the output voltage should be held constant even in total absence of load. The idea is to analyze the consequences of deactivating some phases of the converter in that situation. For the 6-phase converter for instance, the power range can be divided into six equal subranges. The "power-controlled variation of the number of active phases" will consist in sequentially activating and deactivating the phases proportionally to the output power range. The effect of such an operation on the efficiency is presented in Figure 5.17.

It can be seen that for the larger and upper portion of the power range, the efficiency is higher when all the phases are operating than when some of them are deactivated. This is mainly due to the predominance of conduction losses in that upper portion as they are proportional to the square of the RMS current. It is more efficient to share the current among many phases than to reduce the number of active phase. For a converter with  $N_{ph}$  total identical phases, the conduction losses for  $N_{act}$  active phases are given by:

$$P_{N_{act},cd} = N_{act} (R_{Ldc} + R_{DSon}) \left( \frac{I_{Prms}}{N_{act}} \right)^2 = (R_{Ldc} + R_{DSon}) \frac{I_{Prms}^2}{N_{act}} \quad (5.76)$$

It is clear from Equation 5.76 that, the higher the number of phase the lower the conduction losses. It can be noticed however on Figure 5.17 that, for very low power, the conduction losses becomes less important and, the efficiency is higher with reduced number of active phase. It would be therefore interesting of having the possibility to vary the number of active phases in function of the

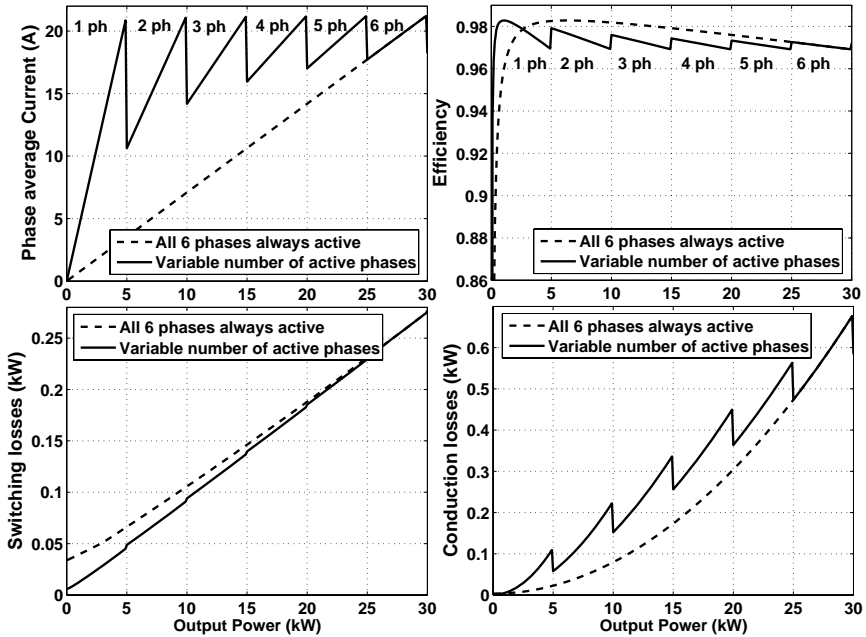


Figure 5.17.: Converter's efficiency with variable, power-controlled, active phase number

output power. A method for reliably doing so is presented below.

- **Power-controlled variation of the number of active phases**

The principle of power-controlled variation of the number of active phases is depicted in Figure 5.18a. The output power is determined from the supercapacitor bank voltage and phase current measurements realized for the purpose of the DC bus voltage regulation. For a  $N_{ph}$ -phase converter,  $N_{ph} - 1$  hysteresis comparators are used to sense the crossing of the  $N_{ph} - 1$  power thresholds  $P_s$  that delimitate the power subranges. The binary output of each comparator serves as activation signal and are used to block or unblock the gate signals of the corresponding phase-leg transistors through logic gate devices as it can be seen on Figure 5.21a. The hysteresis is necessary to avoid oscillations of

the comparators' outputs in case of noisy power signal. The number  $N_{act}$  of active phases is determined by summing up all the comparators' outputs. As the first phase is always active ( $Act1 = 1$ ), "1" is added to the sum to obtain the correct value of  $N_{act}$ .

The simulation curves of this principle are shown in Figure 5.18b for a triangular power shape of 60kW peak to peak. It can be seen that the generation of the activation signals works well both for positive and negative powers.

• **Automatic phase shift-angle adaptation**

It is well known that, the ripple's amplitude of the total output current of a  $N_{ph}$ -phase converter is  $N_{ph}$  times lower than that of a phase current if the  $N_{ph}$  currents are regularly angle-shifted within a period. If the number of active phase varies, the shift-angle should be adapted to the actual number to keep the output current ripple as low as possible. Table 5.8 gives the shift-angle of each phase, referred to the first phase ( $\Theta_1 = 0$ ) and normalized to  $2\pi$ , in function of the number  $N_{act}$  of active phases, for a 6-phase converter ( $N_{ph} = 6$ ).

$N_{act}$	$\Theta_1$	$\Theta_2$	$\Theta_3$	$\Theta_4$	$\Theta_5$	$\Theta_6$
1	0	D-A	D-A	D-A	D-A	D-A
2	0	1/2	D-A	D-A	D-A	D-A
3	0	1/3	2/3	D-A	D-A	D-A
4	0	1/4	1/2	3/4	D-A	D-A
5	0	1/5	2/5	3/5	4/5	D-A
6	0	1/6	2/6	1/2	2/3	5/6

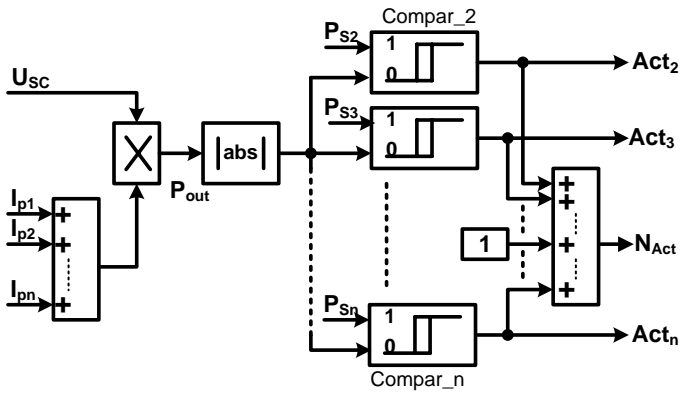
**D-A:** Deactivated ( $\Theta$  set to 0 or  $2\pi$ )

Table 5.8.: Normalized shift-angle versus number of active phase for a 6-phase converter

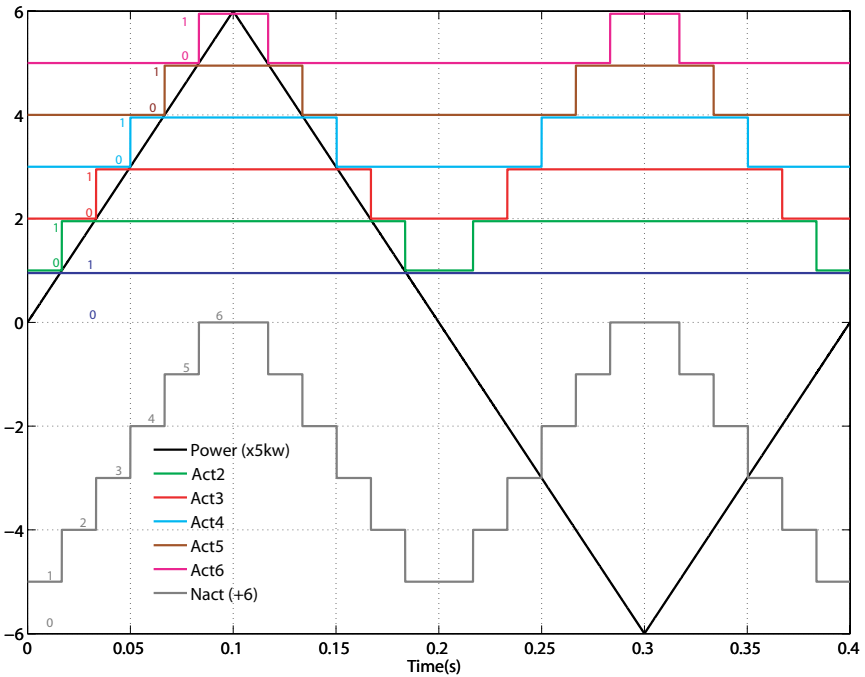
It can be seen from Table 5.8 that the shift-angle  $\Theta_n$  of the  $n^{th}$  phase ( $1 \leq n \leq N_{ph}$ ) can be determined knowing  $N_{act}$  as follow:

$$\Theta_n = 2\pi \left( \frac{n - 1}{N_{act}} \right) \tag{5.77}$$

This determination can be automatically done as shown in Figure 5.19a with a sawtooth signal generator for PWM. The shift-angle of the  $N_{ph} - N_{act}$  deac-



(a) Principle



(b) Simulation

Figure 5.18.: Power-controlled variation of the number of active phases

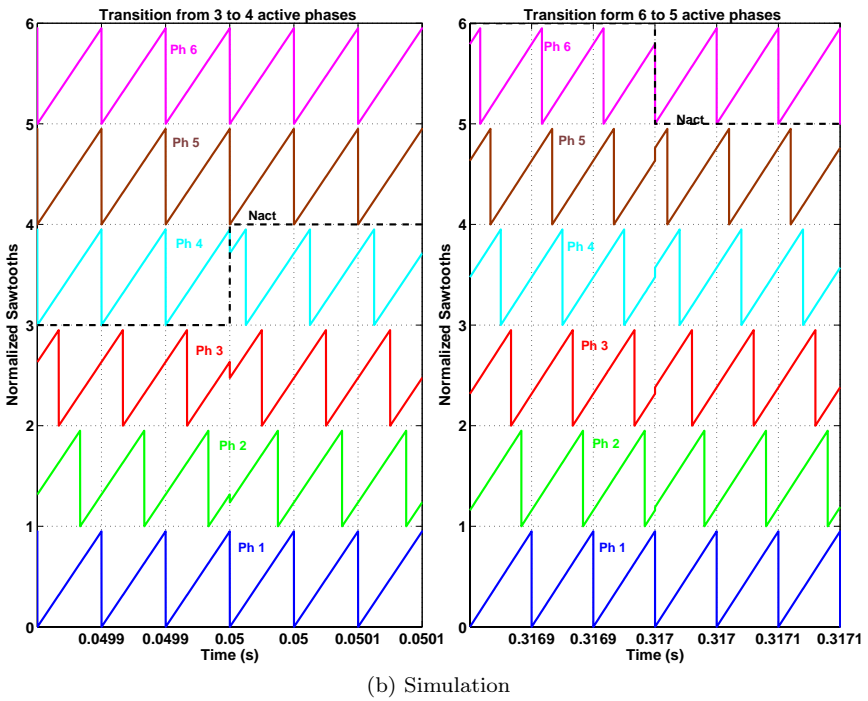
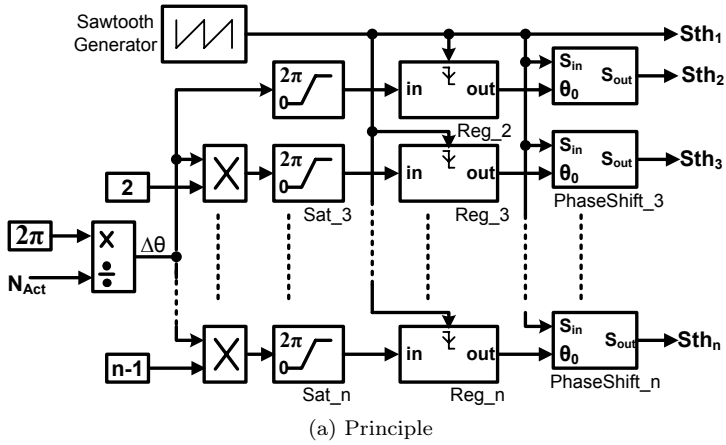


Figure 5.19.: Automatic sawtooth phase shift-angle variation



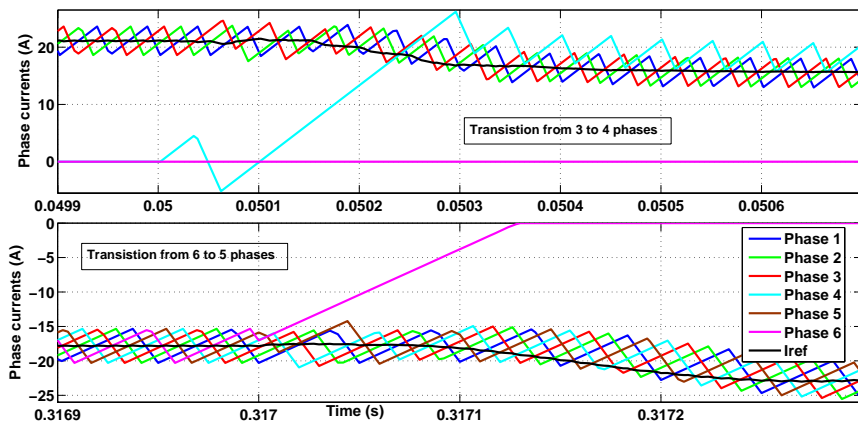


Figure 5.20.: Current waveforms during phase shift-angle variation

tivated phases is set to  $2\pi$  by the saturation blocks so that these phases remain in phase with the reference phase (Phase 1). To avoid frequency shift among the phases, the shift-angle's update for all the phases is synchronized to the falling edge of the reference sawtooth (Phase 1).

The simulation curves of the shift-angle adaptation for the 6 sawtooth signals are presented in Figure 5.19b, for the 3 to 4 and 6 to 5 active phases transitions. It can be seen that the principle works well in both transitions and that, it generates an irregular period for all the phases which are angle-shifted. However, this irregularity has no major impact on the converter's operation as it can be seen on the corresponding current waveforms presented in Figure 5.20, except a small ripple's peak on the total output current that can be observed on the second graph of Figure 5.21b.

#### • DC bus voltage and phase current regulation

It has been seen in Section 5.1 that the DC bus voltage regulation is performed thanks to cascaded voltage and current regulators. In Figure 5.1, a single current regulator is used to control the supercapacitor bank's current. With a multi-phase converter, each phase current must be controlled to ensure an

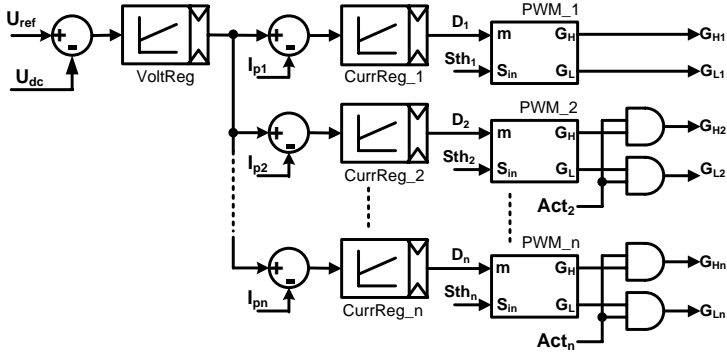
equal share of the output current among the phases. Otherwise, the unavoidable disparities among the components' characteristics would cause unbalance current share and, damageable over-currents may occur in some phases. Individual phase current regulation is also necessary for the effective operation of the active phase number variation's technique as it can be seen on Figure 5.21a.

A single voltage regulator is used to control the DC bus voltage. The voltage regulator generates a common current reference for all the  $N_{ph}$  current regulators; thus, the current reference is inherently adapted to the number of active phases. When a phase is activated, the voltage regulator maintains the current reference until the contribution of that newly activated phase to the total current becomes substantial, then the current reference is accordingly reduced as it can be seen on Figure 5.20. This approach avoids the generation of important voltage peaks or sags during the phases' activation or deactivation. It is therefore unnecessary to divide the current reference by the number of active phases.

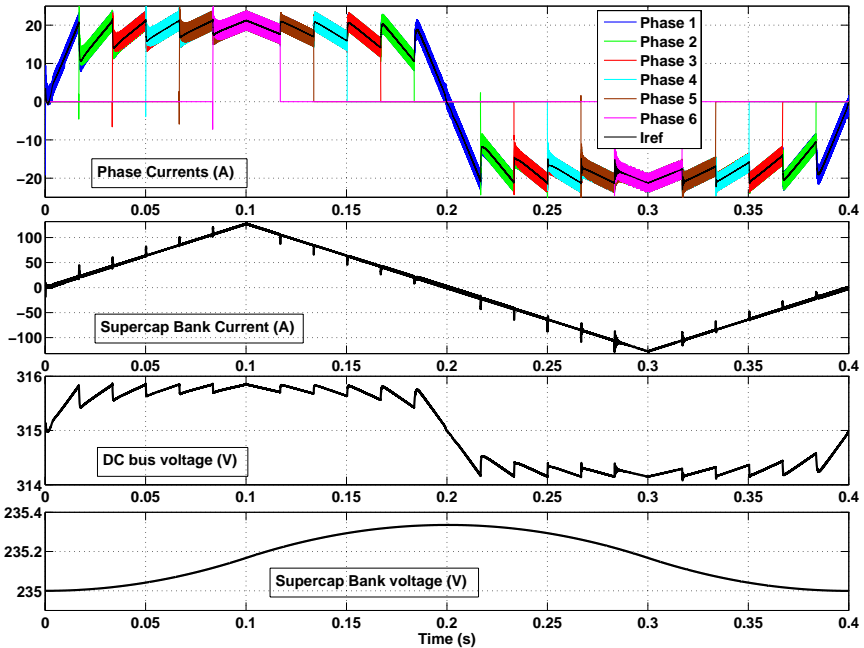
Simulation curves of the DC bus voltage regulation with variable, power-controlled active phase number, in the case of the triangular power shape of Figure 5.18b are shown in Figure 5.21b. It can be seen that the phase activation and deactivation operates very well according to the sequence presented in Figure 5.18b. It can be also observed that the output current's ripple decreases as the number of active phase increases, which confirms the effectiveness of the phases' shift-angle adaptation. The DC bus voltage presents an absolute static error less than 1V, which proves the effectiveness of the proposed voltage regulation technique.

#### • Application to efficiency optimization

The analysis of the efficiency curve of Figure 5.17 has shown that the converter efficiency will be improved if only one phase is activated at very low power (standby operation), then all the phases activated once the power reached a threshold value  $P_{th}$ . Only one comparator is necessary in that case and the principle of phase activation can be simplified as shown in Figure 5.22.  $P_{th}$  should be determined for each application either by efficiency measurement or by accurate evaluation as proposed in Section 5.3.2.1. This will result in a flatter efficiency curve mainly in the low power range.



(a) Principle



(b) Simulation waveforms

Figure 5.21.: DC bus voltage regulation with variable number of active phases

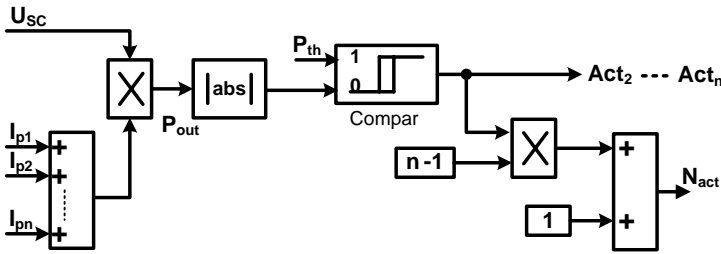


Figure 5.22.: Power-controlled, phase activation for no-load efficiency optimization

- **Fault tolerance capability**

The possibility of activating or deactivating some channels provides the multi-phase converter with some fault tolerance capability mainly for low power operation. In fact, as all the phases are identical, deactivated phases represent some redundancies for activated ones. In case of phase a failure (mainly opened-circuit failure), the faulty phase can be deactivated and easily replaced by a previously deactivated one.

For high power operation, the fault tolerance is difficult to perform as all the phases already operate near their nominal power rating, unless the converter’s design allows to do otherwise. It should be noted that the implementation of the fault tolerance does not require any additional devices, particularly in the case of DSP control for, a leg failure can be easily detected from the existing data (comparison of the measured currents and activation signals).

## 5.4. Overall efficiency of the auxiliary storage subsystem

The overall cycle efficiency of the auxiliary storage can be determined from the efficiencies of the supercapacitor bank and the DC-DC converter evaluated in Sections 5.2.3.1 and 5.3.2.1 respectively. The auxiliary storage subsystem’s

efficiency  $\eta_{as}$  has been defined in Chapter 4 as follow:

$$\eta_{as} = \eta_{bb} \cdot \eta_{sc} \quad (5.78)$$

$\eta_{bb}$  and  $\eta_{sc}$  are the cycle efficiencies of the buck-boost converter and the supercapacitor bank respectively.  $\eta_{sc}$  is given in Equation 5.29. Assuming that the buck and boost operations are perfectly symmetrical,  $\eta_{bb}$  can be obtained from the 1-way efficiency  $\eta_{bb_{1w}}$  defined in Equation 5.75 by:

$$\eta_{bb} = \eta_{bb_{1w}}^2 \quad (5.79)$$

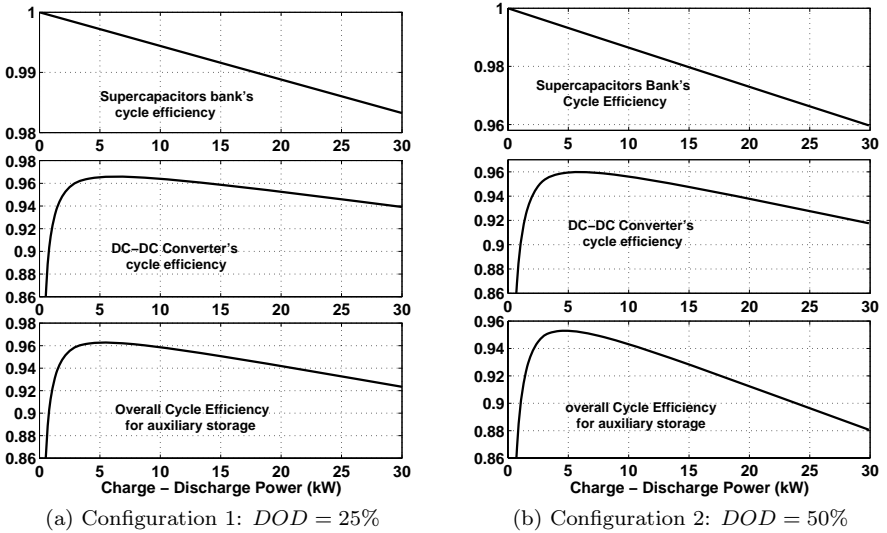


Figure 5.23.: Cycle efficiency of the auxiliary storage subsystem

The round-trip efficiency characteristics for the individual units and the whole auxiliary storage subsystem are represented in Figure 5.23. For both configurations, the efficiency decreases with increasing power. As the minimal output voltage was considered, this decrease is mainly due to the output current's increase accordingly to power. The figure also shows that the first

configuration, which possesses a higher minimum voltage and therefore lower maximum current, exhibits higher cycle efficiency than the second one. These facts show the importance of the “current efficiency” for the supercapacitive auxiliary storage subsystem. Hence, for high power application, the supercapacitor bank’s voltage should be as high as possible to reduce the current, and the converter should be designed to exhibit the highest possible efficient current capability.

For the global efficiency analysis carried out in Section 4.2.2, a 1-way efficiency of 95% was assumed for each unit, which had yielded the value  $0.95^4 = 0.81$  for the round-trip efficiency of the supercapacitive auxiliary storage subsystem. The evaluation’s results reported in Figure 5.23 show that this value can be exceeded by far with an optimized design, which will improve the overall storage system’s efficiency.

## 5.5. Chapter summary

In this chapter, a formal method for sizing the supercapacitor bank so as to meet any voltage and energy requirements was proposed. The efficiency of the supercapacitor bank versus the output power was evaluated and analyzed. This analysis has shown that the efficiency decreases almost linearly with increasing power and that for a given bank reducing the depth of discharge will increase the efficiency because the current rating will decrease. However, a small *DOD* necessitates a high number of cells and therefore induces higher cost, to meet the energy requirement .

The design of a multi-phase DC-DC converter to interface the supercapacitor bank to the DC bus has been also discussed. Its efficiency has been evaluated in function of the output power and number of phases, for two values of the supercapacitor bank’s *DOD*. Its analysis has shown that, like for the supercapacitor bank, the efficiency is higher for the smaller *DOD*, and that it does not necessary increase with increasing number of phase. This is mainly due to the great impacts of the components’ characteristics as, the converter’s design changes accordingly to the phase number. The design will be finally a trade-off between the efficiency and the cost. A technique for a “Power-controlled variation of the number of active phases” has been proposed to improve the converter’s low power operation’s efficiency. Simulation results have prove the

effectiveness of that control technique.

Finally the global efficiency of the supercapacitive auxiliary storage was evaluated from the individual efficiencies of its units. This evaluation has confirmed that very high round trip efficiencies can be achieved with optimized design and control.





# 6. Implementation and Experimental results

In Chapter 3, a control strategy to optimize the efficiency of the pneumatic-to-mechanical conversion was proposed and some simulation results presented and discussed. In Chapter 4, a design and control strategy to provide the storage system with power quality and flexibility was proposed. The development of these strategies has required extensive use of computer calculations and simulations that need be experimentally validated. In this chapter, the test benches realized for that purpose will be described and the experimental results presented and commented.

In the first section, the small bench realized for the test of the pure pneumatic conversion system studied in Section 3.1 will be briefly described, then the first practical results of the Maximum Efficiency Point Tracking strategy recorded from that bench will be presented and commented. The main experimental verifications of the proposed optimization and control strategies have been conducted afterwards on a prototype of the hybrid, hydro-pneumatic and supercapacitors storage system realized at *LEI*. The design and operation of that prototype will be described in the second part of the chapter and the experimental results will be reported. The partial and overall system efficiencies have been also measured and will be presented and discussed in the last part.

## 6.1. Pneumatic conversion system

### 6.1.1. Description of the test bench

Initial investigations on the optimization of pneumatic energy storage carried out at *LEI* were based on the utilization of a pure pneumatic conversion system using a volumetric air machine. The MEPT strategy was developed to optimize the operation of such a machine through speed control. The schematic diagram

of the experimental test-bench realized for that purpose given in Figure 6.1a.

The *ATLAS COPCO*'s LBZ14R-02 air motor, whose characteristics have been presented in Section 3.1.2 was used for the study and experiments. As that machine is not reversible, only the motor operation could be tested. The compressed air is provided by laboratory compressed air network at 10bar. A 90L vessel is used as a storage device with a maximum pressure of 7bar as recommended for the motor. A small MAXON's DC electric machine of 250W is used for the mechanical-to-electrical energy conversion. The DC machine is preferred in order to simplify the energy conversion and the speed control. A full-bridge DC-DC converter is used for the speed control and the power conditioning. A haft-bridge DC-DC converter is used to interface the supercapacitor bank.

For the MEPT experimentation in generation mode, the supercapacitor bank is not necessary and is replaced by a power resistor in oder to have an unlimited and controllable energy consumption. A 24V DC source is used to establish the DC bus voltage before the beginning of the discharge process, so that the converters can operate right away at the valve opening. Analog, sliding mode-controlled current regulators are implemented with the converters on a single power board for a fast and close current control. The other control functions are performed by a DSP board that also ensures the interface with the user through a personal computer. A detailed description of the DSP board is given in Section 6.2.1.2. A picture of the described test-bench is given in Figure 6.1b.

### 6.1.2. Implementation and results of the MEPT strategy

The maximum efficiency point tracking algorithm presented in Section 3.1.4.1, the speed control and DC bus voltage regulation functions are implemented in the DSP board. The pneumatic and mechanical powers are necessary to calculate the motor's efficiency and to perform the MEPT algorithm. Given that no air flow rate sensor is used, the flow rate is determined from the pressure and speed measurements thanks to the variable pressure model given in Equation 3.10. In a similar way, the mechanical torque is determined from the same measurements thanks to Equation 3.8.

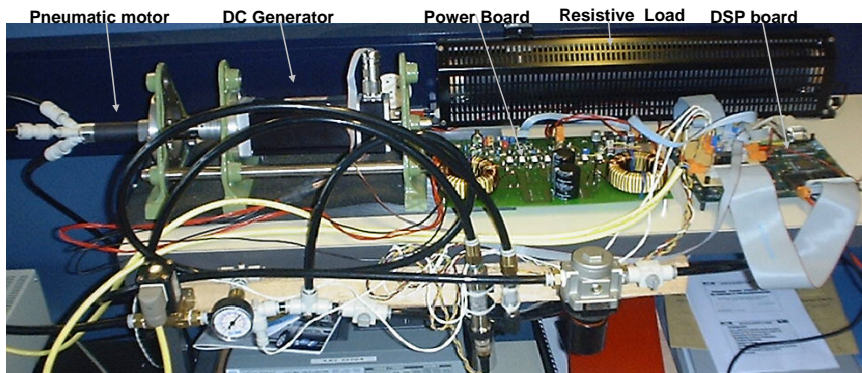
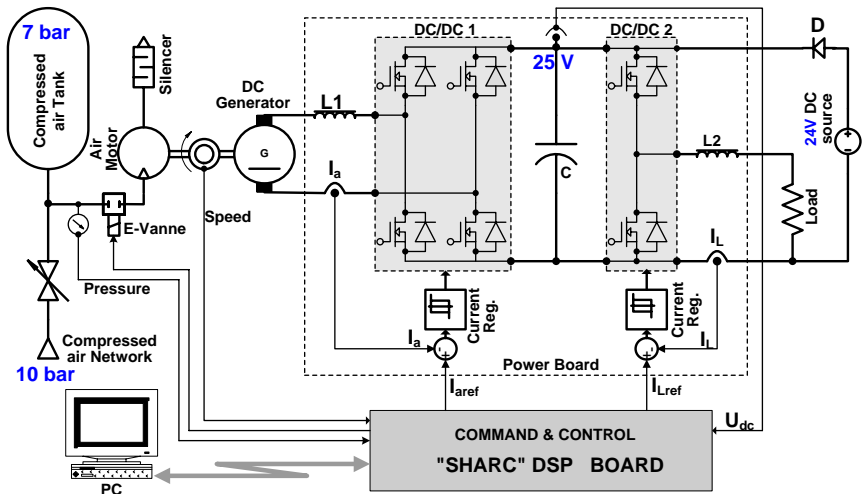
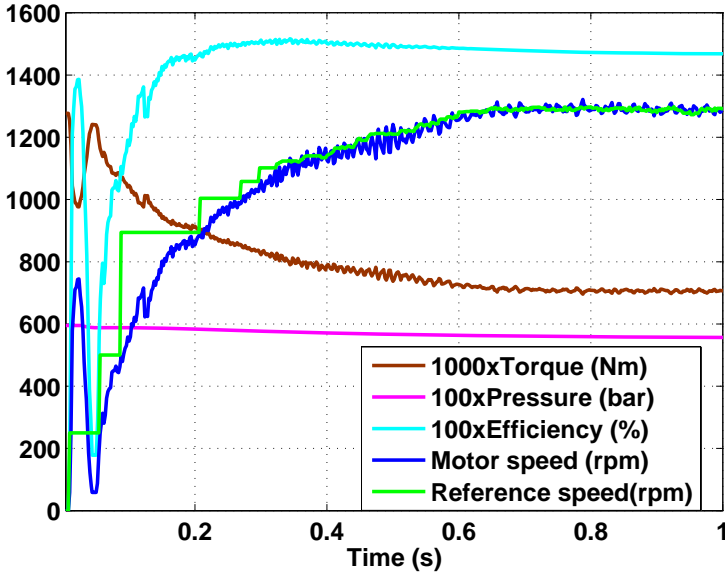
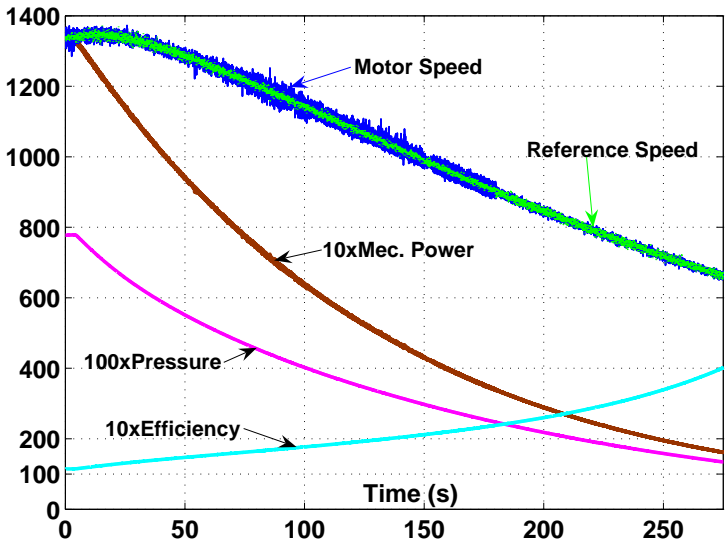


Figure 6.1.: Schematic diagram and Picture of the test-bench realized for the experimental evaluation of the MEPT strategy with pure pneumatic conversion



(a) MEPT startup at 6 bar



(b) MEPT tracking from 8 to 1.6bar

Figure 6.2.: Experimental curves of the MEPT strategy

Figure 6.2a shows the experimental curves recorded for a MEPT startup at 6bar. It can be seen that the system accurately reaches the optimal speed only about 0.7s after the valve is opened, tanks to the “Quadratic Interpolation” technique. This delay is variable because of the random starting torque of the vane type air motor used in the setup. The tracking curves of Figure 6.2b show a speed ripple of about 20rpm, mainly at high pressures. This is inherent to the "Perturbation-Observation" technique used for tracking. The ripple’s amplitude is however small enough to ensure a smooth speed variation. A comparison with Figure 3.11 shows that these curves are in good agreement with the simulation curves.

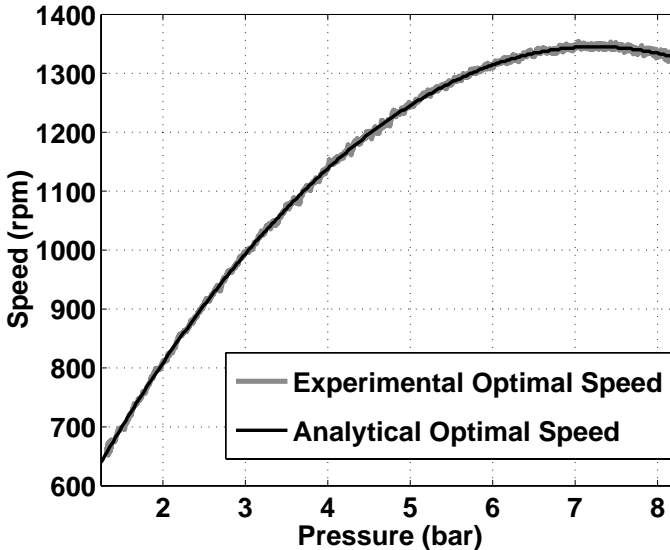


Figure 6.3.: Analytical and practical optimal speeds for the MEPT strategy with pneumatic conversion

The performances of the proposed MEPT algorithm can be well appreciated on Figure 6.3, where the experimental optimal speed is represented together with the analytic one, obtained by derivation of the efficiency expression given in Equation 3.20. It can be seen that the two curves are almost superposed,

which confirms the effectiveness and accuracy of the proposed algorithm.

## 6.2. Hybrid hydro-pneumatic and supercapacitors storage system

The experimental curves of Figure 6.2b confirm that in addition to their low pressure ratings, the efficiency of air machines remains low despite the implementation of the MEPT strategy, as it has been seen in Chapter 3. For those reasons, air machines were quickly abandoned to take advantage of the higher conversion performances of hydraulic machines. A test setup for the hybrid closed gas cycle, hydro-pneumatic and Supercapacitors energy storage system presented in Section 4.1.3, was realized to pursue the experimental investigations. The main goal of that installation was to verify the effectiveness of the MEPT strategy with hydro-pneumatic conversion and to evaluate the performances of the power variation and energy management strategies. A detailed insight on the design and operation of the setup is given in Section 6.2.1 and, the results of the first experiments are reported and commented in Section 6.2.2.

### 6.2.1. Description of the test setup

#### 6.2.1.1. System design

The system design had to be adapted to the laboratory context with as main constraint, the cost minimization through the use of available or low cost devices that allow achieving the experimental goals stated above. The schematic diagram of the dedicated test installation is presented in Figure 6.4. The system can be divided into the following main parts described hereunder: The line source, the active DC load, supercapacitive storage, the hydro-pneumatic storage and the command and control.

**Line supply** In the targeted applications, the energy source would be a PV panel for example, as shown on Figure 6.4. As the investigations are currently focused on the storage system, the PV source is replaced in the laboratory context by a line source with a  $2kW$  of power rating. The system is connected to the line through a manual 3-phase switch.

## 6.2. Hybrid hydro-pneumatic and supercapacitors storage system

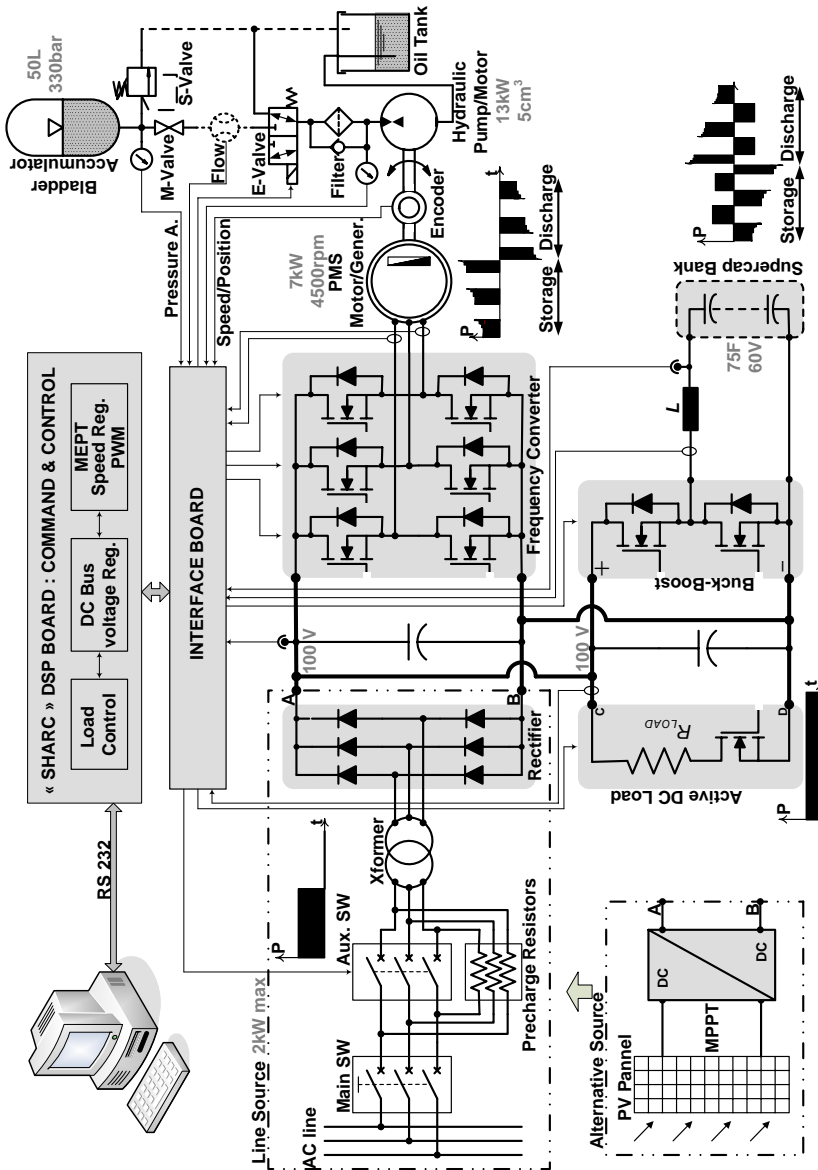


Figure 6.4.: Schematic diagram of the test-setup for hybrid BOP-A and Supercapacitors

A controllable circuit breaker is used to remotely control the connection and to bypass the pre-charge resistors. A 3-phase transformer adapts the line voltage to that of the DC bus and a 3-phase diode bridge rectifies the AC current.

**Active resistive load** An active DC load is used to simulate the energy user. It is composed of power resistors mounted on a dedicated heat sink and a power MOSFET transistor used to vary the load mean power in the range 0 to  $3.5kW$ . In real applications the load would be connected to the DC bus through a line inverter for instance.

**Supercapacitive auxiliary storage** As seen in Chapter 5, this subsystem consists of the supercapacitor bank and the Buck-Boost converter. The used supercapacitor bank was built by the former *MONTENA COMPONENTS* in Fribourg, Switzerland and is composed of 24 cells of 1800F - 2.5V, which gives a total capacitance of 75F and a maximum voltage of 60V. An active symmetrizing system is integrated in the bank.

The Buck-Boost converter is a classical, single-phase non-isolated bidirectional converter as can be seen on the schematic diagram. For the defined DC bus voltage range, power MOSFET transistors are the most suitable switches. A phase-leg power MOSFET module of *IXYS* and a power inductor were used to build the converter.

The DC bus voltage has been set to 100V to avoid a high boost ratio with the supercapacitor bank, but also to remain in the voltage range of battery storage applications for further possible comparison.

**Hydro-pneumatic main storage subsystem** All the components of the hydro-pneumatic storage subsystem were acquired from the industrial market without particular requirements, except for the frequency converter and the permanent magnet synchronous machine.

The frequency converter was built with the same components as the DC-DC converter.

The PMS machine is a dedicated axial flux disc machine adapted to the low DC bus voltage. Its main specifications are summarized in the the following table [103]:



Characteristic	Specification
Type	PMS 120 air cooled
Manufacturer	PERM Motor GmbH, Germany
Power	6.88 kW
Speed	4500 rpm
Torque	14.6 Nm
Voltage	66 V AC
Current	99 A

All the hydraulic components are from *PARKER Hydraulics*. The oil-hydraulic motor/pump is the F11-5 bent axis fixed displacement type, with the following characteristics [76]:

Characteristic	Specification
Type	F11-5
Manufacturer	Parker Hannifin, Sweden
Power	13 kW max continuous
Speed	8500 rpm max continuous
Torque	7.8 Nm @ 100 bar
Displacement	5 cm <sup>3</sup> /rev
Pressure	350 bar max continuous
Flow	41 L/min max continuous

The hydraulic accumulator is a 50L bladder type, with a maximum pressure of 350bar. Many other hydraulic accessories like the oil tank, the manual valve, the electro-valve, the oil filter, the pressure sensors are also used for control and security purposes.

A picture of the test setup is given in Figure 6.5 where the different components can be identified. The main space constraint was to ensure an easy access to all the components. The accumulator is mounted on the wall with dedicated clamp and base brackets. The oil tank is placed a bit higher than the motor-pump to benefit from the hydrostatic pressure and therefore reduce cavitation at the pump intake.

#### 6.2.1.2. System control

The control algorithms are performed by a “SHARC” DSP of *Analog Devices* running at 32MHz [104]. The DSP is embedded in a hardware environment



Figure 6.5.: Picture of the test-setup for hybrid BOP-A and Supercapacitors

containing fast A/D and D/A converter channels, a programmable logic device (FPGA) and some memories (RAM) on a single board. A software environment is available for easy implementation of control functions and easy system management from a personal computer [105]. A RS232 communication link establishes the connection to the DSP board. An additional interface board is used to adapt and redirect the multiple command signals to their respective gates, and to collect and shape the measurements' signals.

The PWM modulators are implemented in the *Xilinx* FPGA circuit [106] and all the other control functions run on the DSP and are programmed in C language [107]. On the basis of the discussion carried out in Section 5.3.1.3, a switching frequency of 10kHz has been chosen for all the modulators. This value corresponds to a control loop period of  $100\mu s$ , which appears fairly reasonable for the application. Within this time, the controller executes all the control functions and updates the modulation index and, with time left for data transfer to the PC as the onboard memory is limited.

### 6.2.2. Implementation and results of the MEPT strategy

#### 6.2.2.1. Implementation of the MEPT strategy

To ease the experimentation of the MEPT strategy, the test setup is modified as shown in Figure 6.6. The auxiliary storage is disconnected and the low power line source is replaced by a more powerful DC source. Thus, the normal intermittent operation can be avoided and the subsystem can operate continuously for longer time, even for a whole charge-discharge cycle, which is important for efficiency measurements as will be seen in Section 6.2.4.1.

The MEPT operation is based on the efficiency-controlled speed adjustment. As the hydraulic machine is directly coupled to the PMS machine, the speed of the first is controlled through the second. A classical field-oriented vector control is implemented in the DSP for that purpose. The speed reference is provided at each optimization loop by the MEPT algorithm after the evaluation and analysis of the hydraulic machine's efficiency. The efficiency evaluation requires the measurement of the mechanical power  $P_{mc}$  and the hydraulic power  $P_{hd}$ .

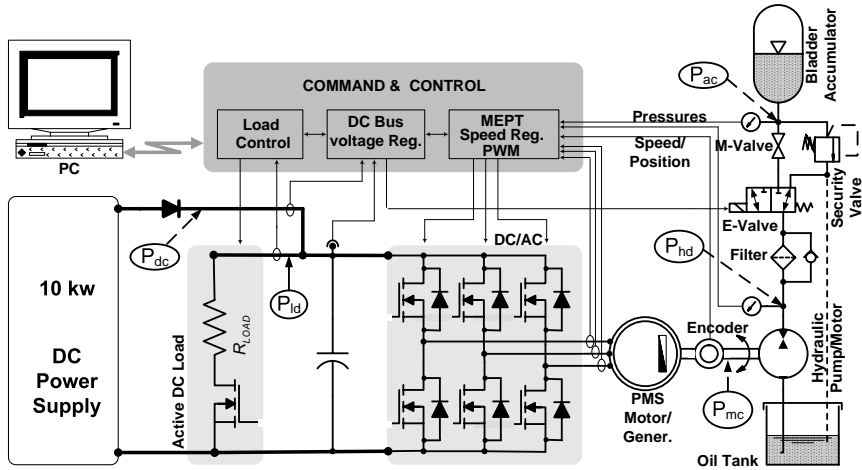


Figure 6.6.: Arrangement for experimental evaluation of MEPT strategy and the main storage subsystem’s efficiency measurement

$P_{mc}$  is determined indirectly from the measurements of the speed and the mechanical torque. The speed is measured through a quadratic encoder. Because of its high cost, the test-setup is not equipped with a torque sensor. Instead, 3-dimensions, torque versus Q-axis current and speed characteristics of the PMS machine, for the motor and generator operations, were previously measured on a dedicated test-bench at the laboratory electrical machines. These characteristics are implemented in the measurement functions and used to determine the mechanical torque from the speed and the phase currents’ measurements.

$P_{hd}$  is determined from the measurements of the pressure and the oil flow rate. For the same economical reasons, the system is not equipped with a flow rate sensor. As oil can be assumed incompressible in the operating pressure range, the flow rate can be easily determined from the speed knowing the displacement. However, for more accuracy, the flow rate versus speed characteristics shown in Figure 3.24 are also implemented in the measurement functions.

### 6.2.2.2. Experimental results of the MEPT strategy

For a fair evaluation of the optimization strategy, the main storage subsystem is firstly operated at constant speed cycles and afterwards at MEPT-controlled variable speed cycles. These cycles are performed within the pressure range of 100 to 200bar.

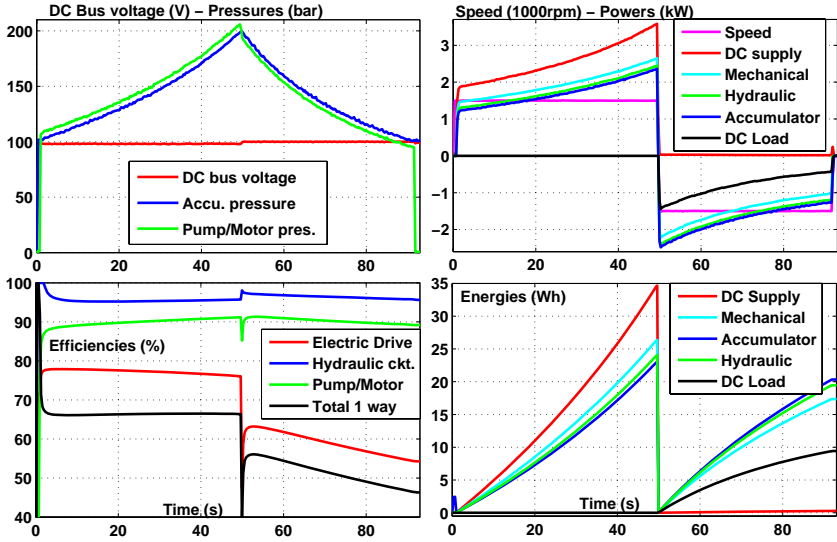
The experimental curves recorded for 1500rpm and 3000rpm constant speed cycles respectively are represented in Figure 6.7. It can be seen on the efficiency graph of Figure 6.7a that the hydraulic machine's efficiency remains around 90% during the whole 1500rpm constant speed cycle. For the 3000rpm cycle, it appears on the corresponding efficiency graph of Figure 6.7bthat, for high pressure, this efficiency is 2 to 3% higher compared to that of the 1500rpm cycle. This remark confirms that high speed operation is more efficient for high pressure than low speed.

The experimental curves recorded for two variable speed cycles are represented in Figure 6.8. The efficiency graphs of that figure show that the hydraulic machine's efficiency is globally higher than the ones obtained for the two constant speed cycles, particularly during the discharge operation.

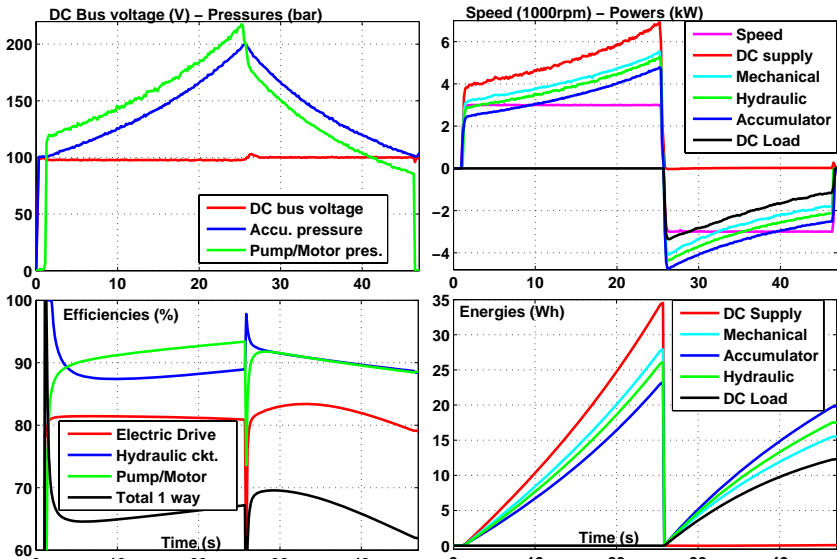
Mode	Characteristics	1500rpm	3000rpm	MEPT 1	MEPT 2
Charge	Mechanical W. (Wh)	26.35	27.90	25.37	27.93
	Hydraulic W. (Wh)	24.03	26.06	23.12	25.46
	<b>Efficiency (%)</b>	<b>91.19</b>	<b>93.40</b>	<b>91.13</b>	<b>91.15</b>
Dis-charge	Hydraulic W. (Wh)	19.44	17.52	19.20	18.99
	Mechanical W.(Wh)	17.34	15.51	18.14	17.85
	<b>Efficiency (%)</b>	<b>89.19</b>	<b>88.52</b>	<b>94.47</b>	<b>93.99</b>
Cycle	<b>Efficiency (%)</b>	<b>81.33</b>	<b>82.67</b>	<b>86.09</b>	<b>85.67</b>

Table 6.1.: Energy efficiency of the hydraulic machine for various operating cycles

A more relevant appreciation can be made by comparing the cycles' efficiencies presented in Table 6.1. It can be seen that the MEPT-controlled cycles' efficiencies are about 4% higher than that of the constant speed cycles. This improvement confirms the effectiveness of MEPT-controlled variable speed op-

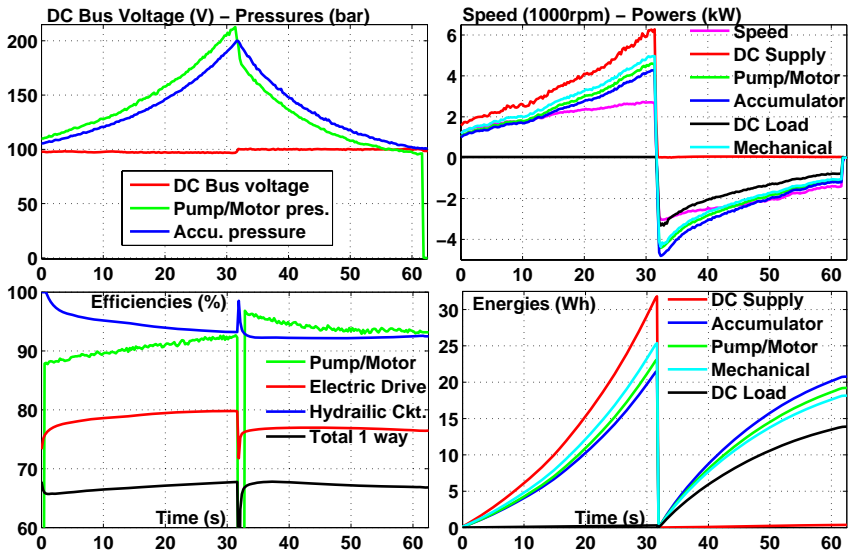


(a) 1500rpm constant speed cycle

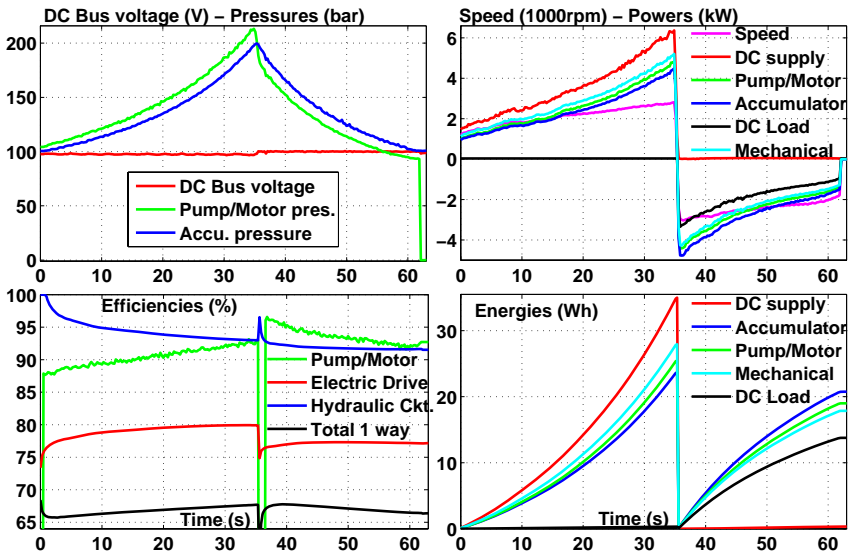


(b) 3000rpm constant speed cycle

Figure 6.7.: Constant speed cycles for the hydro-pneumatic storage



(a) Variable speed cycle 1



(b) Variable speed cycle 2

Figure 6.8.: MEPT-controlled cycles for the hydro-pneumatic storage

eration with hydraulic machines.

Figure 6.9 presents the theoretical optimal speed derived from the interpolated efficiency characteristics of Figure 3.24, together with the experimental optimal speed imposed by the MEPT algorithm. Although there is a common tendency to increase the speed with increasing pressure for the two curves, their values differ notably, particular at high pressure. It is difficult to explain this difference because there is some error related to the interpolated efficiency characteristics as can be seen in Figure 6.10.

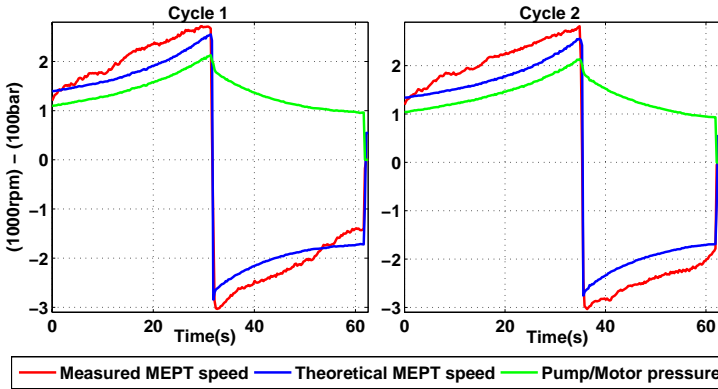


Figure 6.9.: Theoretical and measured optimal speed for the MEPT operation

In any case, the measured maximum efficiencies are in the range indicated by the manufacturer, and the MEPT strategy improves the cycle efficiency of the hydraulic machine. These facts are most important than an exact match between the theoretical and practical optimal speeds, which is difficult to verify. The implications of MEPT strategy on the whole system’s efficiency will be analyzed in Section 6.2.4.



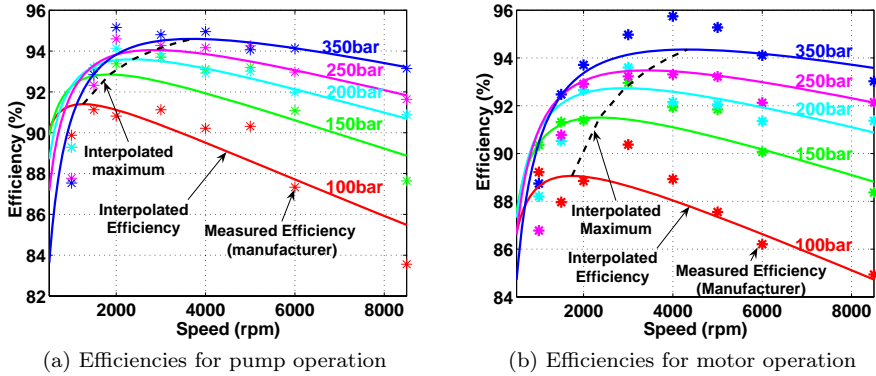


Figure 6.10.: Measured and Interpolated efficiency characteristic for the experimental hydraulic motor/pump

## 6.2.3. Implementation and results of the power variation strategy

### 6.2.3.1. Implementation

It has been seen in Chapter 4 that the power flexibility mainly relies on the intermittent operation of the hydro-pneumatic storage subsystem, associated to the auxiliary storage subsystem. The free-oscillating power modulation mode presented in Section 4.1.2.3 has been adopted for the experiments; the main control parameter of that intermittent operation is therefore the supercapacitor bank's voltage. A constant DC bus voltage guarantees a free power flow between the subsystems.

The principle of the power flow control shown in Figure 4.2 is easily implemented in the DSP. This control function possesses a higher priority than the MEPT control function for obvious security reasons. Its is executed every sampling period. The supercapacitor's depth of discharge is limited to 10V (from 55V to 45V) in order to limit the maximum current, and also to shorten the cycle period so as to register a whole cycle's measurements in the limited onboard memory.

### 6.2.3.2. Experimental results

Figure 6.11 presents the experimental curves of power modulation recorded during a MEPT-controlled storage operation. During this operation, the line and load powers are set to 1.8kW and 0.5kW respectively. As the bank's depth of discharge remains constant, so does the available energy. Hence, the duration of the compression strokes decreases when the pressure and therefore the compressing power increases.

Between two strokes, the supercapacitors are recharged with the constant line power; the recharging time is therefore constant. During that time, some compression heat is exported to the surroundings through the accumulator's wall, which causes its pressure to decrease slightly. It can be seen that the DC bus voltage remains constant whatever power level the hydro-pneumatic storage requires, which confirms the capacity of the auxiliary storage to ensure power quality and flexibility to the whole system. There lies the main advantage of the hybrid topology.

The technique works similarly the other way around as shown on the discharge operation's curves presented in Figure 6.12. During this operation, the line is completely disconnected and the load power is maintained to 0.5kW. When the pressure decreases, so does the available power. Consequently, the supercapacitors' charging power will decrease in such a way that the load power remains constant.

## 6.2.4. Partial and overall system efficiencies measurement

The round trip efficiency is an important characteristic of any storage system as, it determines the portion of energy that can be recovered following a charge-discharge cycle. Although the experimental setup has not been designed with the goal of achieving high efficiency, this characteristic has been measured in order to determine the main critical parts of the system.

### 6.2.4.1. Main storage subsystem's cycle efficiency

The best overall energy efficiency is obtained if all units operate at their optimal conditions. This requirement is difficult to meet with the built experimental setup, particularly for the hydraulic accumulator which requires isothermal

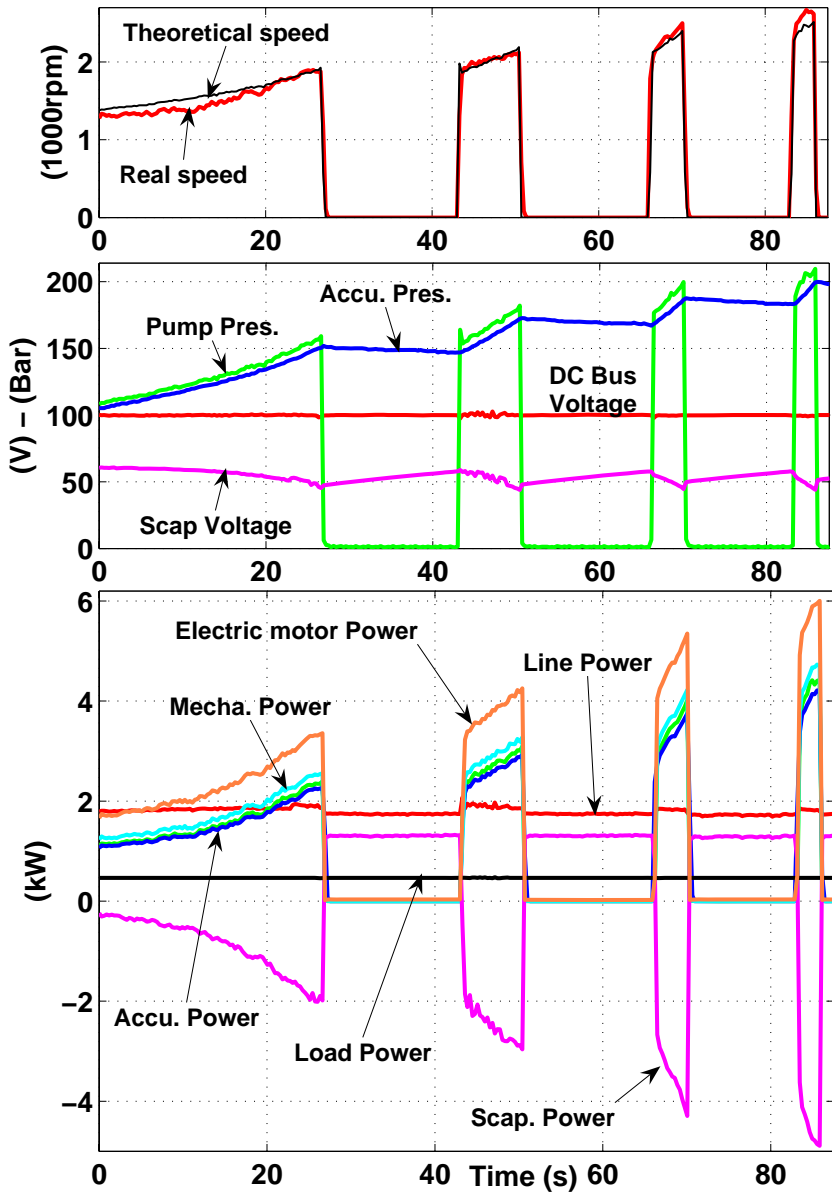


Figure 6.11.: Power modulation during MEPT-controlled storage operation

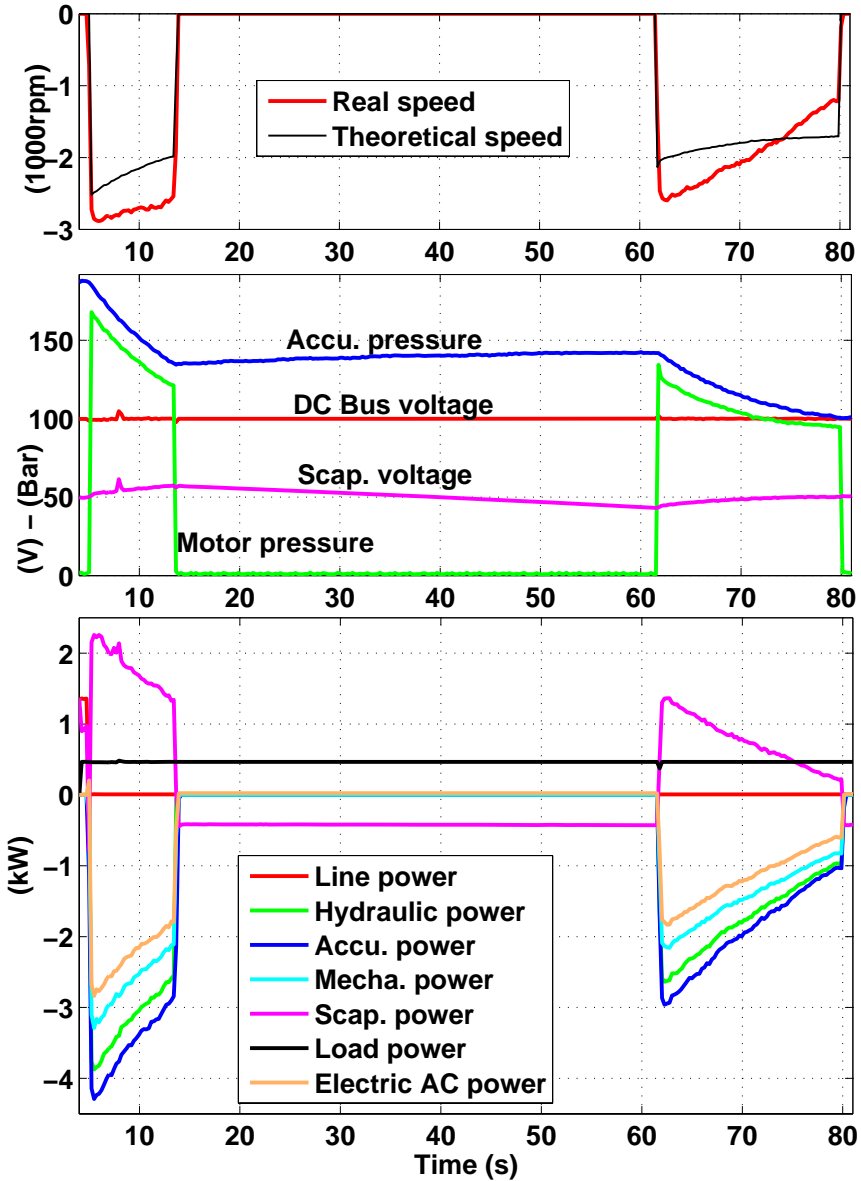


Figure 6.12.: Power modulation during MEPT-controlled discharge operation

compression and expansion. It has been seen in Section 3.2.1.1 that isothermal conditions will be achieved if the filling time constant of the accumulator is much greater than its thermal time constant. For the used 50L accumulator, this condition requires a very low oil flow rate, which is incompatible with the optimal speed of the rotating machines.

Energetically speaking, an ideal isothermal cycle is equivalent to an ideal adiabatic one. Adiabatic cycle would require either a perfectly isolated accumulator (What is not the case in the experimental setup) or a very fast charge-discharge cycle that won't allow any time for heat exchange with the surrounding. This second requirement seems more compatible with the optimal operating conditions of the rotating machines and the volume of the used accumulator. Hence, quasi-adiabatic cycles are realized to have more relevant estimations of the experimental hydro-pneumatic subsystem's efficiency.

For that purpose, the setup is modified as shown in Figure 6.6. The efficiency and energy curves recorded from various cycles are represented in Figures 6.7 and 6.8, and commented below.

#### • Accumulator

The hydraulic accumulator is the main energy storage device of the system. Its cycle efficiency is determined by the ratio of the energy restored during the discharge phase over that one received during the charge. The energy measurements for each operating cycle are given in Table 6.2, with the corresponding cycle efficiencies.

Characteristics	1500rpm	3000rpm	MEPT 1	MEPT 2
Stored energy (Wh)	22.99	23.18	21.55	23.68
Restored Energy (Wh)	20.33	19.81	20.75	20.75
<b>Cycle Efficiency (%)</b>	<b>88.42</b>	<b>85.46</b>	<b>96.28</b>	<b>87.62</b>

Table 6.2.: Round trip efficiency of the hydraulic accumulator for various operating cycles

The table shows that there isn't a particular relationship between the operating speed and the accumulator's cycle efficiency. The average value of

about 89% is very low compared to the expected theoretical efficiency for an isothermal process, the cycle being neither isothermal nor adiabatic due to the time required for the storage and discharge processes. One would have expected a higher efficiency for the 3000rpm cycle as it is the shortest one, but this isn't the case, which suggests that there might be other losses than the thermal losses, for instance the losses related to the oil flow inside the accumulator. It should also be noted that the used accumulator is mainly designed for peak power damping; an appropriate design dedicated to high capacity energy storage applications as considered in this project would probably induce some losses and cost reductions.

• **Hydraulic circuit**

Table 6.3 and the efficiency curves of Figures 6.7 and 6.8 show that the various accessories present in the hydraulic circuit are sources of important losses. It can be seen that these losses increase with the oil flow rate and represent in some cases more than 10% of the power. They are illustrated by the pressure difference between the hydraulic machine and the accumulator. The main lossy elements are the oil filter and the electro-valve because of the important changes in flow section and direction in these devices. An appropriate sizing of the pipe and choice of the sensing and control components would yield a substantial reduction of flow losses.

Mode	Characteristics	1500rpm	3000rpm	MEPT 1	MEPT 2
Charge	Pump W. (Wh)	24.03	26.06	23.12	25.46
	Accu. W. (Wh)	22.99	23.18	21.55	23.68
	<b>Efficiency (%)</b>	<b>95.67</b>	<b>88.94</b>	<b>93.20</b>	<b>93.00</b>
Dis-charge	Accu. W. (Wh)	20.33	19.81	20.75	20.75
	Motor W. (Wh)	19.44	17.52	19.20	18.99
	<b>Efficiency (%)</b>	<b>95.62</b>	<b>88.44</b>	<b>92.53</b>	<b>91.51</b>
Cycle	<b>Efficiency (%)</b>	<b>91.47</b>	<b>78.65</b>	<b>86.23</b>	<b>85.11</b>

Table 6.3.: Energy efficiency of the hydraulic circuit for various operating cycles

• **Hydraulic machine**

The efficiency of the hydraulic machine was discussed in Section 6.2.2.2. The

results summarized in Table 6.1 show that this machine is the stronger link of the conversion chain and that its efficiency will be optimized with the proposed MEPT strategy.

- **Electric drive**

Table 6.4 and the efficiency curves of Figures 6.7 and 6.8 show that the electric drive is the weak link of the experimental conversion chain. The very low efficiency at 1500rpm is probably because this speed is very far from the nominal speed of the PMS machine and the EMF is therefore very low. The choice of the nominal speed wasn't optimal because the characteristics of the hydraulic machine were unknown at the time the electric machine was selected. Nevertheless, there still exist possibilities to achieve high overall efficiency (at least 90% 1-way) for the drive system, i.e the frequency converter and the electrical machine. The experiments have shown that two points are capital for the optimal design and efficient operation of the electric drive in hydro-pneumatic storage applications:

Mode	Characteristics	1500rpm	3000rpm	MEPT 1	MEPT 2
Charge	DC supply W. (Wh)	34.66	34.52	31.81	34.99
	Mechanical W. (Wh)	26.35	27.90	25.37	27.93
	<b>Efficiency (%)</b>	<b>76.02</b>	<b>80.82</b>	<b>79.75</b>	<b>79.82</b>
Dis-charge	Mechanical W. (Wh)	17.34	15.51	18.14	17.85
	Load W. (Wh)	9.41	12.27	13.87	13.78
	<b>Efficiency (%)</b>	<b>54.26</b>	<b>79.11</b>	<b>76.46</b>	<b>77.19</b>
Cycle	<b>Efficiency (%)</b>	<b>41.24</b>	<b>63.93</b>	<b>60.97</b>	<b>61.62</b>

Table 6.4.: Energy efficiency of the Electric drive for various operating cycles

- **The DC bus voltage:** The main argument for the choice of a low DC bus voltage was the compatibility with the low supercapacitor bank's voltage. The study of the auxiliary storage carried out in Chapter 5 has shown the possibility of realizing high efficiency supercapacitive storage for higher voltages. A higher voltage should be chosen for the DC bus to reduce the currents in the drive and therefore increase the efficiency. Classical values of 315V for a single-phase load/line and 540V for a 3-

phase load/line as suggested in Section 5.2.3.2 seem effective for the whole system.

- **The nominal speed:** A high overall efficiency can be expected for the conversion chain only if the optimal speeds of all the rotating machines are compatible. This is not the case for the experimental setup where the nominal speed of the electrical machine is 4500rpm whereas that of the hydraulic machine ranges from 1500rpm to 3000rpm for the considered pressure range. The nominal speed of the electrical machine must be included in the optimal speed range of the hydraulic machine.

- **Round trip efficiency of the main storage subsystem**

The round trip efficiency of main storage subsystem is determined by the ratio of the energy received by the DC load during the discharge phase over that delivered by the DC source during the storage phase. The resulting values are presented in Table 6.5.

Characteristics	1500rpm	3000rpm	MEPT 1	MEPT 2
DC supply energy (Wh)	34.66	34.52	31.81	34.99
Load energy (Wh)	9.41	12.27	13.87	13.78
<b>Cycle Efficiency (%)</b>	<b>27.15</b>	<b>35.54</b>	<b>43.60</b>	<b>39.38</b>

Table 6.5.: Round trip energy efficiency of the main storage subsystem for various operating cycles

These results show that the MEPT-controlled variable speed operation modes yield higher efficiencies than the constant speed operation. However, the experimental round trip efficiency remains very low compared to the theoretical value of 60% expected in Section 4.2.2, with the assumption that every units exhibit a 95% 1-way efficiency. As it has been explained, this is mainly due to the non-optimized design of the experimental setup. The analysis carried out on the individual efficiencies show that possibilities of achieving the goal of 60% round trip efficiency really exist without important development efforts, but simply appropriate design and sizing.



### 6.2.4.2. Auxiliary storage subsystem's round trip efficiency measurement

It has been seen that the auxiliary storage mainly operates in power-controlled mode; its cycle efficiency is therefore measured for different power levels. To effectively do so, the experimental setup is rearranged as shown in Figure 6.13. The line source and the hydro-pneumatic storage subsystem are unused because they won't allow constant power operation. The DC source is programmed in constant power operation mode for the charge phase and the DC load is controlled to absorb a constant power during the discharge. The measurements are performed for the following power levels: 1kW, 2kW, 3kW and 4kW.

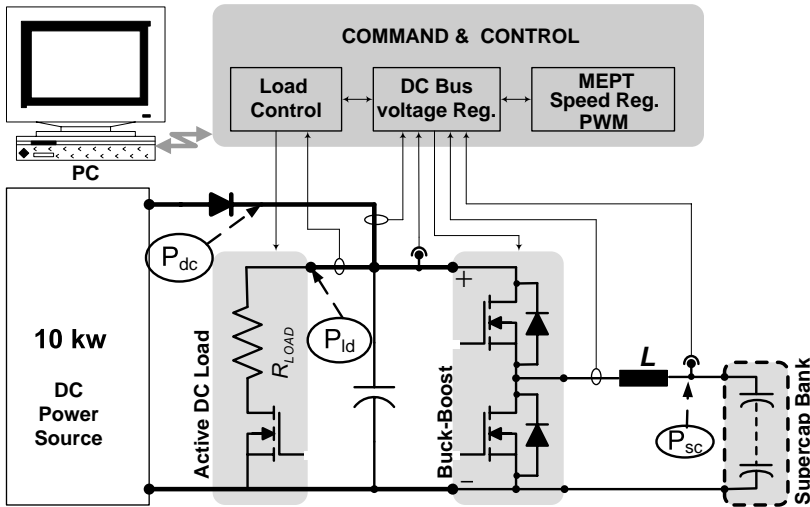


Figure 6.13.: Arrangement for auxiliary storage cycle efficiency measurement

The experimental curves for 1kW and 4kW constant power cycles are presented in Figure 6.14. As the maximum voltage of the DC source is 100V, the DC bus voltage reference is lowered during the charge phase to allow a power flow. The depth of discharge is reduced for the 4kW operation to limit the peak current. The discharge power (imposed by the DC load ratings) is

3.5kW. The curves show that the constant power operation works well: as the voltage increases, the current decreases and vice-versa to maintain the power constant.

• **Round trip efficiency of the Buck-Boost Converter**

The converter’s efficiencies for different phases and power levels are presented in Table 6.6. The efficiency obviously decreases as the power increases. It is slightly lower for boost operation than for buck operation because of the slightly higher voltage ratio that induces higher current. The average cycle efficiency of about 90% is low compared to the efficiency requirements for the auxiliary storage. The evaluation in Section 5.3.2.1 has shown that a cycle efficiency of 95% is achievable with an optimal design.

Mode	Characteristics	1kW	2kW	3kW	4kW
Buck	DC supply energy (Wh)	29.41	28.81	27.71	19.31
	Supercapacitors energy (Wh)	29.07	28.14	27.03	18.83
	<b>Efficiency (%)</b>	<b>98.84</b>	<b>97.67</b>	<b>97.54</b>	<b>97.51</b>
Boost	Supercapacitors Energy (Wh)	25.00	21.85	18.80	11.52
	Load energy (Wh)	23.45	20.28	17.02	10.32
	<b>Efficiency (%)</b>	<b>93.80</b>	<b>92.81</b>	<b>90.53</b>	<b>89.58</b>
Cycle	<b>Efficiency (%)</b>	<b>92.71</b>	<b>90.64</b>	<b>88.30</b>	<b>87.34</b>

Table 6.6.: Cycle energy efficiency of the DC-DC converter for various power levels

• **Round trip efficiency of the supercapacitor bank**

The supercapacitor bank’s cycle efficiency for the different power levels are presented in Table 6.7. These low efficiencies are mainly tributary to the high series resistance of the used, aged bank. Its impact can be observed at the beginning and the end of each phase, on the bank voltage curve of Figure 6.14b. Higher efficiencies can be obtained with recent components as seen in Section 5.2.3.

• **Round trip efficiency of the auxiliary storage subsystem**

The cycle efficiencies of the auxiliary storage for the considered power levels are presented in Table 6.8. These values are simply an image of the superca-

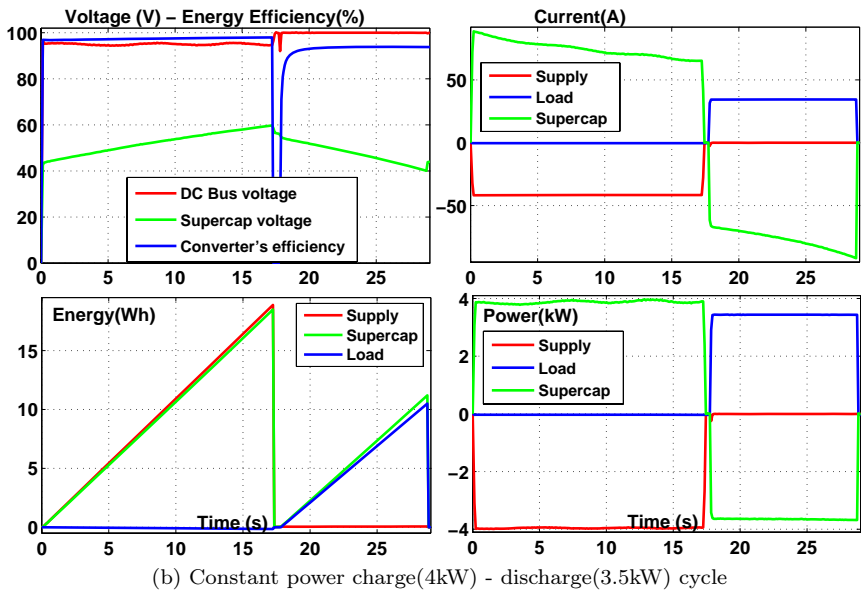
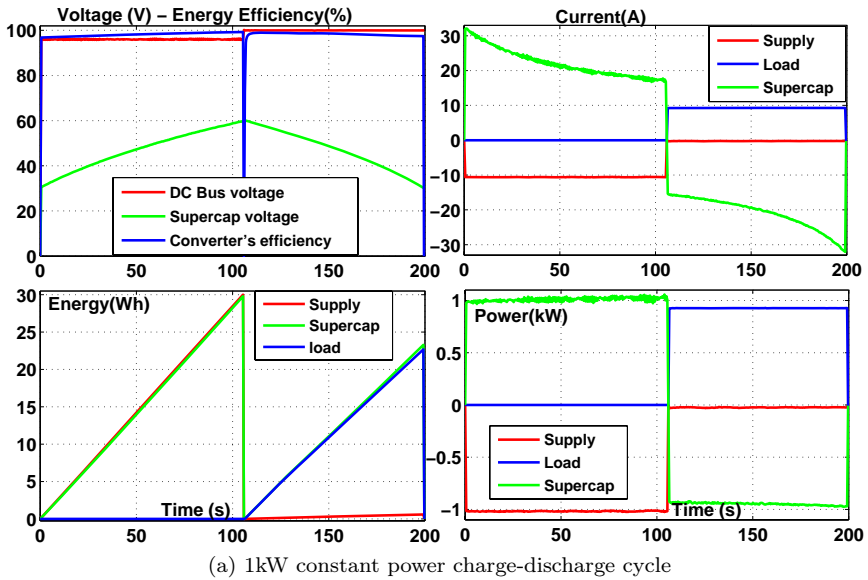


Figure 6.14.: Constant power charge-discharge cycle of the auxiliary storage

Characteristics	1kW	2kW	3kW	4kW
Stored energy (Wh)	29.07	28.14	27.03	18.83
Restored Energy (Wh)	25.00	21.85	18.80	11.52
<b>Cycle Efficiency (%)</b>	<b>85.99</b>	<b>77.64</b>	<b>69.55</b>	<b>61.17</b>

Table 6.7.: Cycle energy efficiency of the supercapacitor bank for various power levels

pacitor bank's efficiencies reported above and are consequently very low. For the same reasons as for the main storage subsystem, these values are not representative of the potential performances of the subsystem; much higher values can be expected.

Characteristics	1kW	2kW	3kW	4kW
DC supply energy (Wh)	29.41	28.81	27.71	19.31
Load Energy (Wh)	23.45	20.28	17.02	10.32
<b>Cycle Efficiency (%)</b>	<b>79.73</b>	<b>70.39</b>	<b>61.42</b>	<b>53.44</b>

Table 6.8.: Round trip energy efficiency of the auxiliary storage subsystem for various power levels

### 6.2.4.3. Overall system's round trip efficiency evaluation

Despite the unsatisfactory efficiency values recorded from the experimental setup, its round trip efficiency is evaluated. The expression of the global system's 1-way efficiency  $\eta_{tl}$  was defined in Equation 4.15 and is rewritten here for convenience.

$$\eta_{tl} = \frac{\eta_{ms}\eta_{as}^2}{1 + D(\eta_{as}^2 - 1)} \quad (6.1)$$

$\eta_{ms}$  and  $\eta_{as}$  are the 1-way efficiencies of the main and the auxiliary storage subsystems respectively, and  $D$  the power modulation duty cycle. This equation shows that the efficiency of the storage system depends on its operating point defined by  $D$ .

In practice, it is rather easier to measure the cycle efficiency of the storage units like the accumulator and the supercapacitor bank as seen with the exper-

imental results just reported. With the assumption that the units' efficiencies are independent of the operation modes (storage or discharge), the round trip efficiency  $\eta_{rt}$  of the global system can be calculated as shown in Equation 4.17 by:  $\eta_{rt} = \eta_{tl}^2$ . Combining this relation with Equation 6.1 gives:

$$\eta_{rt} = \eta_{tl}^2 = \frac{\eta_{c_{ms}} \eta_{c_{as}}^2}{[1 + D(\eta_{c_{as}} - 1)]^2} \quad (6.2)$$

where  $\eta_{c_{ms}}$  and  $\eta_{c_{as}}$  are the cycle efficiencies of the main and auxiliary storage subsystems respectively.

It is difficult to combine the different operating points considered for the measurement of the two subsystems' efficiencies because the storage system goes through all those points during a normal cycle. An order of magnitude of the round trip efficiency is estimated by combining the MEPT1 cycle efficiency (43.60%) for the main storage subsystem with the average cycle efficiency (66.24%) for the auxiliary storage subsystem. The resulting expression is:

$$\eta_{rt} = \frac{0.1913}{(1 - 0.3376 \cdot D)^2} \quad (6.3)$$

The test setup's round trip efficiency  $\eta_{rt}$  is represented in Figure 6.15 as a function the power modulation duty cycle  $D$ , together with the theoretical round trip efficiency estimated in Section 4.2.2. Given the low partial efficiencies, the overall efficiency is obviously low, about haft of the theoretical value expected in Section 4.2.2. When the auxiliary storage is not used ( $D = 1$ ),  $\eta_{rt}$  is equal to the main storage subsystem's cycle efficiency  $\eta_{c_{ms}} = 43.6\%$ . As the contribution of the auxiliary storage increases ( $D$  decreases), the round trip efficiency decreases down to its minimum value defined by  $\eta_{c_{ms}} \cdot \eta_{c_{as}}^2$ . This figure confirms the great impact of the auxiliary storage's performances on the overall system's efficiency.

## 6.3. Chapter summary

In the first section, the small test bench that has served for the first experiments on the proposed MEPT strategy with a pure pneumatic conversion system has been briefly described and some experimental results presented.

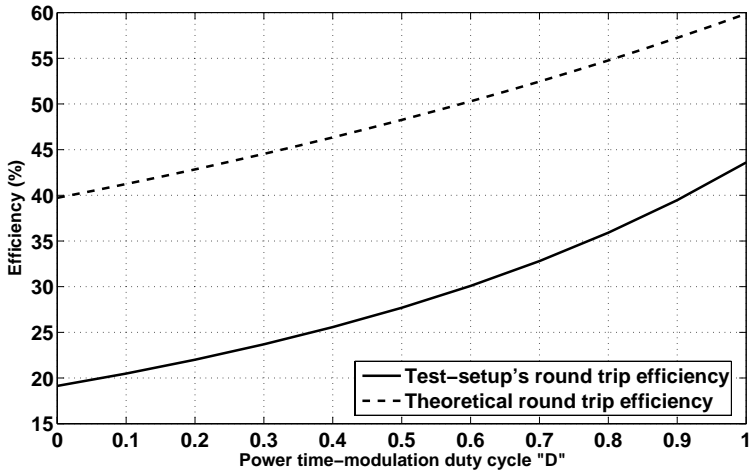


Figure 6.15.: Test setup round trip efficiency versus power modulation duty cycle

These results have shown that the proposed algorithm possesses a fast startup and a smooth tracking capabilities. The comparison of the experimental curves with the simulation curves has shown a good agreement.

In the second section, the design and operation of the first experimental setup for the hybrid hydro-pneumatic and supercapacitors storage has been described. The experimental curves of the implementation of the MEPT strategy with the oil-hydraulic conversion for various charge-discharge cycles have been reported. These curves have shown that, although there are some differences between the theoretical and the measured optimal speeds, the proposed MEPT strategy improves the cycle efficiency of the main storage subsystem by about 4% compared to that of constant speed cycles.

The experimental results of the power variation strategy for the hybrid storage system have also been presented. These results have confirmed the effectiveness of supercapacitive auxiliary storage to provide the storage system with a freely variable and high quality power.

Finally, the results of the partial and overall round trip efficiencies' measurements have been presented. The recorded efficiencies are low compared to the expected theoretical efficiencies, mainly because the test setup design wasn't optimized for efficiency purposes. However, these low efficiencies have confirmed the great impact of the auxiliary storage subsystem's performances on the overall system's efficiency.





# 7. Considerations on Cost, Duty Cycles and Impacts on the Environment

The investigations carried out so far have been mainly focused on the technical performances of the proposed storage technology. Many other aspects are however also important when designing such a system, namely the economical and environmental issues. Although the technical performances were the main object of this thesis, economical and environmental considerations have greatly influenced the choices and approaches adopted all along the project. This chapter aims at briefly discussing those other aspects with regards to the studied storage systems.

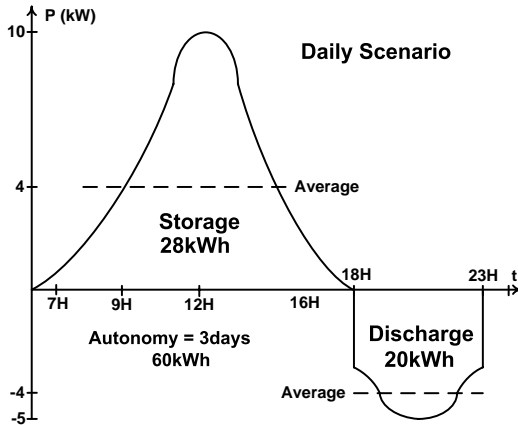
Economical issues will be considered first through a comparative cost evaluation for the two presented hydro-pneumatic storage systems and a lead-acid battery storage system, in the context of a stand-alone photovoltaic home application. Afterwards, the service lifetime will be briefly discussed through a global analysis of the reliability and maintainability of the main units. Finally the recycling possibilities and impacts of the studied systems on the environment will be qualitatively assessed.

## 7.1. Economical considerations: Comparative cost evaluation

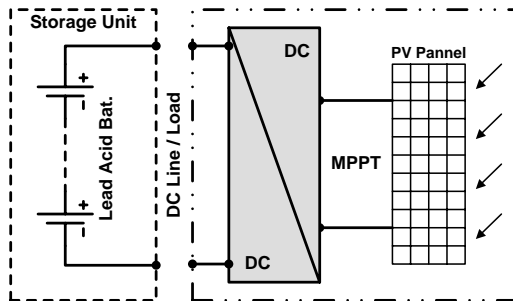
### 7.1.1. Specifications of the studied case

A prospective storage cost evaluation is made for a day-to-night power shift in a stand-alone, photovoltaic-supplied home application. The daily scenario of that application is sketched in Figure 7.1a for a normal sunny day. The

average power of the system is 4kW, the storage peak-power is 10kW and the discharge peak-power is 5kW. A 3-days-autonomy is required, which leads to a storage capacity of 60kWh.



(a) Daily scenario



(b) PV supply and battery storage

Figure 7.1.: Daily scenario and principle PV supply with battery storage system

Three storage technologies are considered with DC voltage output: A tubular plate, lead acid battery system as shown in figure 7.1b and, the hybrid BOP-A and BOP-B systems as shown in Figure 4.6. The minimum service life

requirement is 3'500 cycles, which corresponds to about 10 years with 1 daily cycle.

### 7.1.2. Layouts of the storage technologies

On the basis of the required storage capacity and the energy densities of the considered technologies, the volume and weight of each technology can be estimated. The resultant artist views realized on the basis of the arrangements proposed in [108], is represented in Figure 7.2.

The figure shows that the open gas cycle system (BOP-B) is the lightest and less bulky one. It can be seen also for BOP systems that, the storage capacity is completely separated from the conversion package, which offers more flexibility for the design and sizing of these systems. The storage capacity can be increased or decreased without affecting the power characteristics; thus a small storage capacity can be combined with a high power conversion package and vice-versa.

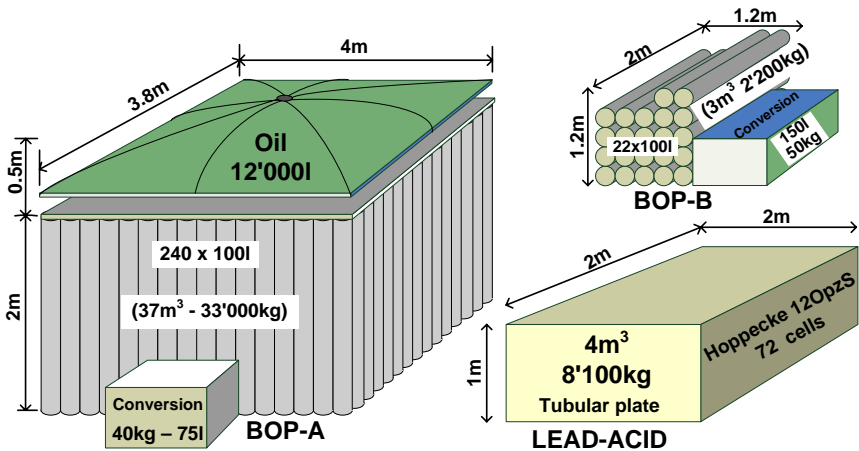


Figure 7.2.: Artist view of the three considered storage technologies for 60kWh capacity

### 7.1.3. Cost evaluation and comparison

Table 7.1 gives the costs for the considered storage technologies and the specified application, evaluated on basis of the current industrial market prices. The costs of the PV panel and its interfacing converter are not taken into account. This figure must be considered as rough estimate as, a lot of ancillaries cannot be integrated in the evaluation at this stage. However, the incurred additional cost could be compensated in an established market.

Once again, BOP-B is by far the cheapest storage solution for the considered application. BOP-A is much more expensive than the other systems, because of the large storage unit related to its low energy density. However, in comparison with lead acid batteries, this high cost is balanced by the high duty cycles inherent to BOP technologies so that the two systems present almost equal specific energy costs.

<b>Characteristic</b>	<b>Lead Acid</b>	<b>BOP-A</b>	<b>BOP-B</b>
Storage cost (€)	18'000	60'000	4'500
Conversion cost (€)	/	15'000	18'000
Technology cost (€)	18'000	75'000	22'500
Operation & Maintenance cost (€)	(30%)	(20%)	(20%)
<b>Total cost(€)</b>	<b>23'500</b>	<b>90'000</b>	<b>28'000</b>
Lifetime (cycles)	3'500	15'000	15'000
<b>Total energy (kWh)</b>	<b>210'000</b>	<b>900'000</b>	<b>900'000</b>
<b>Specific cost (€/kWh)</b>	<b>0.11</b>	<b>0.1</b>	<b>0.03</b>

Price sources: Hoppecke; Hydrel-Parker; Swissoil; Vitkocive SA; Alternativas CMR; Ercteel; (2005)

Table 7.1.: Cost evaluation for the three (60kWh - 10kW peak) storage technologies

Figure 7.3 shows the evolution of the total and specific energy costs for the three considered technologies versus the storage capacity. As can be seen, there is an offset-cost for BOP systems that corresponds to the conversion cost. In addition, BOP-A is more sensitive to the storage capacity than the other sys-

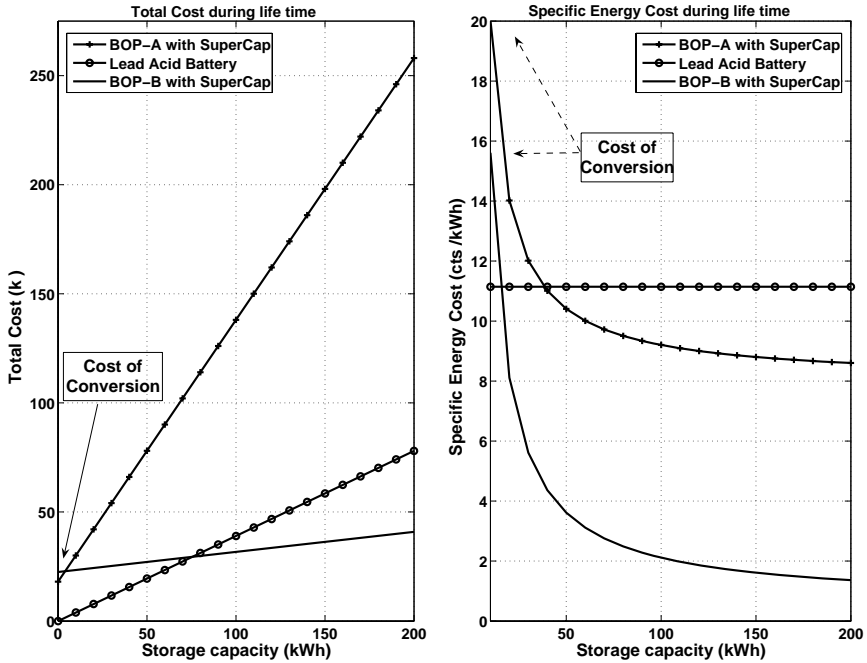


Figure 7.3.: Total-Cost (k€) and specific energy-cost (cts€/kWh) versus storage capacity

tems. These graphs confirm the cost effectiveness of hydro-pneumatic storage systems and particularly the BOP-B, which makes that system very promising as an economically viable storage solution for the targeted applications.

## 7.2. Considerations on duty cycles

Unlike battery storage systems, the studied hybrid, storage systems are the association of many storage and conversion units, as it has been seen on their schematic diagrams in Figure 4.6. The service lifetime of these systems is therefore a statistical combination of the individual reliability and maintainability of the various units which are briefly discussed in the following sections.

### **7.2.1. Service lifetime of storage units**

Two main storage devices are used: The supercapacitors for the auxiliary storage and the hydraulic accumulators (or simply high pressure bottle for BOP-B) for the main storage.

#### **7.2.1.1. Hydraulic accumulators and high pressure vessels**

Most components of hydro-pneumatic systems are mature and well-known industrial designs in terms of reliability and cost. High pressure bottles have been produced for more than a century and hydrostatics are well established in industrial applications. High pressure steel bottles have theoretically unlimited service life as no wearing part. As for accumulators, the piston type is more suitable for the considered applications. In that type, the only wearing parts are seals and bearing rings, that can be easily replaced. It is difficult to find quantitative figures about the duty cycles in public literature because these characteristics depend strongly on the operating conditions and maintenance program. A conservative figure of 20'000 cycles is generally used in standards [108].

#### **7.2.1.2. Supercapacitors**

These devices are relatively recent, but they possess interesting service lifetime characteristics because no mass transport is involved in the electrostatic phenomena, unlike the electrochemical processes of batteries. As static components, they don't suffer from mechanical wear; the main aging effect is related to the electrolyte. Manufacturers announce nowadays a figure of over 1 millions cycles. It should however be noted that, depending on the capacity of the supercapacitor bank, many supercapacitors' cycles are necessary for a single cycle of the main storage system.

### **7.2.2. Service lifetime of conversion units**

Two main types of conversion devices can be distinguished in the storage system: The rotating machines (electric and hydraulic) and the power electronic converters.

### **7.2.2.1. Rotating machines**

Hydraulic and electric machines are mature and well-known industrial devices in terms of reliability and cost. As rotating devices, seals and bearings are the main wearing parts, but they are easy to maintain or replaced. An appropriate maintenance program will ensure long service life to these devices. They are in general designed for tens of thousands of operating hours with good servicing.

### **7.2.2.2. Power electronic converters**

The reliability of power electronic systems is difficult to evaluate as they are relatively complex assemblies. For high power systems (megawatts range) where statistics about failure rates of components, redundancy possibilities and maintenance strategies exist, some reliability figures can be found. Depending on those parameters, service lifetime from a few to tens of years can be expected [109], [110], [111]. For the low power range considered in this study, that data are rather difficult to find. In fact, the most used technologies in that range are relatively recent and in constant evolution to have consistent statistics yet. In any case, the power electronic converters remain statistically the less reliable units of the studied storage systems mainly because of their complexity.

## **7.2.3. Overall system service lifetime**

It is difficult at this stage to determine the service lifetime of the whole system. Even with the assumption that all the units are highly reliable, there is, through the statistical effect of a high number of components, a higher technical risk of failure related to their association. Consistent reliability figures can be given only after years of operation. On the basis of the estimated figures for the different units, the conservative value of 15'000 cycles has been adopted for the purpose of the economical evaluation reported in Section 7.1. However, higher duty cycles are technically achievable.

## **7.3. Environmental issues**

A standard Life Cycle Analysis (LCA) would have been the appropriate method to assess the impacts of the studied storage systems on the environment, from the necessary raw material processing, to the resultant waste, through the user

disposal; but such a task is out of the scope of this thesis. Instead, an overview will be given on the operation impacts, the recycling possibilities and the waste of the used material.

The operation of the storage system involves no harmful processes for the environment as, no greenhouse gas emission and no rejection of toxic or dangerous substances occur. This is inherent to the physics of the storage principle. The main concerns about environmental impacts are related to the energy consumption for material processing and devices manufacturing, and after disposal.

The materials used for the fabrication of the majority of the devices in the storage systems are metals, namely steel, aluminium and copper. They can be found in the pressurized tank, the hydraulic and electric machines, the supercapacitors and the power electronic components. Although the processing of metals is known to be energy-consuming, their recycling possibilities are almost unlimited and, the recycling process is easy and industrially well established. No or very little problematic waste will therefore result from the use of metals. Other materials are also used in the studied system, but in small amounts compared to metals to have significant impacts on the overall system's environmental impacts. They are listed below:

Silicon and plastic will be mainly found in the power electronic devices. Although these are basically non toxic materials, they have a range of environmental impacts. Firstly, their production requires significant quantities of resources, primarily fossil fuels, either to deliver energy for the manufacturing process or as raw material (for plastic). Plastics production also involves the use of potentially harmful chemicals, which are added as stabilizers or colorants. Many of these have not undergone environmental risk assessment and their impact on human health and the environment is currently uncertain. With the increasing demand of silicon for the production of solar cells and the use of plastic for packaging, building, construction, cars manufacturing, etc, the post-consumers recycling of these materials is becoming an important industrial business sector, intended to reduce the resulting waste.

Quaternary salts, organic solvents, active carbon and cellulose are also used in supercapacitors as electrolyte, separator and electrodes respectively. The



only material of possible concern is the organic solvent which, when discarded or disposed of is, according to some regulations, a hazardous waste due to its toxicity and ignitability. Disposal can occur only in properly permitted facilities [112].

Oil is used as power transmitter between the gas and the motor/pump. The closed gas cycle system requires an important amount of oil whereas the quantity is very reduced in the open gas cycle system. Currently, mineral oil is the most used type and can be classified in the same material category as plastic. Possibilities of using vegetal oil exist, but the targeted single liquid in the project is water.

In conclusion, this overview assessment shows that the mainly used materials in the studied storage systems offer important recycling possibilities, therefore very little problematic waste will result from these systems. The main environmental impacts occur during the production and manufacturing processes through energy consumption. Given the potentially high duty cycles associated with these systems, a complete life cycle analysis should result in a positive energetic and environmental balance.



# 8. Conclusion

## 8.1. Contribution and discussion

Pneumatic energy storage was considered with the goal of improving the conversion performances and power capabilities of the dedicated conversion systems.

The analysis of the storage principle has shown that the work potential pneumatic storage relies mainly on the exergy of compressed air and the quality of heat exchange with the surroundings, the inherent advantages being the environmental friendliness and the high compatibility with renewable sources. Recovering electrical energy from compressed air through pneumatics is a reversible process that requires a multiple-step conversion: First, the heat transfer from the surroundings to the compressed air, secondly the pneumatic-to-mechanical conversion, thirdly the mechanical-to-electrical conversion and finally, depending on the application, electric power conditioning. With such a multiple-step conversion, each conversion unit must exhibit a very high efficiency so that an acceptable overall efficiency can be expected.

The investigations were initially focused on the second step of the aforementioned conversion process. Volumetric machines are generally used for that purpose where they operate in constant pressure conditions with an upstream regulation valve. The suppression of the pressure regulation is proposed to avoid the important energy losses related to that process. As a consequence, the volumetric machine must operate at high and variable pressure. An analysis of the efficiency characteristics of this kind of machine shows the existence of a pressure-dependent, optimal speed that corresponds to the maximum efficiency. A Maximum Efficiency Point Tracking (MEPT) strategy is proposed for a real time optimization of the pneumatic-to-mechanical energy conversion efficiency.

This optimization strategy relies on efficiency-controlled, variable speed operation of the volumetric machine, thanks to the electric drive system and a MEPT algorithm. The MEPT algorithm combines quadratic interpolation and the well-known “Perturb-Observe” technique to perform a fast and accurate determination of the optimal speed. Experiments have been successfully conducted both for an air machine and an oil-hydraulic one. The results show that the MEPT-controlled, variable speed operation improves the cycle efficiency of the hydro-pneumatic storage system by about 4% compared to that of a constant speed operation, without use of any additional devices, which confirm the accuracy and effectiveness of the proposed optimization strategy. In addition, the algorithm requires no particular knowledge of the controlled machine and can therefore be used for any kind of volumetric machine. The main difficulty in its implementation is the determination of the appropriate speed increment used by the “Perturb-Observe” technique, that ensures a smooth speed variation while guaranteeing an accurate tracking of the optimal speed.

The main limitation that incurred from the use of the proposed optimization strategy is the loss of the power flexibility due to the MEPT-imposed speed. To circumvent this limitation, the use of a supercapacitive auxiliary storage subsystem is proposed, which leads to the hybrid pneumatics and supercapacitors storage system. A power variation strategy is therefore necessary to provide the whole storage system with high power flexibility and to ease the energy flow management. This strategy is based on an intermittent, time-modulated operation of the main storage subsystem associated with the use of the auxiliary storage subsystem to smooth the resultant pulsating power, through the regulation of the common DC bus voltage. Experimental results confirm the effectiveness of the proposed strategy both for the storage and the discharge operations. The gained power flexibility allows associating subsystems with very different power ratings. Thus, a high storage pressure and therefore high energy density can be achieved from a low power source.

The use of an auxiliary storage increases the complexity of the storage system’s topology, which unavoidably affects its overall conversion efficiency. An efficiency analysis shows that the global system’s efficiency is proportional to the “square” of the auxiliary storage subsystem’s efficiency, which is confirmed by experimental results. Hence, the conversion performances of the auxiliary

storage must be very high to expect a high overall efficiency. A formal method for optimally sizing the supercapacitor bank, so as to meet the voltage and energy requirements while minimizing the cost, is proposed. A control strategy to improve the efficiency of the interfacing multi-phase DC-DC converter, when operating in very low power range (standby operation for instance), is also proposed. This strategy is based on a power-controlled variation of the number active phases. The efficiency analysis shows that in the very low power range, switching losses become more important than conduction losses. Its is therefore more efficient to deactivate a number of unnecessary phases.

Finally, a prospective cost evaluation is made, for a day-to-night power shift in the context of a stand-alone photovoltaic home application. This evaluation compares the studied hydro-pneumatic storage systems and a lead acid battery system. The results show that, in addition to their environmental advantages, the hydro-pneumatic storage systems become more cost effective than the lead-acid battery system for energy capacities larger than a few tens of kWh.

## 8.2. Future work

The final goal of the research project initiated by this thesis is to develop a storage system mainly based on pneumatics with high efficiency, high energy density, high power quality and flexibility, high duty cycles, low cost and low impacts on environment, for the support of renewable energy sources. Despite the obtained results that fulfill some of those requirements, further developments are still necessary, either to complete these results or to surmount the remaining difficulties, in order to effectively achieve all goals. These developments can be classified in two main categories: Thermodynamics and heat transfer on one hand and, electrical machines, power electronics and control on the other hand.

### • Thermodynamics and heat transfer

The open gas cycle hydro-pneumatic storage system using liquid-piston working-chambers with integrated heat exchangers (BOP-B) has been presented as the ideal system to achieve both a high energy density and a high conversion efficiency, at the condition that isothermal compression and expansion be effectively implemented. Modeling and simulations should be done to optimize the design and sizing of the liquid-piston interface system and, to

determine the appropriate components and the optimal operating conditions. A prototype should be built afterwards to verify the quality of heat exchanger and to validate the theoretical results.

As this thesis is being completed, these developments are being initiated in collaboration with specialized laboratories of the Institute of Energy Sciences at EPFL, as it has been explained in Section 3.2.2.

- **Electrical machines, Power electronics and control**

The MEPT strategy proposed for efficiency optimization has been successfully tested with air and then oil-hydraulic volumetric machines. The use of water as the only liquid remains the final goal to improve the environmental compatibility, ease the utilization and reduce the cost of the storage system. For that purpose, the implementation of the MEPT strategy with a water-hydraulic volumetric machine should be studied and tested.

Experimental efficiency measurements show that the electrical drive is the weak link of the main storage subsystem's conversion chain. The drive system needs to be studied more in details and its design needs to be optimized for the particular operating conditions of hydro-pneumatic storage. A dedicated electrical machine is necessary, that exhibits very high efficiency in a wide speed range and both in motor and generator operations. A dedicated DC-DC converter should be also realized for the interface of the supercapacitor bank. The proposed control strategy to improve its efficiency in low power range needs to be experimentally implemented and evaluated.

In addition to the thermodynamic and heat transfer optimization, efficient operation of the liquid-piston system will require an accurate and synchronized operation of the different valves, together with the rest of the system. A global system control strategy should be developed that will ensure an efficient, reliable and secure operation of the hybrid storage system.

# A. Control of the PM Synchronous Machine

## A.1. Principle of Field Oriented Control (FOC) for PMS machine

The Field Oriented Control (FOC) method is used for the control of the PMS machine. This method achieves the best dynamic behavior and is efficient to control a synchronous machine in adjustable speed drive applications with quickly changing speed reference and load in a wide range of speeds, such as considered in this study.

The FOC consists of controlling the stator currents represented by a vector. This control is based on projections which transform a 3-phase time and speed dependent system (a,b,c coordinates) into a 2-coordinate (d,q coordinates) time invariant system. These projections lead to a structure similar to that of a DC machine control. The basic scheme of 3-phase synchronous machine driver using a FOC structure is given in Figure A.1.

There are two reference inputs: The torque component aligned with the q coordinate and, the flux component aligned with the d coordinate. The FOC thus eases the reaching of constant reference (torque component and flux component of the stator current). It also eases the application of Direct Torque control because in the (d,q) reference frame, the expression of the torque is:  $M \propto \psi_r i_q$ . By maintaining the amplitude of the rotor flux  $\psi_r$  at a fixed value, there is a linear relationship between the torque  $M$  and the torque component of the stator current  $i_q$ . Therefore  $M$  can be control by controlling  $i_q$ .

As in synchronous permanent magnet machine the flux is fixed (determined by the magnet), there is no need to create one. Hence, when controlling this

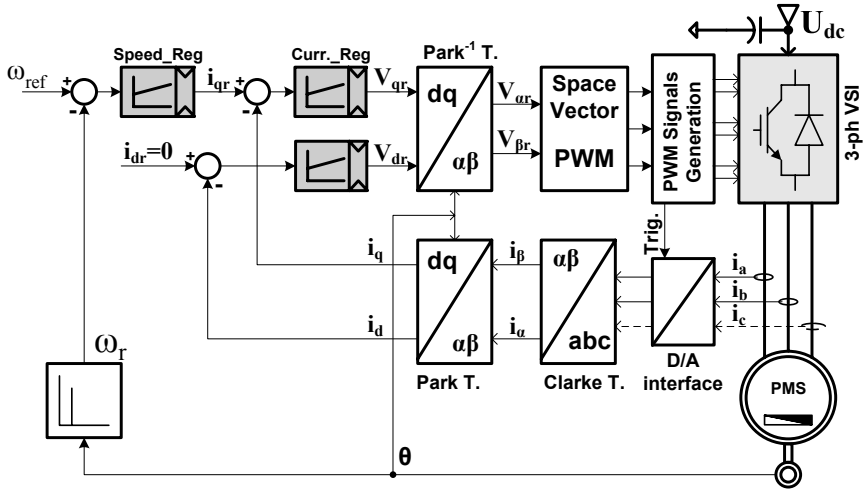


Figure A.1.: Block diagram of a 3-phase synchronous machine driver using a FOC structure

machine in the nominal field region, the d-axis current reference should be set to zero ( $i_{dr} = 0$ ) as can be seen on Figure A.1. This won't be the case if the motor is operated in the field weakening region.

## A.2. Space vector definition and projection

The 3-phases voltages, currents and fluxes of AC-machines can be analyzed in term of complex space vectors [113], [114]. A space vector representation and projections of the stator currents of a 3-phase machine is given in Figure A.2.

Assuming that  $i_a$ ,  $i_b$ , and  $i_c$  are the instantaneous currents in the stator phases, then the complex stator current vector  $\bar{i}_S$  is defined by:

$$\bar{i}_S = k (i_a + \alpha i_b + \alpha^2 i_c) \quad (\text{A.1})$$

where  $\alpha$  and  $\alpha^2$  are the spatial operators:  $\alpha = e^{j2\pi/3}$ ;  $\alpha^2 = e^{j4\pi/3}$  and  $k$  is the transformation constant.



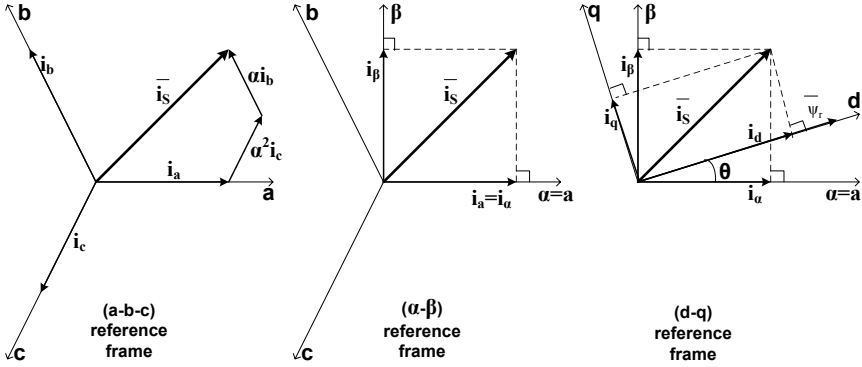


Figure A.2.: Stator current space vector and its components

The transformation from the (a,b,c) reference frame to the (d,q) reference frame is split into 2 steps:

- The Clarke transformation  $(a,b,c) \Rightarrow (\alpha, \beta)$  which outputs a 2-coordinate time variant system.
- The Park transformation  $(\alpha, \beta) \Rightarrow (d,q)$  which outputs a 2-coordinate time invariant system.

**Clarke Transformation** The mathematical relation for the Clarke transformation is:

$$\begin{bmatrix} \alpha \\ \beta \end{bmatrix} = k \begin{bmatrix} 1 & \frac{-1}{2} & \frac{-1}{2} \\ 0 & \frac{\sqrt{3}}{2} & \frac{-\sqrt{3}}{2} \end{bmatrix} \begin{bmatrix} a \\ b \\ c \end{bmatrix}$$

In most cases, the 3-phase system is symmetrical ( $a + b + c = 0$ ). Introducing this relation in Equation A.2 will give:

$$\alpha = k \frac{3}{2} a \quad (\text{A.2})$$

The constant  $k$  can be freely chosen. It is recommended to equalize the  $\alpha$  – quantity and the  $a$  – phase quantity. Then:

$$\alpha = a \Rightarrow k = \frac{2}{3} \quad (\text{A.3})$$

The relation for the Clarke transformation in balanced 3-phase system is therefore:

$$\begin{bmatrix} \alpha \\ \beta \end{bmatrix} = k \begin{bmatrix} 1 & 0 & 0 \\ 0 & \frac{1}{\sqrt{3}} & \frac{-1}{\sqrt{3}} \end{bmatrix} \begin{bmatrix} a \\ b \\ c \end{bmatrix}$$

The resulting relations for the control structure of Figure A.2 are:

$$\begin{aligned} i_\alpha &= i_a \\ i_\beta &= \frac{1}{\sqrt{3}}i_a + \frac{2}{\sqrt{3}}i_b \end{aligned} \tag{A.4}$$

For the control of a symmetrical 3-phase machine, the measurement of only 2 phase currents is necessary.

**Park Transformation** The Park transformation, which is the most important transformation in FOC, projects the 2-phase orthogonal system  $(\alpha, \beta)$  in the (d,q) rotating reference frame. The rotor flux position  $\theta$  is necessary for this transformation as can be seen in Figure A.2. The transformation relations are:

$$\begin{aligned} i_d &= i_\alpha \cos \theta + i_\beta \sin \theta \\ i_q &= -i_\alpha \sin \theta + i_\beta \cos \theta \end{aligned} \tag{A.5}$$

In synchronous machine, the rotor speed is equal to the rotor flux speed. Then  $\theta$  is directly measured by position sensor.

**Reverse-Park Transformation** The control process performed in the (d,q) rotating frame generates two voltage references,  $V_d$  and  $V_q$ , that should be applied to the stator to obtain the expected speed. To be effectively used, these voltages must be brought back into the  $(\alpha, \beta)$  stator frame. This is done through the Reverse-Park Transformation which relations are:

$$\begin{aligned} V_\alpha &= V_d \cos \theta - V_q \sin \theta \\ V_\beta &= V_d \sin \theta + V_q \cos \theta \end{aligned} \tag{A.6}$$

$V_\alpha$  and  $V_\beta$  are used by the Space Vector PWM module to generate the converter's control signals. The principle of this PWM method is presented in the Section A.3.

### A.3. Space vector Pulse Width Modulation (SV-PWM)

The Space Vector Modulation is used to generate the voltages applied to the stator phases. It uses a special scheme to switch the power transistors to generate pseudo sinusoidal currents in the stator phases. This switching scheme comes from the translation of the  $(\alpha, \beta)$  voltage reference vector into an amount of commutation time (on/off) for each power transistor [115].

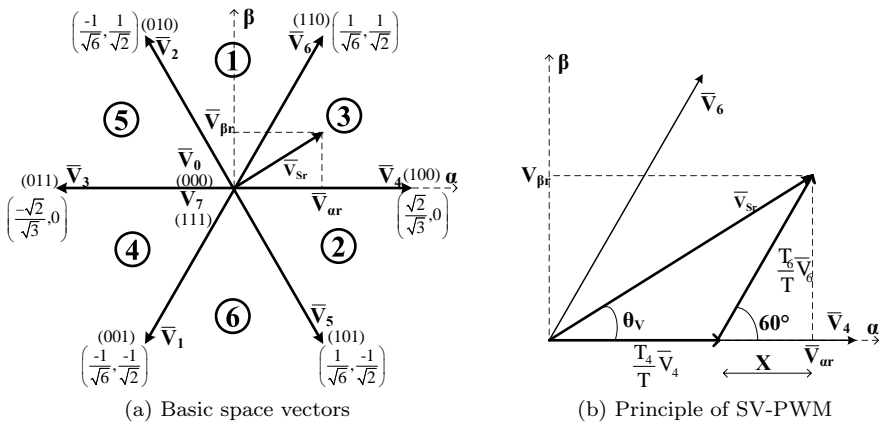


Figure A.3.: Basic space vectors and principle of SV-PWM

Figure A.3a represents the 8 basic space vectors that can be obtained from the 8 possible combinations of the power switches of the 2-level voltage source inverter. These basic vectors comprises 2 null vectors ( $V_0$  and  $V_7$ ), and 6 non-null vectors ( $V_1$  to  $V_6$ ) that define 2 space sectors. The corresponding values of the vector  $(V_\alpha, V_\beta)$  are also given in parenthesis. The method used to approximate the desired stator reference voltage with only 8 possible states of

switches is to combine, in each modulation period  $T$ , adjacent vectors of the reference voltage  $V_{Sr}$  and null vectors, and to modulate the time of application of each adjacent vector.

Figure A.3b illustrates an example where the reference voltage  $V_{Sr}$  is included in sector 3. The adjacent voltages are  $V_4$  and  $V_6$ . The modulation conditions are written as:

$$\begin{aligned} T &= T_4 + T_6 + T_0 \\ V_{Sr} &= \frac{T_4}{T} V_4 + \frac{T_6}{T} V_6 \end{aligned} \tag{A.7}$$

where  $T_4$  is the application time of vector  $V_4$ ,  $T_6$  is the application time of vector  $V_6$  and  $T_0$  is the application time of the null vectors  $V_0$  and  $V_7$ . The determination of  $T_4$  and  $T_6$  are given by simple projections on the  $\alpha$  and  $\beta$  axis. Combining these projections with the values of the basic vectors give the following results.

$$\begin{aligned} T_4 &= \frac{T}{2U_{dc}} \left( 3V_{\alpha r} - \sqrt{3}V_{\beta r} \right) \\ T_6 &= \sqrt{3} \frac{T}{2U_{dc}} V_{\beta r} \\ T_0 &= T - (T_4 + T_6 + T_0) \end{aligned} \tag{A.8}$$

The modulation is done in this way for each sector. The first step is the to determine the sector to which belongs the reference voltage  $V_{Sr}$ . This can be done in many ways from the reference vector  $(V_{\alpha r}, V_{\beta r})$ . One of these ways is the determination of the (a,b,c) normalized components  $(v_a, v_b, v_c)$  of the normalized reference vector  $(v_{\alpha r}, v_{\beta r})$  through the Reverse-Clarke transformation as follow:

$$\begin{aligned} v_a &= v_{\beta r} \\ v_b &= \frac{1}{2} \left( \sqrt{3}v_{\alpha r} - v_{\beta r} \right) \\ v_c &= \frac{1}{2} \left( -\sqrt{3}v_{\alpha r} - v_{\beta r} \right) \end{aligned} \tag{A.9}$$

These voltage are normalized to the nominal phase voltage of the PMS machine. The following code lines give the sector number referred to Figure A.3a as output:

```
If  $v_a > 0$  then  $A = 1$  else  $A = 0$   
If  $v_b > 0$  then  $B = 1$  else  $B = 0$   
If  $v_c > 0$  then  $C = 1$  else  $C = 0$   
 $Sector = A + 2B + 4C.$ 
```



# List of Figures

1.1. Life Cycle and Efficiency of today's main storage technologies (Source: ESA) . . . . .	4
2.1. Principle of CAES system: Schematic of the McIntosh plant in Alabama, USA (From Compressed Air Magazine, September 1990) . . . . .	12
2.2. One-stage arrangement of a AA-CAES system (Source: Alstom Power) . . . . .	14
2.3. Schematic diagram of the uncooled compressed air storage system . . . . .	15
2.4. Principle of the hybrid thermal and compressed air storage system (Source: Active Power, Inc.) . . . . .	16
2.5. Schematic diagram of a Pneumatic storage with volumetric air conversion system . . . . .	18
2.6. Schematic diagram of a pneumatic storage systems with oil-hydraulic conversion . . . . .	19
2.7. Possible steps for the pneumatic energy storage process . . . . .	21
2.8. Possible thermodynamic cycles for the pneumatic energy storage process . . . . .	23
2.9. Thermodynamic transformations involved in the process of closed gas cycle pneumatic energy storage . . . . .	25
2.10. Characteristics of the pneumatic Joule cycle . . . . .	27
2.11. Characteristics of the pneumatic Otto cycle . . . . .	30
2.12. P-V diagram of pneumatic open gas cycle for one volumetric machine's cycle . . . . .	32
2.13. Characteristics of the open gas cycle pneumatic storage . . . . .	33
2.14. Volumetric energy density for closed gas cycle and different value of maximum pressure $p_f$ . . . . .	37

2.15. Optimal compression ratio and maximum volumetric energy density for a closed gas cycle . . . . .	39
2.16. Unused energy and pressure utilization factor of a closed gas cycle pneumatic storage system . . . . .	40
2.17. Energy factor of closed gas cycle pneumatic storage systems . . . . .	41
2.18. Maximum volumetric energy density of closed gas cycle hydro-pneumatic storage systems . . . . .	43
2.19. Volumetric energy density of open gas cycle pneumatic energy storage systems . . . . .	45
2.20. Effect of minimum pressure on the Volumetric Energy Density of Pneumatic storage with Open gas Cycle . . . . .	46
3.1. Principle of Pneumatic energy conversion using volumetric air machine . . . . .	50
3.2. Effects of Relief valve on available pneumatic energy . . . . .	51
3.3. Exergy efficiency of the pressure regulation process . . . . .	53
3.4. Exploded view and cross-section of a low power vane air motor . . . . .	54
3.5. Real and modeled characteristics for the nominal pressure (6.3bar) . . . . .	56
3.6. Real and modeled characteristics for variable pressure . . . . .	57
3.7. Principle of pneumatic-to-mechanical energy conversion . . . . .	58
3.8. Pneumatic-to-mechanical conversion characteristics . . . . .	61
3.9. Efficiency surface of the air motor . . . . .	62
3.10. Schematic representation of the MEPT strategy . . . . .	63
3.11. Simulation curves of MEPT operation . . . . .	65
3.12. Characteristics of the maximum power operating point . . . . .	68
3.13. Flow diagram of the MPPT algorithm . . . . .	69
3.14. Simulation curves of MPPT operation . . . . .	70
3.15. Characteristics of the variable power-controlled operating points . . . . .	71
3.16. Flow diagram of the variable power-controlled startup algorithm . . . . .	72
3.17. Flow diagram of the variable power-controlled tracking algorithm . . . . .	73
3.18. Simulation curves of variable power-controlled operation . . . . .	75
3.19. Types of hydraulic devices used in hydro-pneumatic storage systems (Courtesy of Parker Hydraulics) . . . . .	77
3.20. Example of the efficiency characteristic of an oil-hydraulic machine . . . . .	78
3.21. Principle of pneumatic-to-electric energy conversion for BOP-A . . . . .	79
3.22. Principle of the MEPT strategy for BOP-A . . . . .	80



---

3.23. Simulation curves of a bladder accumulator's charge-discharge cycle . . . . .	83
3.24. Characteristics of the Parker F11-5 oil-hydraulic motor/pump . . . . .	86
3.25. Simulation curves for MEPT strategy applied to BOP-A . . . . .	88
3.26. Layout of "BOP-B": open gas cycle hydro-pneumatic storage system (Courtesy of Cyphelly & Cie) . . . . .	90
4.1. Principle of CASCES system . . . . .	94
4.2. Principle of output power variation . . . . .	96
4.3. Principle of power modulation . . . . .	97
4.4. Control and simulation of fixed-frequency power modulation mode . . . . .	98
4.5. Control and simulation of free-oscillating power modulation mode . . . . .	100
4.6. Schematic diagrams of hybrid, hydro-pneumatics and supercapacitors storage systems . . . . .	101
4.7. Main variables for the hybrid storage system's overall efficiency evaluations . . . . .	103
4.8. Simplified power profiles during the discharge operation mode . . . . .	104
4.9. Estimated global efficiency of hybrid BOP-A with supercapacitors storage system . . . . .	108
4.10. Simplified diagram for layout A . . . . .	110
4.11. Simplified diagram for layout B . . . . .	111
4.12. Simplified diagram for layout C in the context of a PV application . . . . .	112
4.13. Simplified diagram for layout D . . . . .	114
4.14. Simplified diagram for Layout E in the context of a mini water hydraulic application . . . . .	115
4.15. Simplified diagram for Layout F . . . . .	116
4.16. Estimated overall 1-way Efficiency for the 4 presented hybrid layouts . . . . .	121
5.1. Bloc diagram of the auxiliary storage subsystem . . . . .	124
5.2. Detailed and simplified models of a supercapacitor cell . . . . .	126
5.3. Schematic diagram and simplified model of a supercapacitor bank . . . . .	127
5.4. Principle of cell's voltage equalization . . . . .	128
5.5. Equivalent circuits for power-controlled charge and discharge operations . . . . .	133
5.6. Cycle efficiency for a useful energy $W_{scu} = 824.5kJ$ and different values of maximum voltage and $DOD$ . . . . .	138

---

5.7.	Main topologies of isolated bidirectional DC-DC converters . .	139
5.8.	Main topology of Non-isolated bidirectional multi-phase DC-DC Converter . . . . .	140
5.9.	Current shapes for different value of the phase inductance in buck operation . . . . .	142
5.10.	Effect of the phase inductance on the converter's performances	144
5.11.	Phase RMS current versus phase average current . . . . .	145
5.12.	Total conduction losses for the two configurations and different numbers of phase . . . . .	151
5.13.	High side MOSFET switching parameters and simplified waveforms . . . . .	153
5.14.	Low side MOSFET simplified switching waveforms . . . . .	157
5.15.	Total switching losses for the two configurations and different numbers of phase . . . . .	158
5.16.	Converter's efficiency for the two configurations and different numbers of phase . . . . .	159
5.17.	Converter's efficiency with variable, power-controlled, active phase number . . . . .	161
5.18.	Power-controlled variation of the number of active phases . . .	163
5.19.	Automatic sawtooth phase shift-angle variation . . . . .	164
5.20.	Current waveforms during phase shift-angle variation . . . . .	165
5.21.	DC bus voltage regulation with variable number of active phases	167
5.22.	Power-controlled, phase activation for no-load efficiency optimization . . . . .	168
5.23.	Cycle efficiency of the auxiliary storage subsystem . . . . .	169
6.1.	Schematic diagram and Picture of the test-bench realized for the experimental evaluation of the MEPT strategy with pure pneumatic conversion . . . . .	175
6.2.	Experimental curves of the MEPT strategy . . . . .	176
6.3.	Analytical and practical optimal speeds for the MEPT strategy with pneumatic conversion . . . . .	177
6.4.	Schematic diagram of the test-setup for hybrid BOP-A and Supercapacitors . . . . .	179
6.5.	Picture of the test-setup for hybrid BOP-A and Supercapacitors	182
6.6.	Arrangement for experimental evaluation of MEPT strategy and the main storage subsystem's efficiency measurement . . . . .	184

---

6.7.	Constant speed cycles for the hydro-pneumatic storage . . . . .	186
6.8.	MEPT-controlled cycles for the hydro-pneumatic storage . . . . .	187
6.9.	Theoretical and measured optimal speed for the MEPT operation	188
6.10.	Measured and Interpolated efficiency characteristic for the experimental hydraulic motor/pump . . . . .	189
6.11.	Power modulation during MEPT-controlled storage operation .	191
6.12.	Power modulation during MEPT-controlled discharge operation	192
6.13.	Arrangement for auxiliary storage cycle efficiency measurement	197
6.14.	Constant power charge-discharge cycle of the auxiliary storage	199
6.15.	Test setup round trip efficiency versus power modulation duty cycle . . . . .	202
7.1.	Daily scenario and principle PV supply with battery storage system . . . . .	206
7.2.	Artist view of the three considered storage technologies for 60kWh capacity . . . . .	207
7.3.	Total-Cost (k€) and specific energy-cost (cts€/kWh) versus storage capacity . . . . .	209
A.1.	Block diagram of a 3-phase synchronous machine driver using a FOC structure . . . . .	220
A.2.	Stator current space vector and its components . . . . .	221
A.3.	Basic space vectors and principle of SV-PWM . . . . .	223



# Bibliography

- [1] I. E. Agency, “Key world energy statistics 2005,” tech. rep., International Energy Agency, [www.iaea.org](http://www.iaea.org), 2005.
- [2] W. E. Council, “World energy outlook 2004,” tech. rep., World Energy Council, [www.worldenergy.org](http://www.worldenergy.org), 2004.
- [3] W. E. Council, “Survey of energy resources,” tech. rep., World Energy Council, [www.worldenergy.org](http://www.worldenergy.org), 2004.
- [4] I. E. Agency, “Energy to 2050: Scenarios for a sustainable future,” tech. rep., International Energy Agency, [www.iaea.org](http://www.iaea.org), 2003.
- [5] W. E. Council, “Global energy scenario to 2050 and beyond,” tech. rep., World Energy Council WEC, [www.worldenergy.org](http://www.worldenergy.org), 2003.
- [6] W. E. Council, “Reflection on energy and climate change,” white paper, World Energy Council, [www.worldenergy.org](http://www.worldenergy.org), July 2004.
- [7] H. Rudnick, “Risk responsibility for supply in deregulated electricity market: The chilean case,” in *IEEE Power Engineering Society General Meeting*, vol. 1, pp. 525 – 528, July 2003.
- [8] G. Michalik-Mielczarska and W. Mielczarski, “Quality of supply in liberalized electricity markets,” in *Proceedings of the 10th International Conference on Harmonics and Quality of Power*, vol. 1, pp. 1– 6, 2002.
- [9] W. E. Council, “Delivering sustainability: Challenges and opportunities for the energy industry,” statement, World Energy Council, [www.worldenergy.org](http://www.worldenergy.org), 2005.
- [10] I. E. Agency, “Energy technology at the cutting edge,” tech. rep., International Energy Agency, [www.iaea.org](http://www.iaea.org), 2005.

- [11] E. C. C. Research, “Qualitative assessment of non-nuclear energy proposals selected in fp5,” tech. rep., European Commission Community Research, April 2001.
- [12] K. Voorspools, “Sustainability and the future: Rethinking the fundamentals of energy research,” *Renewable and Sustainable energy reviews*, vol. 8, pp. 599 – 608, 2004.
- [13] B. Multon, G. Robin, M. Ruellan, and M. B. Ahmed, “Situation énergétique mondiale à l’aube du 3ème millénaire. perspectives offertes par les ressources renouvelables,” *Revue 3EI*, vol. nř 36, Mars 2004.
- [14] F. Marechal, D. Favrat, and E. Jochem, “Energy in the perspective of the sustainable development : the 2000 W society challenge,” *Conservation and Recycling, Special issue: Sustainability and Renewable Resources*, vol. 44, no. 3, pp. 245–262, 2005. available online via Science Direct.
- [15] E. C. C. Research, “Energy storage: A key technology for decentralised power, power quality and clean transport,” tech. rep., European Commission Community Research, April 2001.
- [16] J. Makansi and J. Abboud, “Energy storage: the missing link of the electricity production and delivery value chain,” tech. rep., Energy Storage Council ESC, May 2002.
- [17] J.-D. Boyes, “Overview of energy storage applications,” in *IEEE PES summer meeting*, (Seattle, Washington), July 2000.
- [18] A. Price, G. Thijssen, and P. Symons, “Energy storage: A solution in network operation,” in *Distributech Europe*, (Vienna - Austria), October 2000.
- [19] P.-C. Symons, “The future of energy storage in a deregulated environment,” in *IEEE PES summer meeting*, (Seattle - Washington), July 2000.
- [20] D. Arvizu, “Fulfilling the promise of renewable energy: a look at the future,” Tech. Rep. PR-100-38345, National Renewable Energy Laboratory (NREL), www.nrel.gov, June 2005 2005.
- [21] D. Espinosa, A. Bernardes, and J. Tenorio, “An overview on the current processes for recycling of batteries,” *Journal of Power Sources*, vol. 135, pp. 311 – 319, 2004.

- 
- [22] C.-J. Rydh, *Environmental Assessment of Battery Systems: Critical Issues for Established and Emerging Technologies*. PhD thesis, CHALMERS University of Technology, Göteborg, Sweden, 2003.
- [23] W.-V. Tore and S. Eckroad, "Improving power delivery through the application of smes," in *IEEE PES meeting*, January 2001.
- [24] J.-D. Boyes and N. Clark, "Flywheel energy storage and superconducting magnetic energy storage (smes) systems," in *Proceedings of IEEE PES meeting*, (Seattle, Washington), July 2000.
- [25] D. Kearney and H. Price, "Assessment of thermal energy storage for parabolic trough solar power plants," in *International Solar energy conference*, pp. 675 – 681, 2004.
- [26] Z. A. Hammoud and M. Lacroix, "A hybrid thermal energy storage system for managing simultaneously solar and electric energy," *Energy Conversion and Management*, vol. 47, pp. 273 – 288, 2004.
- [27] B. Eliasson and U. Bossel, "The future of the hydrogen economy: Bright or bleak?," in *The Fuel Cell Seminar*, (Lucerne - Switzerland), April 2003.
- [28] P. Boulanger and M. Perrin, "Electrolyser, hydrogen storage and fuel cell," wp st5: storage technology report, European Community, INVESTIRE NETWORK, June 2003.
- [29] S. Miyake and S. E. Industries, "Vanadium redox-flow battery for a variety of applications," in *IEEE-PES Summer meeting*, (Vancouver), 2001.
- [30] M. Schreiber, "Field test results for a 1kw - 50kwh vanadium redox-flow battery," in *Proceedings of EESAT conference*, (San Francisco - CA.), DOE - ESA, October 2005.
- [31] D.-T. Bradshaw and M. Ingram, "Pumped hydroelectric storage and compressed air energy storage," in *Proceedings of IEEE-PES summer meeting*, (Seattle, Washington), 2000.
- [32] M. Nakhamkin, R. Wolk, S. V. D. Linden, and M. Pate, "New compressed air energy storage concept improves the profitability of existing simple cycle, combined cycle, wind energy, and landfill gas power plants," in *Proceedings of the ASME Turbo Expo*, vol. 5A, pp. 103 – 110, 2004.
-

- [33] J. Saers, "Thermal and compressed-air energy storage: Next generation of energy storage technology," *Cogeneration and Distributed Generation Journal*, vol. 20, Issue 2, pp. 19 – 33, 2005.
- [34] D. Morrison, "Leveraging thermal and compressed air energy storage," *Power Electronics Technology*, vol. 30, Issue 10, pp. 95 – 96, 2005.
- [35] A. Reller and I. Cyphelly, "Speicherung gasförmiger energienträger: Eine bestandsaufnahme," *VDE Ũ Berichte , Energiespeicher*, vol. 1734, pp. 37 – 45, 2002.
- [36] I. Cyphelly, A. Rufer, P. Brückmann, W. Menhardt, and A. Reller, "Usage of compressed air storage systems," DIS Project 240050, Swiss Federal Office of Energy, [www.electricity-research.ch](http://www.electricity-research.ch), May 2004.
- [37] J. Lefèvre, *Air Comprimé; Tome 2: Utilisation*. Paris - France: Encyclopédie industrielle, 1973.
- [38] B. Gourmelen and J.-F. Leone, "Air comprimé dans l'industrie," *Techniques de l'ingénieur*, vol. Traité Génie Electrique, no. BM 4130, 1997. [www.techniques-ingenieur.fr](http://www.techniques-ingenieur.fr).
- [39] F. D. Yeaple, *Hydraulic and Pneumatic Power and Control: Design, Performance, Application*. Mc Graw Hill, 1966.
- [40] eCompressedair, "Compressed air history," <http://www.ecompressedair.com/library/compressedairhistory.shtml>, Access january 2006.
- [41] J. Prentice, "Compressed air trams," <http://www.tramways.freeserve.co.uk/Tramframe>. <http://mysite.wanadoo-members.co.uk/tramways/Articles/>, Access january 2006.
- [42] D. Self, "Transport museum: Compressed-air propulsion," <http://www.dself.dsl.pipex.com/MUSEUM/TRANSPORT/comprair/>, access January 2006.
- [43] U. MONASH, "The pioneers: An anthology: Victor tatin (1843 - 1913)," <http://www.ctie.monash.edu.au/hargrave/tatin.html>, vol. Access: january 2006.



- 
- [44] S. Robertson, "Pneumatic options," <http://www.aircaraccess.com/>, Access january 2006.
- [45] G. Nègre, "The air car," [www.mdi.lu/](http://www.mdi.lu/); [www.theaircar.com/](http://www.theaircar.com/), access january 2006.
- [46] C. Sutton, "Ucla study suggests air hybrid car could improve fuel efficiency," *UCLA Engineer*, vol. 10, pp. 4 – 5, 2003.
- [47] R. Baxter, *Energy Storage: A Nontechnical Guide*. [www.pennwellbooks.com](http://www.pennwellbooks.com): PennWell Corporation, 2005.
- [48] K.-Y.-C. Cheung, S.-T.-H. Cheung, and R. N. D. Silva, "Large-scale energy storage systems," Tech. Rep. ISE2 2002/2003, Imperial College London, @imperial.ac.uk, 2003.
- [49] A. Marquet, C. Levillain, A. Davriu, S. Laurent, and P. Jaud, "Stockage d'électricité dans les systèmes électriques," *Techniques de l'ingénieur*: [www.techniques-ingenieur.fr](http://www.techniques-ingenieur.fr), no. D4030, 1998.
- [50] R. E. Storage, "Caes technology: Overview," <http://www.ridgeenergystorage.com/caes-overview.htm>, vol. Access january 2006, 2002.
- [51] D.-T. Bradshaw, "Evaluation of sub-surface compressed air energy storage," in *Proceedings of IEEE-PES summer meeting*, (Seattle, Washington), 2000.
- [52] I. Glendenning, "Compressed air storage," *Phys. Technol.*, vol. 12, pp. 103 – 110, 1981.
- [53] S. Zunft, R. Tamme, U. Hartwig, and A. Ternedde, "Thermal energy storage technologies for advanced adiabatic compressed air energy storages (aa-caes)," in *Proceedings of the "Storage for Renewable Energies (STORE)" conference*, (Aix-en-Provence, France), CEA-GENEC, October 2003.
- [54] C. Bullough, C. Gatzien, and C. Jakiel, "Advanced adiabatic compressed air energy storages (aa-caes) for the integration of wind energy," in *Proceedings of the European Wind Energy Conference, EWEC*, (London, UK), November 2004.
-

- [55] H.-J. Kretzshmar, D. Buttig, R. Span, P. Ulbig, and W. Wagner, "Investigations on thermophysical properties of humid air for the aa-caes project," in *Proceedings of the IAPWS annual meeting*, (Vejle), 2003.
- [56] T. Kentschke and H.-J. Barth, "Uncooled compressed air storage in decentralised energy networks," in *Proceedings of the "Storage for Renewable Energies (STORE)" conference*, (Aix-en-Provence, France), CEA-GENEC, October 2003.
- [57] T. Kentschke, *Druckluftmaschinen als Generatorantrieb in Warmluftspeichersystemen*. PhD thesis, Clausthal University, Clausthal, Germany, 2004.
- [58] G. Negre and C. Negre, "Engine or compressor piston control method," *French patent No. FR2769949*, April 1999.
- [59] S. Rothhäuser, *Verfahren zur Berechnung und Untersuchung hydropneumatischer Speicher*. PhD thesis, Rheinisch-Westfälischen Technischen Hochschule, Aachen, 1993.
- [60] K. W. Li, *Applied Thermodynamics: Availability Method and Energy Conversion*. Taylor & Francis, 1996.
- [61] J. Lefèvre, *Air Comprimé; Tome 1: Production*. Paris - France: Encyclopédie industrielle, 1978.
- [62] J. Faisandier and Coll., *Mécanismes Hydrauliques et Pneumatiques*. Paris France: Technique et Ingénierie, 8 ed., 1999.
- [63] B.-V. Karlekar, *Thermodynamics for Engineers*. Prentice-Hall, Inc, 1983.
- [64] L. Borel and D. Favrat, *Thermodynamique et Energétique. 1-De l'énergie à l'exergie*. Lausanne - Switzerland: Presses Polytechniques et Universitaires Romandes PPUR, 2005.
- [65] R. Pandian, F. Takemura, Y. Hayakawa, and S. Kawamura, "Control performance of an air motor," *Proceedings of the IEEE Conference on Robotic & Automation*, pp. pp. 518-524, May 1999.
- [66] Atlas Copco, *LBZ Air Motors Manual, Tools Nr. 9833 8998 03*, 2002.

- 
- [67] C. Hua and C. Shem, "Comparative study of peak power tracking techniques for solar storage systems," *Proceedings of the IEEE Applied Power Electronics Conference and Exposition*, vol. vol 2, pp. pp. 679–683, Feb. 1998.
- [68] D. R. Otis, "Thermal losses in gas-charged accumulators," in *Proceedings of the 8th Intersociety Energy Conversion Engineering Conference*, pp. 198–201, 1973.
- [69] D. E. Winterbone, *Advanced Thermodynamics for Engineers*. Arnold and John Wiley & Sons, 1997.
- [70] A. Pourmovahed and D. R. Otis, "An experimental thermal time constant correlation for hydraulic accumulators," *Journal of Dynamic Systems, Measurements and Control*, vol. 112, pp. 116–121, 1990.
- [71] J. Svoboda, G. Bouchard, and S. Katz, "A thermal model for gas.charged accumulators based on the heat conduction distribution," in *Proceedings of the ASME winter annual meeting on Fluid Transients and Acoustics in the Power Industry*, (San Francisco), pp. 161–167, 1978.
- [72] D. R. Otis and A. Pourmovahed, "An algorithm for computing non-flow gas processes in gas springs and hydropneumatic accumulators," *Journal of Dynamic Systems, Measurements and Control*, vol. 107, pp. 93–96, 1985.
- [73] H. W. Cooper and J. C. Goldfrank, "B-w-r constants and new correlations," *Hydrocarbon Processing*, vol. 46, no. 12, pp. 141–146, 1967.
- [74] B. A. Younglove, *Thermophysical properties of fluids*. American Institute of Physics, 1982.
- [75] J. R. Vilorio, *Hydraulique Industrielle*. DUNOD, 2002.
- [76] Parker Hydraulics, Troohättan, Sweden, *Fixed Displacement Hydraulic Motor/Pump; Series F11/F12*, hy17-8249-uk ed., April 2003.
- [77] J. C. Lassègues, "Supercondensateurs," *Techniques de l'Ingénieur, Traité Génie Electrique*, vol. D3 334, 2000.
-

- [78] S. Buller, E. Karden, D.Kok, and R. W. D. Doncker, "Modeling the dynamic behavior of supercapacitors using impedance spectroscopy," *IEEE Transactions on Industrial Applications*, vol. Volume 38, pp. pp. 1622 – 1626, Nov.-Dec. 2002.
- [79] F. Belhachemi, S. Rael, and B. Davat, "A physical based model of power electric double-layer supercapacitors," in *Proceedings the 2000 IEEE Industry Applications Conference*, vol. vol.5, pp. pp. 3069 – 3076, 8-12 Oct. 2000.
- [80] P. Barrade, "Energy storage and applications with supercapacitors," in *ANAE : Associazione Nazionale Azionamenti Elettrici, 14o Seminario Interattivo, Azionamenti elettrici : Evoluzione Tecnologica e Problematiche Emergenti*, (Bressanone, Italy), 23-26 March 2003.
- [81] P. Barrade, S. Pittet, and A. Rufer, "Series connection of supercapacitors, with an active device for equalizing the voltages," in *PCIM 2000 : International Conference on Power Electronics, Intelligent Motion and Power Quality*, (Nürnberg, Germany), 6-8 June 2000.
- [82] P. Barrade, "Series connection of supercapacitors: Comparative study of solutions for the active equalization of the voltages," in *7th International Conference on Modeling and Simulation of Electric Machines, Converters and Systems, Electrimacs '02.*, (Ecole de Technologie Supérieure (ETS), Montréal, Canada.), 18-21 August 2002.
- [83] H. Späth and K.-P. Becker, "Energy storage by capacitors," *European Transactions on Electrical Power (ETEP)*, vol. Vol. 12, pp. 211–216, May-June 2002.
- [84] P. Barrade and A. Rufer, "Current capability and power density of supercapacitors: considerations on energy efficiency," in *Proceedings of the 10th European Conference on Power Electronics and Applications, EPE 2003, 2-4 September, Toulouse, France.*, 2003.
- [85] W. Lhomme, P. Delarue, P. Barrade, A. Bouscayrol, and A. Rufer, "Design and control of a supercapacitor storage system for traction applications," in *IAS 05 : 2005 IEEE Industry Applications Conference - 40th IAS Annual Meeting*, (Hong Kong), October 2005.

- 
- [86] H. Bühler, *Convertisseurs Statiques*. Collection Electricité, Lausanne, Suisse: Presses Polytechniques et Universitaires Romandes: PPUR, 1991.
- [87] Y. Song and P. Enjeti, "A new soft switching technique for bi-directional power flow, full-bridge dc-dc converter," in *The IEEE Industry Applications Society 37th Annual Meeting*, vol. vol.4, pp. pp. :2314 – 2319, 13-18 Oct. 2002.
- [88] H. Li, F. Peng, and J. Lawler, "A natural zvs high-power bi-directional dc-dc converter with minimum number of devices," in *The IEEE Industry Applications Society 36th Annual Meeting*, vol. Vol. 3, pp. pp. 1874 – 1881, 30 Sept.- 4 Oct. 2001.
- [89] F. Zhang, L. Xiao, and Y. Yan, "Bi-directional dc-dc converter for fuel cell generation system," in *The IEEE Power Electronics Specialists 35th Annual Conference, PESC 04.*, vol. Vol. 6, pp. pp. 4722 – 4728, 20-25 June 2004.
- [90] A. Rufer and P. Barrade, "A supercapacitor-based energy storage system for elevators with a soft commuted interface," *IEEE Trans. on Industry Applications*, vol. Sept-Oct, 2002.
- [91] A. Rufer and H. Ravokratrasolofo, "Static converter for complementary energy storage with batteries and supercapacitors," in *International Conference on Power Electronics, Intelligent Motion and Power Quality, PCIM 99 .*, (Nürnberg, Germany.), 22-24 June 1999.
- [92] P. Dahono, S. Riyadi, A. Mudawari, and Y. Haroen, "Output ripple analysis of multiphase dc-dc converters," in *Proceedings of the IEEE International Conference on Power Electronics and Drive Systems, PEDS '99.*, vol. Vol. 2, pp. pp. 626 – 631, 27-29 July 1999.
- [93] J. Abu-Qahouq, H. Mao, and I. Batarseh, "Multiphase voltage-mode hysteretic controlled dc-dc converter with novel current sharing," *IEEE Transactions on Power Electronics*, vol. Vol. 19, no. Issue 6, pp. pp. 1397 – 1407, 2004.
- [94] Siliconix, *MOSPOWER Applications Handbook*. No. pp. 5.87-6.94, Siliconix, 1984.
-

- [95] J.-J. Huselstein, C. Gauthier, and C. Glaize, "Use of the mosfet channel reverse conduction in an inverter for suppression of the integral diode recovery current," *Proceedings of the 5th European Conference on Power Electronics and Applications*, vol. vol.2, pp. pp. 431 – 436, 13-16 Sep. 1993.
- [96] P. Barrade and A. Rufer, "Cours d'électronique de puissance: Conversion dc/dc." Ecole Polytechnique Fédérale de Lausanne, 2000.
- [97] H. Foch, R. Arches, Y. Chéron, and al., "Alimentation à découpage: Convertisseurs continu-continu non isolés," *Techniques de l'Ingénieur*, vol. Traité Génie Electrique, no. D 3 163, 1999. [www.techniques-ingenieur.fr](http://www.techniques-ingenieur.fr).
- [98] B. Destraz, P. Barrade, and A. Rufer, "A new interleaved multi-channel dc/dc converter specially dedicated to low voltage, high current applications," in *Proceedings of the International Conference on Power Electronics, Intelligent Motion and Power Quality, PCIM 2006.*, (Nuremberg, Germany.), 30 May-1 June 2006.
- [99] F. Blaabjerg and J. Pedersen, "Optimized design of a complete three-phase pwm-vs inverter," *IEEE Transactions on Power Electronics*, vol. Vol. 12, pp. pp. 567 – 577, May 1997.
- [100] S. Linder, *Power Semiconductors*. Lausanne, Switzerland: EPFL Press, 2006.
- [101] B. Baliga, *Modern Power Devices*. New York: John Wiley & Sons, 1987.
- [102] J. Klein, "Synchronous buck mosfet loss calculations with excel model," *Fairchild Semiconductor Application Notes*, vol. AN-6005, 2003.
- [103] Perm Motor GmbH, D-79206 Breisach, Germany, *AC synchronous disc motor generator with permanent magnets*, 2004.
- [104] Analog Devices Inc., Norwood, MA (USA), *ADSP-2106x SHARC User's Manual*, 2nd ed., 1997.
- [105] M. Montemari and M. Nicollerat, *Présentation de la Carte SHARC*. Laoratoire d'Electronique Industrielle (LEI) - Ecole Polytechnique Fédérale de Lausanne (EPFL), CH-1015 Lausanne, 1998.

- [106] Xilinx, San Jose, CA (USA), *XC4000E and XC4000X Series Field Programmable Gate Arrays*, ver. 1.6 ed., may 1999.
- [107] Analog Devices Inc., Norwood, MA (USA), *ADSP-2100 Family C Tools Manual*, 3rd ed., 1995.
- [108] I. Cyphelly and M. Viloz, "Storage technology report: Wpst8-pneumatic storage," tech. rep., Investire Thematic Network, Nov. 2002.
- [109] P. Wikstrom, L. Terens, and H. Kobi, "Reliability, availability, and maintainability of high-power variable-speed drive systems," *IEEE Transactions on Industry Applications*, vol. 36, pp. 231 – 241, Jan.-Feb 2000.
- [110] R.-D. Klug and M. Griggs, "Reliability and availability of megawatt drive concepts," in *PowerCon 2004 International Conference on Power System Technology*, vol. Vol.1, pp. 665 – 671, Nov. 2004.
- [111] R. Bozzo, V. Fazio, and S. Savio, "Power electronics reliability and stochastic performances of innovative ac traction drives: a comparative analysis," in *Proceedings of the IEEE Power Tech Conference*, vol. Vol.3, (Bologna), p. 7, June 2003.
- [112] Maxwell Technologies Inc., CA 92123 San Diego - USA, *Ultracapacitors: Product information sheet*, May 2003.
- [113] Texas Instruments Europe, *Field Orientated Control of 3-phase AC-Motors*, bpra073 ed., February 1998.
- [114] L. Prokop and P. Grasblum, *3-Phase PM Synchronous Motor Vector Control using DSP56F80x*. Motorola Inc., Motorola Czech System Laboratories, an1931/d ed., March 2003.
- [115] E. Simon, *Implementation of a Speed Field Oriented Control of a 3-phase PMS Motor using TM320F240*. Texas Instruments - Digital Control Systems, spra588 ed., September 1999.





# Curriculum Vitae

Sylvain LEMOFOUET-GATSI

Born on 22th May 1970 in Bertoua - Cameroon  
Married, one child

## Education & Experience

- 2002 to date    **Research Assistant & PhD Student**  
*Industrial Electronics Laboratory (LEI)*  
*Swiss Federal Institute of Technology, Lausanne (EPFL)*  
Lausanne - Switzerland
- Research work towards Ph.D degree
  - Miscellaneous projects on power electronics
  - Education assistant for semester and diploma projects
- 2001 - 2002    **Postgraduate Specialization Course in E.E.**  
EPFL, Lausanne - Switzerland
- 1999 - 2001    ◇ **Assistant Lecturer**  
*E.E. Department of the Advanced Teacher's Training*  
*College for Technical Education (ENSET)*  
*University of Douala, Douala - Cameroon*
- ◇ **Application Engineer Consultant**  
*SCR MAYA & Cie, Douala - Cameroon*
- Electrical drive and industrial automation systems

1997 - 1999 **M.Sc. in Pedagogy & E.E.; Major: Electronics**  
*ENSET, University of Douala, Douala - Cameroon*

1991 - 1997 ◊ **Electronics Teacher**  
*Technical high School, Garoua - Cameroon*  
◦ Head of the Electronics Department (1994 - 1997)  
◊ **Application Engineer Consultant** (1994 - 1997)  
*SODECOTON, Garoua - Cameroon*  
◦ U.P.S for computing systems

1988 - 1991 **B.Sc. in Pedagogy & E.E.; Major: Electronics**  
*ENSET, University of Douala, Douala - Cameroon*

1988 **University entrance degree; Major : Electronics**  
*Technical high School of Koumassi, Douala - Cameroon*

## Language

- French **Native language**
- English **Fluent** (written and spoken)

## Publications

- S. Lemofouet, A. Rufer, I. Cyphelly, P. Barrade, F. Grasser, *Principle of a hybrid Compressed Air and Supercapacitors Energy Storage system with Maximum Efficiency Point Tracking*, STORE : Storage for Renewable Energies, 20-21 October 2003, Aix-en-Provence, France. EESAT : Electrical Energy Storage Applications & Technologies, 25-27 October 2003, San Francisco, USA.
- S. Lemofouet, A. Rufer, *Hybrid Energy Storage System based on Compressed Air and Super Capacitors with MEPT (Maximum Efficiency Point Tracking)*, IPEC 2005 : International Power Electronics Conference, 4-8 April, Niigata, Japan. (Reviewed version published in IEEJ Transactions on Industry Applications, Vol. 126, No. 7, 2006;)
- S. Lemofouet, A. Rufer, *Principle of Hybrid Energy Storage Systems based on Hydro-pneumatics and Supercapacitors for Distributed Generation and Renewable Energy Sources Support*, EESAT: Electrical Energy

Storage Applications & Technologies, 17-19 October 2005, San Francisco, USA. (Reviewed version published in IEEE Transactions on Industrial Electronics, special edition on Renewable Energies, Vol. 53, No. 4, August 2006.)

- A. Rufer, S. Lemofouet; *Energetic Performances of a Hybrid Energy Storage System based on Compressed Air and Supercapacitors*; SPEEDAM: International Symposium on Power Electronics, Electrical Drives, Automation and Motion, 23-26 May 2006, Taormina - Italy.
- A. Rufer, S. Lemofouet; *Efficiency Considerations and Measurements of a Hybrid Energy Storage System based on Compressed Air and Supercapacitors*; EPE-PEMC: European Power Electronics Conference, 30-31 August 2006, Portoroz - Slovenia (Best Conference Paper Award).
- S. Lemofouet, A. Rufer, *Hydro-pneumatic Energy Storage Systems for Renewable Sources Support: Principle, Efficiency Optimization Strategies and Possible topologies*, IRES I: International Renewable Energy Storage Conference, 30-31 October 2006, Gelsenkirchen, Germany.
- L. Fleschli, S. Lemofouet, A. Rufer, *A Gradually Controlled Multichannel DC-DC Converter for High Efficiency Applications*, IECON'06: 32nd Annual Conference of the IEEE Industrial Electronics Society, 7-10 November 2006, Paris - France